Department of Electrical and Electronic Engineering

Queen Mary College

(University of London)

PHASE CO-ORDINATE BOND GRAPH ANALYSIS OF MULTIPORT ENERGY SYSTEMS

M. RIDZUAN SALLEH

Thesis presented in the University of London for the degree of Ph.D. in Electrical Engineering

1974

To my parents

'And only parents' love can last our lives'

— Browning

PHASE CO-ORDINATE BOND GRAPH ANALYSIS OF MULTIPORT ENERGY SYSTEMS

ABSTRACT

The analysis of unbalanced power system problems using the method of phase co-ordinates by which the phase quantities are preserved has obvious practical advantages over the transformation methods requiring the phase quantities to be substituted by, for example, symmetrical component and d-q quantities. Since the physical identity of the system is maintained in the phase frame of reference, the matematical models of the system can be subjected to actual operating constraints enabling a unified approach to be adopted in the study of both symmetrical and unsymmetrical conditions.

In this thesis the bond graph techniques are used to model power system components in terms of their phase co-ordinates. The bond graph structure, which is based on energy continuity and power balance, classifies system and sub-systems with respect to the number of energy ports through which energy or power is exchanged with the environment as well as in terms of the particular internal energy transformations involved. The use of bond graphs for the analysis of non-linear electromagnetic systems has resulted in the evolution of a uniform diagramatic structure which represents in a single diagram the basic field properties such as the magneto-motive force and the flux linkages together with the conjugate circuit power variables, voltage and current.

As an extension of this idea, the general n-port electromagnetic and electrostatic field systems are derived in bond graph notations. A very desirable feature of this method of presentation is that there exists a one-to-one correspondence between the bond graph and a computation structure which may be used for the purpose of simulation by either analogue or digital computers.

The general n-port electromagnetic and electrostatic field systems form the basis for the effective modelling of power system components such as rotating machines, transformers and transmission lines. In the investigations of earth faults, these models are simplified in accordance with the need of the particular study but are sufficiently accurate representations to allow predictions on the overall system behaviours.

The bond graph approach is ideally suited to expedite the modelling of dynamic interacting energy systems and when used in conjunction with the computation structure can provide the simulation technique required to model accurately the non-linear behaviours of multiport electromechanical energy converters. The effects of magnetic saturation in synchronous generators are presented in detail.

ACKNOWLEDGEMENTS

No thanks can adequately express my appreciation for the constant encouragement, inspiration and advice I received from my supervisor, Dr. M.A. Laughton, Reader in Electrical Engineering.

My special gratitude is due to Miss C. Smith for typing this thesis in its present fine format.

To the Institut Teknologi Kebangsaan, Malaysia, I am grateful for granting me study leave and financial support to enable me to pursue with the research.

PHASE CO-ORDINATE BOND GRAPH ANALYSIS OF MULTIPORT ENERGY SYSTEMS

TABLE OF CONTENTS

LIST OF FIGURES

LIST OF TABLES

LIST OF PRINCIPAL SYMBOLS

e = effort, emf, generalised force; vector thereof

i = flow, current

λ, p = flux linkage, generalised momentum

q = electric charge, generalised displacement; vector thereof

$\mathcal{F}$ = magnetomotive force or dissipative function

Φ = flux

$\mathcal{R}$ = reluctance

T = steady-state shaft torque or generalised (or quasi) kinetic energy

T^* = generalized kinetic co-energy

ω = angular velocity

E = steady-state phase emf; vector thereof or stored energy

I = steady-state phase current; vector thereof

K = transduction ratio or gyrator modulus; matrix thereof

V = steady-state phase voltage; vector thereof or generalised (or quasi) potential energy

Y = admittance; matrix thereof or energy vector

Z = impedance; matrix thereof or co-energy vector

S = complex phase power or matrix of coefficient

X = primitive quasi displacement

x = primitive quasi velocity; vector thereof

F = primitive quasi force; vector thereof

$\mathcal{L}$ = Lagrangian

f = generalised velocity, vector thereof

M, m = transformer modulus

L = inertance, inductance

L^* = co-inertance

C = compliance, capacitance

R = resistance

P = power

G,r = gyrator modulus

Subscripts

m = magnetizing

ℓ = leakage

a = phase 'a' or armature

b = phase 'b'

c = phase 'c'

F = field

D = direct-axis damper

Q = quadrature-axis damper

s = stator

r = rotor

CHAPTER ONE

INTRODUCTION

1.1 Introduction

This thesis is primarily intended to study the theory involved and the simulation technique required to model power system components in terms of their phase co-ordinates. Traditionally, complicated power system problems have been successfully analysed by manual calculations using transformation methods; and with the advent of modern digital computers it is natural that the same methods are retained adapting the computer to do only the menial chores, once the drudgery of the analyst. The method of phase co-ordinates, however, proposed the retention of the actual phase quantities and avoids the necessity to transform variables. The phase equations are normally more involved, but it is considered that with improved computer methods the solution process needed is within the capability of present-day generation of digital computers.

The modelling of physical systems is guided by two counteracting objectives:

(i) the model must be inclusive, complete, and consistent with the actual device, and

(ii) the model must be simple, basic and non-superfluous.

While the first objective tends to complicate the model by swelling the number of physical properties taken into consideration, the other objective acts as a

retarder on excluding too many significant details. The final model must therefore represent a compromise between these tendencies. Very often, the first step in this compromise is a decision to consider the system lumped rather than distributed.

At the onset of the research work, it was soon realised that a systematic procedure for graphically representing lumped energy systems, unambiguously, was needed. The electric circuit graphs have been extensively developed since 1800, perhaps initiated by Alessandro Volta (1745-1827). The use of circuit graphs in a wide variety of applications and the availability of its associated topological and operation techniques are both impressive and well documented. As such there is a strong appeal in the idea of finding circuit representations for both electrical and non-electrical systems. However, since circuit elements react to potential differences while this property is not universal for elements in nominally analogous fields, this mode of representation is principally ideal only for systems characterised by power variables sharing one common domain. In order to avoid this restrictive nature in the fundamental tool of modelling, a search was made for an alternative graph.

The bond graph concept[1,2] initially proposed about a decade ago is based on energy continuity and power balance. The relationships between bond graphs and several of the other types of known[3] graphs used in engineering system analysis are displayed in Fig. 1-1.

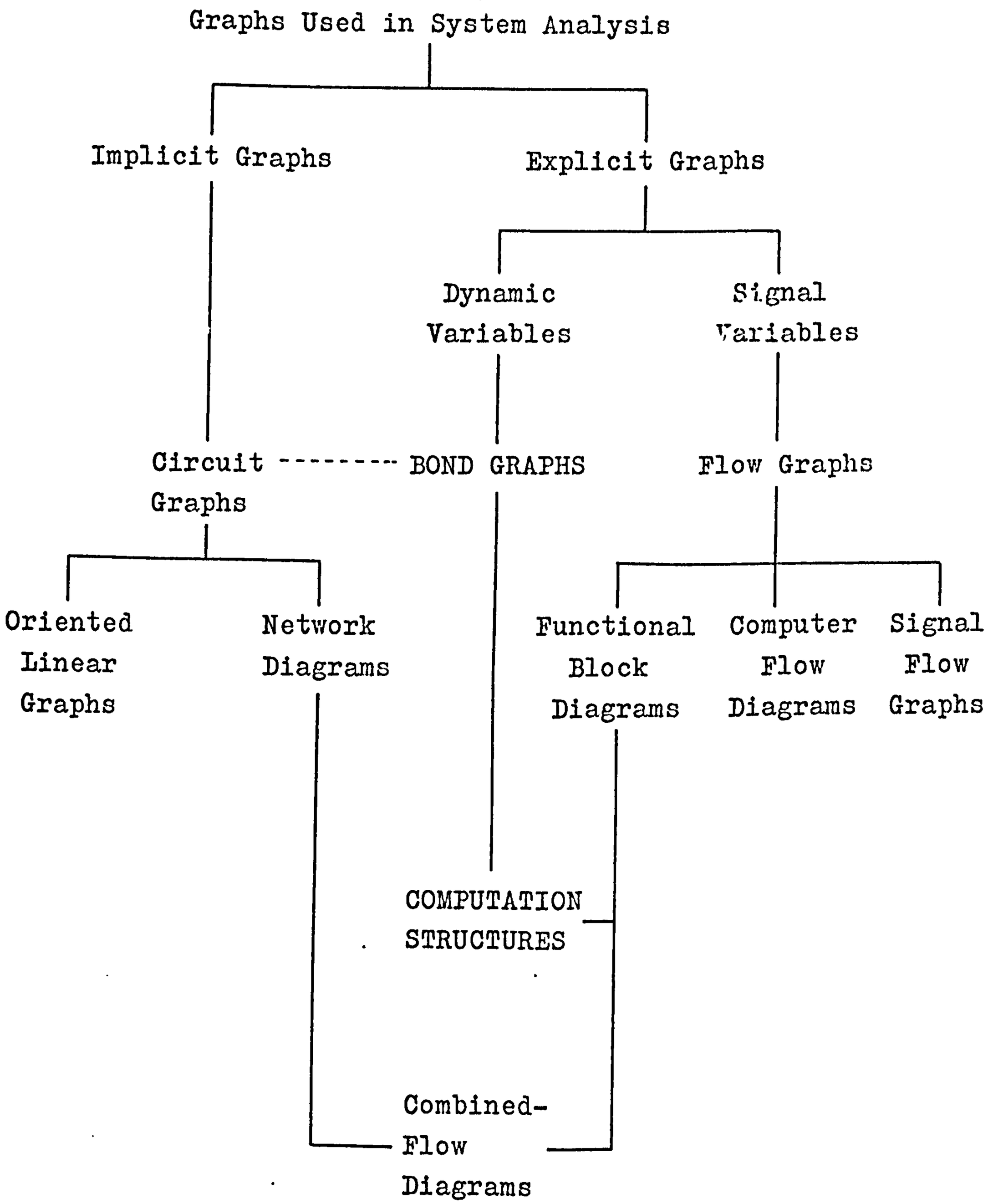

Fig. 1-1 Relationships between Graph Methods Used in Engineering System Analysis

The decision to use bond graphs lies in their ability to provide a comprehensive view of energy and power interactions between topological constraints and 1-port elements. Also the bond graph approach is particularly adaptable when electrical, mechanical and magnetic systems interact within a dynamic structure, since all these systems may be handled conveniently by the same unified method. The clarity and conciseness with which bond graphs depict the nature of dynamic interactions between system components makes them uniquely useful in the application of simulation to design. In a sense, the bond graph representation presents graphically what other techniques express in equations or in the condensed notation of matrices and tensors.

Although the development of bond graphs is perhaps motivated by the need to represent dynamic systems graphically, the conversion of bond graphs into steady-state 'impedance/admittance' graphs in which all dynamic elements are transformed into equivalent impedance/ admittance form, follows in a simple and direct process. In the steady-state bond graph, the impedances and admittances are characterised by the usual complex quantities $Z(j\omega)$ and $Y(j\omega)$ repsectively.

With the bond graph established as the basic modelling tool, its use was initially focused on the energy and power interaction property of the graph. The application of variational principles leads to the view that power-conserving transformations may be regarded as physical devices enforcing constraints and that the extension of energy methods aids in the formulation of physical systems.

In an attempt to simplify the representation of non-linear effects using state-space formulation, it becomes apparent that most non-linear effects in power system engineering can be represented by non-linear dissipative elements which in turn can be characterised by non-linear algebraic equations. Consequently new bond graph devices are introduced to display the non-linear effects graphically. These devices, which will be described in Chapter 2, play an important role in the simulation of non-linear power system components.

1.2 Bond Graph - Historical Background

The introduction of bond graph by Paynter[1,2] is the manifestation of his belief that energy and power alone are the fundamental dynamic variables. In his effort to develop a general theory of engineering systems, the preoccupation with energy flux and power flow is quite evident, and this eventually resulted in the application of the terms 'energy ports', 'power bonds' and 'multiport elements' as early as 1955.

The concept took a major turn in the late 1950's with the realisation that the requisite form of graph lies in the form of structural formulas for chemistry. In 1959 this idea was extended with the introduction of the ideal 3-port energy junction. It was then apparent that two 3-ports bonded together form a 4-port; the process of which may be continued indefinitely to form n-ports of any order whose only requirement at the junction is to ensure that power or energy is conserved.

The system of bond graphs was organised into a

formal discipline by the publication of a book by Paynter[2] in 1961. However, it was not until 1968 when Karnopp and Rosenberg[4] presented a book solely on the definitions of bond graph notations and their applications that bond graph techniques gained greater acceptance and usage.

1.3 Bond Graph - Review of Literature

The bond graph methods, which perhaps was initially created as an alternative to circuit graph methods, can be extended beyond their traditional domains of applicability to include chemical reactions and the types of irreversible thermodynamic interactions of interest in biophysics and other fields[5,6]. The very diversity of the systems studied and the technical fields involved have made it hard for any single individual to keep aware of all the developments in bond graph methods. This short review is not intended to compile all the published literature or to compare the various methods but rather to emphasise the lack of technical papers on the application of bond graph techniques to power system problems.

To the best of the author's knowledge, the only available recorded paper on the use of bond graphs for power system modelling was presented by Paynter[7] in 1960 at the First Congress of the International Federation of Automatic Control, Moscow. In this paper he suggested that power systems consist of elemental parts - the multiport components - which may be treated in precisely analogous fashion to the mutlivalent atoms of structural chemistry. Thus, by considering each and every functional

component of the power system as a multiport sub-system, it is possible systematically to classify and to catalogue all the elemental parts. The assembly of a representation of any particular portion of a large power system merely requires connecting the parts resulting in the construction of an assembly diagram. In a later paper[8] published in 1965, Paynter and Karnopp reaffirmed and extended this conviction by stating that all energy systems are composed of irreducible primitive bond graph sets.

Most of the papers before 1968 originated from the Massachusetts Institute of Technology, often circulated as internal notes, and as such are difficult to obtain. However, after the publication of the book on bond graphs in 1968, a collection of papers on analytical mechanics[9,10], structural dynamics[11] and the problems of vehicle drives[12] began to appear from other sources. The paper on power-conserving transformations[9] is an important contribution since the physical interpretation of the transformations leads to non-traditional system formulations including the use of co-energy expressions for ideal devices which, although conservative, store no energy.

In 1972 a concerted effort was made to present simultaneously a representative group of research papers which indicate the broad scope in the future growth of bond graph theory[13,14,15] and an expansion of the areas of applicability of bond graph methods[16,17,18,19]. A more recent paper by Martens[20] deals with the simulation of non-linear multiport system.

1.4 Thesis Organisation

This thesis is presented in six main chapters and five appendices, with references pertaining to each chapter included in its final section. A feature, inherent in bond graph analysis, which illustrates every facet of a model diagramatically, forms an integral part of the thesis.

In a way, the bond graph concept is somewhat alien to the power system analyst and as such part of Chapter 2 is devoted to the definitions of bond graph notations. The special properties of the gyrator are explored in the latter half of this chapter resulting in the proposal and introduction of the inductive and capacitive mutators as necessary multiports in the graphical representations of non-linear energy systems. With the derivation of the general n-port electromagnetic and electrostatic field systems, it will be shown that the non-linear energy systems can be described by sets of mixed differential/ algebraic equations systematically organised by computation structures which have one-to-one correspondence with bond graphs.

The application of bond graph techniques to power system problems are included in the following two chapters. In Chapter 3 the n-port electromagnetic field system is adapted for steady-state operation and the simplified single-phase transformer is used to model a number of polyphase mutliwinding transformers needed for the analysis of fualt problems. Models of other power system components such as rotating machines and transmission

lines are also derived, in the process of which certain interesting structures are displayed. It is in the opinion of the author that these structures may provide an important clue to the suggestion by Paynter[7,8] that a power system complex can be represented in the same manner as, for example, the macromolecular architecture in chemistry. However, it must be stated here that no scientific evidence can hitherto be found to substantiate this opinion.

The n-port electromagnetic field system is again utilised in Chapter 4 to study the dynamic behaviours of single- and three-phase saturated synchronous generators. The first part of this chapter deals with the theory of rotating machines, derived to ensure that the sets of mixed differential/algebraic equations can be formulated as in Chapter 2. An attempt is made to overcome the difficulties involved in representing the rotor circuits by considering the complicated rotor leakage flux paths. It will also be shown that the computation structures help to organise the system equations systematically and perhaps optimise the solution process for the minimum number of iterations. In fact, Clancy and Fineberg[21] have suggested that some of the major difficulties in digital simulations arise because digital computers are series devices and that unless a sorting algorithm is available to convert the computers into 'pseudo-parallel' devices these difficulties cannot be resolved since most of the existing physical systems are parallel phenomena. The computation structure can be regarded as a sorting algorithm.

In the fifth chapter, the energy and power interactions expressed by bond graphs are investigated using variational principles. A number of power-conserving transformations can be evolved, the physical interpretations of which points to the conclusion that even though no energy is stored in the ideal transformers, yet co-energy expressions can exist which may be used in Lagrangian formulations[13]. The basic and alternative bond graphs for lumped energy systems, formed from transformers and gyrators respectively, are presented. Also methods for formulating non-linear system equations from bond graphs are derived, confirming the need to introduce the mutators to display the non-linear effects graphically.

Chapter 6 attempts to review and unify the contributions made in this thesis. The extensive application of bond graphs to the steady-state and dynamic modelling of power system components shows the flexibility of this approach and may provide future scope for the understanding of the complex energy interactions in these components. It is hoped that this chapter will highlight the ability of the derived technique to model non-linear energy systems.

Appendix A gives details of PHASECO, a program developed by the author for the solution of balanced and unbalanced fault problems in power systems. The program for the simulation of non-linear dynamic systems is a commercial package program and is described in Appendix B. An alternative method for simulation is the implicit integration method and in Appendix C the required derivative approximation is derived.

In Appendix D, data for all the test systems are presented. The simulated oscillograms for a three-phase synchronous generator and an induction motor used in the tests are included in Appendix E. This appendix also displays all the waveforms for the various mmfs and flux linkages.

1.5 References

1. Paynter, H.M.: 'Generalising the Concepts of Power Transport and Energy Ports for System Engineering', ASME Paper 58-A-296, presented at 1958 Annual Meeting, New York, N.Y.

2. Paynter, H.M.: 'Analysis and Design of Engineering Systems', (The MIT Press, Cambridge, Mass., 1961)

3. MacFarlane, A.G.J.: 'Notes on Multi-Port Approach to System Analysis and the Theory of Bond Graphs', Lecture Notes, August, 1965 (Unpublished)

4. Karnopp, D. and Rosenberg, R.C.: 'Analysis and Simulation of Multiport Systems', (The MIT Press, Cambridge, Mass., 1968)

5. Auslander, D.M., Oster, G.F., Perelson, A. and Clifford, G.: 'On Systems with Coupled Chemical Reaction and Diffusion', ASME Journal of Dynamic Systems, Measurements and Control, Series G, 1972, 94, (3), pp. 239-248.

6. Auslander, D.M., Lobdell, T.E., and Chong, D.: 'A Large-Scale Model of the Human Cardiovascular System and its Application to Ballistocardiography', ASME Journal of Dynamic Systems, Measurements and Control, Series G, 1972, 94, (3), pp. 230-238.

7. Paynter, H.M.: 'Computer Representations of Polyphase Alternating Current Systems for Dynamic Analysis and Control', Automatic and Remote Control, Proc. First International Congress of the International Federation of Automatic Control, Moscow, 1960, pp. 1009-1017.

8. Paynter, H.M. and Karnopp, D.C.: 'Design and Control of Multiport Engineering Systems', Automatic and Remote Control, Proc. of International Federation of Automatic Control, Tokyo, 1965, pp. 443-454.

9. Karnopp, D.C.: 'Power-Conserving Transformations: Physical Interpretations and Applications using Bond Graphs', Journal of the Franklin Institute, 1969, 288, (3), pp. 175-201.

10. Karnopp, D.C.: 'Resolution of a Paradox Involving Mechanical Gyrators and Transformers', Journal of the Franklin Institute, 1971, 291, (3), pp. 211-217.

11. Karnopp, D.C.: 'Bond Graph Methods in Structural Dynamics', Society of Automotive Engineers, Paper 710781, September 1971.

12. Karnopp, D.C. and Rosenberg, R.C.: 'Application of Bond Graph Techniques to the Study of Vehicle Drive Line Dynamics', ASME Journal of Basic Engineering, Series D, 1970, 92, (2), pp. 355-362.

13. Brown, F.T.: 'Lagrangian Bond Graph', ASME Journal of Dynamic Systems, Measurement and Control, Series G, 1972, 94, (3), pp. 213-221.

14. Oster, G.F. and Auslander, D.M.: 'The Memristor: A New Bond Graph Element', ASME Journal of Dynamic Systems, Measurement and Control, Series G, 1972, 94, (3), pp. 249-252.

15. Brown, F.T.: 'Direct Application of the Loop Rule to Bond Graphs', ASME Journal of Dynamic Systems, Measurement and Control, Series G, 1972, 94, (3), pp. 253-261.

16. Martens, H.R. and Bell, A.C.: 'A Logical Procedure for the Construction of Bond Graphs in System Modelling', ASME Journal of Dynamic Systems, Measurement and Control, Series G, 1972, 94, (3), pp. 183-188.

17. Wormley, D.N., Grag, D.P. and Richardson, H.H.: 'A comparative Study of the Non-Linear and Linear Performance of Vehicle Air Cushion Suspensions using Bond Graph Models', ASME Journal of Dynamic Systems, Measurement and Control, Series G, 1972, 94, (3), pp. 189-197.

18. Paynter, H.M.: 'The Dynamics and Control of Eulerian Turbomachines', ASME Journal of Dynamic Systems, Measurement and Control, Series G, 1972, 94, (3), pp. 198-205.

19. Rosenberg, R.C.: 'Multiport Models in Mechanics', ASME Journal of Dynamic Systems, Measurement and Control, Series G, 1972, 94, (3), pp. 206-212.

20. Martens, H.R.: 'Simulation of Non-Linear Multiport Systems using Bond Graphs', ASME Journal of Dynamic Systems, Measurement and Control, Series G, 1973, 95, (1), pp. 49-54.

21. Clancy, J.J. and Fineberg, M.S.: 'Digital Simulation Languages: A Critique and a Guide', Proc. of the Joint Computer Conference, 1965, 27, (1), pp. 23-36.

CHAPTER TWO

BOND GRAPH ANALYSIS AND SIMULATION OF MULTIPORT SYSTEMS

2.1 Introduction

The primary aim of this chapter is to construct a general mathematical and graphical model of a collection of resistive, capacitive and inductive multiports which may be used to represent sub-systems consisting of non-linear electromagnetic and electrostatic energy fields. These interactive sub-systems can adequately represent most of the power system components such as rotating machine, transformers and transmission lines.

Hitherto, the network theory approach has always been used in the analysis of power system behaviours and one of the earliest and most widespread use of this theory is in the steady-state analysis of unbalanced polyphase network using symmetrical component theory initially introduced in 1915[1]. With the acceptance of the concept of a circuit as a system of idealized lumped elements, complicated physical devices are then naturally described by their 'equivalent circuits'. A classical general approach to equivalent circuits has been developed by Kron[2,3] by the use of tensor concepts.

The representation of an individual power system component by means of 'electric equivalent circuit' method is well known and perhaps the chief exponent in this field is Slemon[4,5,6]. As an extension of Cherry's concept[7] of duality between electric and magnetic circuits, Laithwaite[8] introduced the 'magnetic equivalent circuit'

which is later developed and used by Fiennes[9] as a new approach to the general theory of electrical machines.

It is with these developments in mind that an attempt is made here to use the Bond Graph Technique[10,11,12,13] to organise a computation structure representing both magnetic and electric fields, rather than considering them separately in two distinct equivalent circuits. The bond graph initially introduced in Section 1.1 has a novel way of organising the computation structure and will be freely used throughout this thesis.

The problem of designing and evaluating an engineering multiport system involves the study of a series of inter-connected components for generating, conditioning, transmitting, and transducing power. The bond graph notation, besides being specially designed to expedite the modelling of physical dynamic systems in which power interactions are important, is ideally suited for the 'molecularization' of engineering multiport systems into multiport components.

The modelling process begins with the basic coupling structure of each component and in a logical step-by-step procedure the complete model is built to satisfy a number of functional considerations inherent to the ideal model. The degree of sophistication of the model is governed by the needs of the particular study; and having achieved the desired component model each model may be connected to represent the complete system by using the principle of causal relations[13].

Consequently, the following sections will be devoted to the basic concepts of bond graphs useful for the analysis

and simulation of power system dynamics; and it is hoped to show that the bond graph approach is conceptually very advantageous as it presents a detailed display of the energy coupling between the mechanical, electrical and magnetic ports of an energy system in a single minimally coded structure suitable for analysis by either analogue or digital computers.

2.2 Representation of Necessary Multiports

The usual definition of a multiport is a subsystem that may interact with other systems through one or more ports[14]. A generalized multiport system shown in Fig. 2-1 is composed of elements from the necessary bond graph set. The collection of C and L multiports is referred to as the storage field and the set of ports associated with it, the storage ports. The dissipation field consists of R elements with its corresponding dissipation ports. The collection of source elements S_e and S_i comprises the source field and its associated ports are the source ports. However, the junction structure is a power-conserving multiport from the collection of elements in the set (TF, GY, IMU, CMU, O, 1) which for the purpose of this study is termed as transformer, gyrator, inductive mutator, capacitive mutator, flow junction and effort junction respectively.

For computational analysis it is important that causality be assigned to the bond graph according to a systematic procedure and the result is that shown in Fig. 2-2. The graph is said to have integration causality, which means that every C-field port and every L-field port is as shown in that figure. The procedure for assigning

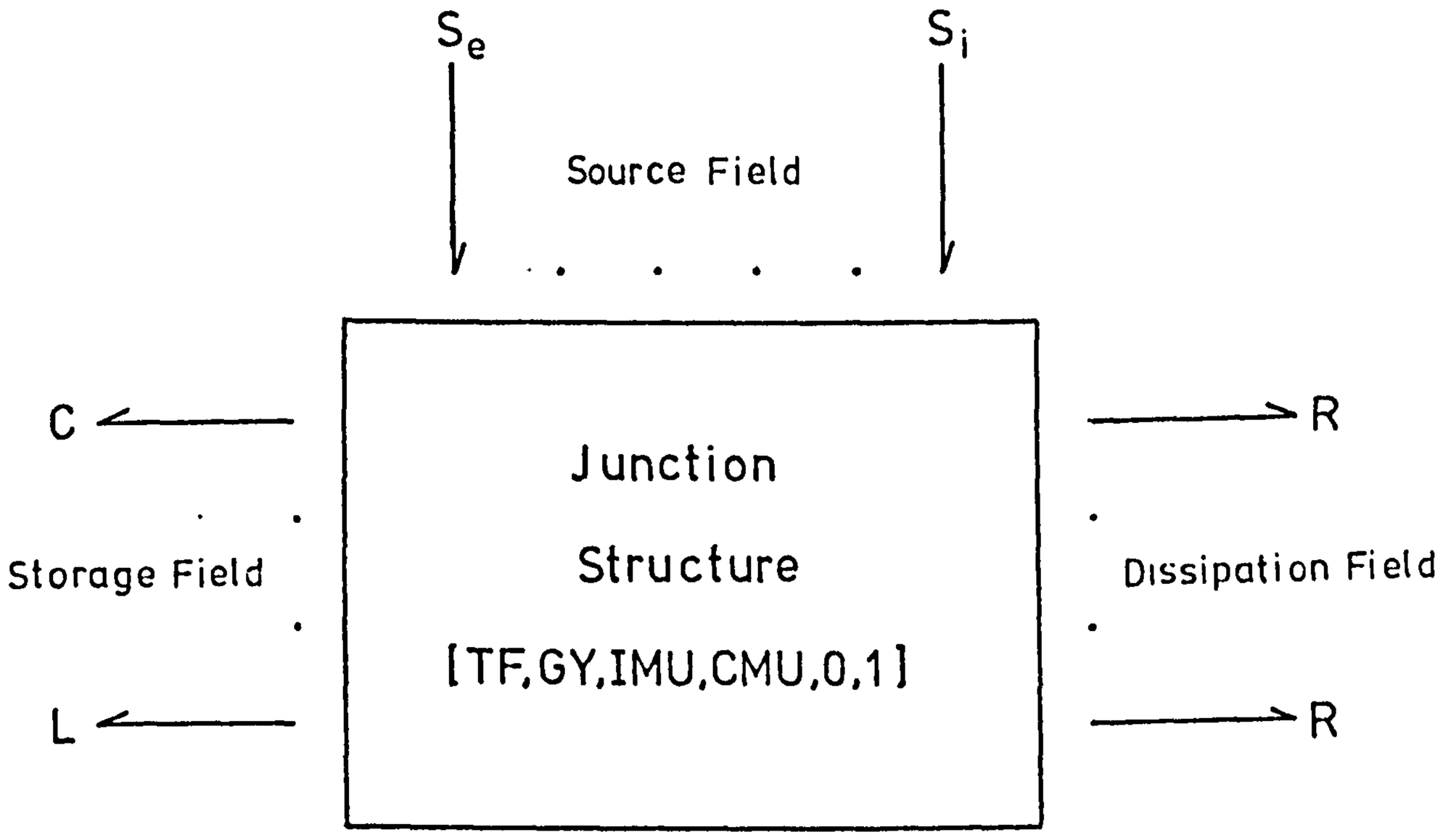

Fig. 2-1 Basic Field of Acausal Multiport System

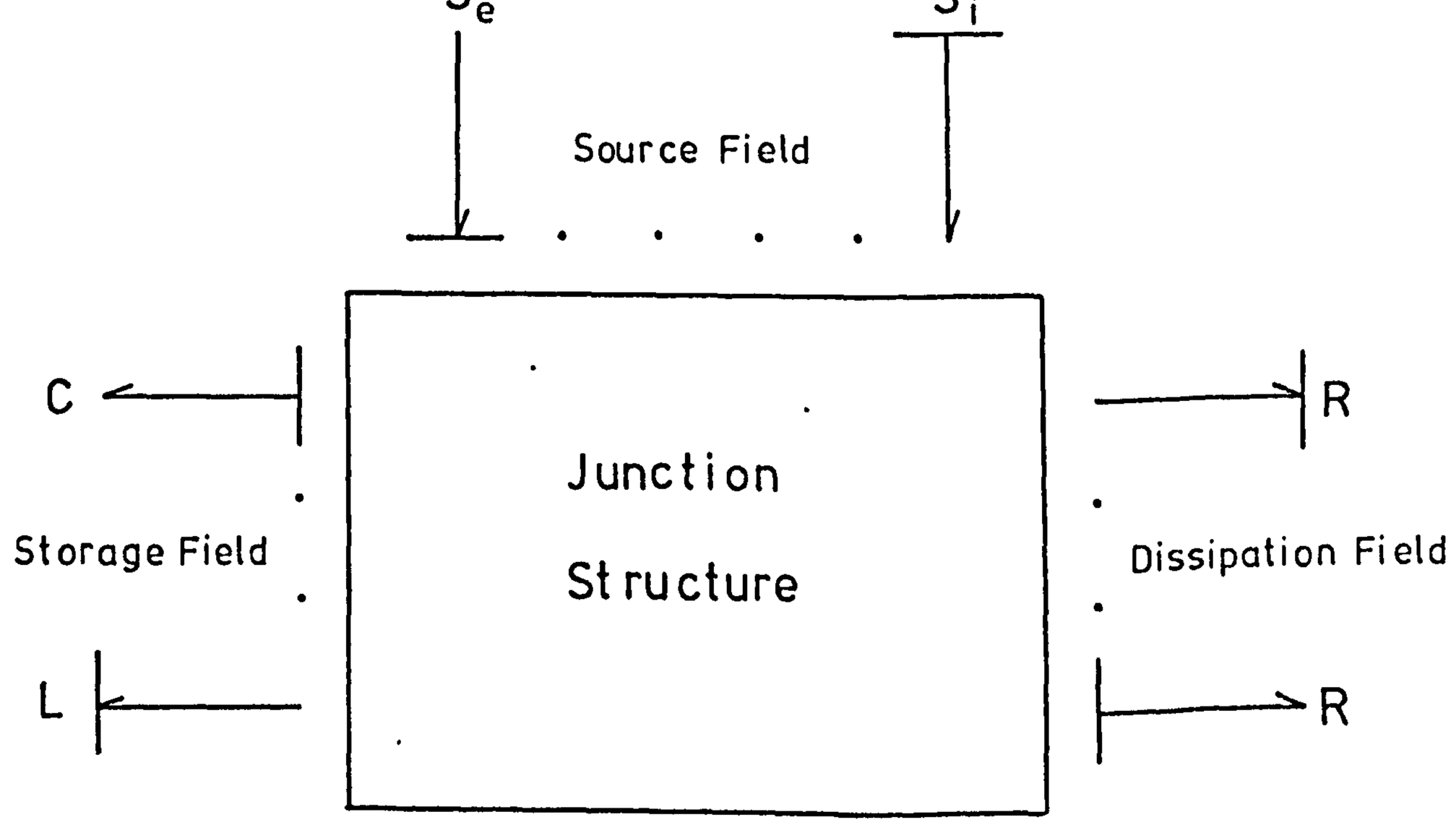

Fig. 2-2 Basic Field of Causal Multiport System

causality will be explained in Section 2.2.4.

2.2.1 Necessary 1-Port Elements

The main characteristic of the 1-port element is that it may be defined in terms of a single pair of energy variables at a port, the effort or emf e(t) and the flow or current i(t), and the time integrals of these quantities,

the flux linkage (or generalized momentum),

$$\lambda(t) = \int^{t} e(t)dt \qquad 2.1$$

and the electric charge (or generalized displacement),

$$q(t) = \int^{t} i(t)dt \qquad 2.2$$

In general the energy U(t) supplied by any 1-port may be written as,

$$U(t) = \int^{t} e(t).i(t)dt \qquad 2.3$$

By considering the nature of energies involved, the 1-ports may be categorized into elements which either dissipate, store or supply energies.

The bond graph representation of the 1-port resistance or dissipative element is shown in Fig. 2-3(a) in which the sign convention implies that the power, e(t).i(t), represents power flowing into the resistance element. For the element to be dissipative it is essential that the curve for the non-linear function $e = F_R(i)$ or $i = F_R^{-1}(e)$ lies in the first or third quadrant as in Fig. 2-3(b) to constrain the static function between e and i such that $e.i \geqslant 0$.

From Eqs. 2.1, 2.2 and 2.3, the energy U(t) may be re-defined as,

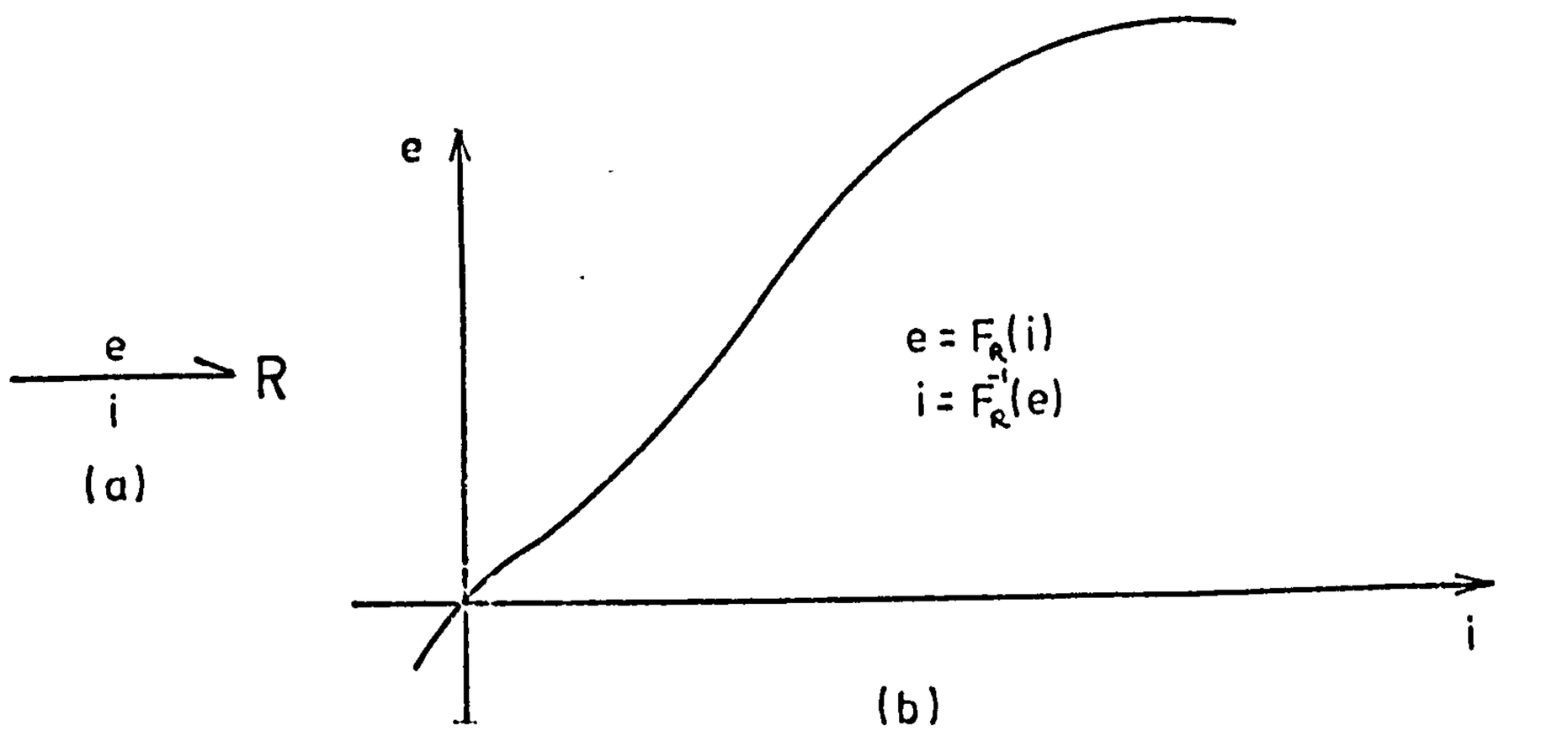

Fig. 2-3 1-Port Resistance Element

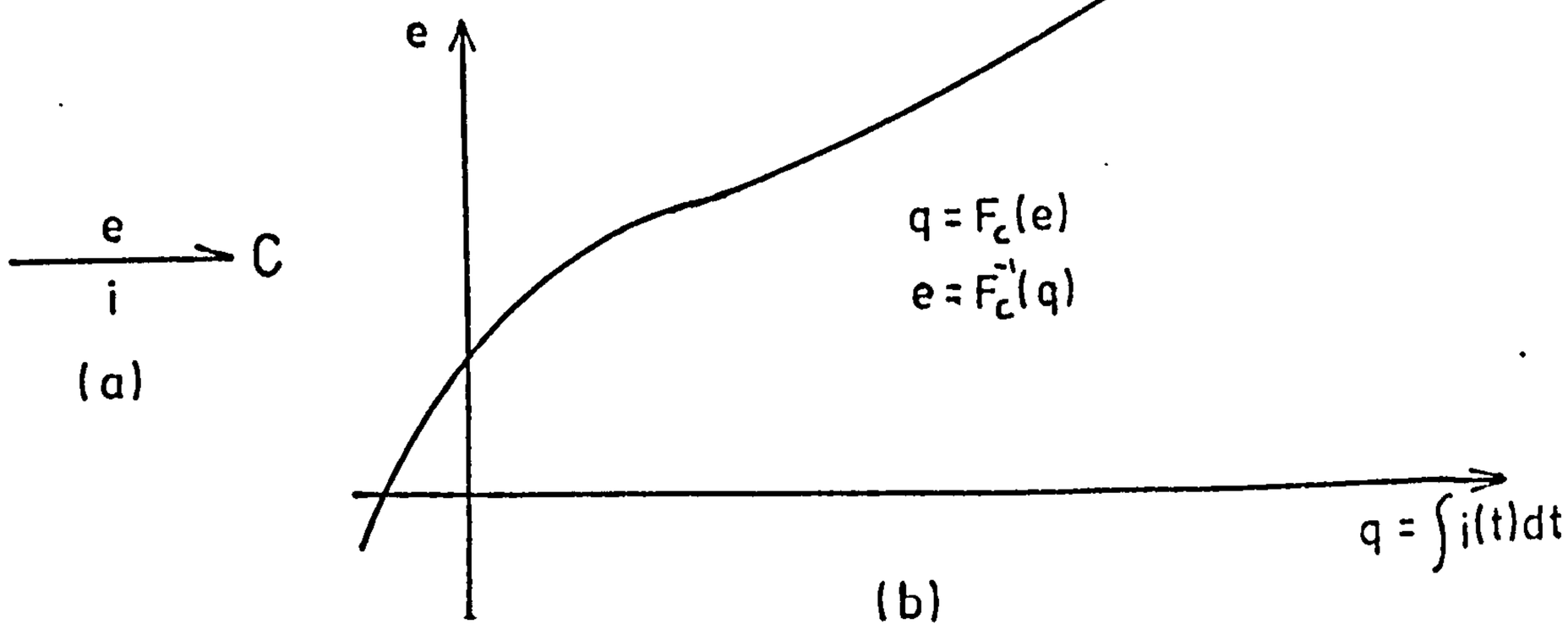

Fig. 2-4 1-Port Capacitance Element

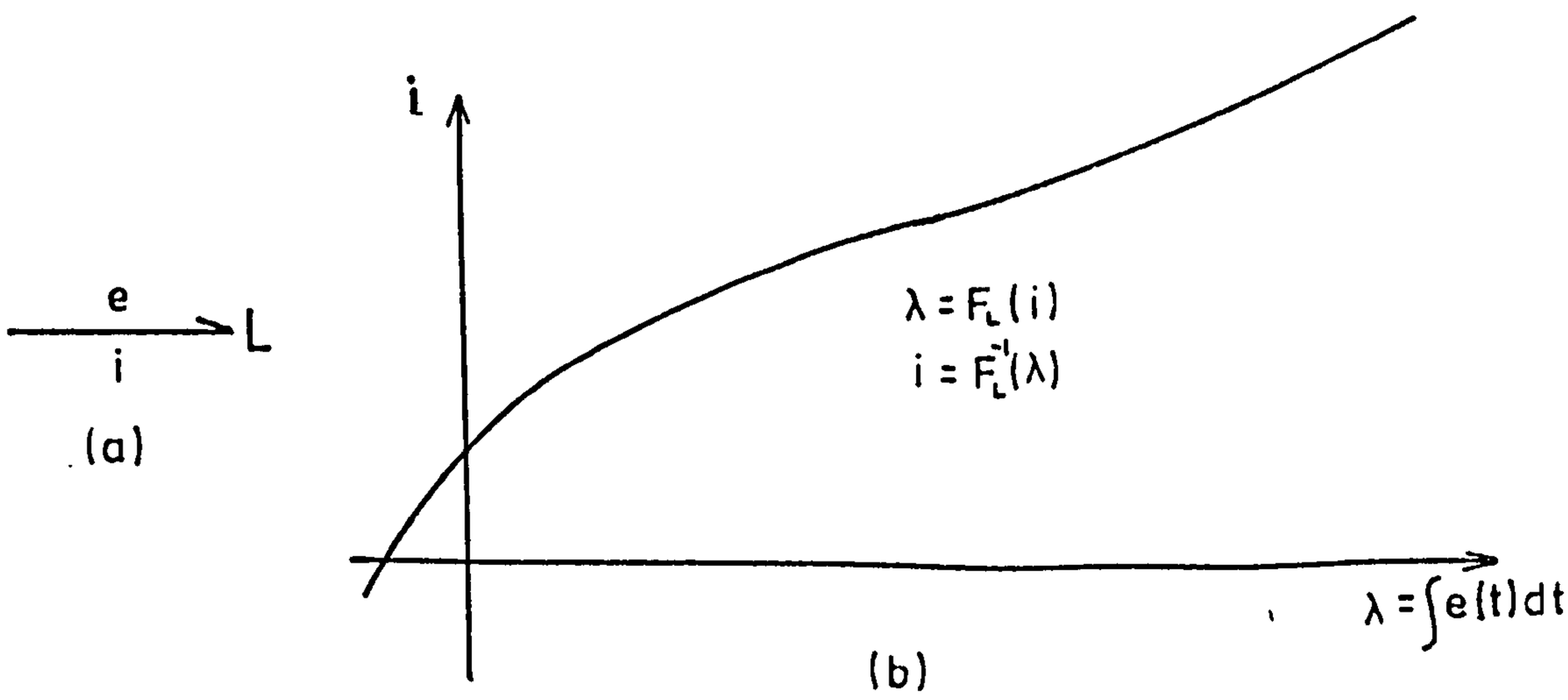

Fig. 2-5 1-Port Inductance Element

$$U(t) = \int^{t} e(t).dq(t) \qquad 2.4$$

and

$$U(t) = \int^{t} i(t).d\lambda(t) \qquad 2.5$$

For the case in which a static relationship exists between e and q, the Eq. 2.4 may be written as,

$$U_q(q) = \int^{q} e(q).dq \qquad 2.6$$

The 1-port element, which exhibit the energy property of having no net change in U_q when either q or e is cycled is called a capacitance element and its representation is shown in Fig. 2-4(a). The most important feature of the capacitance element is the existance of a static relationship between e and q. The actual form of the relation depends upon the integration constant set by the initial condition of q.

Similarly for the case in which a static relationship exists between i and λ, the Eqn. 2.5 may be written as,

$$U_p(\lambda) = \int^{\lambda} i(\lambda)d\lambda \qquad 2.7$$

resulting in the introduction of another conservative element whose storage energy depends on λ (or i) with no set change of U_p involved if either λ or i is cycled. This element, termed as an inductance element has an implied initial condition constraint in the relationship between i and λ. The bond graph representation is shown in Fig. 2-5(a).

The last two 1-port elements to be defined are the effort and flow sources. These sources are assumed to

provide an effort or flow as functions of time without regard to the power delivered or absorbed. The power convention is as indicated in Table 2-1 where e.i is power supplied by the source to the system to which it is connected. These ideal sources are capable of infinite power generation. As such real sources may be modelled by these ideal sources and other elements which may account for the internal characteristics of the real sources which prevent infinite power from being supplied.

Table 2-1 gives a summary of the necessary 1-Ports.

2.2.2 Necessary 2-Port Elements

The basic 2-port elements to be introduced in this section are ideal in the sense that they conserve power. The condition for power conservation at the two ports considered is,

$$e_1(t).i_1(t) = e_2(t).i_2(t) \qquad 2.8$$

One element which satisfied Eq. 2.8 is the ideal transformer. The characteristic of the 2-port transformer is:

$$\begin{bmatrix} e_1 \\ i_1 \end{bmatrix} = \left[\begin{array}{c|c} m & \\ \hline & \frac{1}{m} \end{array}\right] \cdot \begin{bmatrix} e_2 \\ i_2 \end{bmatrix} \qquad 2.9$$

The bond graph of an ideal transformer is shown in Fig. 2-6 together with its electric circuit representation.

Another way of satisfying Eqn. 2.8 is typified by a 2-port element termed as a gyrator which has the following characteristic,

$$\begin{bmatrix} e_1 \\ i_1 \end{bmatrix} = \left[\begin{array}{c|c} & r \\ \hline \frac{1}{r} & \end{array}\right] \cdot \begin{bmatrix} e_2 \\ i_2 \end{bmatrix} \qquad 2.10$$

Table 2-1 Summary of the Necessary 1-Ports

Element	Bond Graph Symbol	Defining Relation	Linear Relation
Effort Source	$S_e \xrightarrow[i]{e}$	$e = S_e(t)$ i arbitrary	$e = S_e(t)$
Flow Source	$S_i \xrightarrow[i]{e}$	$i = S_i(t)$ e arbitrary	$i = S_i(t)$
Resistance	$R \xleftarrow[i]{e}$	$e = F_R(i)$ $i = F_R^{-1}(e)$	$e = R\,i$ $i = G\,e = e/R$
Capacitance	$C \xleftarrow[i]{e}$	$\dot{q} = i$ $q = F_c(e)$ $e = F_c^{-1}(q)$	$q = C\,e$ $e = q/C$
Inductance	$L \xleftarrow[i]{e}$	$\dot{\lambda} = e$ $\lambda = F_L(i)$ $i = F_L^{-1}(\lambda)$	$\lambda = L\,i$ $i = \lambda/L$

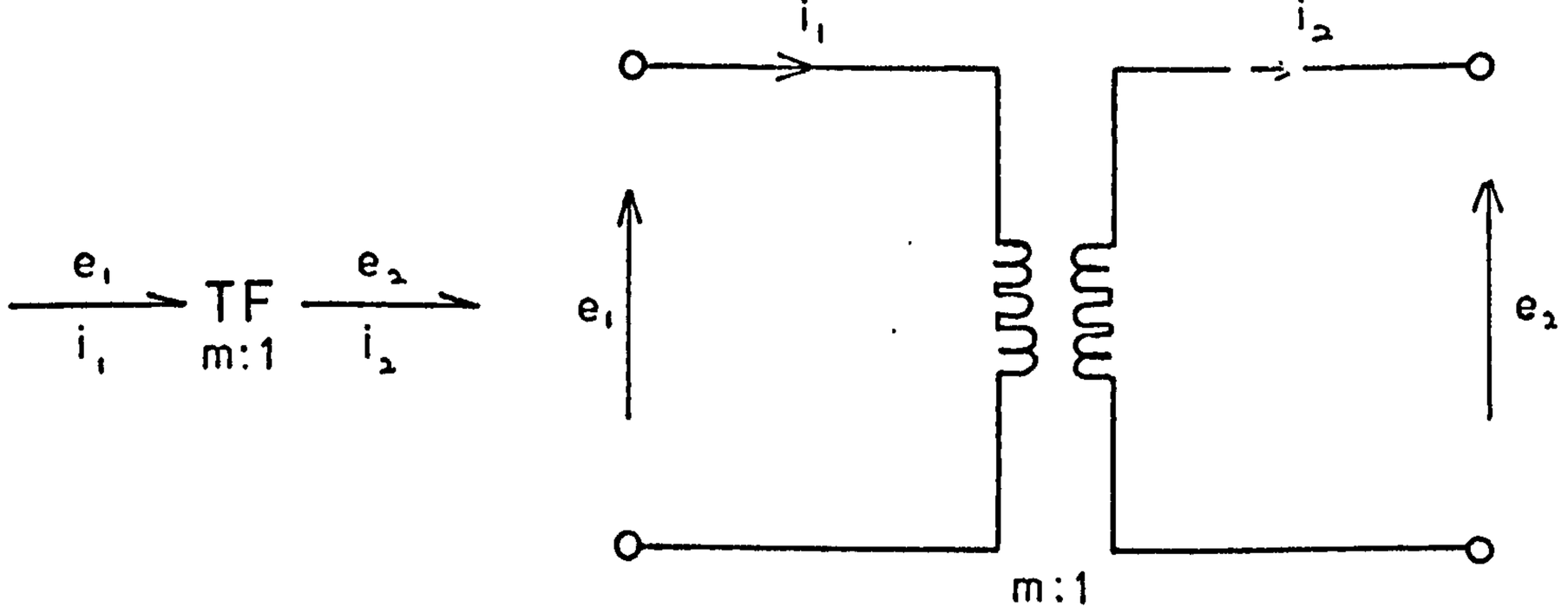

Fig. 2-6 Basic 2-Port Ideal Transformer

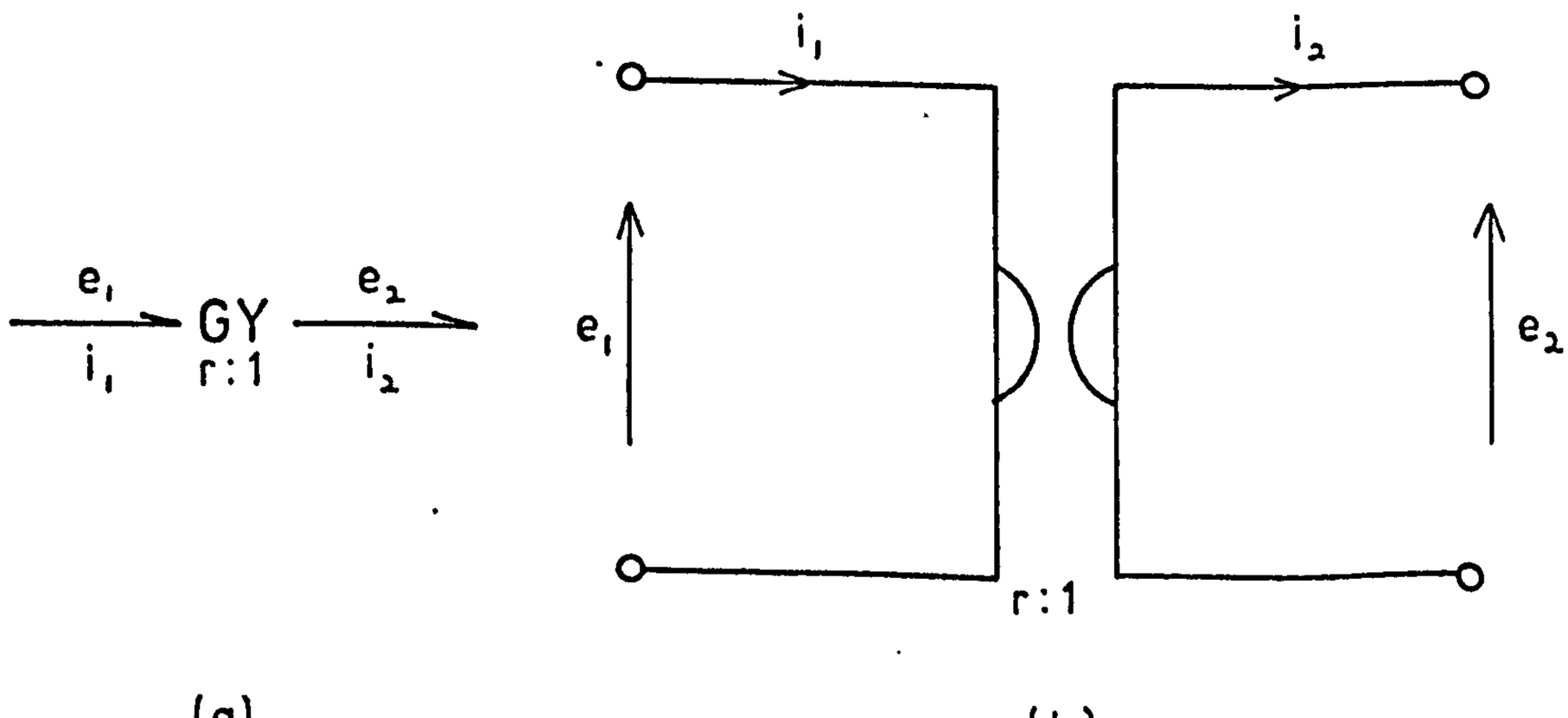

Fig. 2-7 Basic 2-Port Ideal Gyrator

One special feature of the transformer and the gyrator is that power is conserved even when the modulus m of the - TF - or the modulus r of the - GY - is not constant.

The modulated transformer is defined by the symbol:

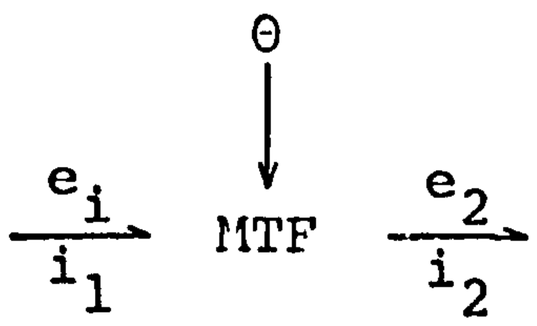

where two power bonds and one signal flow are shown. A modulated transformer is an element like a transformer but in which the modulus may vary as a function of some variable, Θ.

Similarly, a modulated gyrator is defined as an element that satisfies the gyrator relations in Eqn. 2.10, but in which the modulus r is a function of some variable. The symbol for a modulated gyrator is:

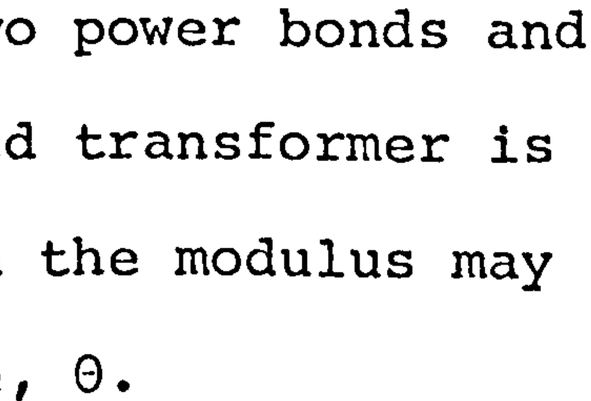

The gyrator has two very interesting properties. A cascade combination of two gyrators is equivalent to a transformer, as shown below

$e_1 = r_1 i_2 \qquad r_2 i_2 = e_3 \qquad e_1 = (r_1/r_2)e_3$

$r_1 i_1 = e_2 \qquad e_2 = r_2 i_3 \qquad (r_1/r_2)i_1 = i_3$

In principle a transformer may be regarded as a cascade combination of two gyrators. Also the gyrator has the ability to transform a non-linear capacitance into a non-linear inductance, and vice versa, thus:

$$\xrightarrow[i_1]{e_1} \underset{r:1}{GY} \xrightarrow[i_2]{e_2} C$$

$$e_1 = ri_2 \qquad \ldots \text{(i)}$$

$$i_1 = e_2/r \qquad \ldots \text{(ii)}$$

$$e_2 = F_c^{-1}(q_2) \qquad \ldots \text{(iii)}$$

Using Eqn. 2.2 with (ii) and (iii)

$$i_1 = \frac{F_c^{-1}(q_2)}{r} = \frac{F_c^{-1}\left(\int^t i_2(t)dt\right)}{r}$$

From (i)

$$\int^t e_1(t)dt = r\int^t i_2(t)dt$$

Thus

$$i_1 = \frac{F_c^{-1}\left(\int e_1(t)dt\right)}{r^2}$$

And from Eqn. 2.1

$$i_1 = \frac{F_c^{-1}(\lambda_1)}{r^2}$$

The last equation agrees with the definition of inductance as given in Table 2-1 but the transformed inductance has a value dependent upon the square of r.

The gyrator with its special property of transforming one type of 1-port storage element to another has similar characteristics to a device, termed as a mutator, introduced by Chua[15] in his paper on non-linear network elements.

A laboratory model of the mutator which is an active 2-port linear network has been built using lumped components.

In the same paper Chua showed that there are three classes of mutators - an L-R mutator, a C-R mutator, and an L-C mutator. An L-R mutator is characterized by the property that if a non-linear resistance with an e-i curve is connected across port two of this element, the resulting one-port network, seen across port one, becomes a non-linear inductance in the sense that it can be characterized by a λ-i curve, or by an i-λ curve which is identical to the original e-i curve. The converse is true and in view of this the mutator may be regarded as a reversible two-port element.

This concept of defining a 2-port element, having the property such that a non-linear resistance may be transformed into a non-linear inductance, or a non-linear capacitance, can be extended for the general case in which the terminal electrical power may be coupled to the electromagnetic or electrostatic field energy through a 2-port element. Since both the field energy and the terminal power share a common intensive variable a simple integral relationship must exist between the field energy and the terminal power.

From Eqns. 2.1 and 2.2 and using the D-operator,

$$\lambda(t) = e(t)/D \qquad 2.11$$

$$q(t) = i(t)/D \qquad 2.12$$

With the condition for conservation of power being satisfied, the characteristic of the element derived from Eqn. 2.11 is:

$$\begin{bmatrix} \lambda_1 \\ i_1 \end{bmatrix} = \left[\begin{array}{c|c} 1/D & \\ \hline & 1 \end{array}\right] \cdot \begin{bmatrix} e_2 \\ i_2 \end{bmatrix} \qquad 2.13$$

This new 2-port element is termed as an inductive mutator and has an important transformation operator which relates the applied power at the terminal, minus resistive losses, to the field energy associated with an inductive coil terminal. The inductive mutator is a reversible two-port element. It has the same causality as the transformer, but unlike the latter it has the special function of mutating the instantaneous port variable while maintaining power conservation. The bond graph structure is:

$$\xrightarrow[i_1]{\lambda_1} \text{IMU} \xrightarrow[i_2]{e_2}$$

The corresponding element in the electrostatic field energy domain is the capacitive mutator whose characteristic may be obtained by satisfying both Eqns. 2.8 and 2.12 thus:

$$\begin{bmatrix} e_1 \\ q_1 \end{bmatrix} = \left[\begin{array}{c|c} 1 & \\ \hline & 1/D \end{array}\right] \cdot \begin{bmatrix} e_2 \\ i_2 \end{bmatrix} \qquad 2.14$$

Consequently, it has a property corresponding to that of the inductive mutator. The capacitive mutator mutates the terminal electrical power into the instantaneous stored electrostatic field energy and vice versa. The bond graph representation is:

$$\xrightarrow[q_1]{e_1} \text{CMU} \xrightarrow[i_2]{e_2}$$

2.2.3 Necessary 3-Port Elements

With only 1-ports and 2-ports available the only bond graph structures which may be constructed are long chains of 2-ports with 1-port terminations. As such it is necessary to have 3-ports as many more configurations are possible since two 3-ports bonded together form a 4-port. The process may be continued indefinitely to form n-ports of any order.

The two necessary 3-ports to be described are ideal in the power conserving sense. The first to be considered is the flow junction. The symbol for this element is a '0' with three bonds emanating from it; thus

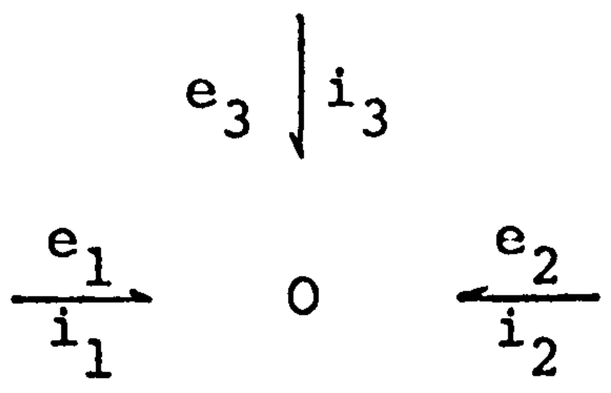

The power-conserving relation is given by:

$$e_1(t).i_1(t) + e_2(t).i_2(t) + e_3(t).i_3(t) = 0 \qquad 2.15$$

As the flow junction is a common effort junction, the relations for the element may be written as:

$$e_1(t) = e_2(t) = e_3(t) \qquad 2.16$$

and from Eqn. 2.15

$$i_1(t) + i_2(t) + i_3(t) = 0 \qquad 2.17$$

The dual of the flow junction is the effort junction represented by the symbol '1' with three attached bonds:

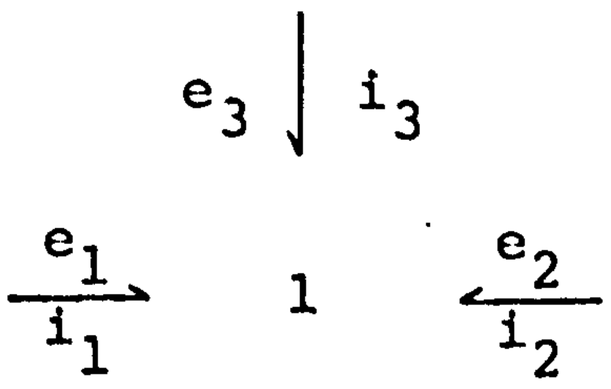

Satisfying the power conservation requirement of Eqn. 2.15 and noting that an effort junction is a common flow junction, the relations for this element are:

$$i_1(t) = i_2(t) = i_3(t) \qquad 2.18$$

and

$$e_1(t) + e_2(t) + e_3(t) = 0 \qquad 2.19$$

The three-port 0- and 1- junctions can be easily generalized by joining them through a number of single bonds to form a n-port junction. A summary of the necessary 2-ports and 3-ports is given in Table 2-2.

2.2.4 Causality for the Necessary Multiports

The effort and flow sources are the most easily discussed from a causal point of view. By definition, a source impresses either an effort or flow time history upon whatever system is connected to it. Thus the only permissible causalities for source elements are:

S_e ——e——| and S_i |——i——

which ensure that the effort, S_e and flow, S_i are the respective inputs into the systems to be connected.

However, the 1-port resistance is normally indifferent to the causality imposed upon it and as long as both the functions $F_R(i)$ and $F_R^{-1}(e)$ exist and are known, there is no reason for preferring one causality over the other.

The characteristic of the 1-port capacitance and 1-port inductance elements are expressed as static relations between e and $q = \int^t idt$ and i and $\lambda = \int^t edt$ respectively. Considering the capacitance element from Table 2-1 the characteristic may be rewritten as:

Table 2-2 Summary of the Necessary 2-Ports and 3-Ports

Element	Bond Graph Symbol	Defining Relation
Transformer	$\xrightarrow[i_1]{e_1}$ TF m:1 $\xrightarrow[i_2]{e_2}$	$e_1 = m e_2$ $m i_1 = i_2$
Gyrator	$\xrightarrow[i_1]{e_1}$ GY r:1 $\xrightarrow[i_2]{e_2}$	$e_1 = r i_2$ $r i_1 = e_2$
Inductive Mutator	$\xrightarrow[i_1]{\lambda_1}$ IMU $\xrightarrow[i_2]{e_2}$	$\lambda_1 = e_2/D$ $i_1 = i_2$
Capacitive Mutator	$\xrightarrow[q_1]{e_1}$ CMU $\xrightarrow[i_2]{e_2}$	$e_1 = e_2$ $q_1 = i_2/D$
Flow Junction	$\xrightarrow[i_1]{e_1}$ 0 $\xleftarrow[i_2]{e_2}$ $e_3 \uparrow i_3$	$e_1 = e_2 = e_3$ $i_1 + i_2 + i_3 = 0$
Effort Junction	$\xrightarrow[i_1]{e_1}$ 1 $\xleftarrow[i_2]{e_2}$ $e_3 \uparrow i_3$	$i_1 = i_2 = i_3$ $e_1 + e_2 + e_3 = 0$

$$e = F_c^{-1}\left(\int^t i\,dt\right) \text{ and } i = \frac{d}{dt}\left[F_c(e)\right] \qquad 2.20$$

in which causality is implied by the form of the equation. When i(t) is the input to the capacitance element, e(t) is given by a static function of the time integral of i(t). However, when e(t) is the input, i(t) is the time derivative of a static function of e(t). This implies that there are two types of causality, the integral causality and derivative causality respectively.

Since the inductance is the dual of the capacitance element, similar effects occur with the two choices of causality. From Table 2-1, the inductance element characteristics are:

$$i = F_L^{-1}\left(\int^t e\,dt\right) \text{ and } e = \frac{d}{dt}\left[F_L^{-1}(i)\right] \qquad 2.21$$

In both cases it is often preferred to use the integral causality in system representation so as to put the system into a form convenient for simulation. The presence of a derivative causality indicates the need for defining an equivalent element before the bond graph is constructed[13].

For the necessary 2-ports, a total of two possibilities for the assignment of causality exist for each element. As soon as one of the e(t)'s or i(t)'s has been assigned as an input to the — TF —, the other e(t) or i(t) is constrained to be an output by Eqn. 2.9. As such the only two possible choices for causality for the transformer are ├— TF —┤ and —┤ TF ├— .

The constraint imposed by Eqn. 2.10 determines the only permissible causal choices for the — GY — as being

—| GY |— and |— GY —| , since either e(t) or i(t) must be assigned as an input. Similarly, considering Eqns. 2.13 and 2.14 and assigning the appropriate input, the two classes of mutators have identical causality to that of the transformer. This is shown in Table 2-4.

The causal properties of 3-port flow junctions and effort junctions are somewhat similar to those of the necessary 2-ports. Although each bond of the 3-port, if considered alone, could have either of the two possible causalities assigned, not all combinations of bond causalities are permitted by the characteristic relations of the element.

For the flow junction, Eqns. 2.16 and 2.17 indicate that all efforts on all bonds are equal and the sum of the flows must be zero. Thus, if on any bond the effort is an input to the flow junction, then all other efforts are determined to be the outputs at all the other bonds. Conversely, if the flows on all bonds but one are inputs to the flow junction, Eqn. 2.17 states that the flow on the remaining bond is determined and must be an output of the junction.

As the effort junction is the dual of the flow junction, the same considerations apply except that the roles of the effort and flow are interchanged and that Eqns. 2.18 and 2.19 are used instead.

Tables 2-3 and 2-4 give the causal forms for the necessary 1-ports, 2-ports and 3-ports.

Table 2-3 Causal Forms for the Necessary 1-Ports

Element	Acausal Graph	Causal Graph	Causal Relation
Effort Source		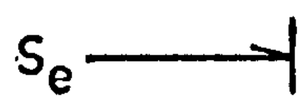	$e(t) = S_e(t)$
Flow Source			$i(t) = S_i(t)$
Resistance	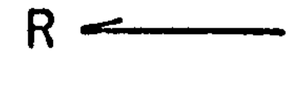	 	$e = F_R(i)$ $i = F_R^{-1}(e)$
Capacitance		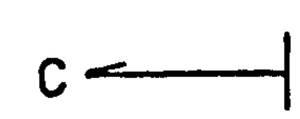 	$e = F_c^{-1}(\int i\,dt)$ $i = \frac{d}{dt}[F_c(e)]$
Inductance		 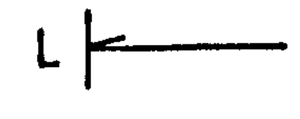	$i = F_L^{-1}(\int e\,dt)$ $e = \frac{d}{dt}[F_L(i)]$

Table 2-4 Causal Forms for the Necessary 2-Ports and 3-Ports

Element	Acausal Graph	Causal Graph	Causal Relation
Transformer		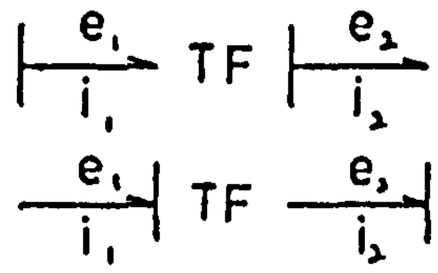	$e_1 = m e_2$ $i_2 = m i_1$ $i_1 = i_2/m$ $e_2 = e_1/m$
Gyrator	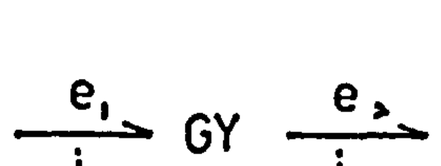	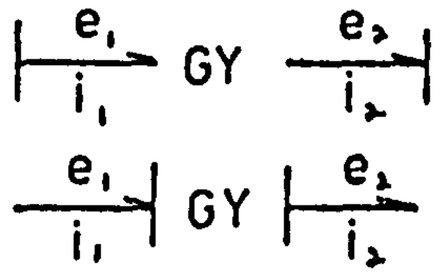	$e_1 = r i_2$ $e_2 = r i_1$ $i_1 = e_2/r$ $i_2 = e_1/r$
Inductive Mutator	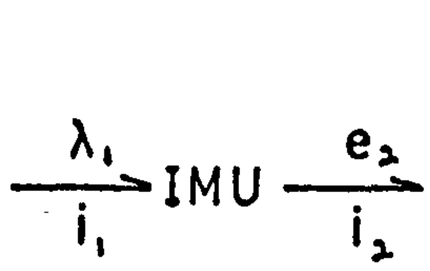	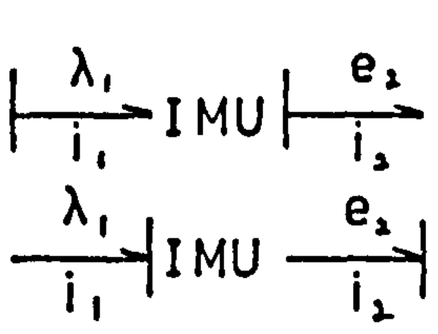	$\lambda_1 = e_2/D$ $i_2 = i_1$ $i_1 = i_2$ $e_2 = D\lambda_1$
Capacitive Mutator	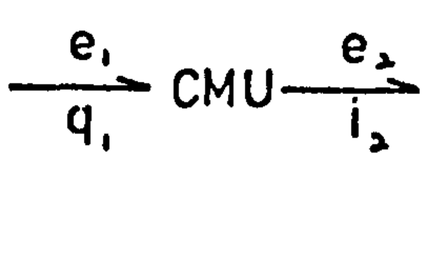	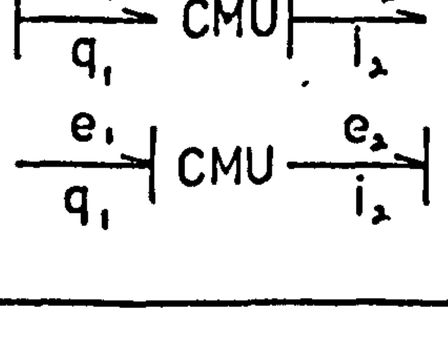	$e_1 = e_2$ $i_2 = Dq_1$ $q_1 = i_2/D$ $e_2 = e_1$
Flow Junction		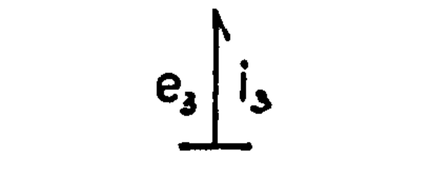	$e_3 = e_1$ $e_3 = e_1$ $i_1 = -(-i_2 + i_3)$
Effort Junction	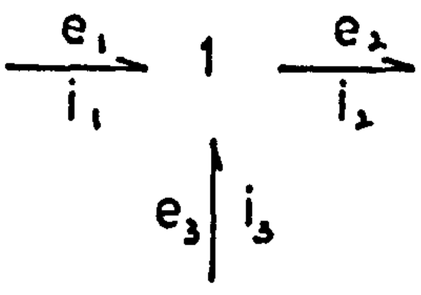	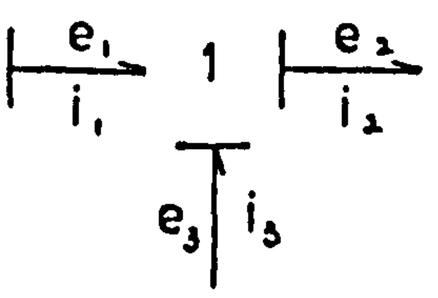	$i_2 = i_1$ $i_3 = i_1$ $e_1 = -(-e_2 + e_3)$

2.3 Bond Graph Computation Structures[13]

A principal motivation for generating a bond graph computation structure for a physical system stems from a desire to conduct a simulation of the transient response. In order to derive a computation structure to correspond to a given bond graph it is necessary to augment the bond graph, and substitute signals and signal relations for the bonds and multiports, respectively. Table 2-5 presents ways in which augment bond graph elements may be replaced by signal relations[13].

Similarly ideal 2-ports and n-ports may be represented by the computation structure as shown in Table 2-6. In the non-linear case, the transformer and gyrator two-ports may have the moduli m and r as functions of the state.

2.3.1 Structure for Electric Circuit

The conversion of a bond graph to a computation structure, shown as an example in Fig. 2-8, involves the following steps[13]:

(i) augment the bond graph;

(ii) draw pairs of directed effort-flow signal pairs to replace the bonds;

(iii) substitute the equivalent signal relations for the bond graph elements as indicated in Tables 2-5 and 2-6.

An electrical circuit example is shown in Fig. 2-8 in which the circuit is first converted to an augment bond graph, (i); then the bond graph is converted to a computation structure. There is no necessity to write any equation.

Table 2-5 Computation Structures for the Necessary 1-Ports

Causal Element	Non-Linear Form	Linear Form	Causal Relation
S_e ⟶|	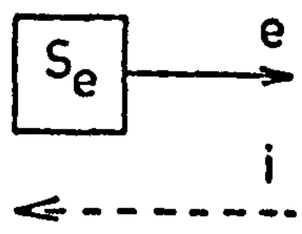	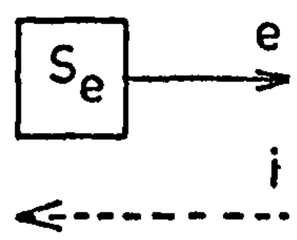	$e(t) = S_e(t)$
S_i |⟶	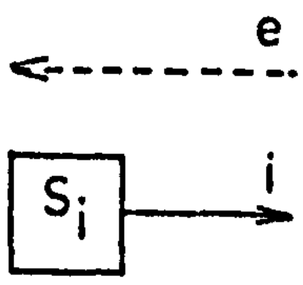	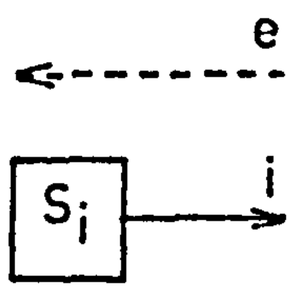	$i(t) = S_i(t)$
R ⟵|	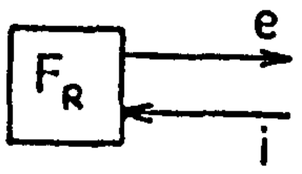	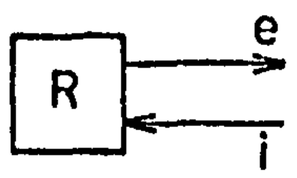	$e = F_R(i)$
R |⟵	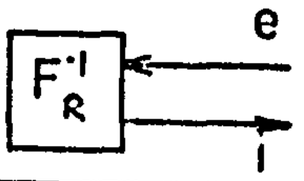	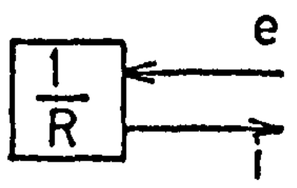	$i = F_R^{-1}(e)$
C ⟵|	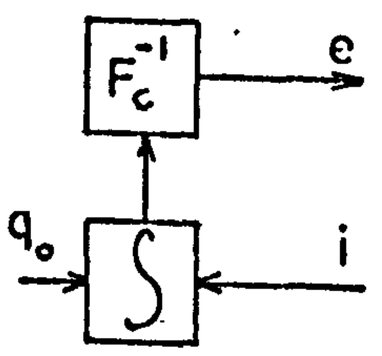	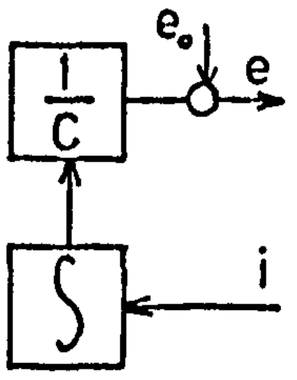	$e = F_c^{-1}(\int_{-\infty}^{t} i\,dt)$
L |⟵	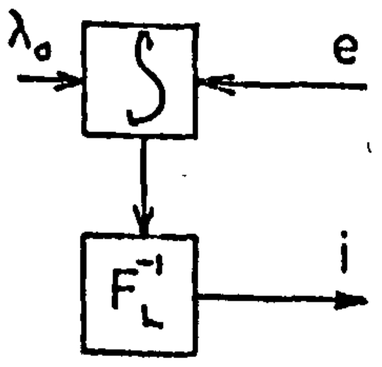	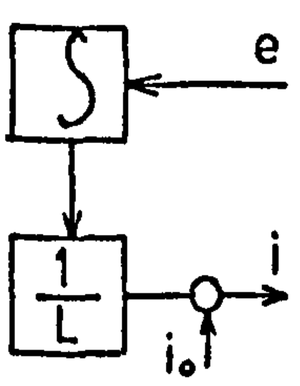	$i = F_L^{-1}(\int_{-\infty}^{t} e\,dt)$

Table 2-6 Computation Structures for the Necessary 2-Ports and n-Ports

Causal Element	Non-Linear Form	Linear Form	Causal Relation
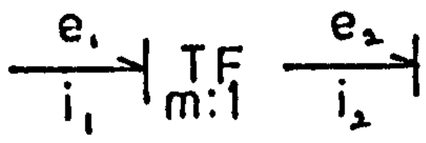	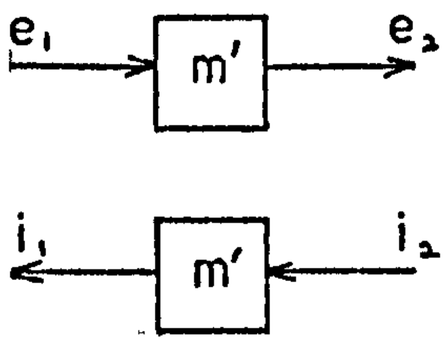	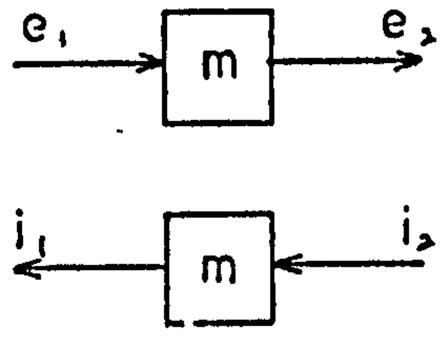	$e_1 = m e_2$ $i_2 = m i_1$
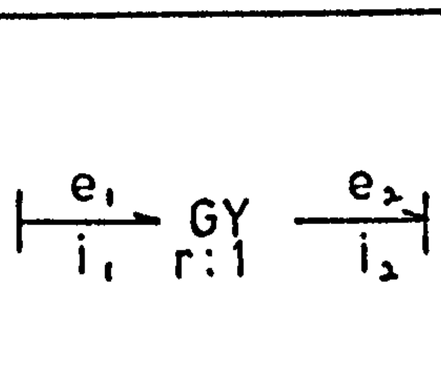	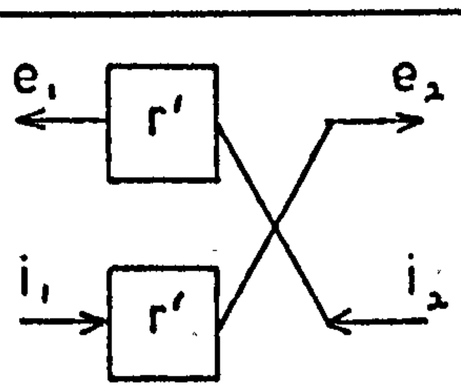	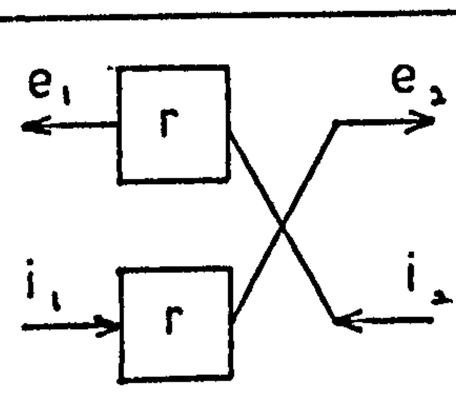	$e_1 = r i_2$ $e_2 = r i_1$
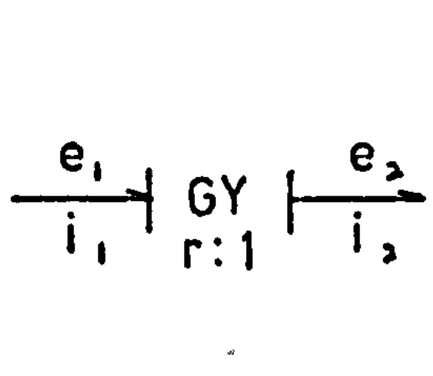	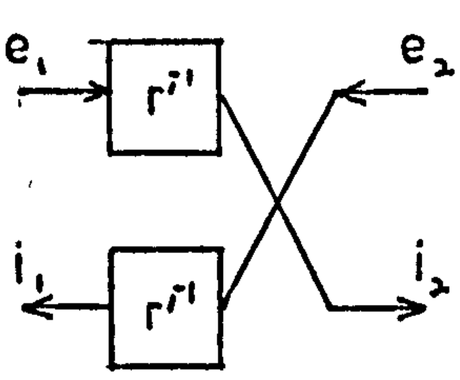	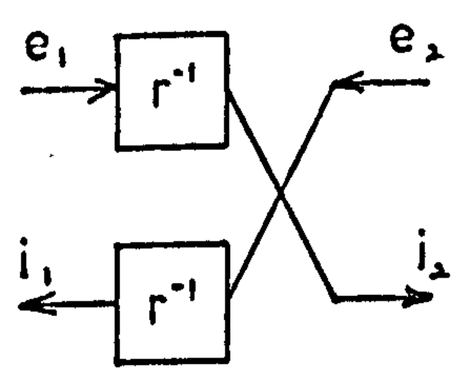	$i_1 = e_2 / r$ $i_2 = e_1 / r$
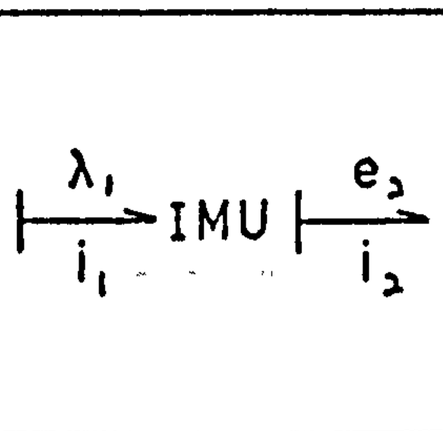	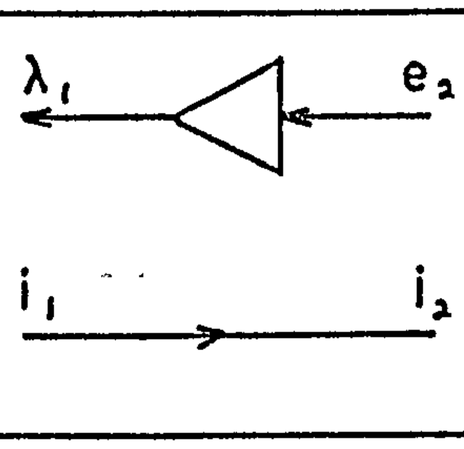	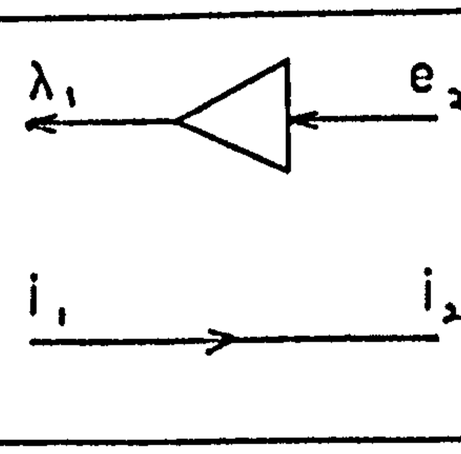	$\lambda_1 = e_2 / D$ $i_2 = i_1$
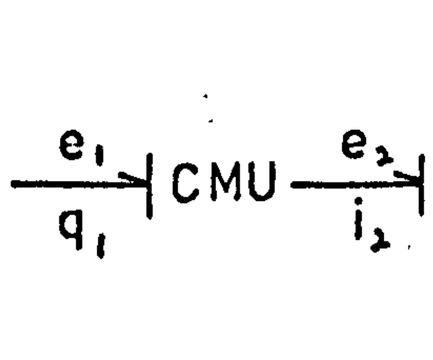	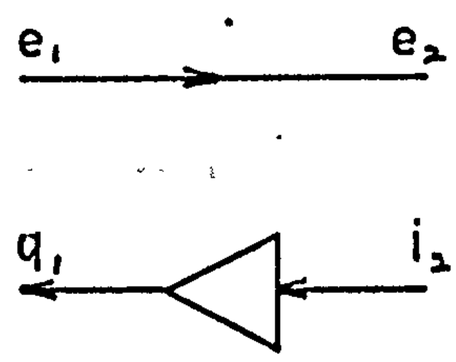	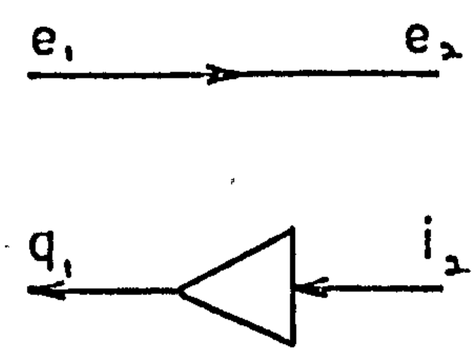	$e_2 = e_1$ $q_1 = i_2 / D$
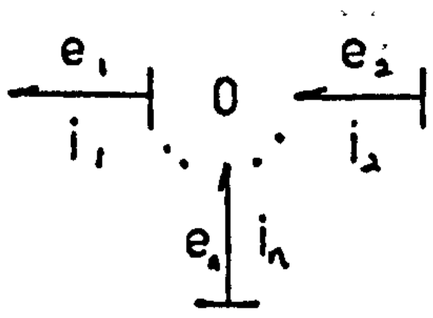	No Non-Linear Form	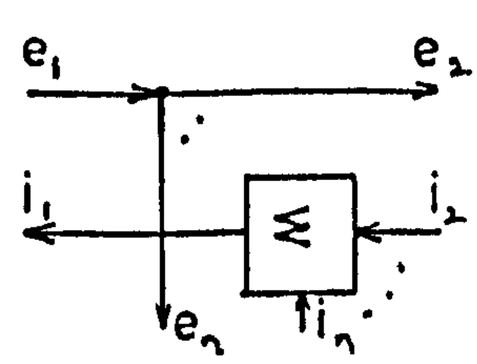	$e_2 = e_1$ $e_n = e_1$ $i_1 = -\sum_{k=2}^{n} i_k$
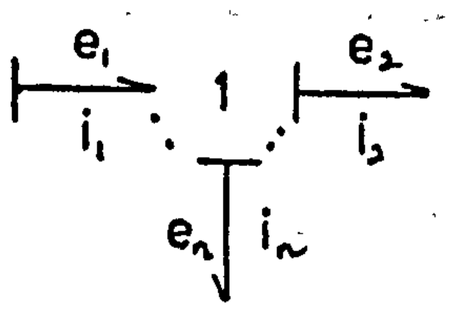	No Non-Linear Form	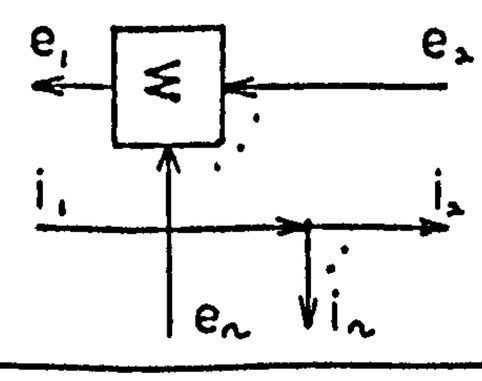	$e_1 = -\sum_{k=2}^{n} e_k$ $i_2 = i_1$ $i_n = i_1$

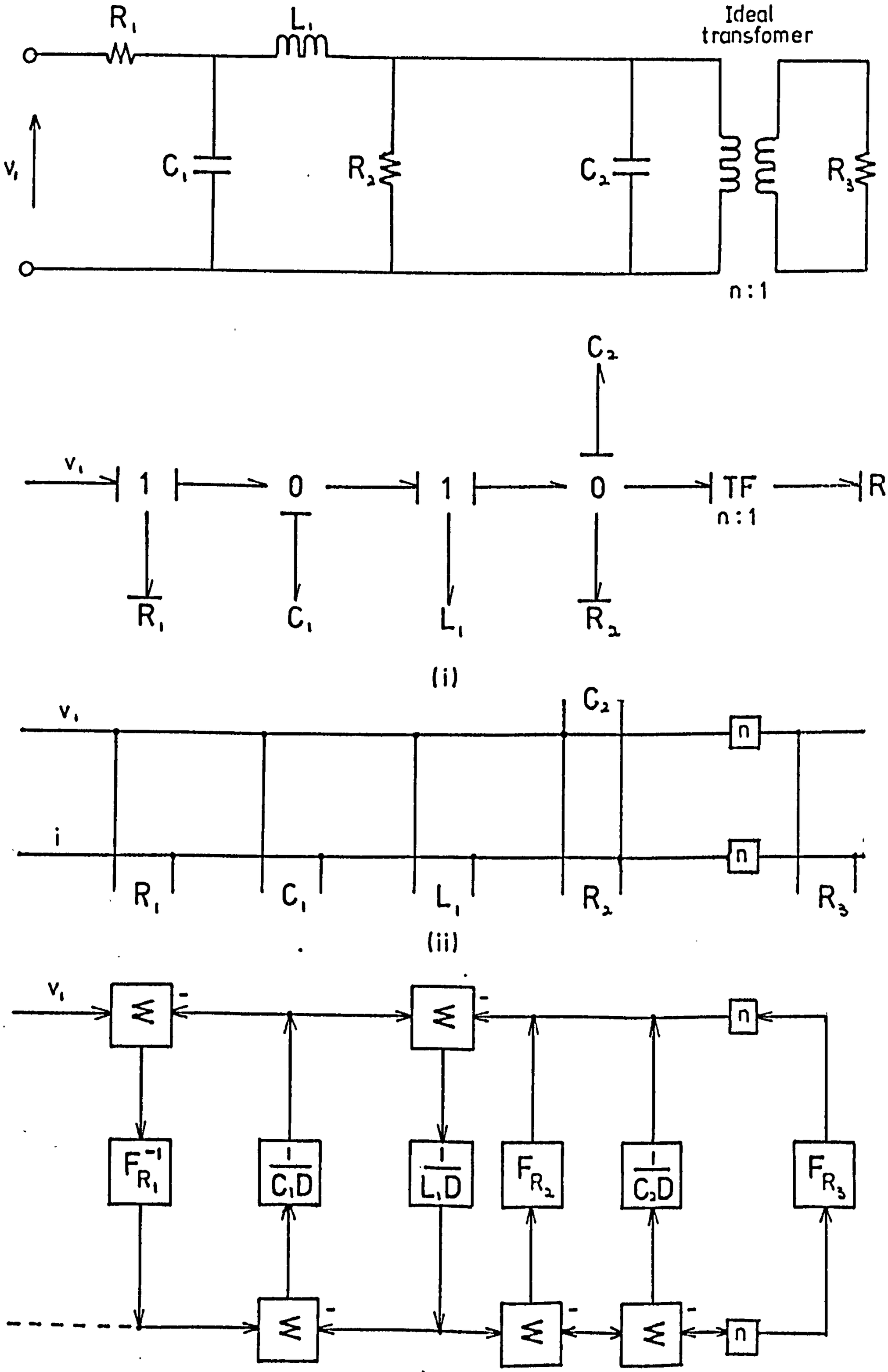

Fig. 2-8 Conversion of a Bond Graph into a Computation Structure

2.3.2 Non-linear Inductance

One of the limitations in representing non-linear inductance by the standard power variables, voltage and current, is that graphical representation of the field systems by the usual equivalent circuit methods is rather complicated. The bond graph approach enables the instantaneous field energy distribution and the terminal power to be linked by an ideal 2-port element and thus making it possible to be represented by an unambiguous elegantly coded diagram. This structure will represent the field in terms of the flux linkage and the current, which are the electromagnetic energy variables.

For a magnetic system comprising of a single exciting coil of resistance R, as shown in Fig. 2-9, the instantaneous value of the emf e(t) is given by[16]:

$$e = \frac{d\lambda}{dt} \qquad 2.22$$

where λ is the instantaneous value of the flux linkage with the circuit; the sign is positive for increasing flux.

The flux linkage is defined as:

$$\lambda = N\Phi \qquad 2.23$$

where Φ is the flux linking all N turns of the winding; and the magnetomotive force, or mmf of the coil has the following relationship with the current:

$$\mathfrak{F} = Ni \qquad 2.24$$

The differential energy stored in the magnetic field supplied by the electrical source in time dt is:

$$dW_{elec} = ei\ dt \qquad 2.25$$

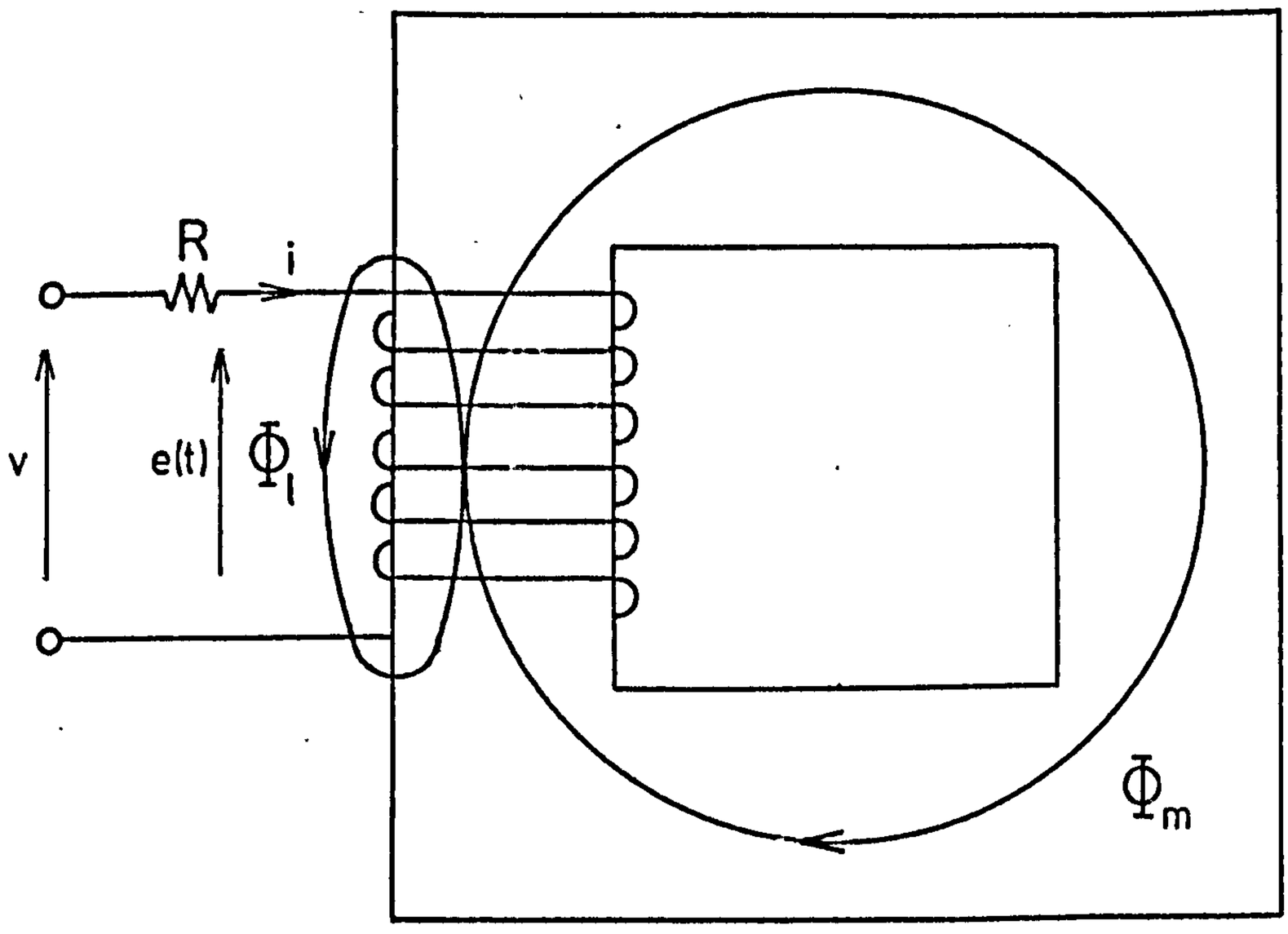

(a)

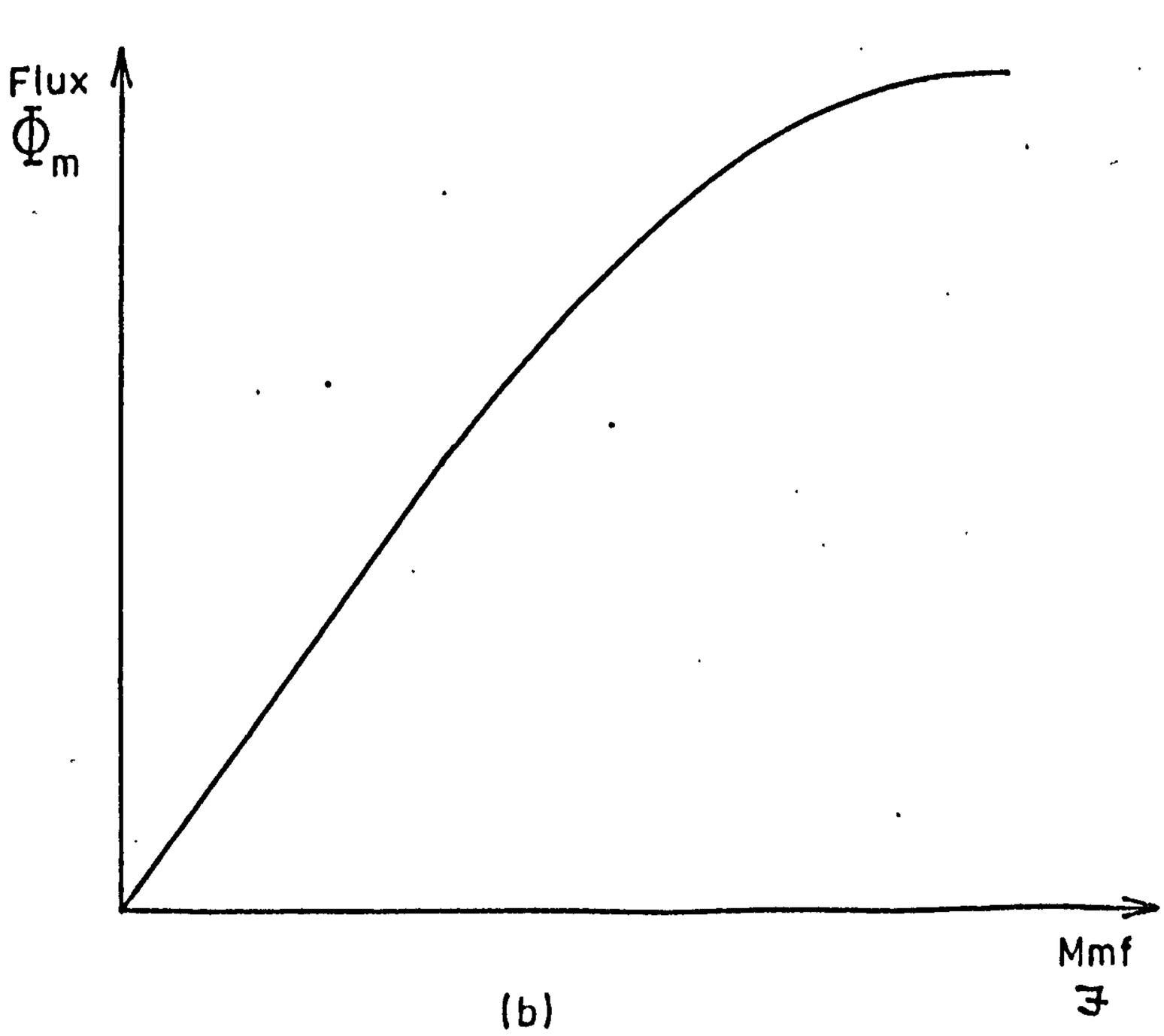

(b)

Fig. 2-9 One-Port Electromagnetic Field Element with Flux-Mmf Characteristic

and from Eqns. 2.22, 2.23 and 2.24, the energy equation may be written as:

$$dW_{elec} = id\lambda$$
$$= Nid\Phi = \mathfrak{F}d\Phi \qquad 2.26$$

A change in the flux, due to either a change in the excitation or by mechanical motion or both, results in a flow of energy in the circuit expressed by Eqn. 2.26.

For the case in Fig. 2-9(a), the mechanical structure is rigid and as such the electrical energy supplied to the field must ideally equal the energy stored in the field. Thus:

$$dW_{fld} = dW_{elec} = id\lambda \qquad 2.27$$

and the total energy stored in the field may be expressed in terms of the magnetic variables as:

$$W_{fld} = \int_{\lambda}^{\lambda_2} i(\lambda)d\lambda = \int_{\Phi}^{\Phi} \mathfrak{F}(\Phi)d\Phi \qquad 2.28$$

As indicated by Eqn. 2.28, the mmf $\mathfrak{F}(\Phi)$ is a function of the flux Φ and can be determined from the coil geometry, the magnetic path and properties of the core material of the coil. The relationship of the flux and mmf is governed by the characteristic shown in Fig. 2-9(b). The slope of this curve may be expressed by the non-linear variable $\mathcal{R}'$, called the reluctance:

$$\mathcal{R}'^{-1} = \frac{\Delta\Phi}{\Delta\mathfrak{F}} \qquad 2.29$$

The introduction of the variable reluctance, $\mathcal{R}'$, enables the non-linear relationship of the flux and mmf to be determined easily. Eqn. 2.29 may also be expressed by a simple algebraic equation thus:

$$\Phi = \frac{\mathcal{F}}{\mathcal{R}} \qquad 2.30$$

where $\mathcal{R}$ is the slope at a given operating point on the flux-mmf curve. Eqn. 2.30 is a short-hand notation of Eqn. 2.29, with total non-linear characteristic included. As such substituting Eqns. 2.23 and 2.24 into Eqn. 2.30 gives the flux linkage as:

$$\lambda = \frac{N^2 i}{\mathcal{R}} \qquad 2.31$$

The electromagnetic fields in power system studies are complicated by the presence of leakage fluxes, which link the coil but do not traverse the main core. Although these fluxes contribute significant effects on the resultant dynamic behaviours of power system components, the linear characteristic[16] of these fluxes can be exploited and used to good advantage for organising the basic framework of the computation structures.

As indicated in Fig. 2-9(a), the total flux of the magnetic system considered, consists of leakage flux, Φ_ℓ, whose path is through the air and the main flux, Φ_m, which occurs in the ferro-magnetic material making up the core. These fluxes are expressed by:

$$\Phi_m = \frac{\mathcal{F}}{\mathcal{R}_m} = \frac{Ni}{\mathcal{R}_m} \qquad 2.32$$

and

$$\Phi_\ell = \frac{\mathcal{F}}{\mathcal{R}_\ell} = \frac{Ni}{\mathcal{R}_\ell} \qquad 2.33$$

where $\mathcal{R}_m$ is the effective reluctance of the path through the main core and $\mathcal{R}_\ell$ is the effective reluctance of the path through the surrounding air.

The total flux linkage in the coil is:

$$\lambda_t = N\Phi_m + N\Phi_\ell$$

$$= \lambda_m + \lambda_\ell$$

$$= \frac{N^2 i}{\mathcal{R}_m} + \frac{N^2 i}{\mathcal{R}_\ell} \qquad 2.34$$

From Eqn. 2.22 the total flux linkage may also be expressed by:

$$\lambda_t = \int^t e(t)dt \qquad 2.35$$

Since the leakage flux is assumed linear, a leakage inductance constant, L_ℓ, may be defined as:

$$L_\ell = \frac{\lambda_\ell}{i} = \frac{N^2}{\mathcal{R}_\ell} \qquad 2.36$$

The bond graph incorporating Eqns. 2.23 and 2.24, for the main flux and resultant mmf respectively, and Eqn. 2.32 may be represented by:

$$\xrightarrow[i]{\lambda_m} \underset{N:1}{TF} \xrightarrow{\Phi_m} \mathcal{R}_m$$

where $\mathcal{R}_m$, the non-linear reluctance of the path through the main core is defined by the flux-mmf characteristic of Fig. 2-9(b). The equation for this relationship is:

$$\begin{bmatrix} \lambda_m \\ i \end{bmatrix} = \left[\begin{array}{c|c} N & \\ \hline & 1/N \end{array}\right] \cdot \begin{bmatrix} \Phi_m \\ \mathcal{F} \end{bmatrix} \qquad 2.37$$

Taking into account the leakage flux and the coil resistance, R, the bond graph of the complete non-linear magnetic system using the inductive mutator previously

defined, is shown in Fig. 2.10(a). It is evident that the inductive mutator performs the important role of linking the power at the terminal to the instantaneous electromagnetic field energy residing in the coil. Without the introduction of this device it would not be possible to represent the non-linear inductance in the easily comprehensible diagram of Fig. 2-10(a). The computation structure derived from the bond graph is accompanied in Fig. 2-10(b).

2.3.3 Non-linear Capacitance

If it is desired to build a capacitor of which the capacitance can be calculated accurately, the stray field occurring at the edges must be overcome. Usually a guard ring whose potential is maintained at the same value as that of the central electrode, but from a separate source can provide a uniform flux density over the central electrode and as such a linear equation may be used to calculate the capacitance.

A non-linear capacitance may be considered to have two types of energy fields, namely the uniform field occurring in the immediate vicinity of the electrodes and the complex stray field whose pattern is defined by a number of factors including the geometric configuration and size of the electrodes, the dielectric material and the surrounding fields.

The purpose of this section is to represent a simple capacitance energy system consisting of two parallel electrodes in bond graph notations. The stray field can be characterised by a non-linear function, the evaluation of which shall not be pursued here.

The capacitor to be considered has two equal

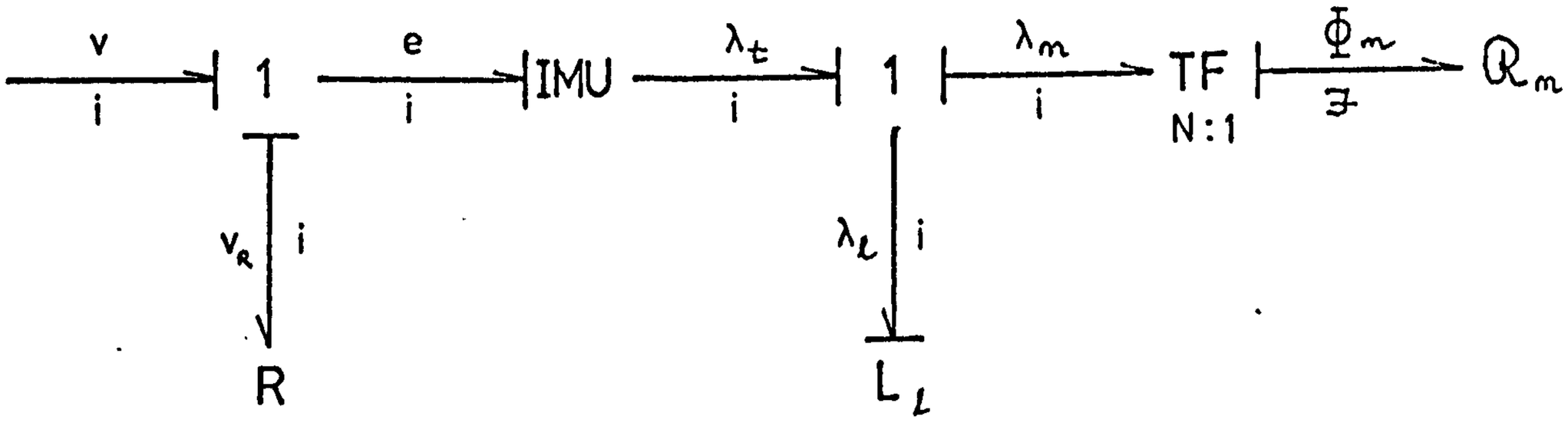

(a)

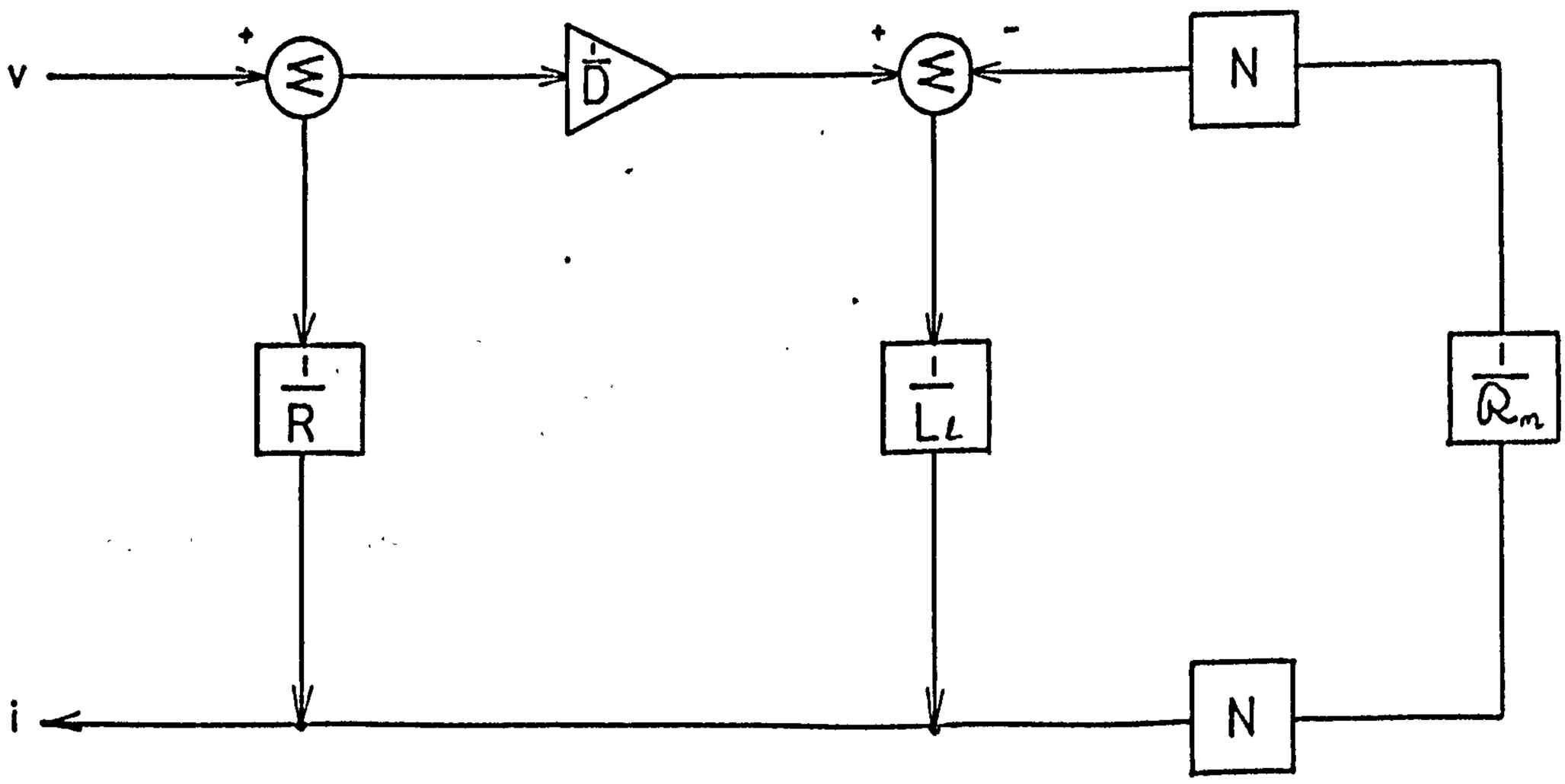

(b)

Fig. 2-10 Bond Graph and Computation Structure for a Non-Linear Inductance

conducting electrodes, placed parallel to one another at a distance, D, bounding a dielectric of permittivity K as shown in Fig. 2-11(a). Each electrode with an area A carries Q quantity of charge.

Then the electromotive force or emf produced by the uniform energy field between the electrode is[17]:

$$e = \int_{o}^{D} \frac{4\pi Q}{KA}\, dx$$

$$= \frac{4\pi QD}{KA}$$

$$= \frac{Q}{C} \qquad 2.38$$

where $C = \frac{KA}{4\pi D}$ is the linear capacitance due to the uniform field between the electrodes.

Taking the stray field into consideration, the emf, e, is partly generated by this field and is given by:

$$e = \int \frac{4\pi Q_s}{K_s A_s}\, dy$$

$$= F_c^{-1} \left(\int^{t} i_s dt\right) \qquad 2.39$$

where i_s is the current associated with the charge Q_s. This equation represents the effect caused by the stray field. The integration limits; the permittivity, K_s; the effective electrode area, A_s, as well as the stray charge, Q_s, cannot be easily determined and thus the evaluation of the stray capacitance is difficult to attain.

In an ideal capacitor, when the electrodes have accumulated a quantity of charge, $(Q + Q_s)$, determined by

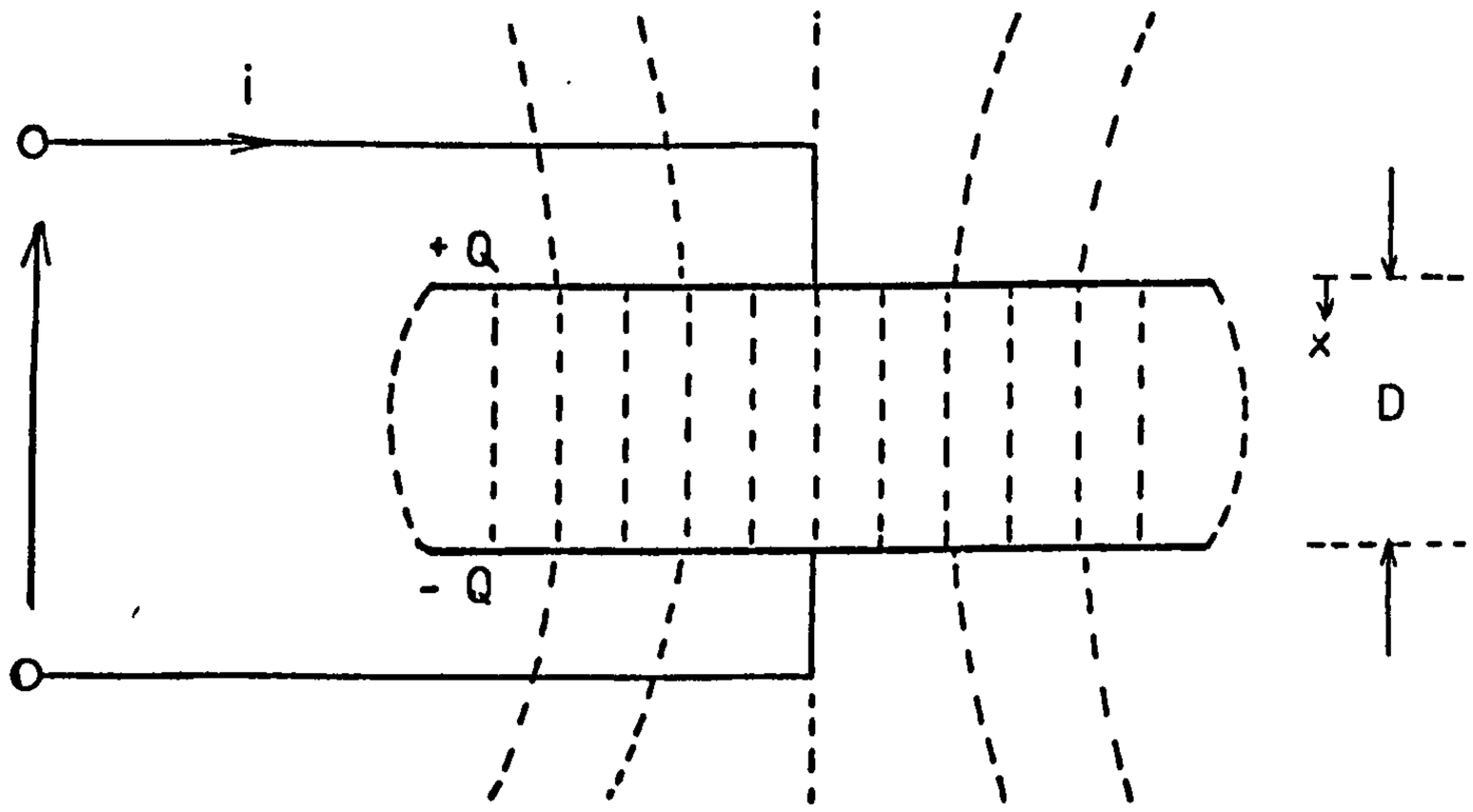

(a)

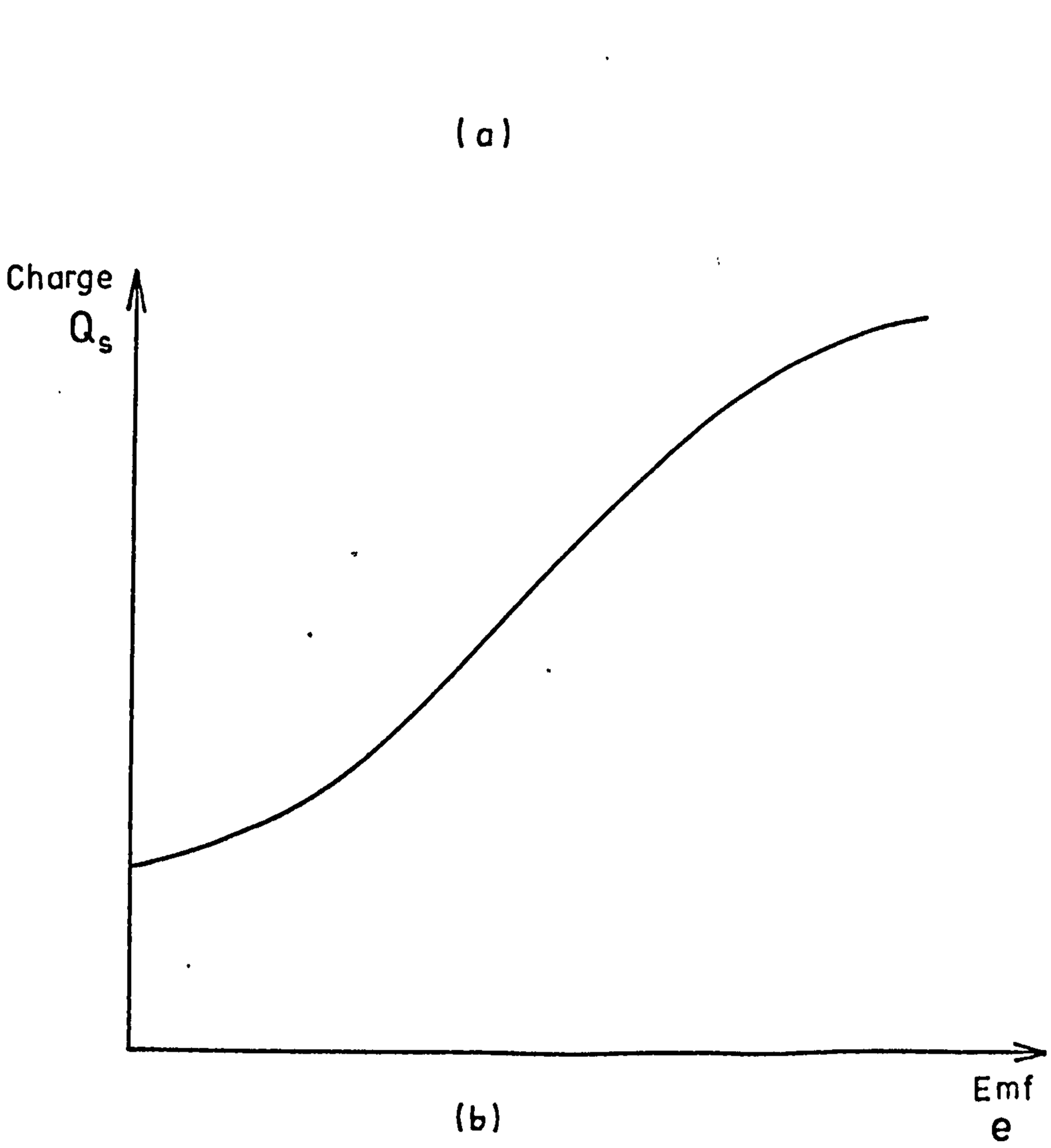

(b)

Fig. 2-11 One-Port Electrostatic Field Element with Charge-Emf Characteristic

the emf, e, the current ceases to flow. With all practical dielectric a small current continues to flow, but dies away gradually over a long period of time. In the bond graph notation of Fig. 2-12, this phenomenon is represented by the non-linear resistance, R. The function,

$F_c^{-1}\left(\int^t i_s dt\right)$, generated by the stray field is shown in the same figure as $\mathcal{C}_s$.

For the case of the non-linear capacitance, the capacitive mutator bridges the terminal power with the instantaneous electrostatic field energy in the bond graph of Fig. 2-12(a).

2.4 Analysis of Multiport Energy Systems

In this section a general method of analysis of multiport electromagnetic and electrostatic energy systems will be presented. Computation structures for these n-port systems can be easily derived using the technique explained in previous sections. The bond graph unique property of organising system equations will be deployed fully and consequently the analysis and simulation can be easily handled by a digital computer.

Previous work in the simulation of multiport electromagnetic system, such as the rotating machine and the power transformer by digital computers, involve the handling of large inductance matrix which has to be inverted at every integration steps[18,19]. In the analysis of a saturated synchronous machine, a modified and complicated inductance matrix has to be introduced and similar matrix inversions are necessary[20].

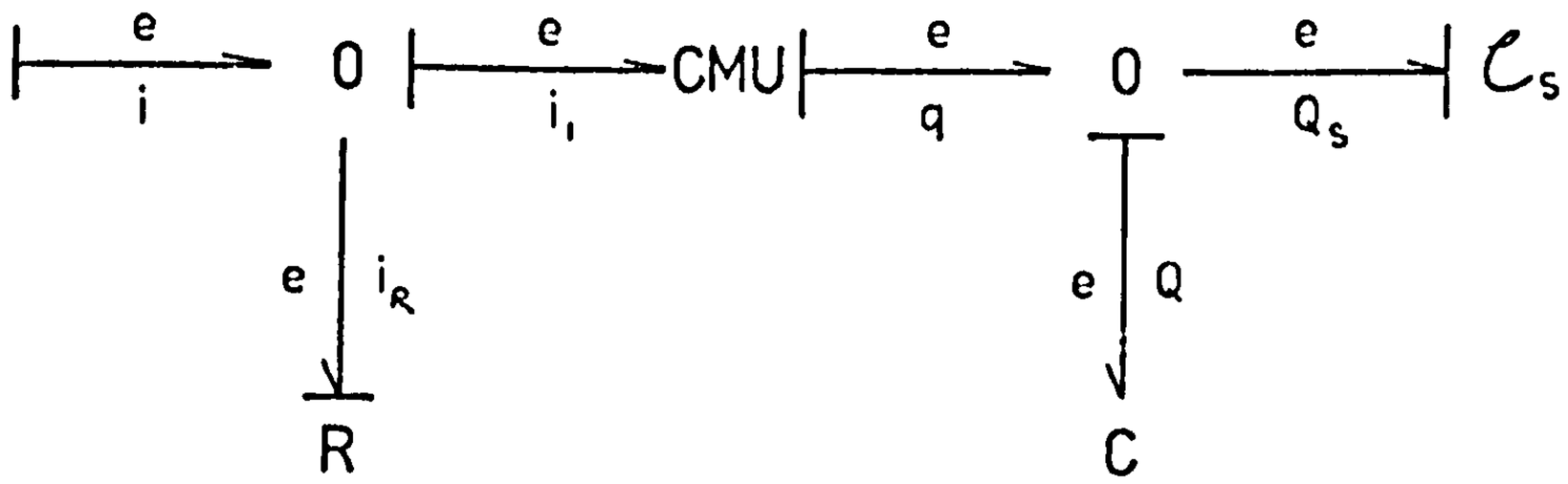

(a)

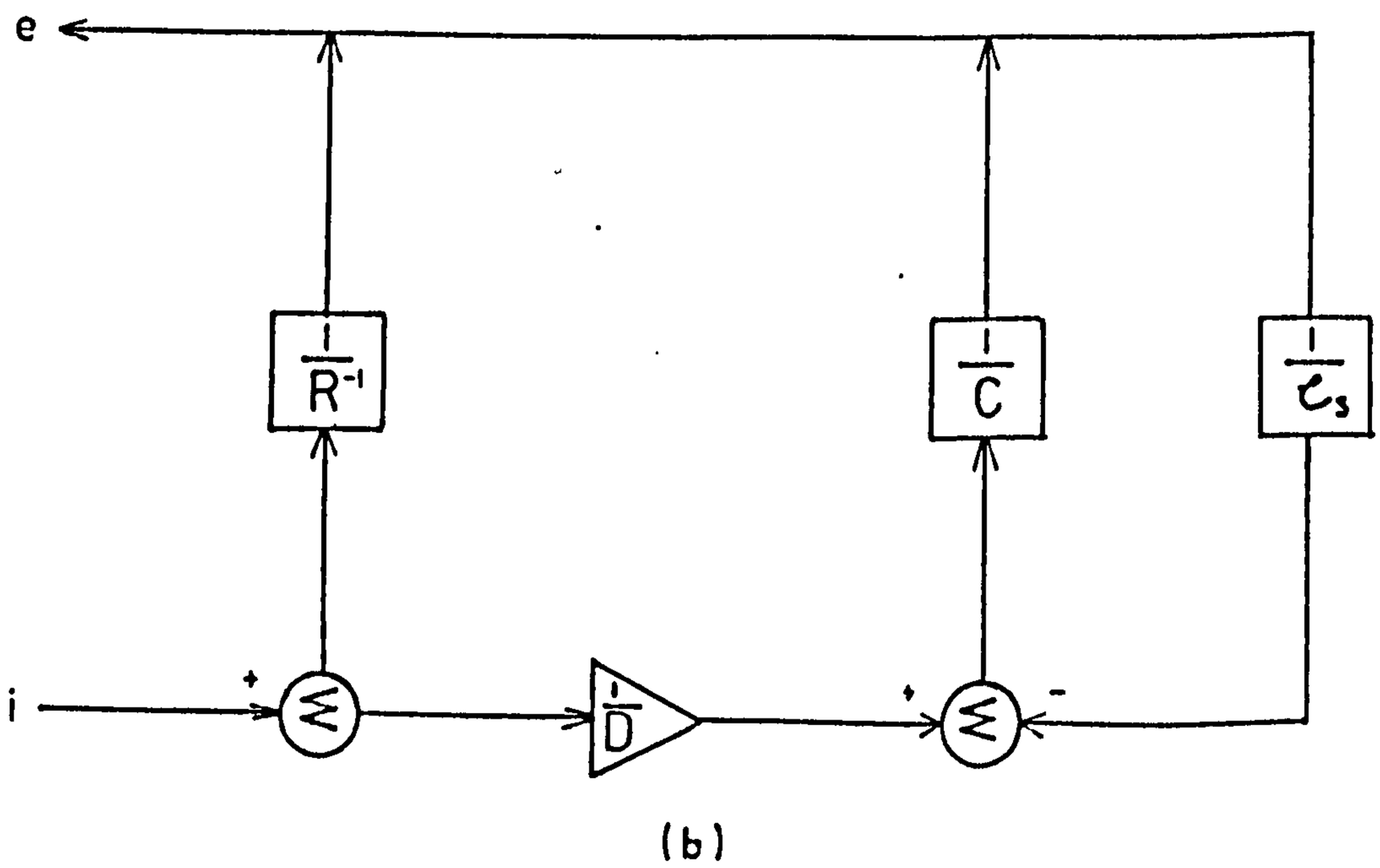

(b)

Fig. 2-12 Bond Graph and Computation Structure for a Non-Linear Capacitance

The approach using the bond graph computation structure avoids the necessity of inverting the matrix and provides a unified method for both linear and non-linear cases. As such saturated and unsaturated rotating machine can be simulated without further alteration to the system equations. In a later chapter the technique involved will be explained in detail.

2.4.1 Electromagnetic Field System

One of the most useful phenomena in power system engineering is perhaps the interaction of several energy ports by means of a common magnetic field, which appears in the simple single-phase transformer as well as in the rotating machine with several damper and compensation windings.

As an example of an inductive field system a toroidal with n coils will be considered. For the general case, a rigid core structure is chosen so as to reduce the introduction of extra variables. A schematic diagram of this coil is shown in Fig. 2-13(a) indicating that there are (n + 1) flux paths consisting of the n leakage fluxes and the single mutual flux which results from the net mmf of the n coils.

Generalising Eqn. 2.24 for n coils, the net or resultant mmf is:

$$\mathcal{F}_m = \sum_{p=1}^{n} N_p i_p \qquad 2.40$$

where N_p and i_p are the number of turns and the terminal current of the pth coil respectively.

Similarly from Eqn. 2.30, the main flux is:

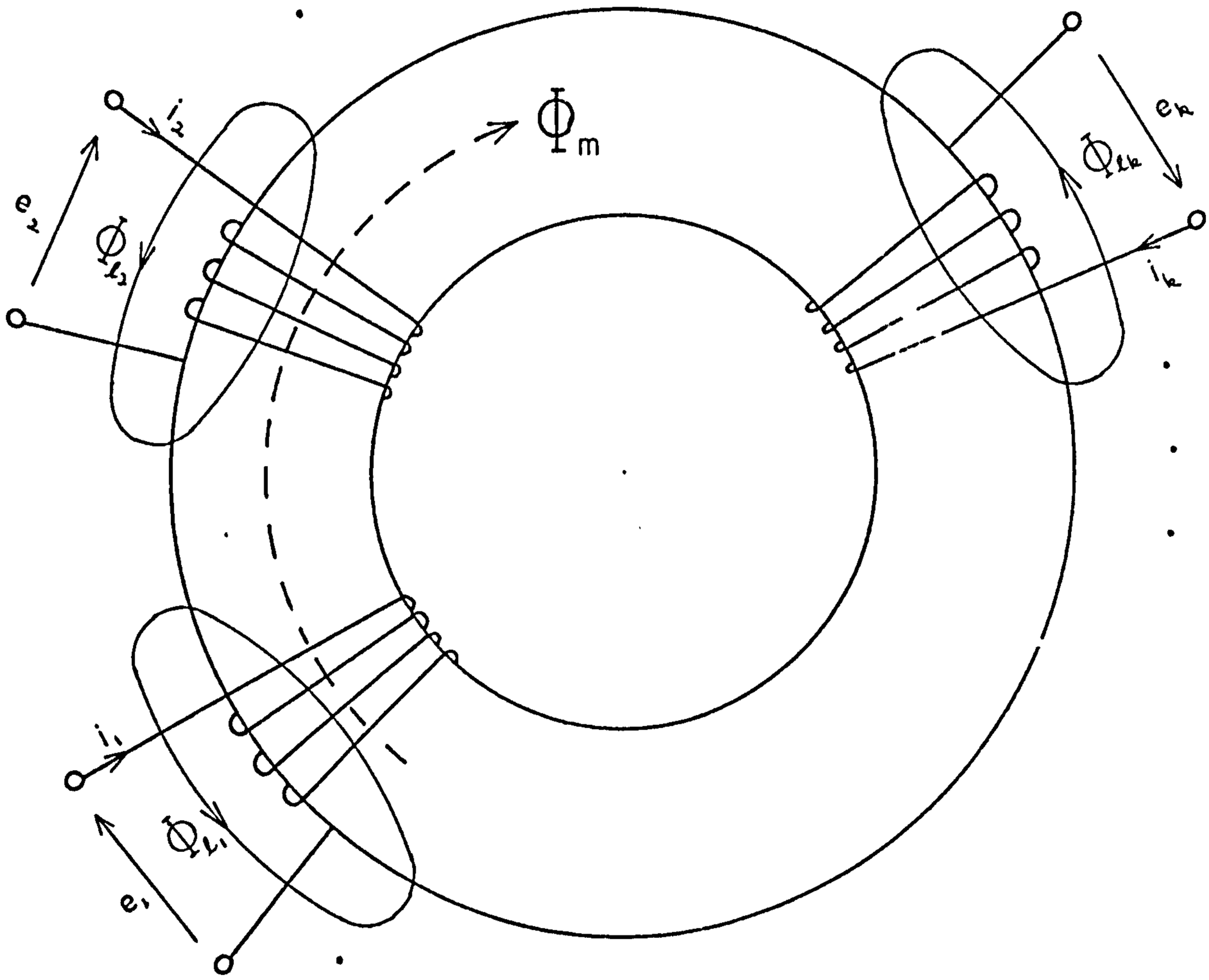

(a)

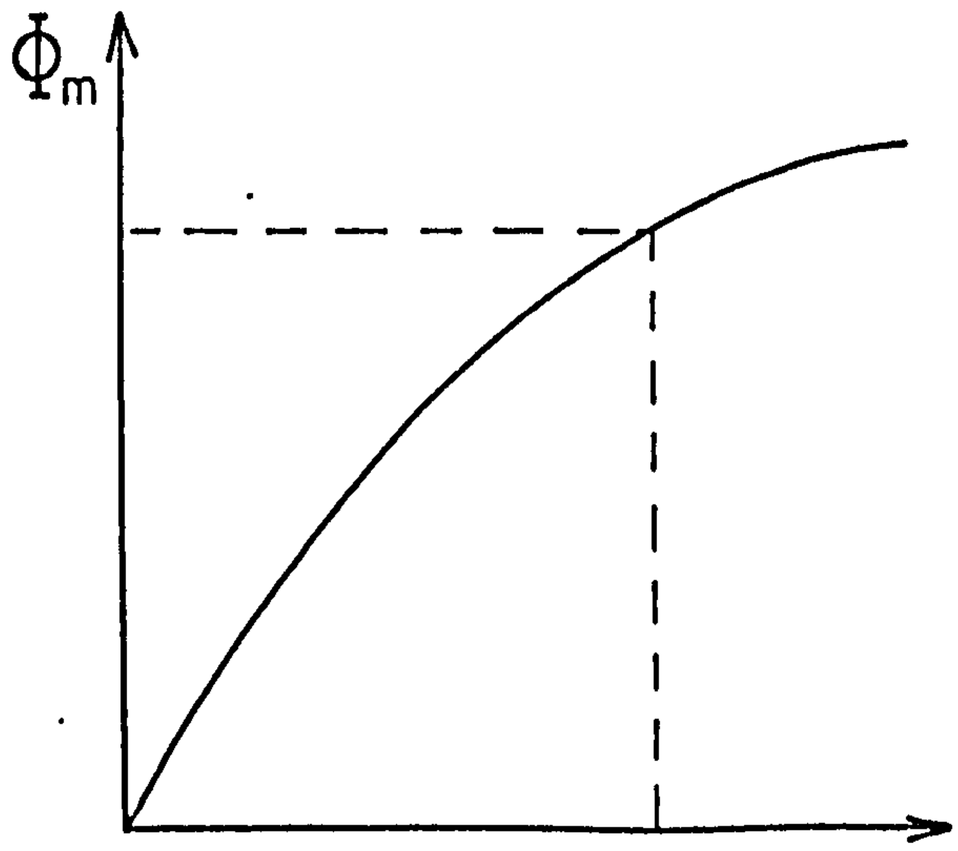

(b)

Fig. 2-13 The General n-Port Electromagnetic Field System

$$\Phi_m = \frac{\mathcal{F}_m}{\mathcal{R}_m}$$

$$= \frac{1}{\mathcal{R}_m} \sum_{p=1}^{n} N_p i_p \qquad 2.41$$

where $\mathcal{R}_m$ is the effective reluctance of the path through the main core and is defined by the $\Phi_m - \mathcal{F}_m$ characteristic of Fig. 2-13(b).

The total flux linkage of the kth toroidal coil may be derived from Eqns. 2.34 and 2.36, thus

$$\lambda_k = L_{\ell k}\, i_k + N_k\, \Phi_m \qquad 2.42$$

This flux linkage is constrained by the kth terminal voltage expressed by:

$$\lambda_k = \int^t e_k(t).dt \qquad 2.43$$

The bond graph representation of the general n-port electromagnetic field system is shown in Fig. 2-14(a) which completely describes Eqns. 2-40, 2.41, 2.42 and 2.43 in a concise coded-structure. The computation structure of Fig. 2-14(b) is derived directly from the bond graph.

The computation structure of Fig. 2-14(b) suggests that Eqns. 2.40, 2.41 and 2.42 may be expressed by a single equation defined by the effort junction between the IMU and the TF at the kth coil, thus:

$$\lambda_k = L_{\ell k}\, i_k + \frac{N_k}{\mathcal{R}_m} \sum_{p=1}^{n} N_p i_p \qquad 2.44$$

$$= \left(L_{\ell k} + \frac{N_k^{\,2}}{\mathcal{R}_m}\right) i_k + \frac{N_k}{\mathcal{R}_m} \sum_{\substack{p=1 \\ p\neq k}} N_p i_p \qquad 2.44$$

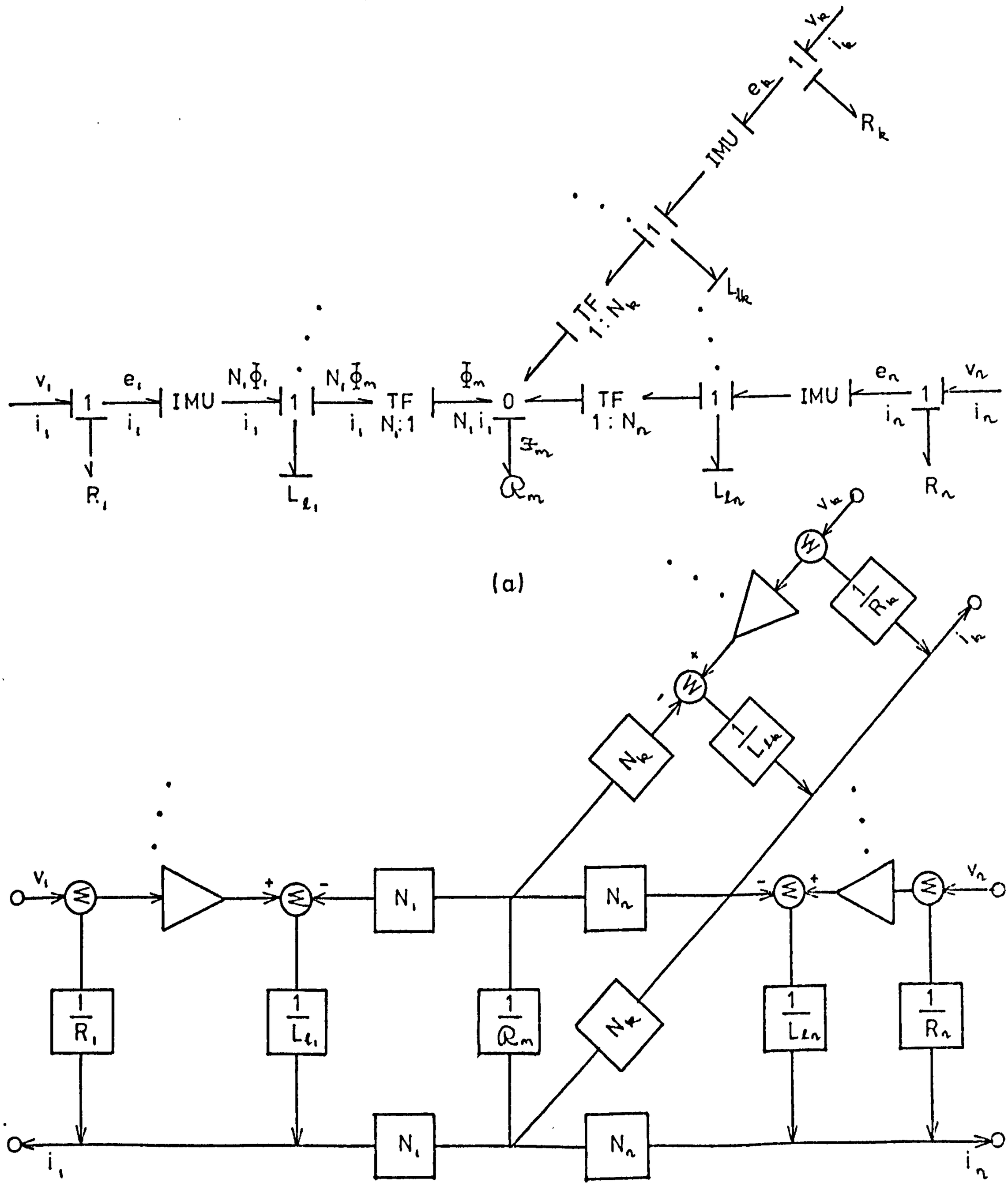

Fig. 2-14 Bond Graph and Computation Structure for the n-Port Electromagnetic Field System

Also from the causality assigned at the same effort junction, the current in the kth coil is defined completely by the leakage inductance, $L_{\ell k}$, since the output variable is i_k, hence:

$$i_k^{q+1} = \frac{1}{L_{\ell k}} \left[\lambda_k - \frac{N_k}{\mathcal{R}_m} \sum_{p=1}^{n} N_p i_p^{q} \right]$$

$$= \frac{1}{\left(L_{\ell k} + \frac{N_k^2}{\mathcal{R}_m}\right)} \left[\lambda_k - \frac{N_k}{\mathcal{R}_m} \sum_{\substack{p=1 \\ p \neq k}} N_p i_p^{q} \right] \qquad 2.45$$

As there are n coils, the solution will involve n equations of the same form as Eqn. 2.45. As stated earlier the reluctance, $\mathcal{R}_m$, is the slope associated with the flux-mmf characteristic of Fig. 2.13(b) and can be considered to be linear over an incremental section of the curve. As such Eqn. 2.45 can be assumed to be linear over a small excursion of the operating point on the non-linear curve. The standard method for the solution of linear equations such as the Gauss-Seidel and the Newton-Raphson methods may be used to solve the current equation provided the constraint at the coil terminal imposed by Eqn. 2.43 is adhered.

Rewriting the constraint equation with the resistance of the kth coil, R_k, considered, thus:

$$\dot{\lambda}_k = \nu_k + i_k^{q} R_k \qquad 2.46$$

then the total flux linkage may be evaluated using the usual numerical integration methods. The flux linkage, λ_k, obtained at the qth iteration is substituted into

Eqn. 2.45 and the instantaneous value of the current at the kth coil can then be determined.

This method is capable of solving both linear and non-linear electromagnetic field systems. The flux-mmf characteristic introduces the desired relationship between Φ_m and $\mathfrak{F}_m$ into Eqn. 2.45. This characteristic is read into the equation, using the $\mathfrak{F}_m$ known, by the normal interpolation method.

Another obvious advantage of this method is that the leakage inductances, the coil turns ratios and the resistances can all be calculated from design data. Thus, the dynamic behaviour of the electromagnetic system can be predicted at the 'drawing board' stage as this method avoids the use of the inductance matrix which may have to be measured experimentally. A detailed procedure for organising Eqns. 2.45 and 2.46 in a form suitable for input into digital computer involving the computation structure will be discussed in a later chapter.

2.4.2 Electrostatic Field System

In power system engineering the electrostatic field contributes a negligible part in the electro-mechanical energy conversion processes. Its effect is more significant in the study of transient in transmission lines and in the design of transformer tanks.

In this section the n-port electrostatic field system as shown in Fig. 2-15 is considered. The difficulty of determining the stray field tends to limit the usefulness of the subsequent method developed. However, the main aim of including this section is to show the versatility of the

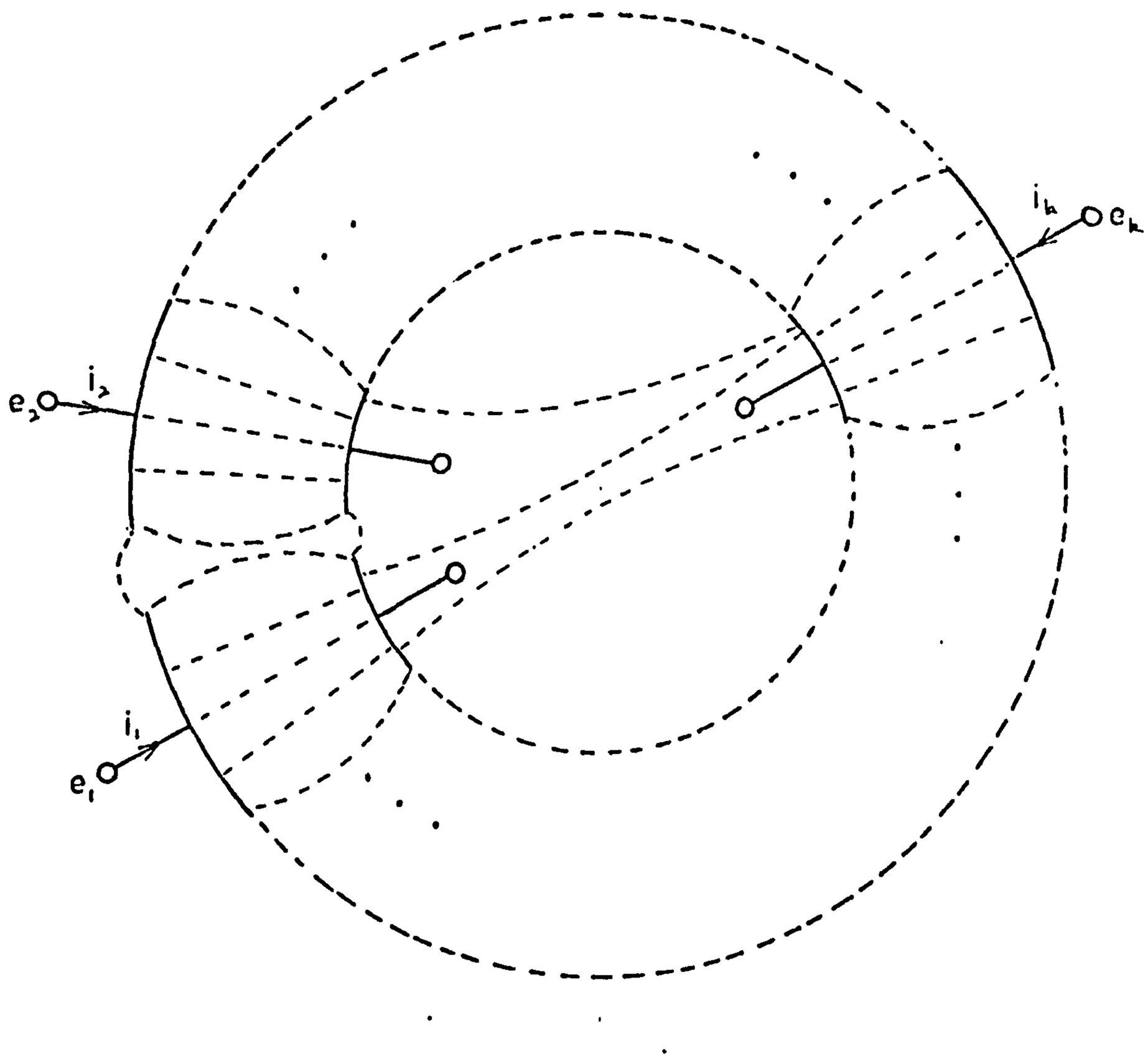

Fig. 2-15 The General n-Port Electrostatic Field System

analytical method evolved from the bond graph structure.

The charge which contributes to the stray fields emanating from any electrode can be deduced from Eqn. 2.39 as:

$$Q_s = F_c \left(\sum_{p=1}^{n} a_p e_p \right) \qquad 2.47$$

where a_p is the coefficient determined by the stray fields and e_p is the emf at the pth terminal. In general the capacitance associated with $F_c \left(\sum_{p=1}^{n} a_p e_p \right)$ may be written as C_s.

The charge between the pair of electrodes at the kth terminal which generates the uniform field is:

$$Q_k = e_k C_k \qquad 2.48$$

and thus the total charge on the kth electrodes is:

$$Q_{Tk} = Q_k + Q_s$$

$$= e_k C_k + Q_s \qquad 2.49$$

The total charge, Q_{Tk}, is constrained by the kth terminal current and is expressed as:

$$Q_{Tk} = \int^{t} i_k(t).dt \qquad 2.50$$

The general n-port electrostatic field system is represented in bond graph notation as in Fig. 2-16(a) in which the structure completely defines Eqns. 2.47, 2.48, 2.49 and 2.50.

From the computation structure of Fig. 2-16(b), the total charge for the kth electrodes, Q_{Tk}, may be expressed in terms of the terminal emf, e_k:

$$Q_{Tk} = e_k C_k + F_c \left(\sum_{p=1}^{n} a_p e_p \right) \qquad 2.51$$

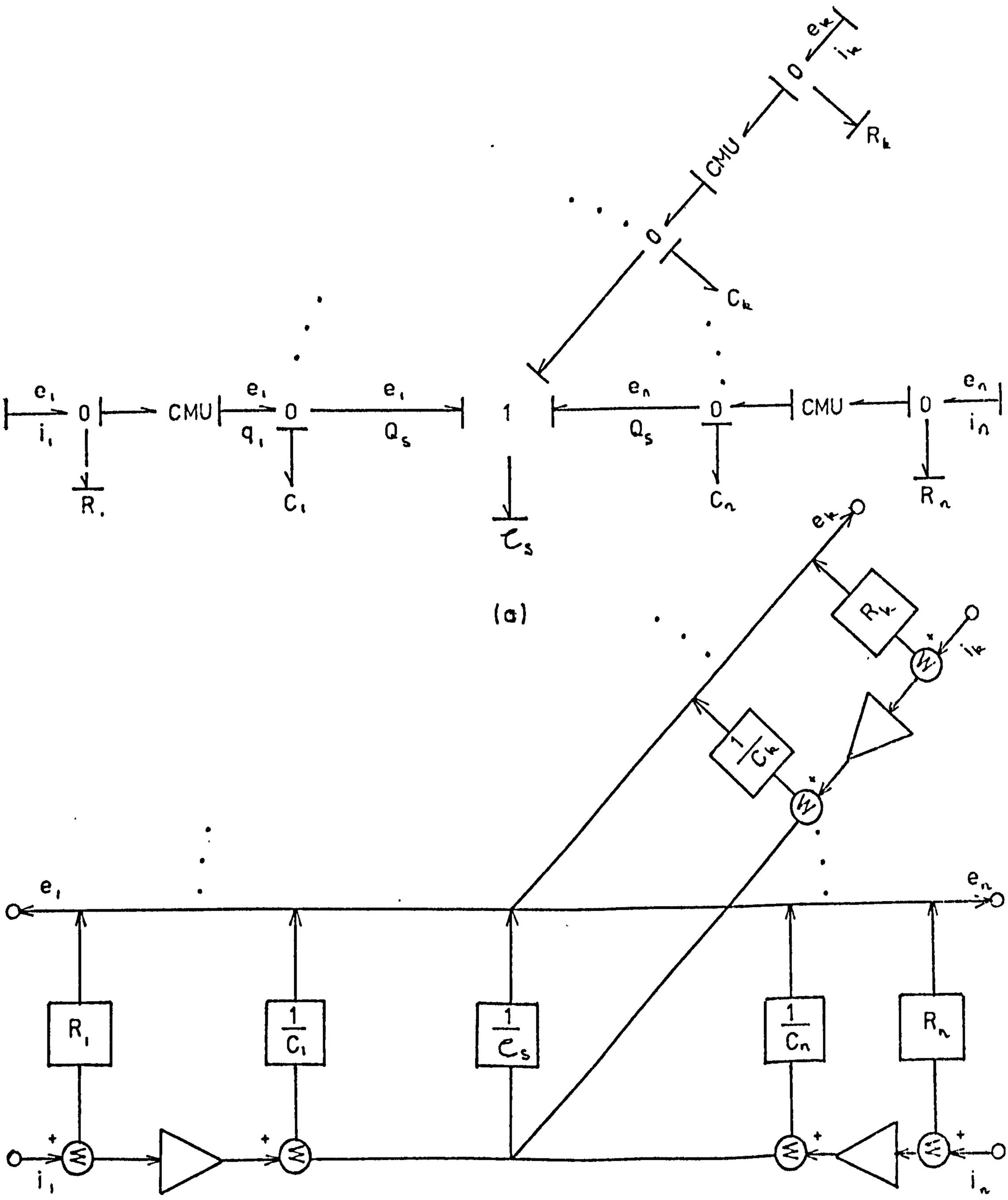

(b)

Fig. 2-16 Bond Graph and Computation Structure for the n-Port Electrostatic Field System

The flow junction, containing the capacitance, C_k, defines the kth terminal emf as:

$$e_k^{q+1} = \frac{1}{C_k} \left[Q_{Tk} - F_c \left(\sum_{p=1}^{n} a_p e_p^{q} \right) \right] \qquad 2.52$$

The solution of Eqn. 2.52 is similar to that of Eqn. 2.45. However, the constraint imposed at the kth terminal with the non-linear dielectric resistance, R_k, considered is:

$$\dot{Q}_{Tk} = i_k + \frac{e_k^{q}}{R_k} \qquad 2.53$$

Comparing Eqns. 2.45 and 2.46 for the electromagnetic system with Eqns. 2.52 and 2.53 for the electrostatic system, the equations involved are similar; however, two different energy domains are considered. Should a duality exist between the systems, such property may be useful in analysing a system in which the dual provides an easier approach to the solution.

2.5 Conclusions

The first part of this chapter attempts to present the basic rules for using the bond graph notations. Most of these materials are covered in the references given. However, in the latter part, the bond graph technique is extended by the introduction of the new two-port elements, the inductive and capacitive mutators, to link the instantaneous electromagnetic and electrostatic energy fields to the electrical power at the terminals.

The mutators enable the complete electromagnetic and electrostatic field systems to be presented in a unified

elegantly coded structure which may be used to assemble the system equations for solution by either analogue or digital computers.

In the next chapter the bond graph approach will be used to model system components such as rotating machine, transformer and transmission line in the phase co-ordinate representation. Steady state unbalanced polyphase fault analysis using these models will be studied.

Simulation of the dynamic behaviour of a medium-sized synchronous generator using the bond graph technique discussed, will also be attempted. The results obtained will be compared with experimental test results.

2.6 References

1. Stokvis, L.G.: 'Analysis of unbalanced load treated as equivalent to two balanced loads', Elect. World, 1915, 65, pp.1111-1115.

2. Kron, G.: 'Tensor Analysis of Networks' (Wiley, New York, 1951)

3. Kron, G.: 'Equivalent Circuit of Electric Machinery' (Wiley, New York, 1951)

4. Slemon, G.R.: 'Magnetoelectric Devices' (Wiley, New York, 1966)

5. Slemon, G.R.: 'Equivalent Circuits for Transformers and Machine including Non-linear Effects', Proc. IEE, 1953, 100, Pt. IV, pp 129-143.

6. Slemon, G.R.: 'Analytical Models for Saturated Synchronous Machine', Trans. IEEE, March/April 1971, PAS-90, (2), pp 409-417.

7. Cherry, E.C.: 'The Duality between Interlinked Electric and Magnetic Circuits and the Formation of Transformer Equivalent Circuits', Proc. of the Physical Soc., 1949, 62, pp 101.

8. Laithwaite, E.R.: 'Magnetic Equivalent Circuits for Electrical Machines', Proc. IEE, 1967, 114, (11), pp 1805-1809.

9. Fiennes, J.: 'New Approach to General Theory of Electrical Machine using Magnetic Equivalent Circuits', Proc. IEE, 1973, 120, (1), pp 94-104.

10. Paynter, H.M.: 'Generalising the Concepts of Power Transport and Energy Ports for System Engineering', ASME Paper 58-A-296, presented at 1958 Annual Meeting, New York, N.Y.

11. Paynter, H.M.: 'Analysis and Design of Engineering Systems' (The MIT Press, Cambridge, Mass., 1961)

12. Paynter, H.M.: 'Computer Representations of Polyphase Alternating Current Systems for Dynamic Analysis and Control', Automatic and Remote Control, Proc. First International Congress of the International Federation of Automatic Control, Moscow, 1960, pp 1009-1017.

13. Karnopp, D. and Rosenberg, R.C.: 'Analysis and Simulation of Multiport Systems' (The MIT Press, Cambridge, Mass, 1968)

14. Rosenberg, R.C.: 'State-Space Formulation for Bond Graph Models of Multiport Systems', ASME Journal of Dynamic Systems, Measurement and Control, Series G, 1971, 93, (1), pp 35-40.

15. Chua, L.O.: 'Synthesis of New Non-linear Network Elements', Proc. IEEE, 1968, 56, (8), pp 1325-1340.

16. Fitzgerald, A.E. and Kingsley, C.: 'Electric Machinery' (McGraw-Hill, New York, 1961)

17. Carter, G.W.: 'The Electromagnetic Field' (Longmans, London, 1967)

18. Reddy, G. and Jones, C.V.: 'Line-to-line Short Circuit of Synchronous Machine: Illustration of Computer-Aided Machine Analysis', Proc. IEE, 1971, 118, (1), pp 161-169.

19. Subramaniam, P. and Malik, O.P.: 'Digital Simulation of Synchronous Generator in Direct-Phase Quantities', Proc. IEE, 1971, 118, (1), pp 153-160.

20 Reddy, G., Ali, A.M. and Jones, C.V.: 'Computer-Aided Analysis of Saturated System', Proc. IEE, 1971 118, (12), pp 1791-1799.

CHAPTER THREE

STEADY-STATE ANALYSIS OF MULTIPORT ENERGY SYSTEMS

3.1 Introduction

In this chapter the main goal is to built up a model of a power system complex from a study of the system components and subsequently to demonstrate successful prediction of many features of the real system. Bond graph models of the power system components are derived using the notations developed in Chapter Two and an assembly[1] of these components representing the complete system is used to calculate fault currents under varying fault conditions. The transformer representation may be evolved directly from the bond graph structure for the general n-port electromagnetic field system which constitutes the necessary ingredient for the modelling of a number of polyphase multi-winding transformers. However, the rotating machine model uses a modified form of the electromagnetic field system with particular considerations made involving the basic gyrator action of the machine.

The suitability of a particular component model can partly be judged on the basis of its effect on the system performance. In the studies considered, models of components are as simple as possible and yet, when assembled into the system, are sufficiently accurate representations of the components to allow prediction of the effects of changes in component parameters and configurations on the overall system behaviours. Since only steady-state conditions are considered, there is no necessity to obtain the dynamic computation structure but instead the nodal

admittance matrix is formed from the bond graph of each component.

One of the interesting features of the bond graph approach is that models automatically tend to be represented in the phase frame of reference. As such the analysis of power system by this method must be oriented to account for the actual phase variables used. The method of phase co-ordinates, proposed by Laughton[2,3], is ideally suited for solution of balanced and unbalanced fault problems and may be used to test the validity of the alternative models derived from the bond graph methods.

Problems in polyphase circuit theory have been extensively studied by many authors, namely, Fortescue[4], Clarke[5], Kimbark[6] and Koga[7]. The symmetrical component theory developed since 1915 for the analysis of unbalanced system behaviours offers an admirable measure of unbalanced system operation. However, the assembly of sequence components and the solution of sequence equations can be quite involved, particularly in the case of systems where mutual coupling exists between the sequence networks. Alternatively, transformation methods[5,6,7] have been introduced to overcome the difficulties encountered in using symmetrical components.

The method of phase co-ordinates, however, uses the actual system phase voltages, currents and impedances and thus avoids the necessity of transforming variables and of departing from the physical component models. In this chapter this method will be used in conjunction with the bond graph models developed for the power system components.

Also in this chapter it is hoped to show that the bond graph technique is equally adaptable for steady-state operations. Under this condition, the power system component models are relatively simpler and as such may provide a better understanding of the modelling technique involved before proceeding with the dynamic studies in Chapter Four.

3.2 Rotary Energy Converters

A vast collection of literature has been available since 1910[8] which concerns itself with the many problems of rotating electrical machines. Much of this work is directed towards establishing the relation between the machine parameters and the steady-state load-performance characteristics of machines. While some attention has been given to the transient performance of electrical machines under starting or fault conditions, the attention to transient problems has been much less extensive than that concerned with the steady-state load performance. However, in the next chapter dynamic problems will be treated in detail using the bond graph concept while in this section an effort will be made to derive a model of the three-phase synchronous generator suitable for steady-state studies.

Under balanced steady-state conditions, the representation of one phase of the three-phase synchronous machine by the equivalent phase circuit where the machine appears as a voltage source with an internal impedance has been extensively used for a variety of studies. In the present context the model will be based on such a representation; however, consideration will be made to enable the machine to operate in an unbalanced three-phase mode.

3.2.1 Basic Rotating Machine

Electromechanical energy conversion can occur when two or more coils move relative to each other or when some object with magnetic properties is moving in the interacting magnetic fields. The inductances of the coils then become functions of the geometry of field distribution and the magnetic properties of the surrounding space.

A two-winding structure as illustrated in Fig. 3-1 may be considered to be so designed that one coil is fixed with respect to the magnetic structure and the second coil is so arranged that it can be rotated with respect to the fixed coil assembly. The mutual inductance, M_{12}, between the two coils will vary with angle, θ. It will be a maximum when the flux linking the rotating coil is maximum and it will be zero when the flux linkages are zero, the situation that exists at $\theta = \frac{\pi}{2}$ and $\frac{3}{2}\pi$ respectively.

It can be shown[9] that the electrical energy input, when only M_{12} varies with position, is:

$$dW_{elec} = I_1 \frac{d\lambda_1}{dt} \cdot dt + I_2 \frac{d\lambda_2}{dt} \cdot dt$$

$$= 2\, I_1\, I_2\, dM_{12} \qquad 3.1$$

where λ_1 and λ_2 are the flux linkages with coils 1 and 2 respectively, with I_1 and I_2 being their respective coil currents.

The energy originally stored in the mutual field is:

$$W_{fld} = I_1\, I_2\, M_{12} \qquad 3.2$$

Therefore, the change in energy stored in the mutual field is:

$$dW_{fld} = I_1\, I_2\, dM_{12} \qquad 3.3$$

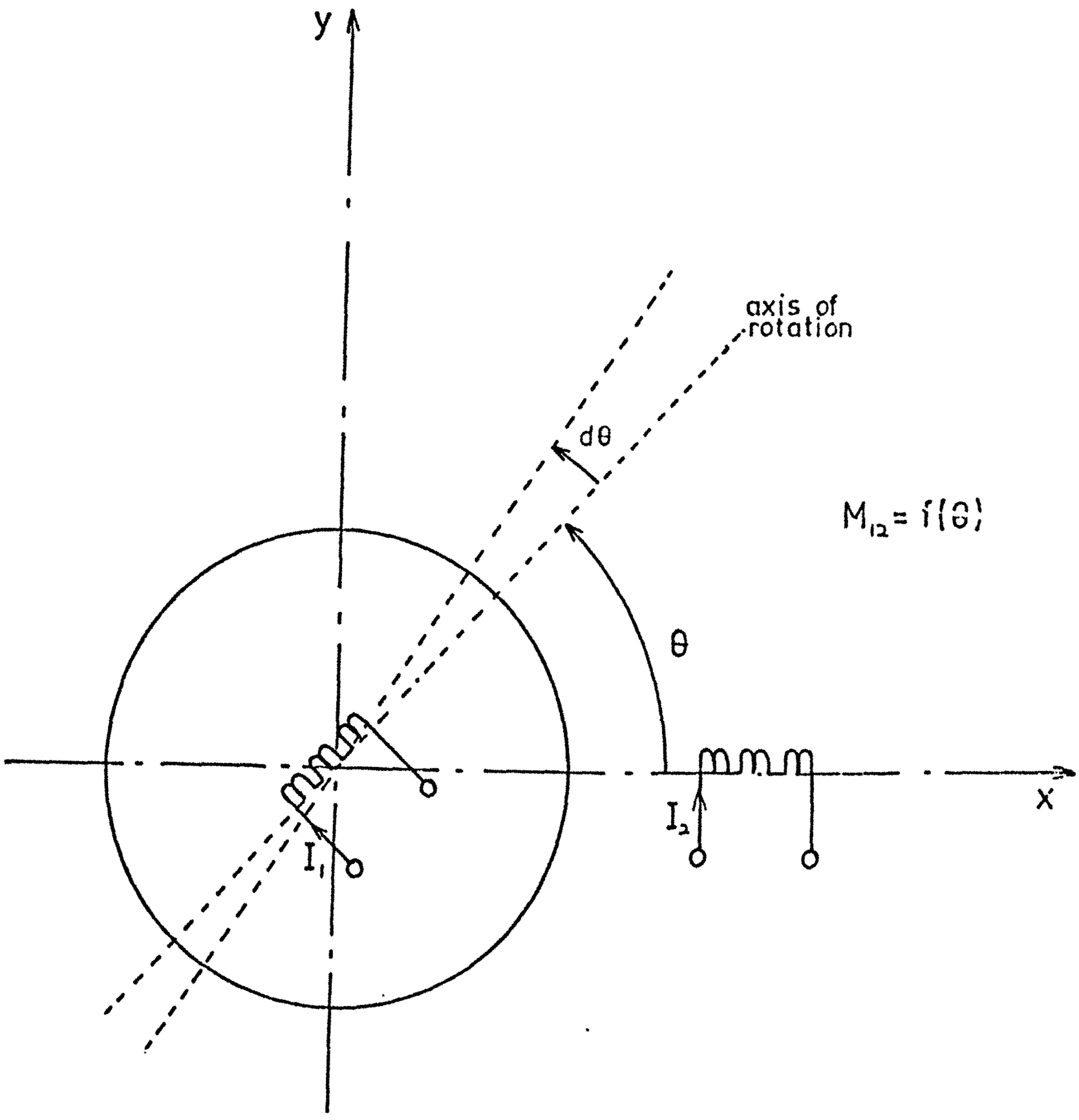

Fig. 3-1 Schematic Diagram of Basic Rotating Machine

and the incremental mechanical work done is:

$$dW_{mech} = T_e \, d\Theta$$

$$= dW_{elec} - dW_{fld}$$

$$= I_1 \, I_2 \, dM_{12} \qquad 3.4$$

where T_e is the excitation torque. For the case in which only M_{12} varies with Θ and the self inductances, L_{11} and L_{22}, being constant, then the torque developed may be obtained from Eqn. 3.4 as:

$$T_e = I_1 \, I_2 \, \frac{dM_{12}}{d\Theta} \qquad 3.5$$

If coil 1 is excited with coil 2 on open circuit, the emf, E_2, induced in coil 2 may be expressed by:

$$E_2 = I_1 \, \frac{dM_{12}}{d\Theta} \, .\omega \qquad 3.6$$

where ω is the speed of rotation of coil 1. Thus Eqns. 3.5 and 3.6 may be written in matrix form as:

$$\begin{bmatrix} E_2 \\ \\ I_2 \end{bmatrix} = \left[\begin{array}{c|c} \cdot & r \\ \hline \frac{1}{r} & \end{array}\right] \cdot \begin{bmatrix} T_e \\ \\ \omega \end{bmatrix} \qquad 3.7$$

where $r = I_1 \, \frac{dM_{12}}{d\Theta}$. Comparing Eqn. 3.7 with Eqn. 2.10 it is evident that the ideal rotating machine with no reluctance torque component has a characteristic identical with that of a gyrator whose modulus, r, is a function of I_1, M_{12} and Θ.

3.2.2 Synchronous Generator

The polyphase synchronous generator is the standard device used in power systems for converting rotary mechanical

energy into electromagnetic energy. Viewed in the present context this component is simply a transducer modulated by the direct current in the field windings on the rotor.

For the general three-phase case, under steady-state conditions, the synchronous generator may be considered as a primitive lossless transducer of the form:

$$\left.\begin{aligned} E &= K\omega \\ T &= KI \end{aligned}\right\} \qquad 3.8$$

where $[T,\omega]$ are the steady-state values of shaft torque and speed and $[E,I]$ are the steady-state values of the matrix of phase emfs (E_a, E_b, E_c) and the matrix of phase currents (I_a, I_b, I_c) respectively. The gyrator modulus matrix, $K = (K_a, K_b, K_c)$, depends upon the field excitation current, I_F, and the magnetizing inductance, M_F. Eqn. 3.7 is a special case of the general form expressed by Eqns. 3.8.

From the expression for steady-state no-load voltage[10], the gyrator modulus matrix may be derived as:

$$\left.\begin{aligned} K_a &= \frac{1}{\sqrt{2}}\ M_F\ I_F \angle 0^\circ \\ K_b &= \frac{1}{\sqrt{2}}\ M_F\ I_F \angle -120^\circ \\ K_c &= \frac{1}{\sqrt{2}}\ M_F\ I_F \angle\ 120^\circ \end{aligned}\right\} \qquad 3.9$$

and from which the phase emfs or the no-load voltages, (E_a, E_b, E_c), may be expressed by;

$$E_a = \frac{1}{\sqrt{3}} (K_c - K_b)\omega \qquad)$$

$$= j \frac{M_F \omega I_F}{\sqrt{2}} \angle 0^\circ \qquad)$$

$$E_b = \frac{1}{\sqrt{3}} (K_a - K_c)\omega \qquad)$$

$$= j \frac{M_F \omega I_F}{\sqrt{2}} \angle -120^\circ \qquad) \qquad 3.10$$

$$E_c = \frac{1}{\sqrt{3}} (K_b - K_a)\omega \qquad)$$

$$= j \frac{M_F \omega I_F}{\sqrt{2}} \angle 120^\circ \qquad)$$

A three-phase synchronous machine represented by a voltage source with internal admittance in each phase, has a bond graph for phase 'a' given by:

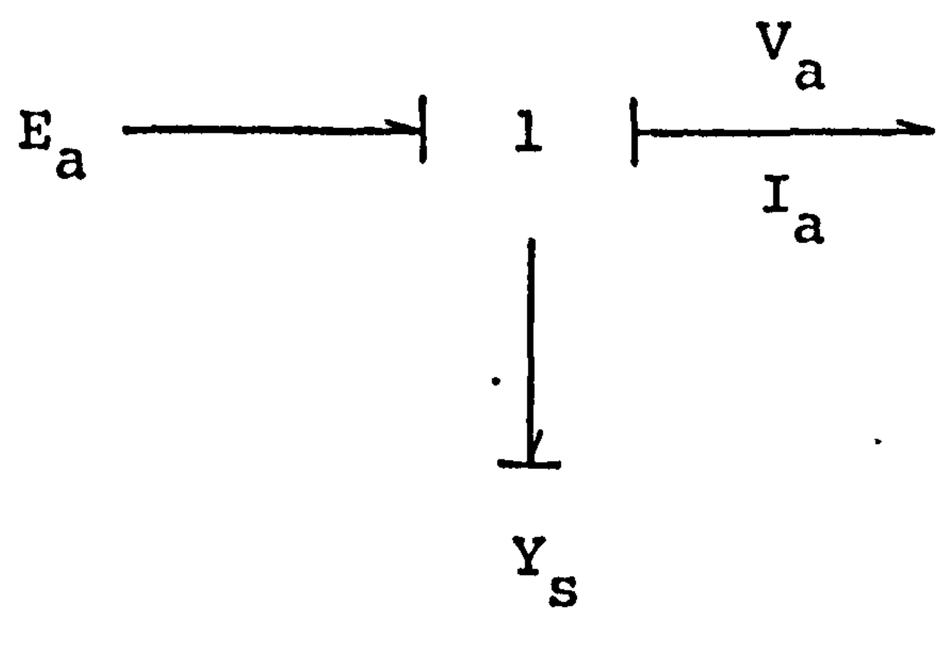

From Eqns. 3.10, the phase emf E_a, can be shown to consist of two components, $K_c\omega/\sqrt{3}$ and $K_b\omega/\sqrt{3}$. Thus, the above bond graph can be modified as;

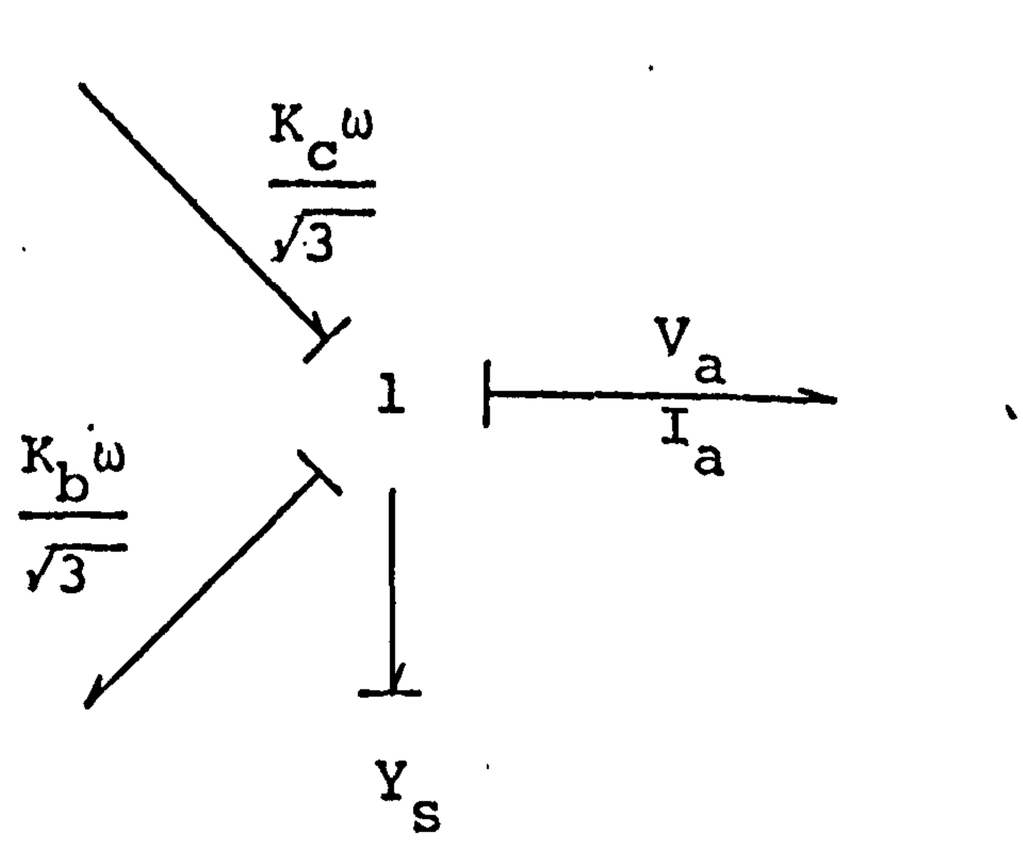

The structure shown can also be derived for the other phases.

In order to proceed with the modelling of steady-state synchronous machine, it is necessary to introduce the concept of 'phase' torque. The total torque, T, expressed in terms of the 'phase' torques T_a, T_b and T_c (= $T/3$), is:

$$T = T_a + T_b + T_c$$

$$= T/3 + T/3 + T/3 \qquad 3.11$$

and in terms of the phase currents is:

$$T = \frac{P}{\sqrt{3}} \left[K_a(I_b - I_c) + K_b(I_c - I_a) + K_c(I_a - I_b) \right] \qquad 3.12$$

where P is the number of pole pairs.

The transducer relationships between the rotational speed ω, torques T_a, T_b and T_c, and phase currents I_a, I_b and I_c, can be represented by the modulated gyrator, thus:

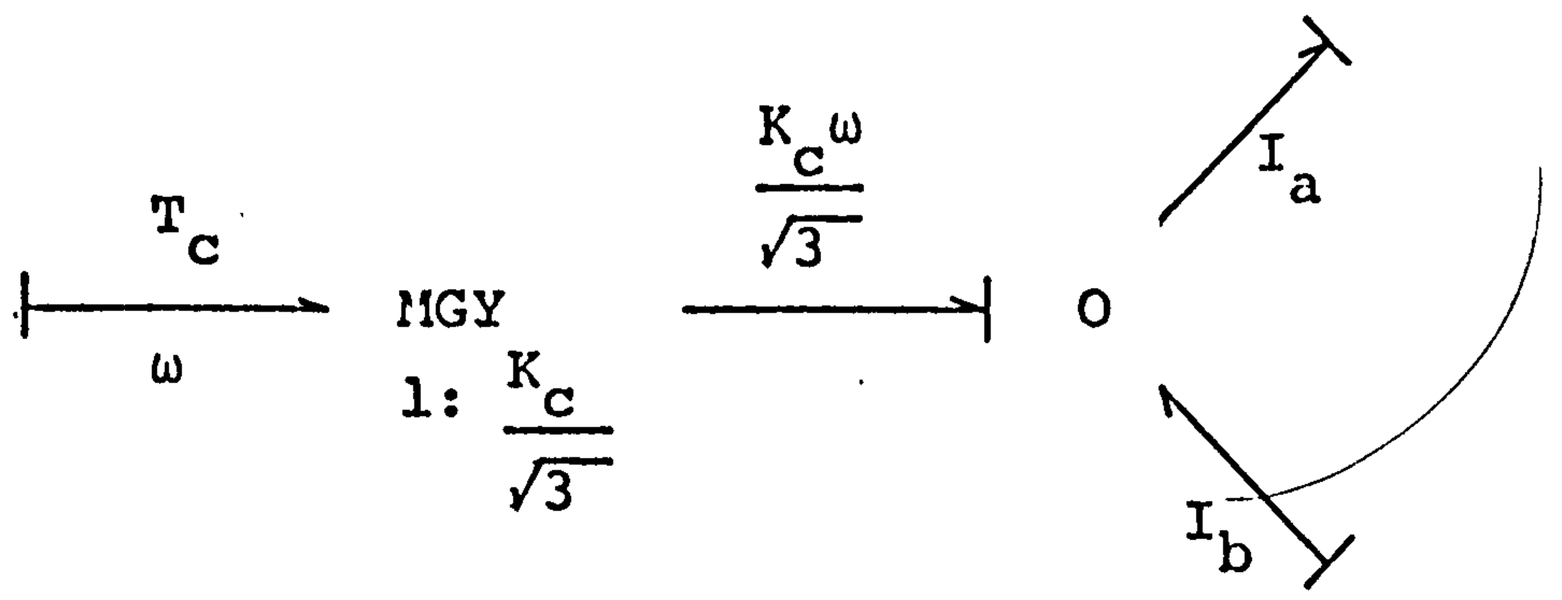

By appropriately arranging the bond graph structures for each electrical and mechanical phases, derived as shown, the bond graph for the three-phase synchronous generator may be represented by Fig. 3-2. This diagram shows that the mechanical energy is transferred through three separate 0-junctions each having one-third of the total torque. However, in actual fact there exists only one mechanical port and that the representation chosen serves only to simplify the diagram.

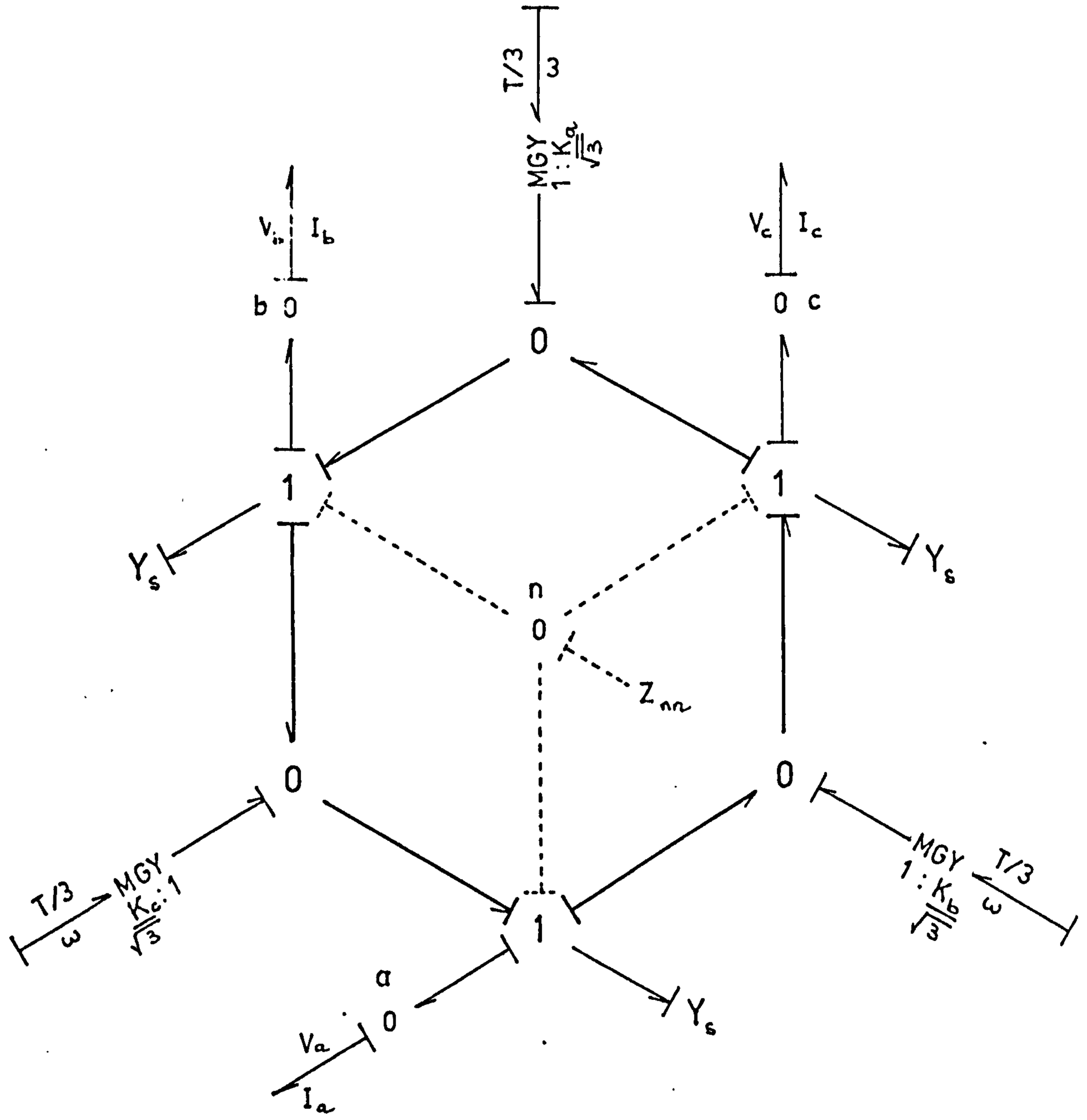

Fig. 3-2 Bond Graph Representation of a Three-Phase Synchronous Generator (Steady-State Condition)

The generator model of Fig. 3-2 is ideal for use in three-phase load flow studies where the real power is supplied by the mechanical torque at synchronous speed and the reactive power is governed by the excitation current. The effects of unbalanced operations may be included in the gyrator modulus matrix, K, which is a function of the phase angles.

The admittance, Y_s, can either be the synchronous admittance which consists of both magnetizing and leakage admittances[11] or the appropriate generator admittances, being sub-transient values for circuit-breaker ratings and transient values for protective gear applications. This method of representation requires that the operating conditions and the internal admittance of the synchronous generator are initially known.

It will be shown at a later chapter that the hexagonal structure in Fig. 3-2 assumes a similar role in the dynamic representation of the three-phase synchronous generator. The neutral node, n, is shown in the same figure with the dotted line indicating the bonds for a generator with an earthing impedance, Z_{nn}.

However, in some studies, quite often the sequence quantities are given instead. For normal balanced machine designs where the machine may be adequately represented in symmetrical component analysis by the three uncoupled sequence admittances y_1, y_2 and y_o, the phase admittance matrix Y_{abc} may be constructed from the sequence admittances using the relationships[12]:

$$Y_{abc} = \frac{1}{3}\begin{bmatrix} Y_0+Y_1+Y_2 & Y_0+\alpha Y_1+\alpha^2 Y_2 & Y_0+\alpha^2 Y_1+\alpha Y_2 \\ Y_0+\alpha^2 Y_1+\alpha Y_2 & Y_0+Y_1+Y_2 & Y_0+\alpha Y_1+\alpha^2 Y_2 \\ Y_0+\alpha Y_1+\alpha^2 Y_2 & Y_0+\alpha^2 Y_1+\alpha Y_2 & Y_0+Y_1+Y_2 \end{bmatrix} \quad 3.13$$

where $\alpha = 1\angle 120^o$ and Y_1, Y_2, Y_0 are the positive-, negative- and zero-sequence admittances respectively. In this representation, the zero-sequence admittance Y_0, can be made to include the earthing admittance of the synchronous generator.

The current equations for a star-connected synchronous generator with earthed neutral may be written as:

$$I_{abc} = y_1 E_{abc} - Y_{abc} V_{abc} \quad 3.14$$

where E_{abc} is the matrix for the equivalent voltage source per phase and V_{abc} is the matrix of voltages at the terminal nodes.

3.3 Energy-Transfer Devices

This section includes a study of the single-phase two-winding transformer, a device which consists of two coils which are fixed with respect to each other and with respect to the magnetic material making up the structure. Although the transformer is not an energy-conversion device, it is an indispensable component in many energy-conversion systems.

The bond graph for the n-port electromagnetic field system has been developed in Chapter 2 and from this structure, the bond graph of the two-port single-phase transformer may be derived. For the particular study in

this chapter the model is simplified by considering the following assumptions:

(i) the effective reluctance of the magnetic path through the main core, $\mathcal{R}_m$, is negligible;

(ii) the effective reluctances of the magnetic paths through the surrounding air for both windings are represented by a single equivalent reluctance; and,

(iii) only steady-state operating conditions are considered.

From this simple model, the bond graph of the single-phase two-winding transformer in terms of the equivalent leakage admittance and turns ratio may be obtained.

3.3.1 Basic Single-Phase Transformer

In the study of system unbalanced problems using the actual system phase voltages, currents and admittances, a major difficulty concerns the representation of transformers. Laughton[2,3] has derived a single-phase transformer model in phase co-ordinates which is used to develop the phase equivalent circuits of a number of balanced and unbalanced polyphase multiwinding transformers.

The transformer model, developed from the bond graph of the electromagnetic system of Chapter 2, not only reaffirms the validity of the previous model[2] but also has the advantage of being derived from the general non-linear two-winding transformer which may then be reduced in a simple step-by-step method to a model suitable for this particular study. The assumptions made in Section 3.3 are used in the reduction process.

The non-linear two-winding transformer is shown in

Fig. 3-3(a) and with the definition of the leakage inductances, $L_{\ell 1}$ and $L_{\ell 2}$, in terms of the leakage reluctances, $\mathcal{R}_{\ell 1}$ and $\mathcal{R}_{\ell 2}$, and turns ratio, α and β, given by[11]:

$$L_{\ell 1} = \frac{\alpha^2}{\mathcal{R}_{\ell 1}}$$

$$= \frac{\alpha \Phi_{\ell 1}}{i_1} \qquad 3.15$$

$$L_{\ell 2} = \frac{\beta^2}{\mathcal{R}_{\ell 2}}$$

$$= \frac{\beta \Phi_{\ell 2}}{i_2} \qquad 3.16$$

where the equivalent variable turns ratio α and β may be expressed in per-unit quantities as $(1+t_\alpha)$ and $(1+t_\beta)$ respectively, the bond graph representation may be redrawn as shown in Fig. 3-3(b). Assuming that the effective relunctance of the magnetic path through the main core, $\mathcal{R}_m$, is negligible, the reduced bond graph of the single-phase two-winding transformer is represented by Fig. 3-3(c) where the equivalent leakage reluctance can be expressed as:

$$\frac{1}{\mathcal{R}_e} = \frac{1}{\mathcal{R}_{\ell 1}} + \frac{1}{\mathcal{R}_{\ell 2}}$$

$$= \frac{L_{\ell 1}}{\alpha^2} + \frac{L_{\ell 2}}{\beta^2} \qquad 3.17$$

Under steady-state conditions, the inductive mutator becomes a 1:1 transformer since $e = j\omega\lambda$, and assuming that the coil resistances, R_1 and R_2, can be included in the admittance Y_t (or $1/z_t$), the bond graph may be simplified to that shown in Fig. 3-4(a).

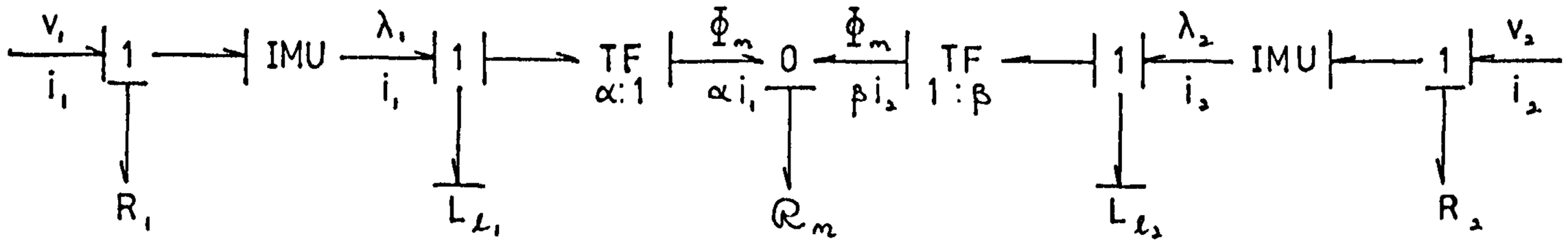

(a)

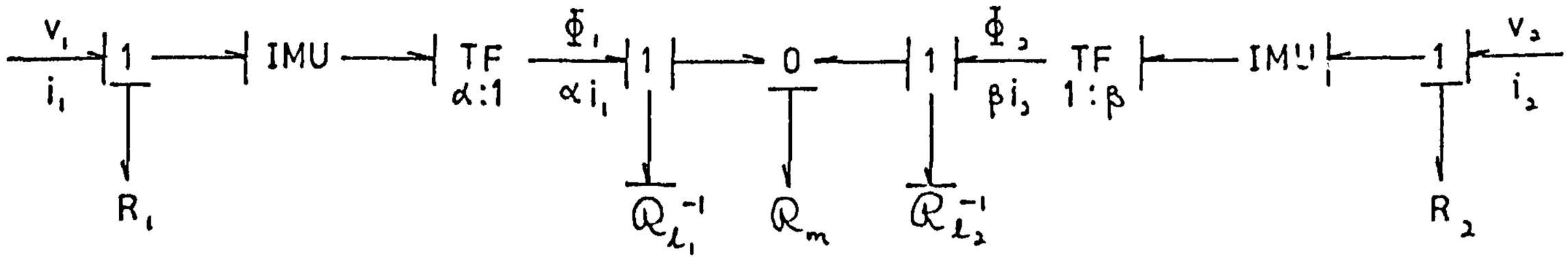

(b)

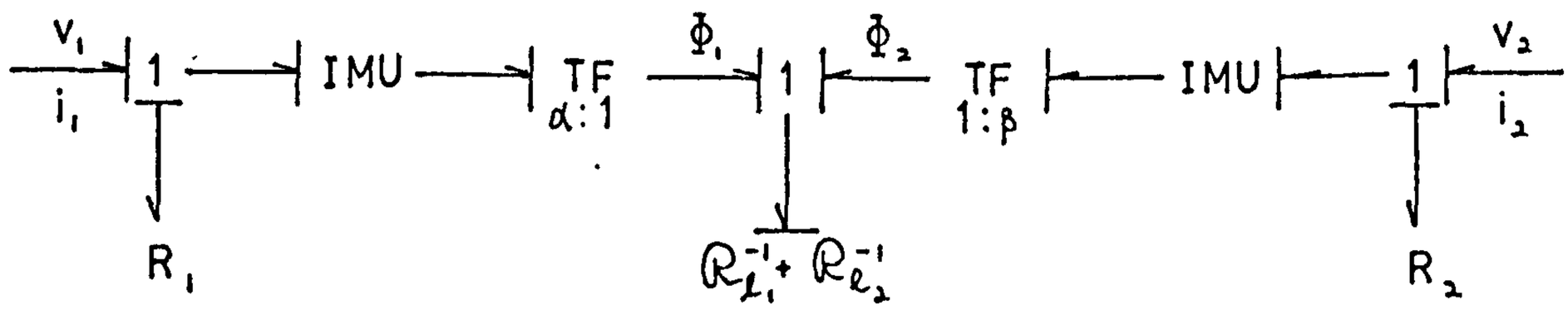

(c)

Fig. 3-3 Bond Graphs of a Single-Phase Two-Winding Transformer

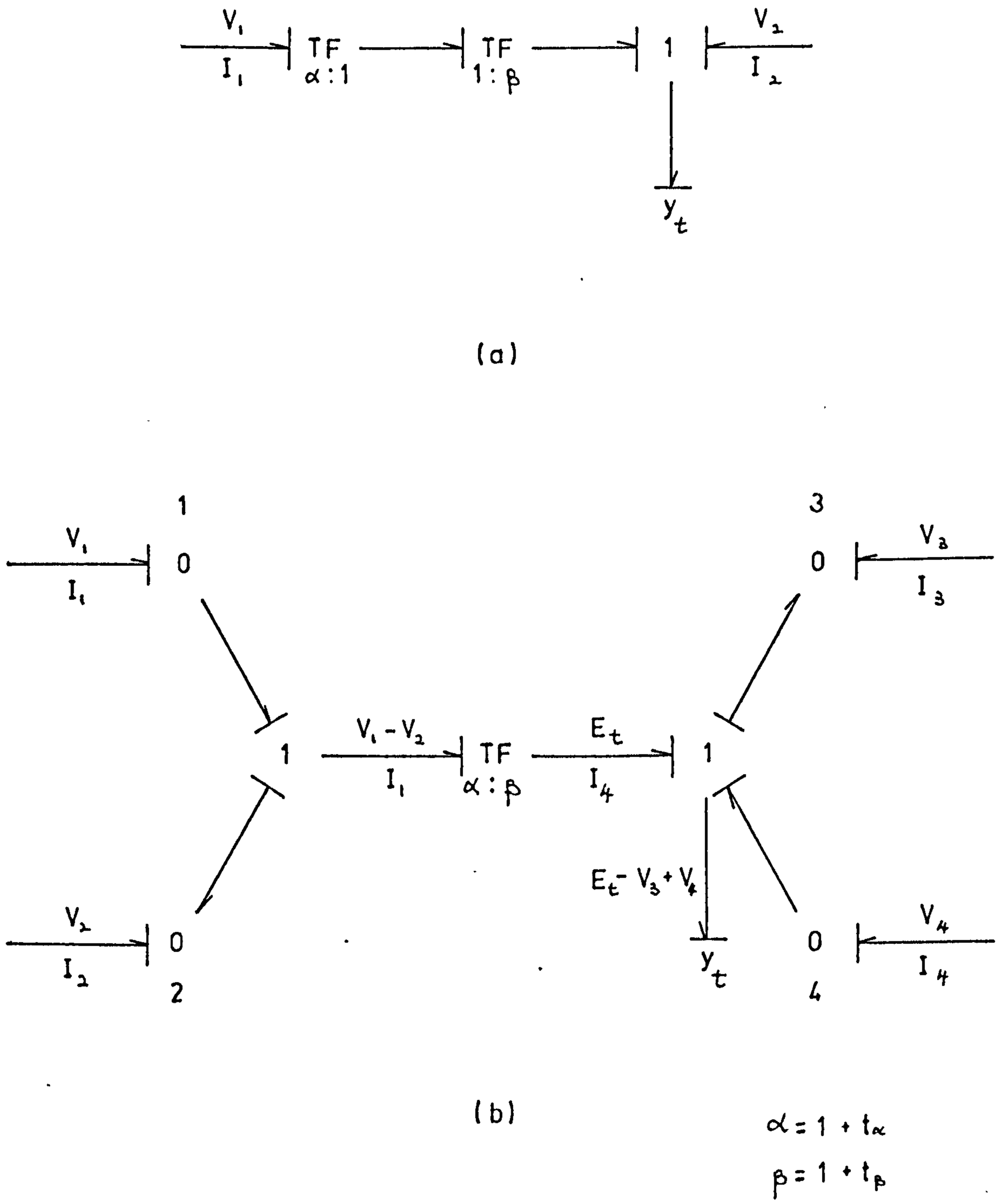

Fig. 3-4 Simplified Bond Graphs of a Single-Phase Two-Winding Transformer (Steady-State Condition)

The equivalent leakage impedance $\mathcal{Z}$, may be defined in terms of the coil leakage impedances $\mathcal{Z}_1$ and $\mathcal{Z}_2$ for coils 1 and 2 respectively as:

$$\mathcal{Z} = \frac{j\omega L_{\ell 1}}{\alpha^2} + \frac{j\omega L_{\ell 2}}{\beta^2}$$

$$= \frac{\mathcal{Z}_1}{\alpha^2} + \frac{\mathcal{Z}_2}{\beta^2} \qquad 3.18$$

Thus the equivalent leakage impedance referred to coil 2 is:

$$\mathcal{Y}_t = \beta^2 \mathcal{Z} = \frac{\beta^2}{\alpha^2} \mathcal{Y}_1 + \mathcal{Y}_2$$

$$= \mathcal{Y}'_1 + \mathcal{Y}_2 \qquad 3.19$$

which is the sum of the leakage impedances, $\mathcal{Y}'_1$ and $\mathcal{Y}_2$, with $\mathcal{Y}_1$ referred to coil 2. If it is required to float the transformer in order to eliminate earth connection, the bond graph takes the form shown in Fig. 3-4(b) where the four necessary nodes defined by the 0-junctions are clearly labelled.

From the relationships across the ideal transformer, shown in Fig. 3-4(b):

$$\left.\begin{aligned} \frac{V_1 - V_2}{\alpha} &= \frac{E_t}{\beta} \\ \frac{I_1}{\beta} &= \frac{I_4}{\alpha} \end{aligned}\right) \qquad 3.20$$

the nodal current at node 4 can be evaluated at the effort junction containing Y_t as:

$$I_4 = (E_t - V_3 + V_4) \frac{Y}{\beta^2} \qquad 3.21$$

where $y = 1/\mathcal{Z}$ is the equivalent leakage admittance and $Y_t = y/\beta^2$. Using Eqn. 3.20, the nodal current is

$$I_4 = \left[\frac{\beta}{\alpha}(V_1 - V_2) - V_3 + V_4\right]\frac{Y}{\beta^2}$$

$$= \left[\frac{Y}{\alpha\beta}(V_1 - V_2) + \frac{Y}{\beta^2}(V_4 - V_3)\right] \qquad 3.22$$

Similarly using Eqn. 3.20 the nodal current at node 1 is:

$$I_1 = \frac{\beta}{\alpha} I_4$$

$$= \left[\frac{Y}{\alpha^2}(V_1 - V_2) + \frac{Y}{\alpha\beta}(V_4 - V_3)\right]$$

$$= \left[\frac{Y}{\alpha^2}(V_1 - V_2) + \frac{Y}{\alpha\beta}(V_1 - V_3) - \frac{Y}{\alpha\beta}(V_1 - V_4)\right]$$

$$= I_p + I_q - I_r \qquad 3.23$$

The nodal currents at nodes 2 and 3 may be derived using Eqns. 3.22 and 3.23, with the relationships in Fig. 3-4 (b) thus:

$$\left.\begin{aligned} I_2 &= -I_1 \\ I_3 &= -I_4 \end{aligned}\right) \qquad 3.24$$

The bond graph describing Eqns. 3.23 may be represented by:

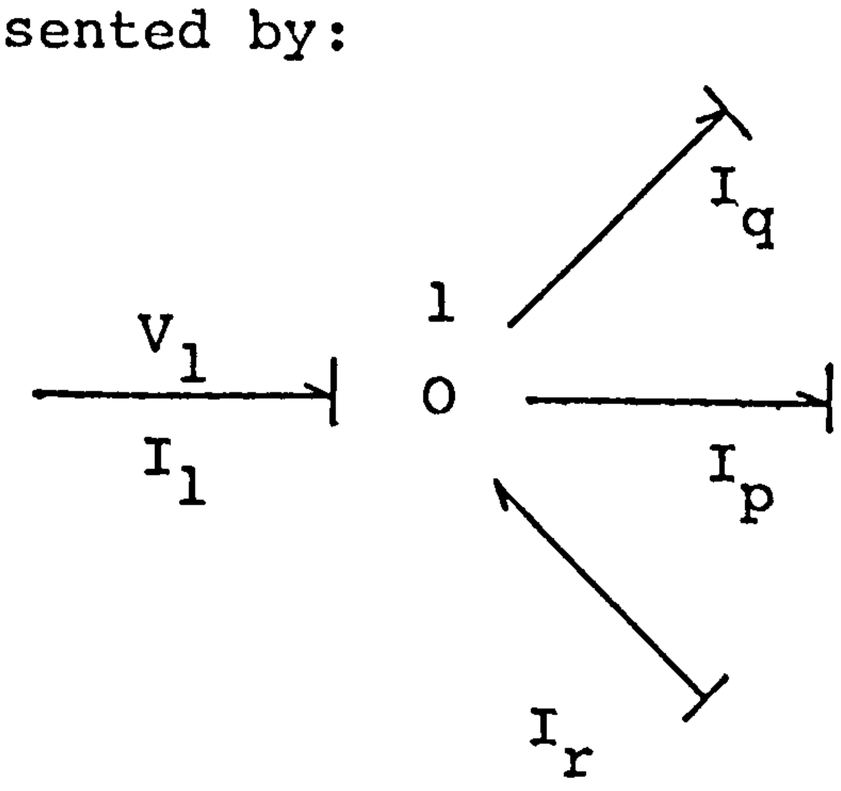

where I_p, the current in the bond between nodes 1 and 2 can be represented by the bond graph;

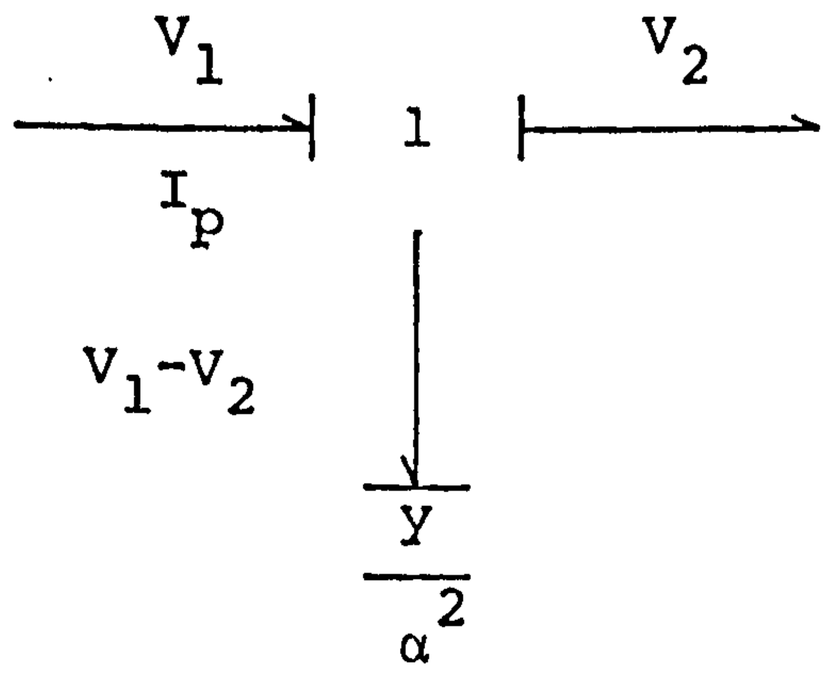

The currents, I_q and I_r, have similar bond graphs; and with all the structures determined the complete bond graph for node 1 as expressed by Eqn. 3.23 may be derived.

The process may be repeated for all the other nodes. When the resulting bond graphs are correctly assembled, the equivalent bond graph of the single-phase transformer may be represented by Fig. 3-5.

The term 'equivalent' used to describe the transformer above refers to the corresponding form of the simplified model of Fig. 3-4(b), with the assumptions of Section 3.3 considered. In the equivalent model the ideal TF is replaced by passive elements.

In matrix form, Eqns. 3.22, 3.23 and 3.24 may be expressed as:

$$I = YV \qquad 3.25$$

where $[I,V]$ are the steady-state values of the matrix of injected nodal currents (I_1, I_2, I_3, I_4) and matrix of nodal voltages (V_1, V_2, V_3, V_4) respectively; and Y is the nodal admittance matrix. By noting the algorithm[13] for forming the matrix Y, the bond graph of Fig. 3-5 may be used to assemble the nodal admittance matrix.

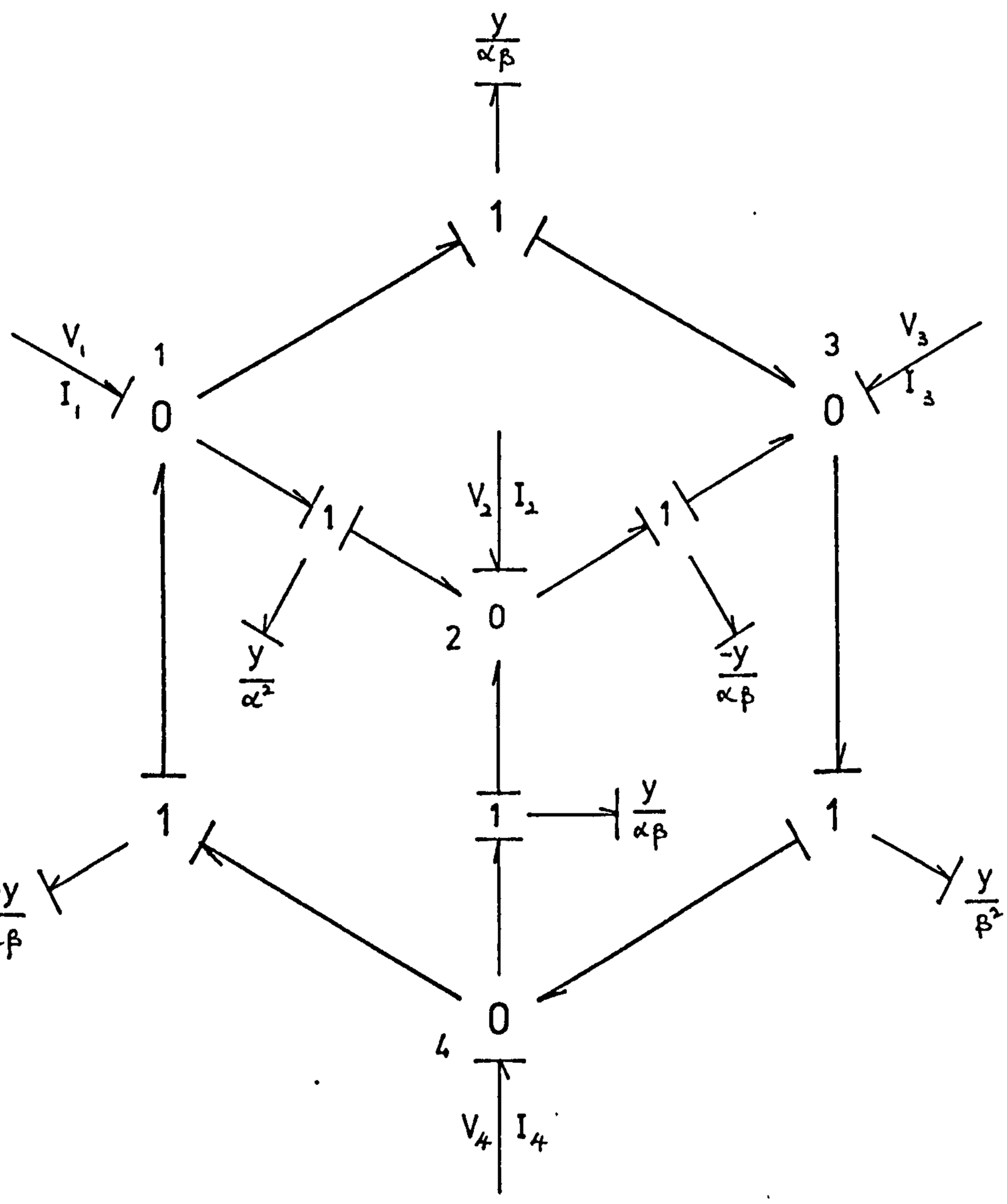

$\alpha = 1 + t_\alpha$

$\beta = 1 + t_\beta$

Fig. 3-5 Equivalent Bond Graph of the Single-Phase Two-Winding Transformer

The equivalent bond graph for the single-phase transformer of Fig. 3-5 may be regarded as consisting of two distinct structures, the hexagonal structure which forms the outer ring and the star structure within this ring. In fact all the multiwinding transformers developed in this chapter possess certain combinations of these structures.

3.3.2 Three-Phase Two-Winding Transformers

In the preceding section, a simple transformer model, shown in Fig. 3-4(b), is used as the basis for constructing a bond graph representation of a single-phase two-winding variable-turns ratio transformer. This structure termed as the equivalent bond graph of the single-phase transformer is shown in Fig. 3-5, and may be used in combinations to represent all the possible three-phase power transformers.

An alternative method involves using directly the simple transformer model mentioned above. Form Fig. 3-4(b), the bond graph for the delta-star transformer may be assembled as shown in Fig. 3-6 by joining the secondary nodes end to end. Following the same procedure for deriving Eqns. 3.20 and using Fig. 3-6, the relationship across the ideal transformer is:

$$\left.\begin{aligned} \frac{V_A - V_N}{1 + t_\alpha} &= \frac{E_t/\sqrt{3}}{1 + t_\beta} \\ \\ \frac{I_A}{1 + t_\beta} &= \frac{I_t/\sqrt{3}}{1 + t_\alpha} \end{aligned}\right\} \qquad 3.26$$

where E_t and I_t are the line-to-line voltage and current respectively between nodes 'b' and 'c'. The current, I_t,

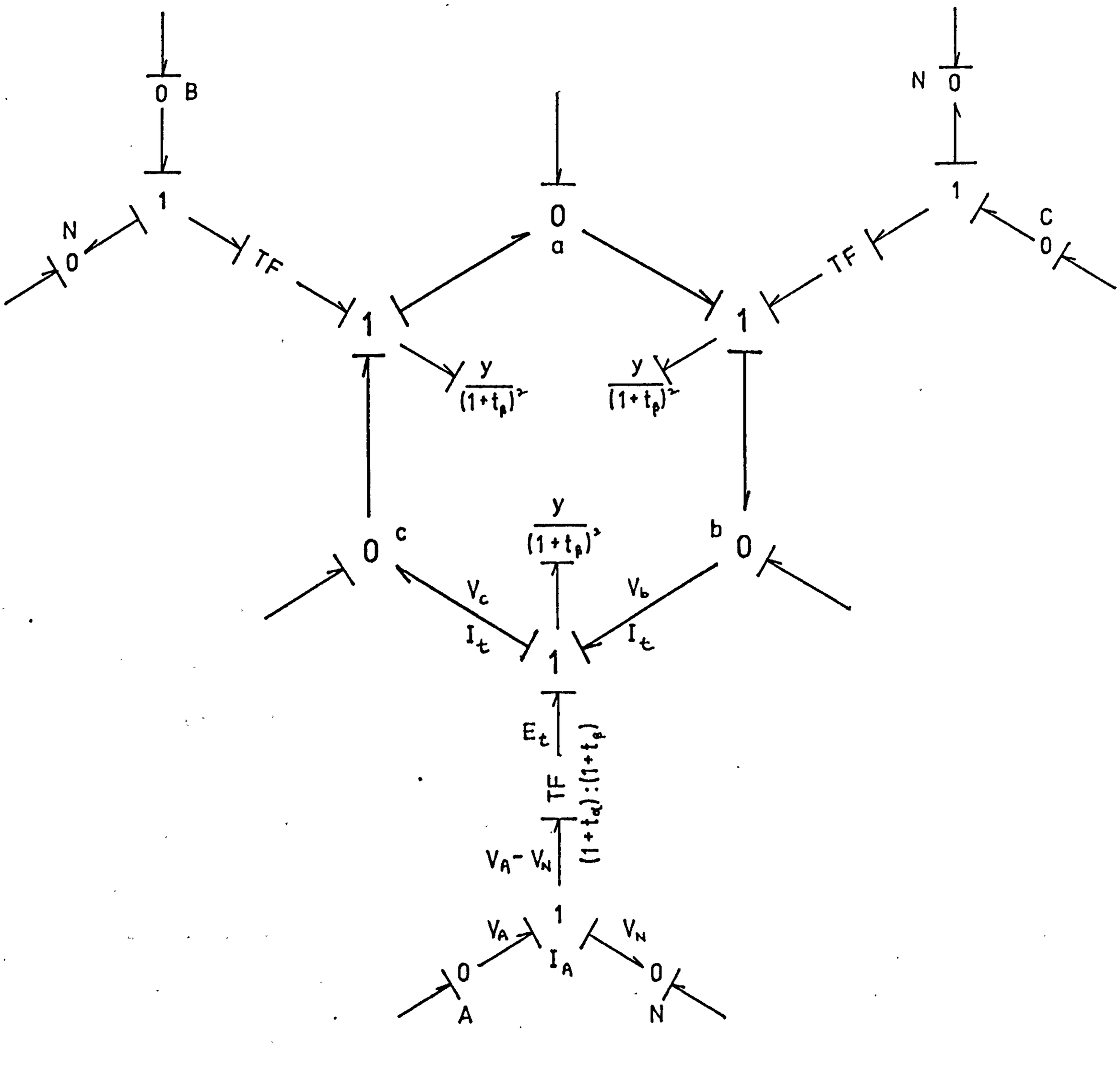

Fig. 3-6 Bond Graph Representation of a Delta-Star Transformer

can be evaluated at the effort junction containing $y/(1 + t_\beta)^2$ as;

$$I_t = (E_t + V_b - V_c) \frac{y}{(1 + t_\beta)^2} \qquad 3.27$$

Using Eqns. 3.26 and 3.27, the current injected into node 'A' may be expressed as:

$$I_A = \left[\frac{y(V_A - V_N)}{(1 + t_\alpha)^2} + \frac{y(V_b - V_c)}{\sqrt{3}(1 + t_\alpha)(1 + t_\beta)} - \right]$$

$$= \left[\frac{y(V_A - V_N)}{\alpha^2} + \frac{y(V_b - V_c)}{\alpha\beta} \right]$$

$$= \left[\frac{y(V_A - V_N)}{\alpha^2} + \frac{y(V_A - V_C)}{\alpha\beta} - \frac{y(V_A - V_b)}{\alpha\beta} \right] \qquad 3.28$$

where $\alpha = (1 + t_\alpha)$ and $\beta = \sqrt{3}(1 + t_\beta)$

Similarly considering nodes, B, C, N, n, a, b and c, the equivalent bond graph of the delta-star transformer may be represented by Fig. 3-7 from which the nodal admittance matrix may be derived. It may be noted that the 0-junction for node 'A' expresses graphically the expanded form of Eqn. 3.28. The neutral although shown as three separate nodes, all labelled N, should in fact be represented by only one common node. This is done to avoid complicating the diagram.

A delta-delta transformer formed from the simplified bond graph of the single-phase transformer of Fig. 3-4(h) is shown in Fig. 3-8. Following the same steps taken for the delta-star transformer, the equivalent bond graph of the delta-delta transformer may be represented by Fig. 3-9.

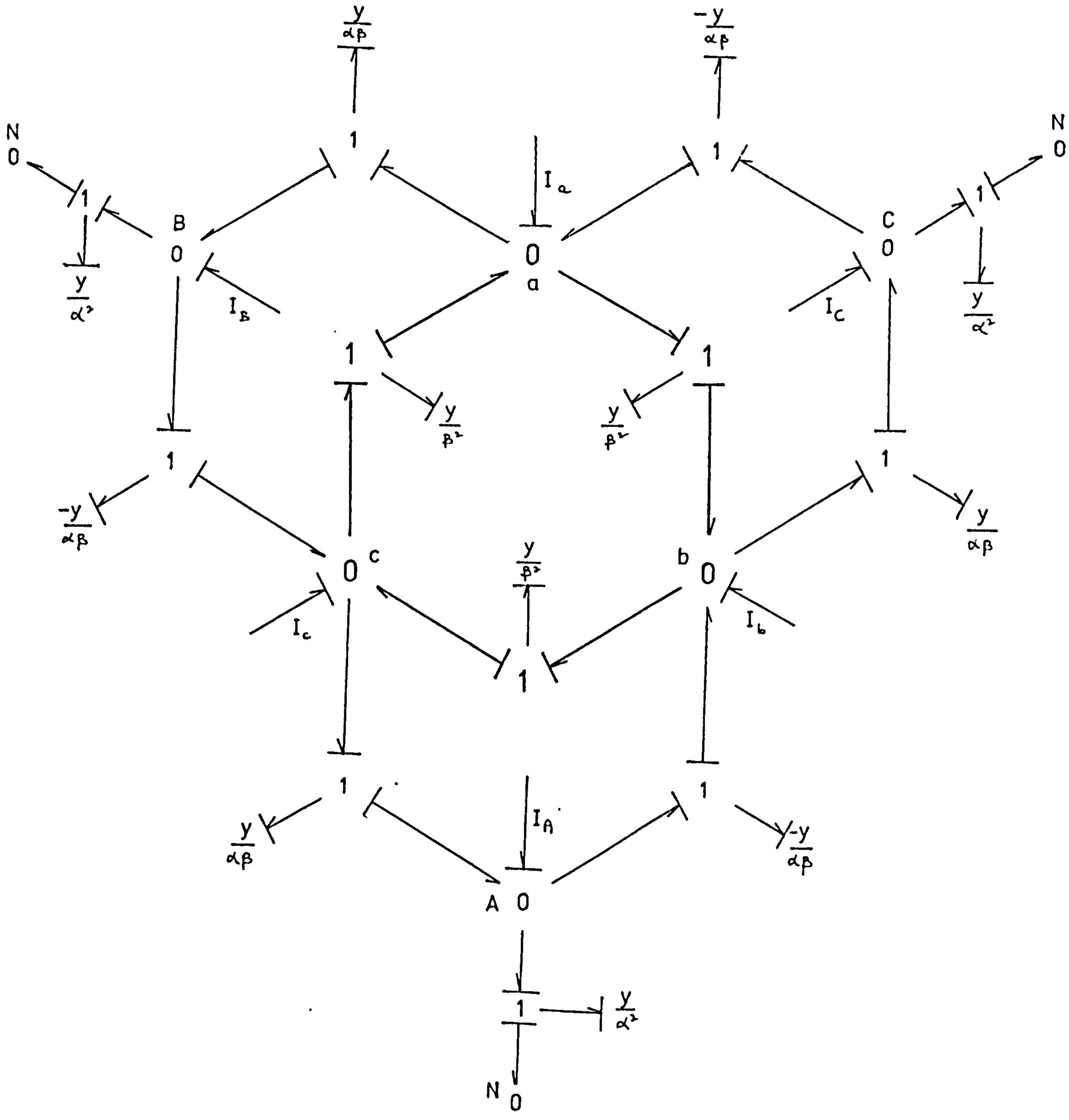

Fig. 3-7 Equivalent Bond Graph of the Delta-Star Transformer

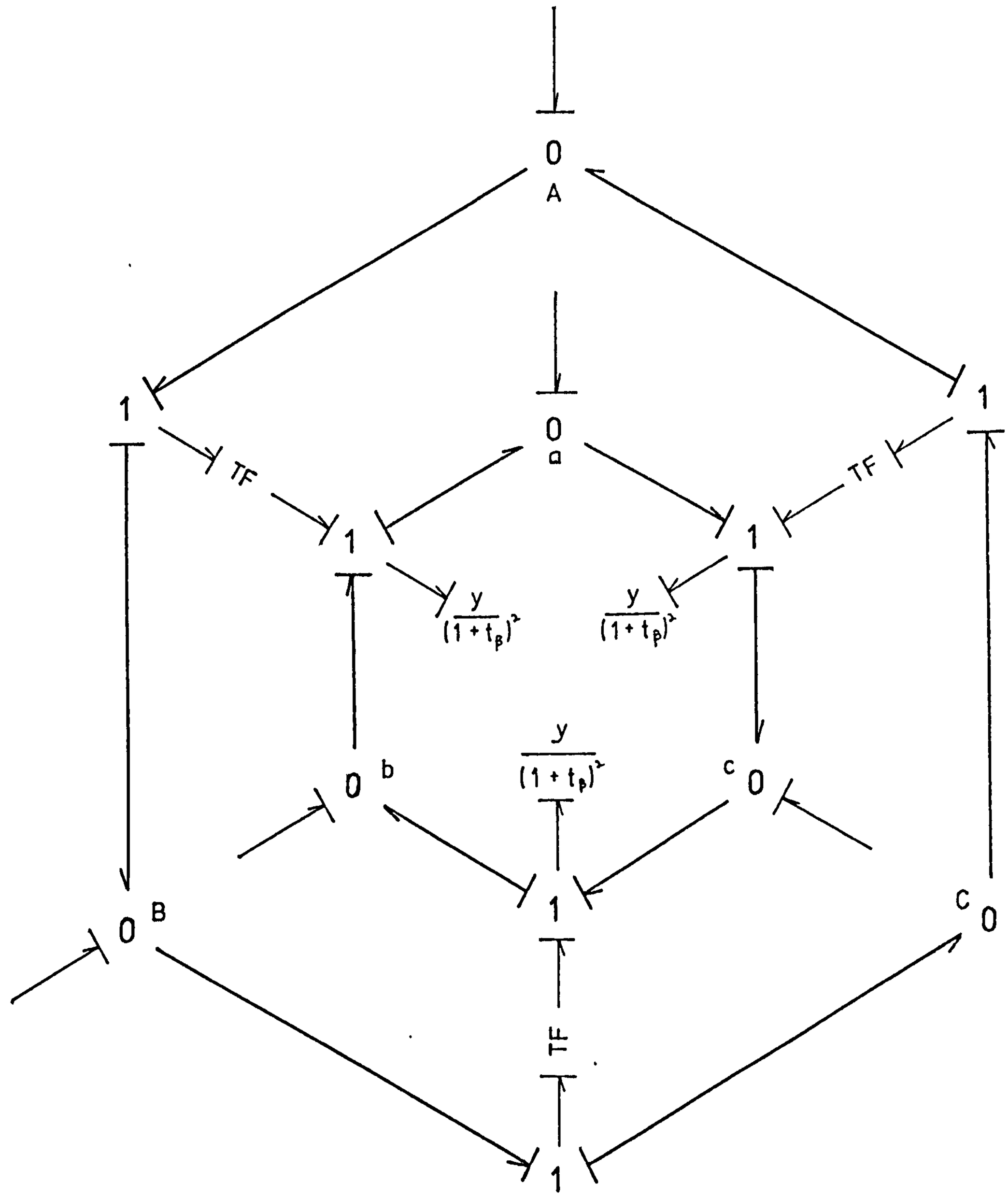

Fig. 3-8 Bond Graph Representation of a Delta-Delta Transformer

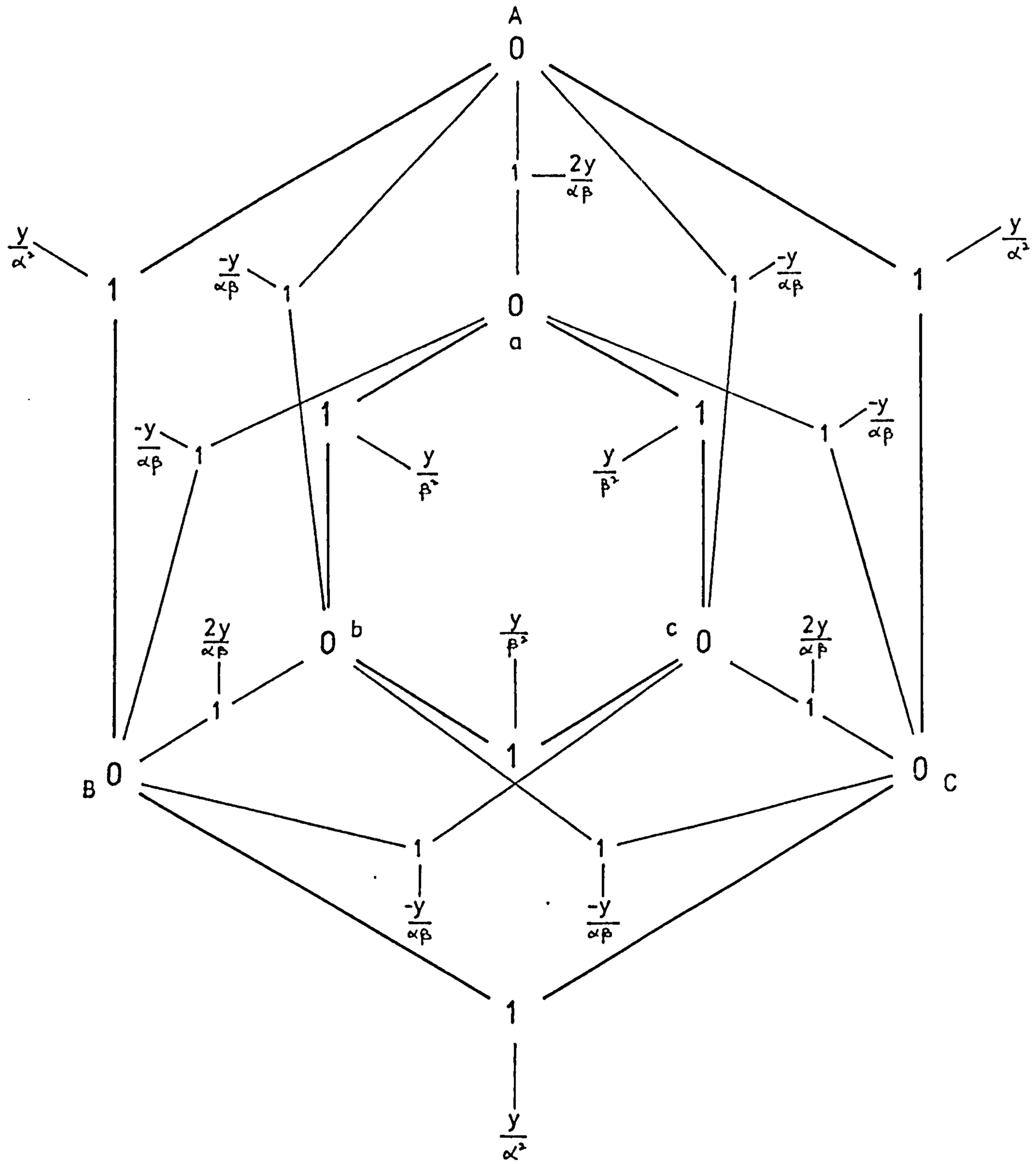

Fig. 3-9 Equivalent Bond Graph of the Delta-Delta Transformer

Since the equivalent bond graph of both the delta-star and delta-delta transformers may be derived directly from the equivalent bond graph of the single-phase transformer, it is not surprising that these three-phase transformers clearly exhibit the presence of both the hexagonal and the star structures. In fact based on these structures the star-star and the open-delta transformer representations may be evolved.

In general the nodal voltage and current equations for the three-phase transformer may be expressed by:

$$\begin{bmatrix} I_{ABC} \\ \\ I_{abc} \end{bmatrix} = \left[\begin{array}{c|c} Y_p & Y_q \\ \hline Y_r & Y_s \end{array}\right] \cdot \begin{bmatrix} V_{ABC} \\ \\ V_{abc} \end{bmatrix} \qquad 3.29$$

where the values of the sub-matrices Y_p, Y_q, Y_r and Y_s are determined by the structure and connection of the three-phase transformer. Using either Fig. 3-4(b) for the simplified bond graph or Fig. 3-5 for the equivalent bond graph of the single-phase transformer and considering the types of transformer connections, the sub-matrices may be found from the bond graphs such as that shown in Figs. 3-7 and 3-9; thus:

a) Delta-Star Earthed

$$Y_p = (y/\alpha^2)1$$

$$Y_q = Y_r = (y/\alpha\beta)\cdot\begin{bmatrix} 0 & 1 & -1 \\ -1 & 0 & 1 \\ 1 & -1 & 0 \end{bmatrix} \qquad 3.30$$

$$Y_s = (y/\beta^2)\cdot\begin{bmatrix} 2 & -1 & -1 \\ -1 & 2 & -1 \\ -1 & -1 & 2 \end{bmatrix}$$

where $\alpha = (1 + t_\alpha)$, $\beta = \sqrt{3}\ (1 + t_\beta)$ and 1 is the unit matrix. The values of α and β take into account the variable turns ratio on both the primary and secondary windings. However, if no tapping is used, t_α and t_β are both zero. For the delta-star transformer with earthed neutral, the bond graph is similar to that of Fig. 3-7 but with the neutral node, N, eliminated since $V_N = 0$.

b) Star-Star Earthed

$$\left.\begin{aligned} Y_p &= (y/\alpha^2)\ 1 \\ Y_q &= Y_r = (-y/\alpha\beta)\ 1 \\ Y_s &= (y/\beta^2)\ 1 \end{aligned}\right\} \qquad 3.31$$

where $\alpha = (1 + t_\alpha)$ and $\beta = (1 + t_\beta)$.

For the cases in which the neutral nodes are not connected directly to earth, the sub-matrices have to be altered accordingly and the nodal voltages and currents are related by:

$$\begin{bmatrix} I_{ABCN} \\ \\ I_{abcn} \end{bmatrix} = \left[\begin{array}{c|c} Y_p' & Y_q' \\ \hline Y_r' & Y_s' \end{array}\right] \cdot \begin{bmatrix} V_{ABCN} \\ \\ V_{abcn} \end{bmatrix} \qquad 3.32$$

where the values of the sub-matrices Y_p', Y_q', Y_r' and Y_s' include new matrix elements from the addition of the two neutral nodes, N and n. However, the rows and column containing these new nodes may be eliminated, thus reducing Eqn. 3.32 to the same form as Eqn. 3.29.

(c) Delta-Delta

$$Y_p = (y/\alpha^2) \cdot \begin{bmatrix} 2 & -1 & -1 \\ -1 & 2 & -1 \\ -1 & -1 & 2 \end{bmatrix} \qquad 3.33$$

$$Y_p = Y_r = -(\alpha/\beta)\ Y_p$$

$$Y_s = (\alpha^2/\beta^2)\ Y_p$$

where $\alpha = \sqrt{3}\ (1 + t_\alpha)$ and $\beta = \sqrt{3}\ (1 + t_\beta)$

(d) Open-Delta

$$Y_p = (y/\alpha^2) \cdot \begin{bmatrix} 2 & -1 & -1 \\ -1 & 1 & 0 \\ -1 & 0 & 1 \end{bmatrix}$$

$$Y_q = Y_r = -(\alpha/\beta)\ Y_p$$

$$Y_s = (\alpha^2/\beta^2)\ Y_p$$

where $\alpha = \sqrt{3}\ (1 + t_\alpha)$ and $\beta = \sqrt{3}\ (1 + t_\beta)$

3.3.3 Three-Phase Three-Winding Transformers

The method developed for representing a single-phase transformer can be extended to three-circuit transformers and autotransformers, and to any multiwinding transformer regardless of the number of circuits. In reference 2 a comprehensive collection of the transformer connection tables is presented. Similar results can be obtained by using appropriate combinations of the equivalent bond graphs for the three-phase two-winding transformers from which the nodal current equations for the three-winding transformers may be derived. As an example, a star-star-delta transformer may be assembled from paralleling one

star-star and two star-delta equivalent transformers, each paralleled in turn.

In the analysis of three-winding transformers, there are occasions when the tertiary variables are of no particular interest to the analyst and as such these may be eliminated using standard matrix reduction formula. The reduced nodal current equations will then have the form shown in Eqn. 3.29 which have not only fewer nodes but may also ensure a better numerical stability in the eventual solution process.

3.4 Energy-Transmitting Devices

When all three phases of an overhead or underground transmission line must be represented, as for example in unsymmetrical fault conditions or for unbalanced loads, a generalized three-wire model will be required, governed by equations of the form:

$$\left.\begin{aligned} \frac{dV}{dx} &= ZI \\ \frac{dI}{dx} &= YV \end{aligned}\right) \qquad 3.35$$

where V and I are the steady-state three-phase voltage and current matrices while Z and Y are the series impedance and shunt admittance matrices, respectively. The variable, x, measures the distance along the line from the receiving end.

These generalized transmission line equations include the effects of mutual electrostatic and electromagnetic induction between phase wires and with respect to the ground plane. For design and operating studies over a

range of conditions at normal system frequency, such lines may be effectively represented in an 'equivalent pi' model. Furthermore, leakage conduction is generally very small, so that a simple -C-L-R-C- equivalent circuit can be employed, which permits the terminal capacitances to be added at each system node.

3.4.1 Basic Single-Phase Transmission Line

The general form of Eqn. 3.35 may be modified to consider the solution of the single-phase transmission line with the impedance and admittance uniformly distributed as shown in Fig. 3-10 where zdx is the series impedance of an elemental length of the line, and ydx is its shunt admittance.

The solved differential equations for the phase voltage and current at any point on the line may be expressed in hyperbolic functions as[13]:

$$\left.\begin{aligned} V &= V_r \cosh \gamma x + I_r Z_c \sinh \gamma x \\ I &= I_r \cosh \gamma x + \frac{V_r}{Z_c} \sinh \gamma x \end{aligned}\right) \qquad 3.36$$

where V_r and I_r are the receiving end voltage and current respectively; $Z_c = \sqrt{z/y}$ is the characteristic impedance; $\gamma = \sqrt{yz}$ is the propagation constant and x is the point on the line from the receiving end.

In most cases it is convenient to consider the uniformly distributed transmission line as a configuration of lumped parameters and this may be achieved by finding the equivalent circuit which represents the line accurately in so far as measurements at the ends of the line are concerned. For the purpose of the present study the

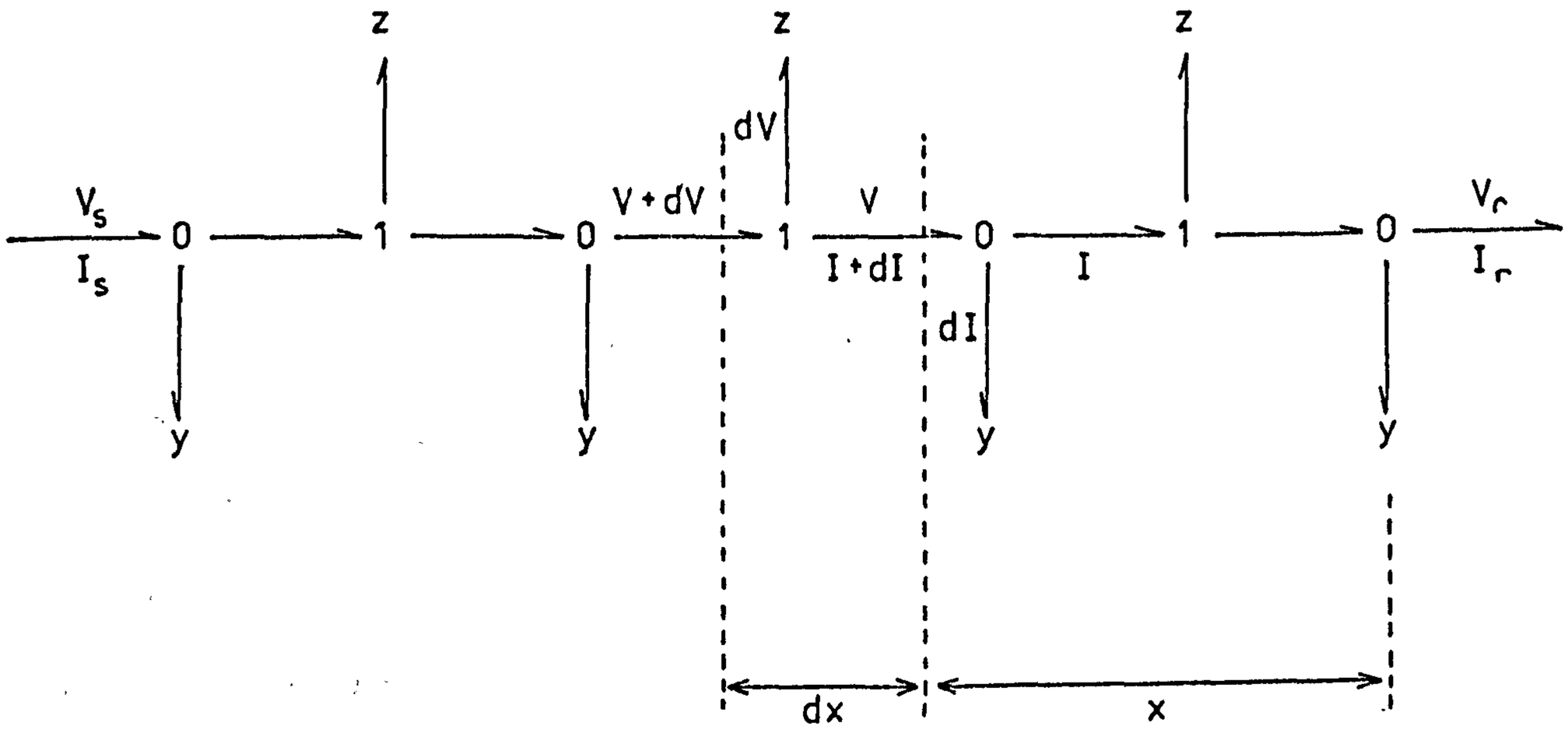

Fig. 3-10 Bond Graph Representation of a Transmission Line with Uniformly Distributed Impedance and Admittance

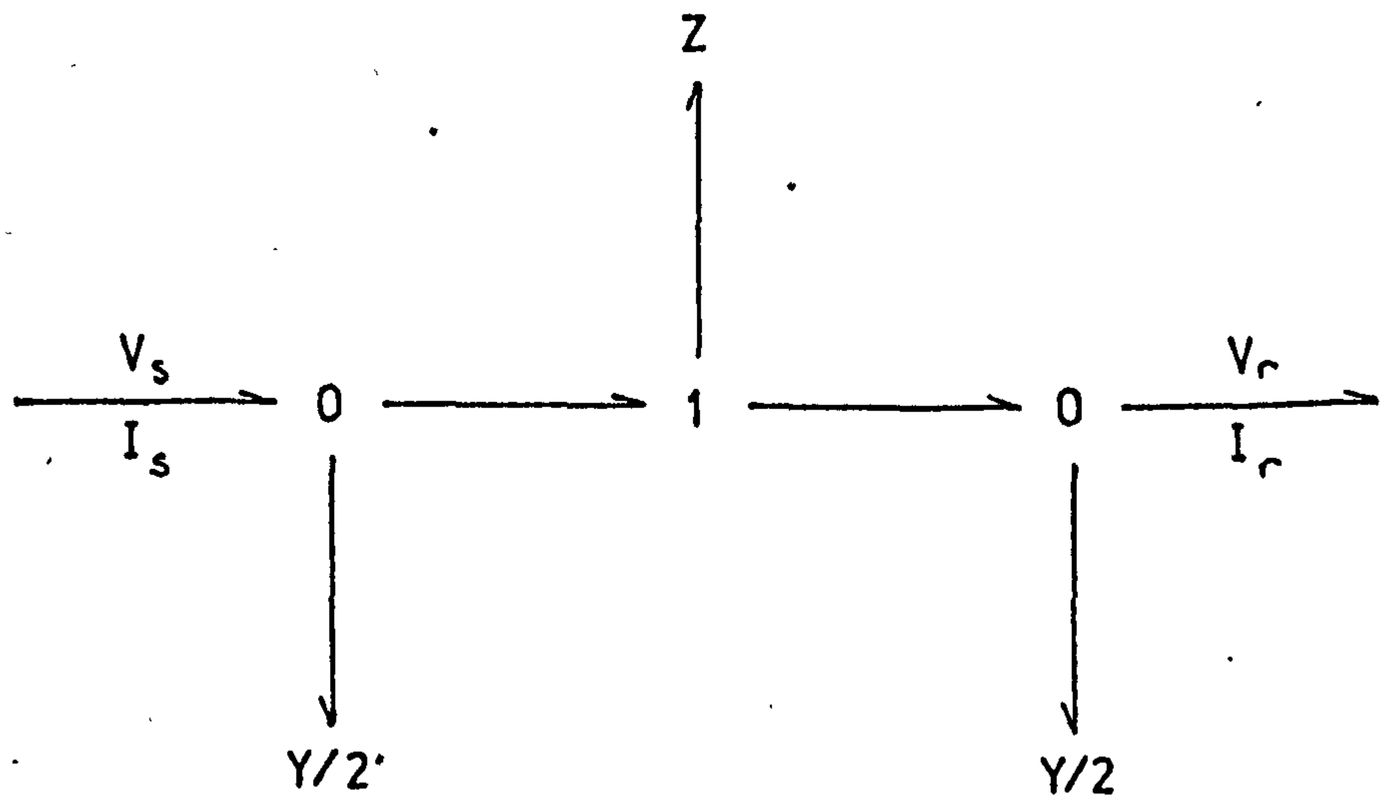

Fig. 3-11 Bond Graph Representation of the Equivalent-Pi Transmission Line

equivalent pi model is used and is shown in Fig. 3-11. The series impedance, Z, and shunt admittance, Y/2 can be derived as[13],

$$\left.\begin{aligned} Z &= Z_s \frac{\sinh \gamma\ell}{\gamma\ell} \\ \text{and} \quad \frac{Y}{2} &= \frac{Y_s}{2} \frac{\tanh \alpha\ell}{\gamma\ell} \end{aligned}\right\} \qquad 3.37$$

where $Z_s = z\ell$ is the total series impedance of the line of length ℓ and $Y_s = y\ell$ is its total shunt admittance.

The ABCD constants which are widely used in power system analysis can adequately describe the characteristic of the transmission line. These constants relate the sending and receiving end variables as follows:

$$\begin{bmatrix} V_s \\ I_s \end{bmatrix} = \left[\begin{array}{c|c} A & B \\ \hline C & D \end{array}\right] \cdot \begin{bmatrix} V_r \\ I_r \end{bmatrix} \qquad 3.8$$

where V_s and I_s are the sending end voltage and current respectively. For the equivalent pi representation, the ABCD constants may be defined as:

$$\left.\begin{aligned} A &= \cosh \gamma\ell \\ B &= Z_c \sinh \gamma\ell \\ C &= \frac{1}{Z_c} \sinh \gamma\ell \\ D &= \cosh \gamma\ell \end{aligned}\right\} \qquad 3.39$$

The constants of long transmission lines involve hyperbolic functions of $\gamma\ell$, where $\gamma\ell$ is complex. Evaluation of the hyperbolic functions can be tedious and time consuming; however, a set of charts have been published[14] from which

the real and imaginary components of the complex ABCD constants can be read.

3.4.2 Three-Phase Transmission Lines

A three-phase transmission line represented only by the series impedance, Z_{abc}, may have current equations of the form:

$$\begin{bmatrix} I_{ABC} \\ I_{abc} \end{bmatrix} = \left[\begin{array}{c|c} Y_1 & Y_2 \\ \hline Y_3 & Y_4 \end{array}\right] \cdot \begin{bmatrix} V_{ABC} \\ V_{abc} \end{bmatrix} \qquad 3.40$$

where the sub-matrices $Y_1 = Y_4 = Z_{abc}^{-1}$ and $Y_2 = Y_3 = -Z_{abc}^{-1}$; V_{ABC} and V_{abc} are column sub-matrices representing the voltages along the conductors carrying the currents in the sub-matrices I_{ABC} and I_{abc}, respectively. The effects of earth wires may be included in Y_1, Y_2, Y_3 and Y_4 since the extra nodes imposed by the addition of these new conductors can be eliminated by matrix reduction formula resulting in the final equation having the same form as Eqn. 3.40.

In the equivalent pi model with one half of the transmission line equivalent shunt admittance, Y, connected to each end of the line, Eqn. 3.40 can be modified as:

$$\begin{bmatrix} I_{ABC} \\ I_{abc} \end{bmatrix} = \left[\begin{array}{c|c} Y_1+\frac{Y}{2} & Y_2 \\ \hline Y_3 & Y_4+\frac{Y}{2} \end{array}\right] \cdot \begin{bmatrix} V_{ABC} \\ V_{abc} \end{bmatrix} \qquad 3.41$$

For the three-phase transmission line whose characteristics are described by the ABCD constant, the voltage and current relationships may be written as:

$$\begin{bmatrix} V_{ABC} \\ I_{ABC} \end{bmatrix} = \left[\begin{array}{c|c} A & B \\ \hline C & D \end{array}\right] \cdot \begin{bmatrix} V_{abc} \\ I_{abc} \end{bmatrix} \qquad 3.42$$

which can be modified to the same form as Eqn. 3.40 and given by:

$$\begin{bmatrix} I_{ABC} \\ I_{abc} \end{bmatrix} = \left[\begin{array}{c|c} DB^{-1} & C-DB^{-1}A \\ \hline B^{-1} & -B^{-1}A \end{array}\right] \cdot \begin{bmatrix} V_{ABC} \\ V_{abc} \end{bmatrix} \qquad 3.43$$

The similarity between the three-phase and single-phase impedance/admittance matrices is evident - each element in the single-phase matrix is replaced by the appropriate 3 x 3 impedance/admittance sub-matrix. The bond graph of the transmission line described by either Eqns. 3.41 or 3.43 has the same structure as the delta-delta transformer of Fig. 3-9, but with $\alpha = \beta = 1.0$.

3.5 Energy Transducers

The representation of loads appropriate to the subject of investigation is an important requirement in system studies and basically at least two different approaches are possible. For any group of loads, curves of the steady-state demand of MW and MVAr as a function of voltage and frequency can be derived. However, although in dynamic studies both may vary and as such influence the outcome of the result, in fault studies this form of representation is quite adequate. An alternative approach is to represent the load as consisting of a combination of

constant impedance loads and motors. There are many possible variations of this method and in this section the loads will be categorised into separate passive and active loads.

As the phase frame of reference will be used throughout this chapter, the loads have to be represented by their equivalent three-phase obtained from the usual one-line diagram. Also the load admittance must be expressed in a form suitable for incorporating into the general nodal admittance equations, thus:

$$YV = I \qquad 3.44$$

where Y is the nodal admittance matrix and represents the admittances in and between all three phases of the system; V and I are the phase voltage and current column matrices respectively.

3.5.1 Passive Loads

This group embraces those loads having constant impedance which is not a function of system voltage or frequency and is comparatively simple to represent in fault studies. For any node k and with the load represented by the complex phase power, S_k, the phase current injected into the node is given by:

$$I_k = \frac{S^*_k}{V_k} \qquad 3.45$$

where S^*_k is the conjugate of the complex power and V_k is the phase-to-earth voltage. If a load can be characterised by a passive admittance per phase, y_{ko}, Eqn. 3.45 becomes

$$I_k = y_{ko} V_k \qquad 3.46$$

By substituting Eqn. 3.46 into Eqn. 3.44 it can be shown that for passive loads the passive admittances are added to the diagonal elements of Y of Eqn. 3.44. If the load has unequal positive-, negative- and zero-sequence admittances the 3 x 3 passive admittance matrix formed to replace y_{ko} has to be transferred to supplement the appropriate block diagonal 3 x 3 sub-matrix of Y.

3.5.2 Active Loads

The main consituents of the active loads in power system studies are the synchronous and induction motors. The synchronous motors are used where large loads are to be driven, where high or variable power factors are needed, where frequent partial voltage dips occur and the motor must ride through these, where maximum clearance is needed between the moving and fixed parts, and where a number of drives must act exactly in step. For many industrial drives where a simple, reliable machine is the first requirement induction motors are used.

The equations governing the phase currents injected into a star-connected synchronous or induction motor with an impedance earthed neutral are[3]:

$$\begin{bmatrix} I_a \\ I_b \\ I_c \\ I_n \end{bmatrix} = \begin{bmatrix} Y_{aa} & Y_{ab} & Y_{ac} & -y_o \\ Y_{ba} & Y_{bb} & Y_{bc} & -y_o \\ Y_{ca} & Y_{cb} & Y_{cc} & -y_o \\ -y_o & -y_o & -y_o & Y_N \end{bmatrix} \cdot \begin{bmatrix} V_a \\ V_b \\ V_c \\ V_n \end{bmatrix} - \begin{bmatrix} y_1 E_a \\ y_1 E_b \\ y_1 E_c \\ -y_o E_n \end{bmatrix} \qquad 3.47$$

where I_n is the current injected into neutral node n, and is usually zero, E_n is the sum of the phase emfs, and is also zero since $E_n = E_a + E_b + E_c = 0$, y_o and y_1 are the zero- and positive-sequence admittances of the motor respectively and $Y_N = 3y_o + Y_{nn}$, where Y_{nn} is the earth admittance. The remaining admittance matrix elements are defined by the phase admittance matrix Y_{abc} as in Eqn. 3.13.

In general, Eqn. 3.47 may be written as:

$$I_{abcn} = -y_1 E_{abcn} + Y_{abcn} V_{abcn} \qquad 3.48$$

where E_{abcn} is the matrix for the equivalent voltage sources per phase including the neutral and V_{abcn} is the matrix of voltages at the terminal nodes and the neutral. With the appropriate sign change to account for motor action, it is evident that Eqn. 3.14 for the synchronous generator and Eqn. 3.48 have the same form. Thus, the basic representation used is an infinite system acting behind a reactance appropriate to the system contribution to fault level. The bond graph of Fig. 3-2 may be used to represent the active load by modifying the direction of the power flow.

The currents expressed in Eqn. 3.48 can be substituted into Eqn. 3.44 and by transferring the Y_{abcn} V_{abcn} terms to the left-hand side, Eqn. 3.44 becomes

$$Y'V' = I' \qquad 3.49$$

where Y' is the supplemented phase admittance matrix and I' is a column matrix whose elements are of the form $y_1 E$ or are zero.

3.6 Bond Graphs and Phase Co-ordinate Analysis

The symmetrical component theory has always been generally used in unbalanced fault studies using digital computers. However, difficulties may arise from problems associated with untransposed transmission lines and other unbalanced system components, or faults where the number of phases is greater than three, as in rectifier transformers or less than three, as in many distribution system feeders, and the analysis of simultaneous faults at different locations in the system. As such there is a need to represent systems in terms of the actual variables instead of the transformed quantities used in symmetrical component methods.

Using the bond graph models developed, the physical identity of the system is preserved and the actual phase voltages, currents and impedances may be used directly avoiding the necessity to transform into the symmetrical component co-ordinates.

In the method of phase co-ordinates, the general form of the nodal admittance equations, shown in Eqn. 3.44, is often preferred. In order to account for the generator and load admittances the equations are modified resulting in the formation of the supplemented nodal phase admittances matrix as shown in Eqn. 3.49.

The procedure to form the supplemented nodal phase admittance matrix from the matrices representing the system components, may be illustrated by considering the sample power system shown in Fig. 3-12. The component matrices derived in previous sections are obtained from bond graph models which ensure that the causalities of

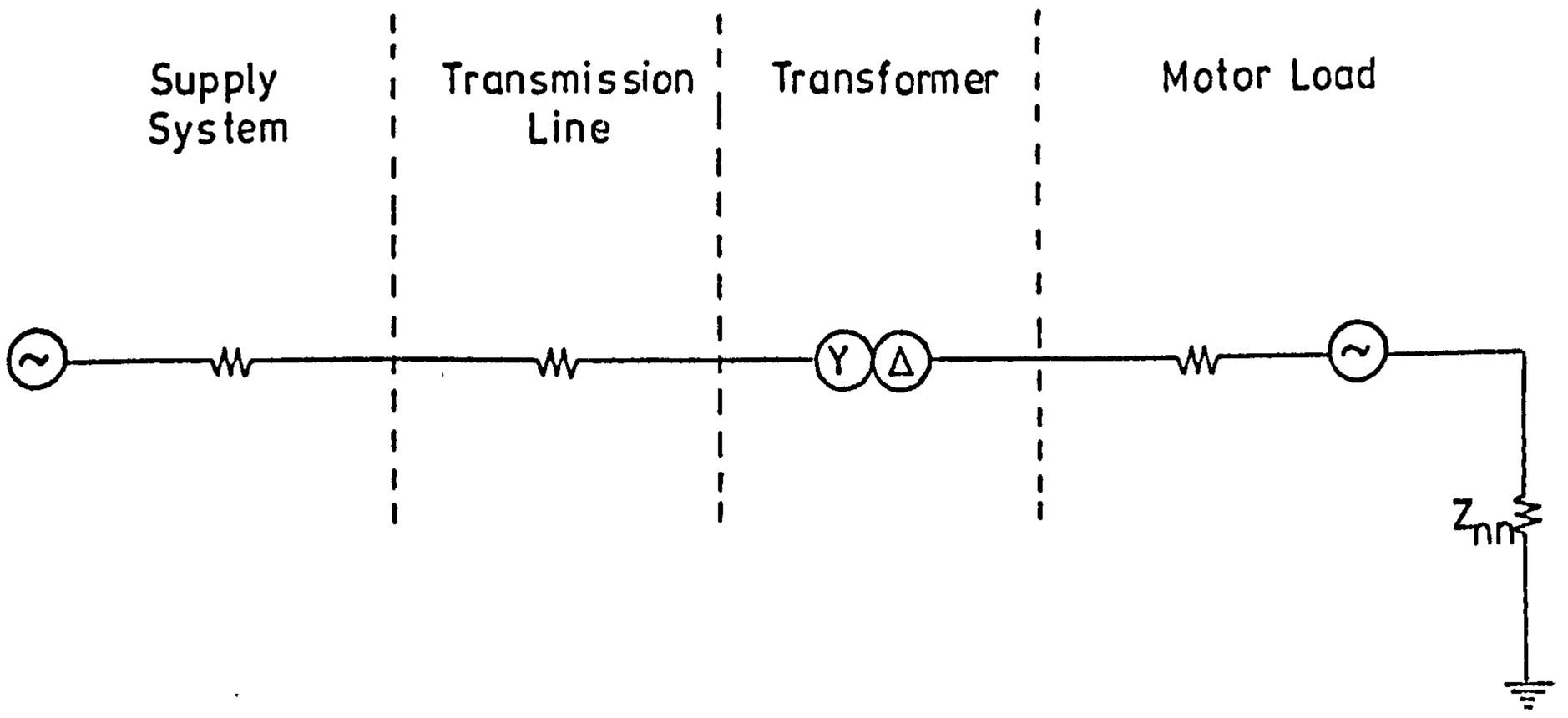

Fig. 3-12 One-Line Diagram of a Sample Power System

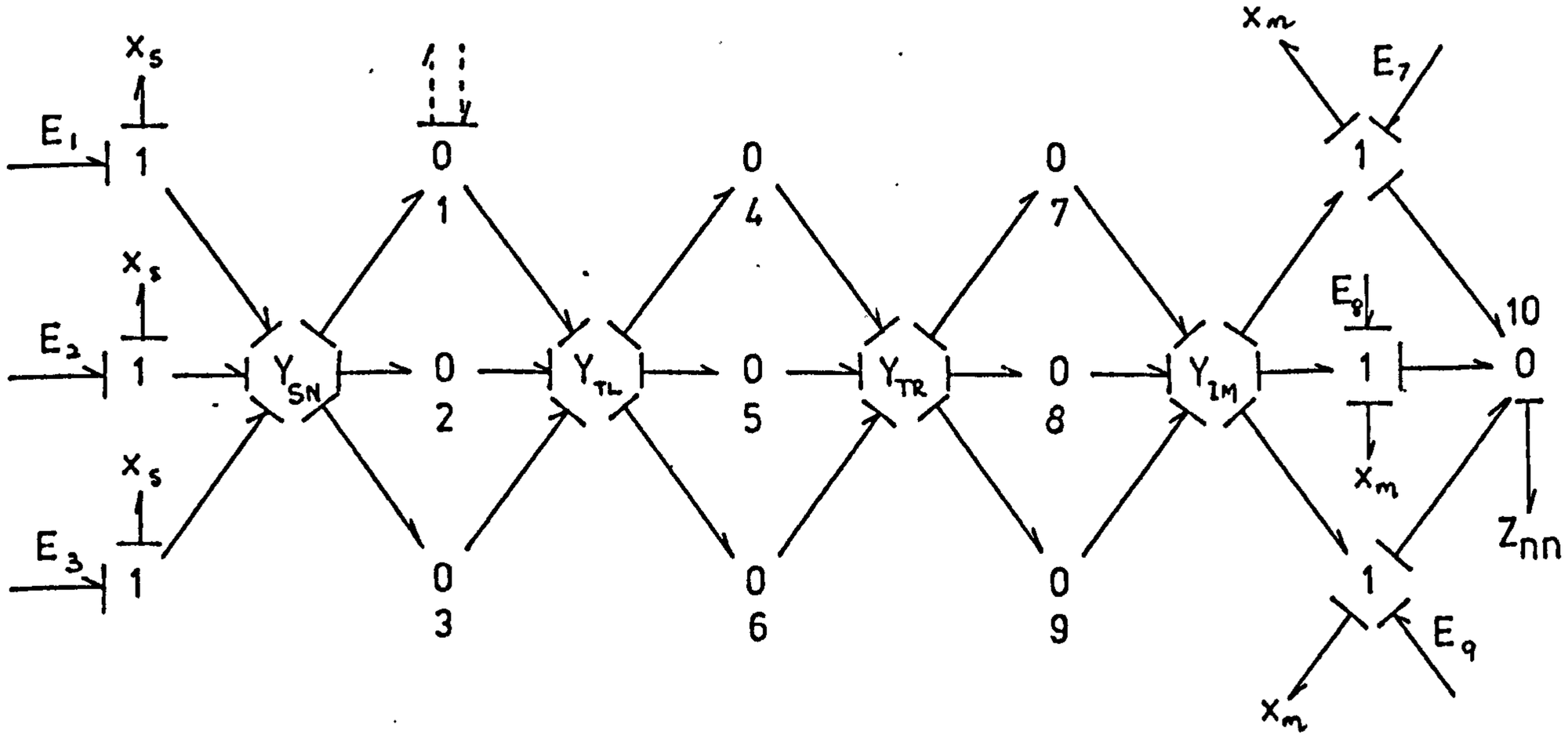

Fig. 3-13 Bond Graph Representation of the Sample Power System

these admittance matrices are as shown in Fig. 3-13. Taking the current injected into each component as positive and vice-versa, the resultant prefault nodal current at each of the numbered node from 1 to 10 is zero.

The nodal admittance matrix for the ten nodes may be formed[13] with the values of the diagonal and off-diagonal elements dictated by the manner in which the system components are connected. In the bond graph of Fig. 3-13, the causalities of the voltage sources for both the synchronous generator and the induction motor are valid and as such the supplemented nodal phase admittance matrix can be formed by incorporating the component matrices, Y_{SN} and Y_{IM}, into the nodal admittance matrix.

From Eqns. 3.14, 3.29, 3.40 and 3.47 defining the component matrices for synchronous generator, transformer, transmission line and induction motor respectively, the supplemented nodal phase admittance matrix for the sample system of Fig. 3-12 may be expressed as:

$$\begin{bmatrix} Y_{SN}+Y_{TL} & -Y_{TL} & 0 & 0 \\ -Y_{TL} & Y_{TL}+Y_p & Y_q & 0 \\ 0 & Y_r & Y_s+Y_{IM} & -3Y_o \\ 0 & 0 & -Y_o 1 & Y_N \end{bmatrix} \cdot \begin{bmatrix} V_{123} \\ V_{456} \\ V_{789} \\ V_{10} \end{bmatrix} = \begin{bmatrix} Y_s E_{123} \\ 0 \\ Y_m E_{789} \\ 0 \end{bmatrix} \qquad 3.50$$

where the sub-matrices Y_p, Y_q, Y_r and Y_s for the delta-star earthed transformer are defined in Eqn. 3.30 and 1 is the unit matrix. The system equations written as in Eqn. 3.50 is suitable for solution by the method of phase co-ordinates using the available computer methods[17].

3.6.1 Computer Methods for Steady-State Analysis

The nodal admittance matrix methods[3,15,16] for fault analysis using digital computers are often superior to that of the mesh method of analysis which are difficult to code in system terms. The advantage of using the nodal admittance matrix is further enhanced when the method of solution requires the phase co-ordinate approach.

A computer program based on this approach has been successfully used for the analysis of all types of fault conditions including simultaneous faults at different geographical locations. This program requires a core storage of 150K for a seventy nodes problem. A modified version of this program specially adapted for use on ICL 1900 series machines and suitable only for earth fault solutions has been developed using overlaid technique resulting in a reduction of the core storage to 48K for the same problem. The details of this package program, labelled as PHASECO, are included in Appendix A.

Viewed in the present context only phase-to-earth faults will be considered in this chapter. There are two possible approaches to the solution of this type of fault, namely, the distributed source method and the source transformation method.

3.6.2 Distributed Source Method

The prefault equations in the form of Eqn. 3.49 is the general expression for Eqn. 3.50. The structures and elements of the supplemented nodal phase admittance matrix, Y', depend upon the nature and connection modes of the components which constitute the complete power system.

For the solution of earth faults by distributed source method, Eqn. 3.49 is rearranged and for the kth node, the voltage may be expressed as:

$$^{p+1}V_k = \frac{1}{Y'_{kk}} \left(Y_k E_k - \sum_{m=1}^{k-1} Y'_{km} {}^{p+1}V_m - \sum_{m=k+1}^{n} Y'_{km} {}^{p}V_m\right) \qquad 3.51$$

where y_k and E_k are the source admittance and emf respectively at node k, Y'_{kk} is the kth principal diagonal element of the supplemented nodal admittance matrix, $^{p+1}V_k$ is the fault voltage at node k after p+1 iterations. The term $y_k E_k$ is zero for nodes other than those with synchronous generators or active loads. The fault voltages are constrained to zero for all the nodes where phase-to-earth short-circuits occur.

The short circuit currents for multiphase earth faults occurring at nodes q and r may be solved by constraining the voltages V_q and V_r to zero in Eqn. 3.51 and can be represented by:

$$\left.\begin{aligned} I_q(sc) &= \sum_{m=1}^{n} Y'_{qm} V_m - I'_q \\ I_r(sc) &= \sum_{m=1}^{n} Y'_{rm} V_m - I'_r \end{aligned}\right) \qquad 3.52$$

where I_q and I_r are the prefault currents as expressed in Eqn. 3.49, Y'_{qm} and Y'_{rm} are the elements of the qth and rth row of the matrix Y'.

3.6.3. Source Transformation Method

This method applies the Norton's theorem, or superposition methods[18], and requires that the supplemented nodal impedance matrix, Z', be obtained by inverting Y'.

If the voltage drop caused by the fault current is known, this current may be determined for an equivalent current source acting alone at the point of fault. The fault conditions are obtained by superposition. Under earth fault conditions, the voltage drop at the faulted node prior to analysis is known and may be effectively used in this method.

From the supplemented nodal impedance matrix structure:

$$Z' = Y'^{-1} = \begin{bmatrix} Z'_{11} & Z'_{12} \cdots Z'_{1q} \cdots Z'_{1r} \cdots Z'_{1n} \\ Z'_{21} & Z'_{22} \cdots Z'_{2q} \cdots Z'_{2r} \cdots Z'_{2n} \\ \vdots & \vdots \quad \vdots \quad \vdots \quad \vdots \\ Z'_{q1} & Z'_{q2} \cdots Z'_{qq} \cdots Z'_{qr} \cdots Z'_{qn} \\ \vdots & \vdots \quad \vdots \quad \vdots \quad \vdots \\ Z'_{r1} & Z'_{r2} \cdots Z'_{qr} \cdots Z'_{rr} \cdots Z'_{rn} \\ \vdots & \vdots \quad \vdots \quad \vdots \quad \vdots \\ Z'_{n1} & Z'_{n2} \cdots Z'_{nq} \cdots Z'_{nr} \cdots Z'_{nn} \end{bmatrix} \qquad 3.53$$

the short-circuit currents can be found for simultaneous earth faults at nodes q and r as:

$$\begin{bmatrix} I_q(sc) \\ I_r(sc) \end{bmatrix} = \begin{bmatrix} Z'_{qq} & Z'_{qr} \\ Z'_{rq} & Z'_{rr} \end{bmatrix}^{-1} \cdot \begin{bmatrix} V_q \\ V_r \end{bmatrix} \qquad 3.54$$

where V_q and V_r are the respective prefault phase-to-earth voltages and I_q and I_r are the fault currents injected into nodes q and r.

The short-circuit currents can be solved from Eqn. 3.54 and the node voltages may then be derived by superposition of the voltages, due to the short-circuit current I_j acting alone, onto the prefault voltages V_i; thus:

$$V_i(sc) = V_i + \sum_j Z'_{ij} I_j(sc) \qquad 3.55$$

where i = 1,2,3...n and j = q,r.

3.6.4 Results of Analysis

In order to prove the validity of the various component models developed, results of three-phase fault studies of a test power system, consisting of six generators, twelve transformers, seventeen transmission lines and nine passive loads, are compared with those obtained by other methods, namely:

i) Nodal iterative method[13] whose nodal admittances are obtained from the one-line diagram, and

ii) Source transformation method using the nodal impedance matrix derived by inverting the nodal admittance matrix from (i).

A schematic representation of the test power system used in the analysis is shown in Fig. 3-14 where the components are described by their respective matrices. With the appropriate causalities imposed on the system, the supplemented nodal admittance matrix similar to that of Eqn. 3.50 may be derived. The package program PHASECO, developed for earth fault studies, is used to analyse the system under three-phase symmetrical fault conditions using both the distributed source and the source transformation methods. The results are as shown in Table 3-1.

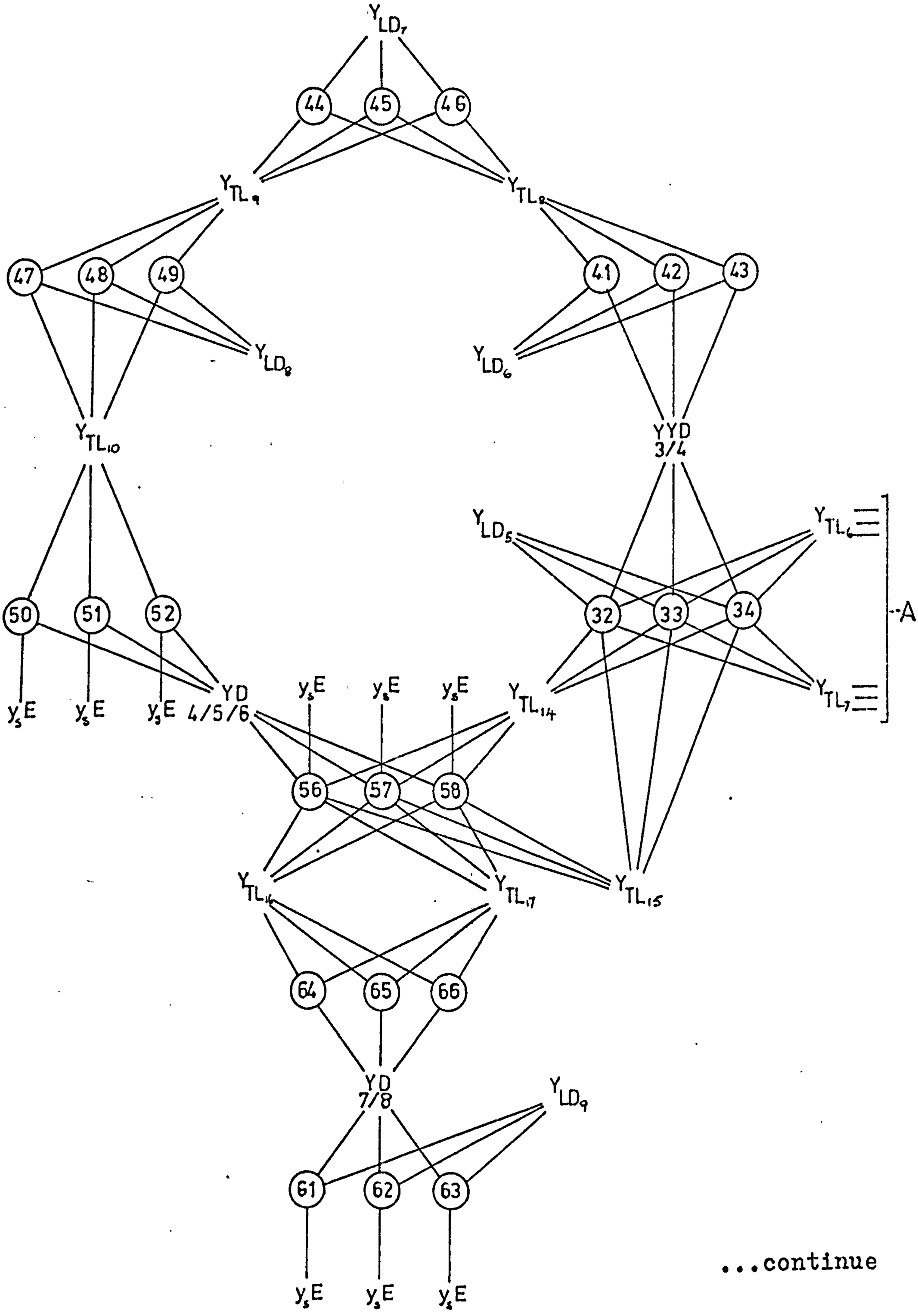
Y_{LD_7}
44
45
46
Y_{TL_9}
Y_{TL_8}
47
48
49
41
42
43
Y_{LD_8}
Y_{LD_6}
$Y_{TL_{10}}$
YYD 3/4
Y_{LD_5}
Y_{TL_6}
50
51
52
32
33
34
A
Y_{TL_7}
YD 4/5/6
y_sE
$Y_{TL_{14}}$
56
57
58
$Y_{TL_{16}}$
$Y_{TL_{17}}$
$Y_{TL_{15}}$
64
65
66
YD 7/8
Y_{LD_9}
61
62
63

...continue

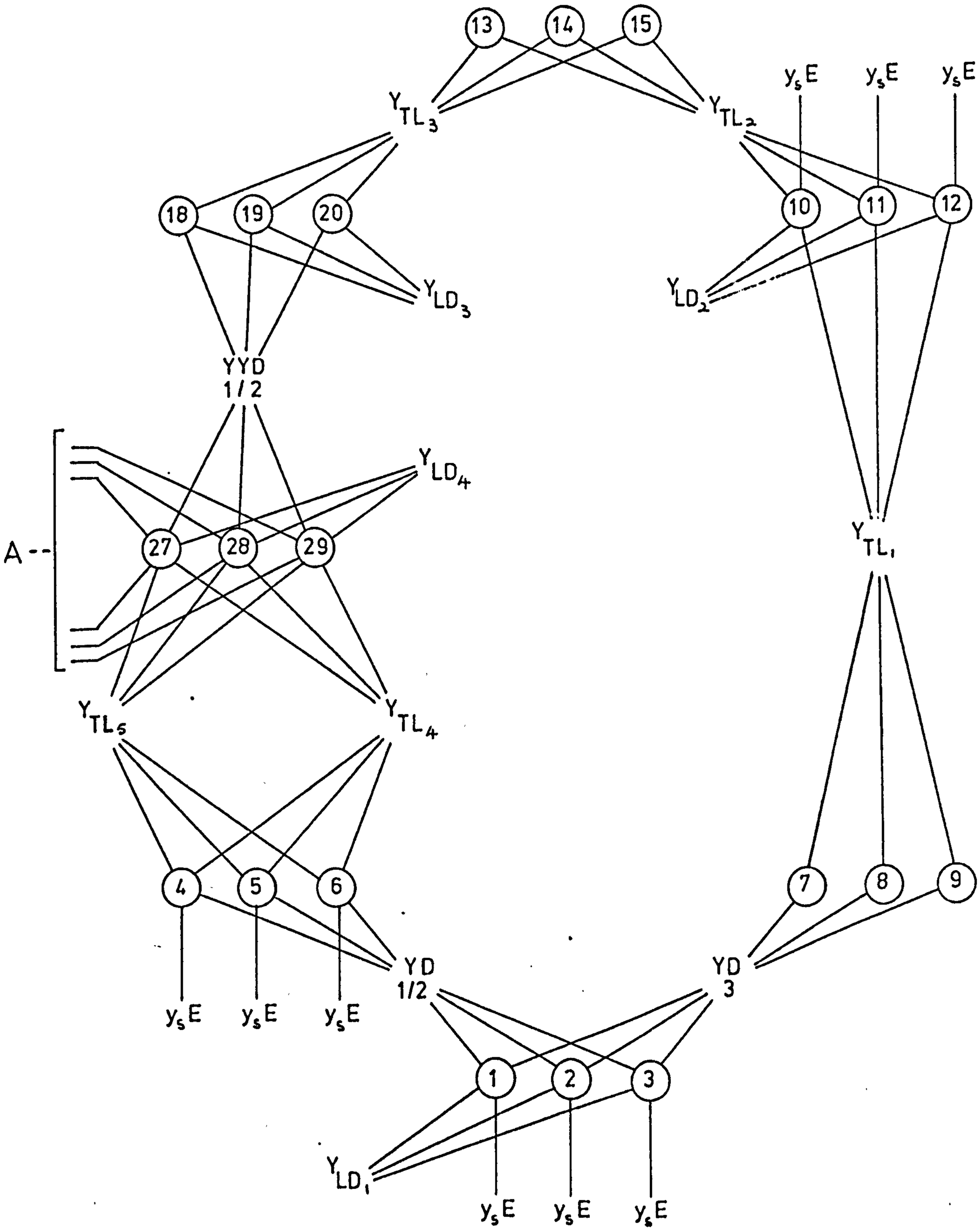

Fig. 3-14 A Schematic Representation of the Power System used in the Analysis

Table 3-1 Fault Levels (MVA) for 3-P Short-Circuit— Three-Winding Transformers Represented by all their Windings

Faulted Nodes	4/5/6	18/19/20	27/28/29	50/51/52	56/57/58
Method (i)	1445	463	1397	1410	1728
Method (ii)	1476	480	1425	1400	1791
Distributed Source	1413	525	1373	1326	1701
Source Trans.	1413	525	1373	1326	1701

In the above table the discrepancies in the results obtained from methods (i) and (ii) may be due to the use of different programs, solved by entirely two different computers. Apart from this there are relatively good agreements between the methods used. The three-winding transformers shown in Fig. 3-14 as YYD(1/2) and YYD(3/4) have tertiary windings which are not connected to any other system component. Thus the models for these transformers may be simplified by neglecting the tertiary windings. The results shown below validate this assumption.

Table 3-2 Fault Levels (MVA) for 3-P Short-Circuit— Three Winding Transformers Represented by only Two Windings

Faulted Nodes	4/5/6	18/19/20	27/28/29	50/51/52	56/57/58
Distributed Source	1406	439	1358	1325	1697
Source Trans.	1406	439	1358	1325	1697

One of the main advantages of using the phase co-ordinate method is that symmetrical as well as unsymmetrical fault problems can be solved with minor or no alteration to the nodal admittance/impedance matrix. As such a unified approach subjected to appropriate constraints may be used to deal with all types of fault conditions.

3.7. Conclusions

In this chapter bond graph models of power system components have been derived from the general n-port electromagnetic field system described in Chapter 2. This system may not be used in its original form, but by appropriately restructuring the system a whole family of electromagnetic devices may be evolved. Perhaps, this is hardly surprising since the electromagnetic field plays an important role in power system engineering, appearing in devices ranging from the simple static reactors to the more complex synchronous generators.

The transmission line in this chapter is modelled as an equivalent pi circuit. However, if a dynamic representation is required the n-port electromagnetic and electrostatic field systems, modified accordingly or otherwise, may be effectively used.

Although the bond graph of the synchronous generator is derived by considering the fundamental gyrator action of the device, it will be shown in the next chapter that the dynamic model of the generator evolves from the n-port electromagnetic field system which when subjected to steady-state conditions assumes the hexagonal strucure as shown in Fig. 3-2.

The n-port electromagnetic field system, which represents dynamic interactions, may be easily modified for steady-state operations. For linear systems under this conditon, the mutators become 1:1 transformers and the admittance Y(D), where D = d/dt, imposed by the steady-state constraint of the form $e^{j\omega t}$, is characterized by the complex quantities Y(jω). For a given frequency ω, the admittance is a complex number; it may be expressed as magnitude and phase angle.

For the studies in this chapter, the basic requirement involves the construction of the bond graphs and the subsequent assembly of the supplemented nodal phase admittance matrix. In the process of modelling power system components, the system nodes are represented by 0-junctions and the causality of each component model is arranged to enable the admittance elements to be easily derived by noting the algorithm for forming the admittance matrix.

The bond graph obtained for the power transformers exhibit certain interesting features such as the recurrence of the hexagonal and star structures in all the possible transformer connections. In fact the hexagonal structure seems to play an important role in the bond graph modelling of most, if not all, three-phase power system components. Perhaps, this may suggest the inherent exchanges of power between the three phases in the system, normally characterized by the mutual couplings.

3.8 References

1. Paynter, H.M.: 'Computer Representations of Polyphase Alternating Current Systems for Dynamic Analysis and Control', Automatic and Remote Control, Proc. First International Congress of the International Federation of Automatic Control, Moscow, 1960, pp. 1009-1017.
2. Laughton, M.A.: 'Analysis of Unbalanced Polyphase Networks by the Method of Phase Co-ordinates, Part I, System Representation in Phase Frame of Reference', Proc. IEE, 1968, 115, (8), pp. 1163-1173.
3. Laughton, M.A.: 'Analysis of Unbalanced Polyphase Networks by the Method of Phase Co-ordinates, Part 2, Fault Analysis', Proc. IEE, 1969, 116, (5), pp. 857-865.
4. Fortescue, C.L.: 'Method of Symmetrical Co-ordinates Applied to Solution of Polyphase Networks', Trans. Amer. Inst. Elect. Engrs., 1918, 37, Pt. II, pp. 1027-1140.
5. Clarke, E.: 'Circuit Analysis of A-C Power Systems - Vol. I', (Wiley, New York, 1943).
6. Kimbark, E.W.: 'Power System Stability - Vol. I', (Chapman and Hall, London, 1952).
7. Koga, N.: 'Transformation Circuit of Alpha, Beta, and Zero Components and its Application', Ohm, 1956, 43, (2), pp. 235-240.
8. Blondell, A.L.E.: 'Synchronous Motors and Converters', translated by C.O. Mailboux, additional chapters by C.A. Adams, (McGraw-Hill, New York, 1913).
9. Ellison, A.J.: 'Electromechanical Energy Conversion', (Harrap, London, 1970).

10. Adkins, B.: 'The General Theory of Electrical Machines', (Chapman and Hall, London, 1964).

11. Fitzgerald, A.E. and Kingsley, C. Jr.: 'Electric Machinery', (McGraw-Hill, New York, 1961).

12. Lewis, W.E. and Pryce, D.G.: 'The Application of Matrix Theory to Electrical Engineering', (Chapman and Hall, London, 1966).

13. Stevenson, W.D.: 'Elements of Power System Analysis', (McGraw-Hill, New York, 1962).

14. Povejsil, D.J. and Johnson, A.A.: 'A Per-Unit Interpretation of Transmission Line Constants', Trans. AIEE, 1951, 70, pp. 194-200.

15. John, M.N.: 'A General Method of Digital Network Analysis particularly suitable for use with Low-Speed Computers', Proc. IEE, 1961, 108A, pp. 369-382.

16. Brameller, A. and Denmead, J.K.: 'Some Improved Methods for Digital Network Analysis', Proc. IEE, 1962, 109, Part A, pp. 109-116.

17. Stagg, G.W. and El-Abiad, A.H.: 'Computer Methods in Power System Analysis', (McGraw-Hill, New York, 1968).

18. Laughton, M.A.: 'Thevenin and Norton Theorems - Generalisation and Dualities', Int. J. Elect. Engrg. Education, 1969, 71, pp. 255-263.

CHAPTER FOUR

DYNAMIC ANALYSIS OF MULTIPORT ELECTROMECHANICAL ENERGY CONVERTERS

4.1 Introduction

The dynamics of a power system are determined to a great extent by the inherent designed characteristics of the synchronous generators and the impedances prevailing within the system. The synchronous generator appears to be the source of almost all electrical energy up to now and even in the foreseeable future. It will not change radically in form except that the generating capacity of units may increase. The integration of many generators and perhaps many generating plants into a computer-controlled complex system will require not only detailed knowledge of the characteristics of generators but also an understanding of the effects of these characteristics on the dynamic operation of the system in which the generator is a small but exceedingly important part. The principal objective of this chapter is to present a simulation technique, using the bond graph notation discussed in Chapter two, for predicting the terminal characteristics of the synchronous generators.

Historically, the analysis of various classes of electromechanical devices - like solenoids, rotating machines, capacitor microphone - has been attempted largely on their own, using what happened to be the most suitable approach for every particular class. Attention was confined to steady-state, and only seldom was transient operation considered.

With the development of the theory of transformation, Kron[1] pioneered the generalised treatment of rotating machinery using tensor analysis. Gibbs[2,3] and Adkins[4] extended Kron's work and gave greater uniformity between different branches of the subject. An intensive coverage of the transformation theory used in machine analysis was presented in a book by Jones[5] in 1967. His basic philosophy on the generalised theory may be summarised in the following statement: 'The performance of any machine under any condition of operations may be analysed or predetermined in terms of measurements made solely at the terminals and shaft of the machine when the machine is stationary'. The measurements referred to are primarily measurements of inductance.

It would therefore be doubtful whether dynamic studies of machine based on data obtained when the machine is stationary would not give erroneous results. In fact Jones' results[5] on such test gave a marked disparity between experimental and simulated peaks which he believed was contributed by three distinct sources:

(i) the unknown change in saturation during the subtransient phase had been neglected,

(ii) the representation of solid iron damping by two isolated coils was somewhat idealistic, for example, the response of the iron to sudden short circuit may be different from its response to steady-state A.C. used in standstill test,

(iii) the difficulty in analysing systems where three coils are in the same axis, that is, share essentially the same iron circuit.

Recently, Reedy, Ali and Jones[6] presented a paper on the analysis of saturated magnetic systems in which the problems associated with (i) and (ii) are solved ingeniously. The method requires the formulation and eventual inversion of a non-linear inductance matrix at each integration step. However, the derivation of this matrix is rather involved even for a single-phase machine.

An alternative approach to the solution of saturated magnetic systems has been proposed in Chapter two. Based on the bond graph for the n-port electromagnetic field system, a unified method for the dynamic solution of electromechanical energy converters can be formulated. In this method a set of mixed differential/algebraic equations derived from a bond graph of the magnetic system is solved directly, thus avoiding the need to assemble and to invert the inductance matrix.

The bond graph approach which will be used for transient studies of saturated synchronous generators requires the predetermination of the no-load magnetisation characteristics. However, with increased use of the digital computers, these characteristics may be predicted easily from design data by the use of discrete elements, often guided by flux plots.

An interesting feature of the proposed method is that the dynamic behaviours of rotating machines can be determined to a good degree of accuracy at the design stage before commencing production when extensive alterations could be a major cost factor.

4.2 Predetermination of the No-load Magnetisation Characteristics of Rotating Machines

This section is intended as a survey of the field of research, involving the electromagnetic energy conversion process, in predicting the internal machine parameters, forces and losses using digital computers. The approach differs from that in this thesis in that emphasis is channelled into the internal operation of the machine to find the flux plots and radial air-gap inductions.

Past efforts in this field are mainly in finding the no-load characteristics. Binns[7] in 1965 calculated the no-load characteristics by a detailed application of the electromagnetic laws with the aid of a computer. He assumed a waveform of flux at the centre of the air-gap to determine the quantities of flux passing through each of the flux paths. The rotor leakage flux is added to the useful flux, and then, since the cross-sectional area of iron at any point on a path can be found, the variation of the flux density along each path can be calculated. From the value of the flux density, the field strengths are obtained from a knowledge of the magnetisation characteristics of the iron. Hence, by taking a considerable number of points along each flux path and determining the field strength at each point, it is possible to integrate the field strength along the path and obtain the drop in magnetic potential along each flux path of the machine.

The mmf drop thus obtained for each section are used to determine the rotor current. If the assumed distribution is correct, each section will require the same rotor current.

If there is a significant discrepancy in these values, the assumed distribution is modified until the difference is negligible. This flux distribution is then used to calculate the open-circuit voltage of the machine.

In 1971 Chari and Silvester[8] treated the same work as above using the method of finite elements. Recently Fuch and Erdelyi[9,10] determine the distribution of radial magnetic induction on the stator bore and the flux plots in the corss-section of a 200 MVA synchronous generator at no-load, three-phase short circuit and at balanced lagging and leading loads. Also the influence of saturation on the direct and quadrature reactances is studied.

It is felt, however, that the method of determining the short circuit characteristics from flux plotting is quite inefficient in terms of computer time and core size. As such it would be logical to consider the use of a predetermined no-load characteristic which is relatively easy to evaluate, in conjunction with the simulation technique developed in this thesis, for predicting the terminal characteristics of a machine. Should it be necessary to study in detail the flux plots and distribution of radial magnetic induction, the determined stator, field and damper currents obtained from the bond graph analysis are relatively accurate to be used as initial values in the method proposed by Fuch and Erdelyi, while ensuring numerical convergence even at high level of saturation.

4.2.1 Numerical Formulation of Differential Equations for the Analysis of Magnetic Field Problems

In the study of the magnetic field problems in machine the fundamental requirement is to reduce the machine into discrete elements. The boundaries and interfaces between regions tend to be regarded essentially as a nuisance and the calculation is directed more to the region interiors, which are commonly divided into grids with resulting large number of nodes formed.

A great deal of literature[11,12,13] is available in methods of solving differential equations essential for the solutions of magnetic field problems, such as the predetermination of the no-load magnetisation characteristics of rotating machines. In this section the analysis is limited to two-dimensional fields, so that the grid is planar and the vector property of the potential $\underline{A}$ can be ignored.

The simplest formulation is in terms of the magnetic potential, Ω in a current-free region such as in the air-gap, stator yoke and regions which are not in the proximity of the current carrying coils. With the nodes spaced in the rectangular array as shown in Fig. 4-1, the grid element between nodes 0 and 1 can be regarded as the rectangular strip ABCD, whose reluctance is:

$$\mathcal{R}_{01} = \frac{1}{\mu \eta_0} \cdot \frac{2h_1}{h_2 + h_4} \qquad 4.1$$

where μ is the relative permeability and η_0 is the primary magnetic constant, that is the ratio B/H in vacuum. The flux in the element is given by:

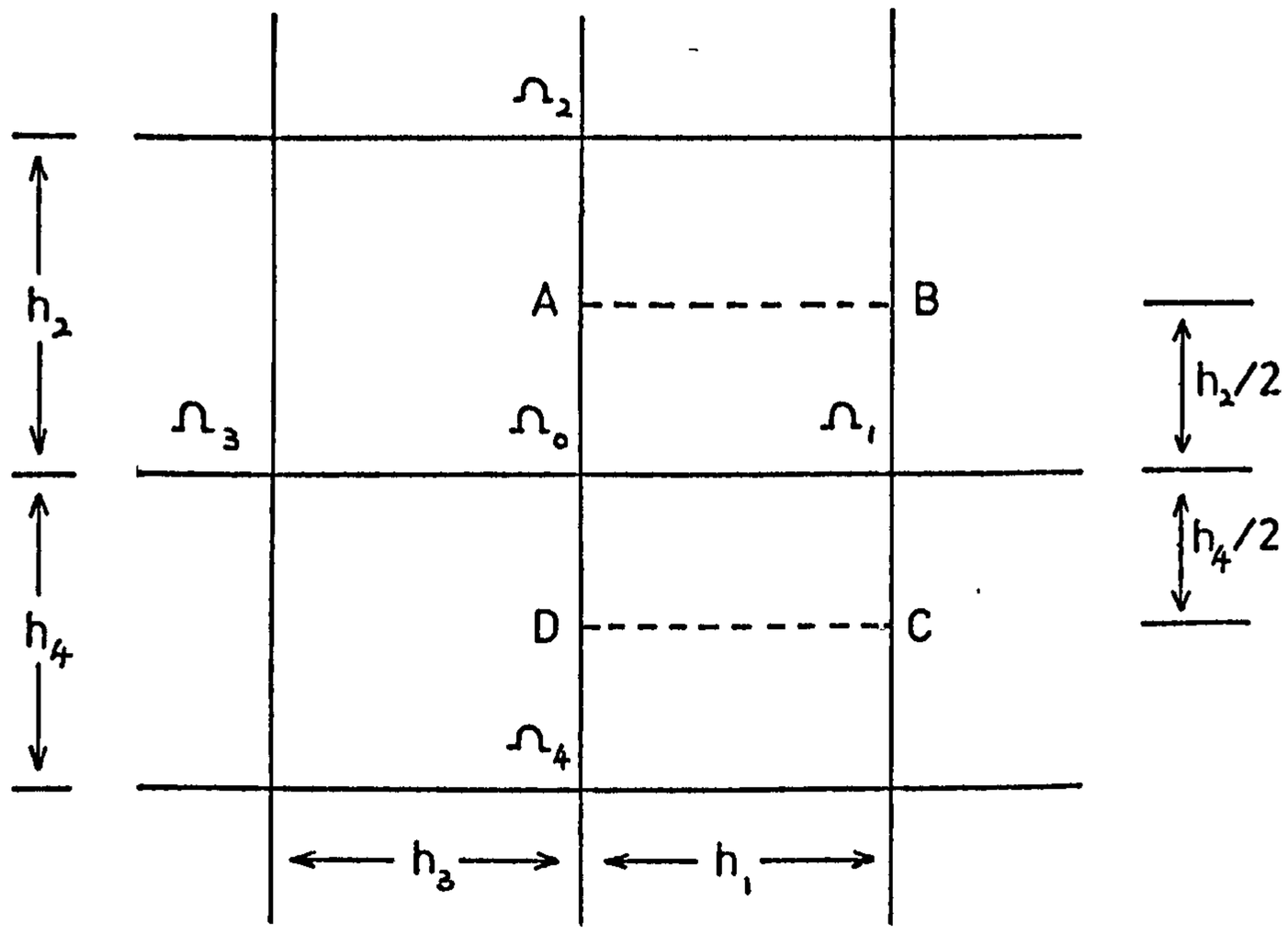

Fig. 4-1 Grid System for a Simple Two-Dimensional Field

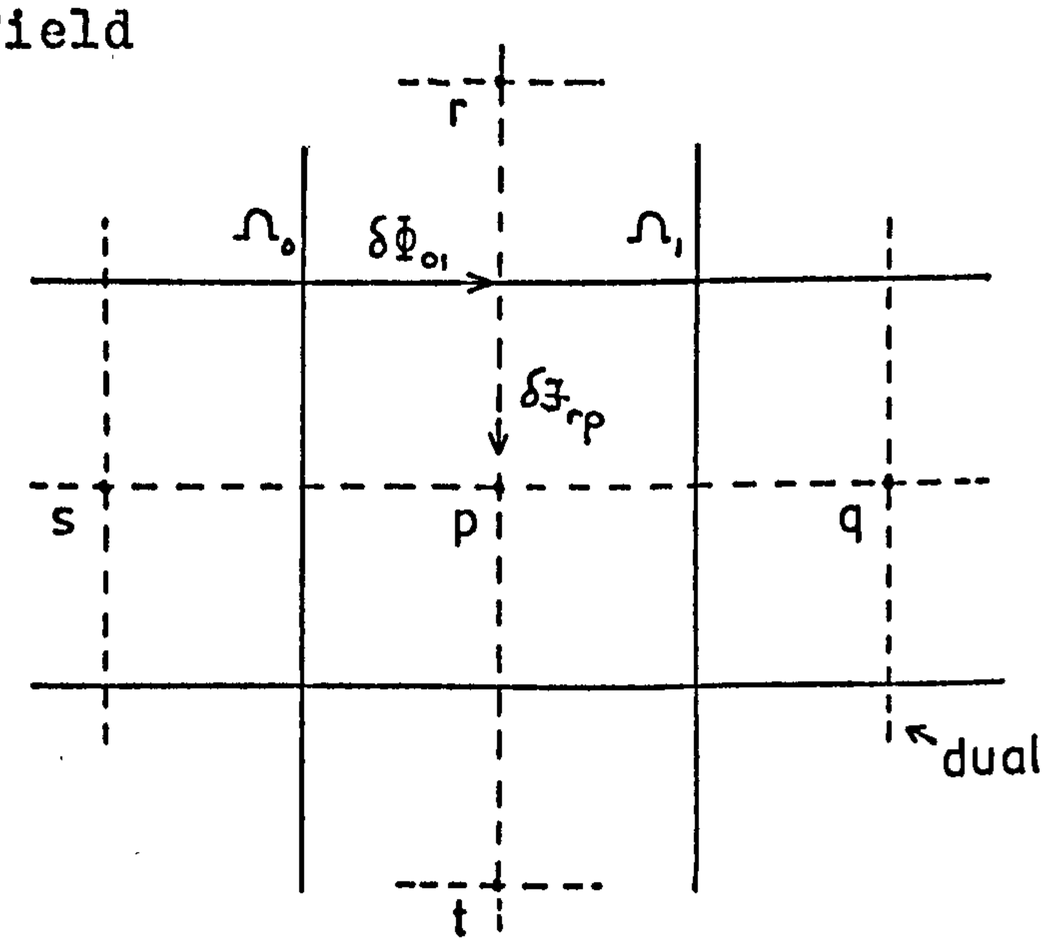

Fig. 4-2 Derivation of the Dual of the Grid System

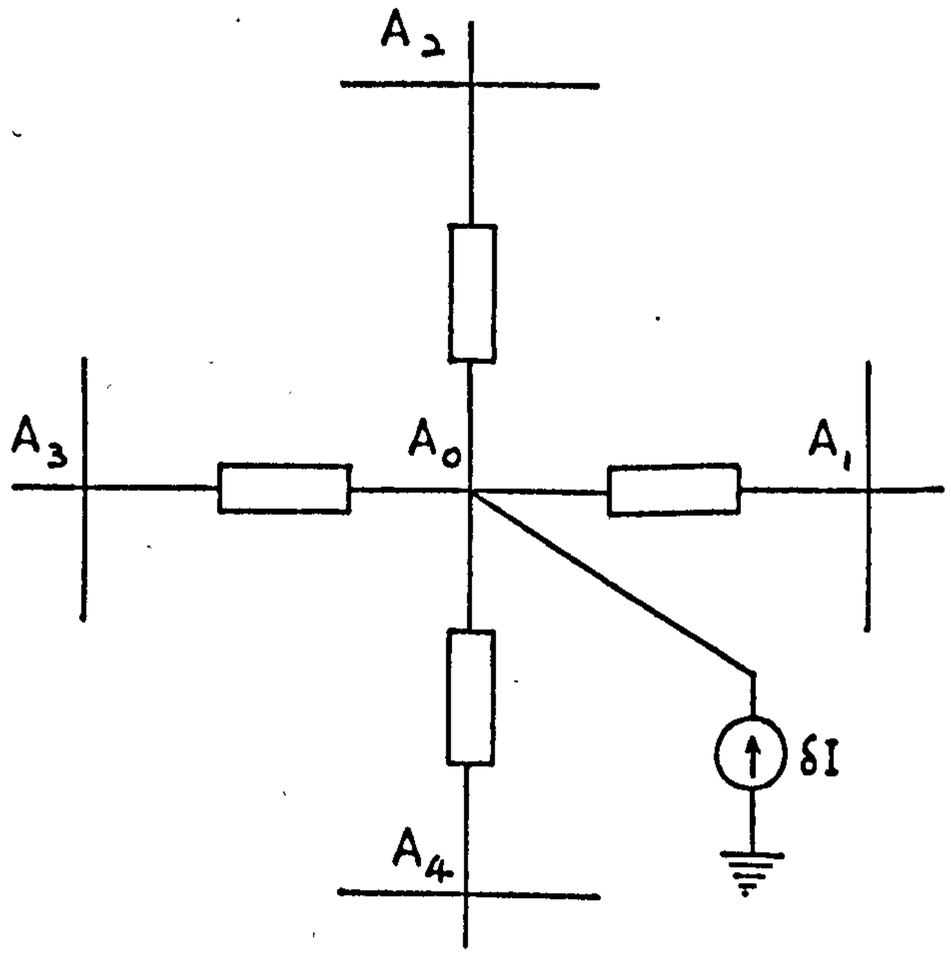

Fig. 4-3 Grid System for Current Carrying Region

$$\textcircled{H}_{10} = \frac{(\Omega_1 - \Omega_0)}{\mathcal{R}_{01}} \qquad 4.2$$

so that the condition that fluxes into node 0 sum to zero is:

$$\frac{h_2+h_4}{2}\left(\frac{\Omega_1-\Omega_0}{h_1}+\frac{\Omega_3-\Omega_0}{h_3}\right)+\frac{h_1+h_3}{2}\left(\frac{\Omega_2-\Omega_0}{h_2}+\frac{\Omega_4-\Omega_0}{h_4}\right)=0 \qquad 4.3$$

assuming the permeability is uniform. This is the same result as is usually obtained by dividing by the volume per unit length associated with node 0, which is $(h_1 + h_3)(h_2 + h_4)/4$.

Since the grid of Fig. 4-1 is mesh fed, a simple potential function Ω cannot be defined without replacing all the linkages by equivalent elements. As such in a current-carrying region it is necessary to transform the grid of Fig. 4-1 into its dual.

The dual of a two-dimensional grid shown in Fig. 4-2 can be obtained by placing a new node in every mesh, and replacing each reluctance by a quantity termed as magnetic conductance situated physically at right angles to it. Potential difference in the original grid becomes the flow quantity in the dual, defined as

$$\delta \mathcal{F}_{rp} = \Omega_0 - \Omega_1 \qquad 4.4$$

and vice versa, the flux linkage as

$$\delta\Phi_{01} = A_p - A_r \qquad 4.5$$

where A denotes the potential function in the dual.

The dual of Fig. 4-1 is a similar grid in which the typical node is spaced relative to its neighbours in the same manner as in the original grid. The typical magnetic

conductance is now given by:

$$\frac{\delta\mathcal{F}}{\delta A} = \frac{1}{\mu\eta_0} \frac{h_2 + h_4}{2h_1} \qquad 4.6$$

In the current carrying region the mmf associated with the node is

$$\delta I = J(h_1 + h_3)(h_2 + h_4)/4 \qquad 4.7$$

where J is the current density. Adding the five infeeds to node O, and dividing by the area, gives:

$$\frac{1}{\mu\eta_0} \frac{2}{h_1+h_3} \left(\frac{A_1-A_0}{h_1} + \frac{A_3-A_0}{h_3}\right) + \frac{1}{\mu\eta_0} \frac{2}{h_2+h_4}\left(\frac{A_2-A_0}{h_2} + \frac{A_4-A_0}{h_4}\right)$$

$$= -J \qquad 4.8$$

in which the sign convention is arbitrary, and that shown corresponds to a choice of the vector potential $\underline{A}$ in the same direction as J. This is the network form of the differential equation for $\underline{A}$, which is

$$\nabla^2 A = -\mu\eta_0 J \qquad 4.9$$

It corresponds to the grid connections shown in Fig. 4-3, in which δI is assumed to be specified, and is therefore represented by a current generator.

From the method explained above the no-load magnetisation characteristics may be predetermined by using Eqns. 4-3 and 4.8 or a modified from of both. A number of numerical techniques[14] are available for solution by digital computers. However, this line of research shall not be pursued here but rather the simulation technique to be presented will presuppose the existence of accurate no-load characteristics which may be obtained by the digital computer technique shown above or otherwise.

4.3 Computer Methods for the Analysis of Non-linear Mixed Differential/Algebraic Equations

As indicated in Chapter two, the terminal solutions of either electromagnetic or electrostatic field systems or a mixture of both require a routine capable of handling mixed differential/algebraic equations. In the past it is normal for system equations to be manipulated in a way suitable for solution by the usual numerical integration techniques such as the Euler, modified Euler, Picard and Runge-Kutta methods[15,16]. These methods are only suitable for linear systems unless special provisions[6] are made otherwise.

In this section two methods of solution of mixed differential/algebraic equation shall be presented. The first was used by Hirst[17] in investigating lumped thermodynamic models having unstable regimes of operation. The method involves the use of the Runge-Kutta-Merson in conjunction with the Newton-Raphson methods.

The alternative method was used by Martens[18] in a bond graph solution of a simple non-linear hydraulic system. The technique referred to as the implicit integration method[21,22] involved basically the approximation of the derivative of the dependent variables in terms of the Taylor expansion and the solving of the evenutal algebriac equations by a single Newton iteration process.

4.3.1 Runge-Kutta-Merson/Newton-Raphson Method

Mixed differential and algebriac equations consisting of p first order x derivatives and q algebriac dependent variables, y, may in general be written as:

$$\dot{x}_r = F_r\left[t, \underline{x}(t), \underline{y}(t) \right] \qquad 4.10$$

$$\text{and} \quad 0 = G_s\left[t, \underline{x}(t), \underline{y}(t) \right] \qquad 4.11$$

where $\underline{x}(t) = x_1, x_2 \ldots x_p$; $\underline{y}(t) = y_1, y_2 \ldots y_q$; $r = 1, 2 \ldots p$ and $s = 1, 2 \ldots q$. The method of solving Eqns. 4.10 and 4.11 involve the determination of $\underline{x}(t)$ using the previous value of $\underline{y}(t)$ and then updating $\underline{y}(t)$ by the Newton-Raphson iteration using the new value of $\underline{x}(t)$.

In the standard Runge-Kutta method the changes in the values of the dependent variables are calculated from a given set of formulas that are expressed in terms of the derivative evaluated at predetermined points. Merson suggested a fourth order method which, in certain circumstances, provided a technique for automatic interval adjustment[19].

The modification of the fourth order Runge-Kutta integration formula for a particular value of the dependent variable, $x_i(t)$, is:

$$x_i^{n+1}(t) = x_i^{n}(t) + \tfrac{1}{2}(k_{i1} + 4k_{i4} + k_{i5}) \qquad 4.12$$

where $x_i^{n}(t)$ is the known value of $x_i(t)$ at time t_n, $x_i^{n+1}(t)$ is the value obtained for $x_i(t)$ at time $t_{n+1} = t_n + h$ and

$$\begin{aligned}
k_{i1} &= {}^{1}/_{3}h\, F_i\left[t_n, \underline{x}^n, \underline{y} \right] \\
k_{i2} &= {}^{1}/_{3}h\, F_i\left[t_n + {}^{1}/_{3}h, \underline{x}^n + \underline{k}_1, \underline{y} \right] \\
k_{i3} &= {}^{1}/_{3}h\, F_i\left[t_n + {}^{1}/_{3}h, \underline{x}^n + \tfrac{1}{2}\underline{k}_1 + \tfrac{1}{2}k_2, \underline{y} \right] \qquad 4.13 \\
k_{i4} &= {}^{1}/_{3}h\, F_i\left[t_n + \tfrac{1}{2}h, \underline{x}^n + {}^{3}/_{8}\underline{k}_1 + {}^{9}/_{8}\underline{k}_3, \underline{y} \right] \\
k_i5 &= {}^{1}/_{3}h\, F_i\left[t_n + h, \underline{x}^n + {}^{3}/_{2}\underline{k}_1 - {}^{9}/_{2}\underline{k}_3 + 6\underline{k}_4, \underline{y} \right]
\end{aligned}$$

where $\underline{k}_1 = k_{11}, k_{21} \ldots kp_1$ and similarly for $\underline{k}_2$, $\underline{k}_3$, $\underline{k}_4$ and $\underline{k}_5$; also $h = t_{n+1} - t_n$ is the time step and $F_i\left[t_n, \underline{x}^n, \underline{Y}\right]$ is the derivative of x_i at solution time t_n.

From Eqns. 4.12 and 4.13 the values of $\underline{x}$ and $\underline{k}$ may be calculated given values of $\dot{x}$ at each value of time. At the end of each attempted step carried out according to the above equations, the Merson truncation error formula below is evaluated for each dependent variable $x_i(t)$,

$$e_i = \frac{1}{5R_i} \left| \left(k_{i1} - {}^{9}/_{2}\, k_{i3} + 4k_{i4} - \tfrac{1}{2}k_{i5}\right) \right| \qquad 4.14$$

where R_i is a normalising parameter whose value depends on the error checking mode. When relative error mode is required $R_i = |x_1|$ and in absolute error mode $R_i = 1$.

When the error is within bounds for every $\underline{x}$, the step is accepted and a new one commenced. Otherwise, h is halved and a new attempt is made until a minimum step size is reached. If the largest error is less than $\frac{1}{32}$nd of its error bound value, the step size is doubled. Again this process continues until either the largest error is satisfactory or the minimum step size is reached.

At the start of a solution and before the commencement of a new step, the Runge-Kutta-Merson/Newton-Raphson routine solves the algebriac equations using the Newton-Raphson method[20]. The difference between the newly calculated value of $\underline{Y}$ and the best previous value is calculated thus:

$$\underline{e} = \left[\underline{Y}^{n+1}(t) - \underline{Y}^{n}(t)\right] \qquad 4.15$$

where $\underline{e} = e_1, e_2 \ldots e_q$, and in which $\underline{Y}^{n+1}(t)$ and $\underline{Y}^{n}(t)$

are the new and previous values of $\underline{y}$ in the algebraic equations respectively.

If all $\underline{e}$ are within the specified bounds, the existing $\underline{y}$ values are retained and the Runge-Kutta-Merson process continues using the latest set of $F_r\left[t, x(t), y(t)\right]$ values. Should one or more $\underline{e}$ values exceed the specified bounds the Newton-Raphson correction routine begins.

Each new value of $\underline{y}$ in the algebriac equations is multiplied in turn by a fixed factor $(1 + \delta)$ where $\delta << 1.0$ and the resulting changes $\Delta\underline{e}$ in the $\underline{e}$ values are found as a result of the perturbations. The changes $\Delta\underline{e}$ are used to compute the Jacobian matrix. Thus, the element in the sth row and bth column is:

$$J_{sb} = \frac{\Delta e_s}{(y_b(t)\delta)} \qquad 4.16$$

for $s = 1, 2, \ldots q$ and where $y_b(t)$ is the variable preturbed by a factor $(1 + \delta)$ and q is the number of dependent variables of the algebraic equations. If $y_b(t)$ is zero, then $y_b(t)\delta$ is replaced by a non-zero quantity based on the magnitude of the error, e_b.

A set of linear algebraic equations is formed thus:

$$\left[\underline{J}\right]\left[\underline{C}\right] = -\left[\underline{e}\right] \qquad 4.17$$

where $\underline{C}$ the correction value vectors. Using Gauss elimination these correction values are solved. The latest values of $y_b(t)$ are changed to $\left[y_b(t) + KC_b\right]$, where K is the Newton-Raphson correction step factor and is always set to its maximum specified value for the first calculation attempt with a new Jacobian.

If the worst error, as defined in Eqn. 4.15, increased following a Newton-Raphson correction step, the value of K is halved and the resulting smaller correction is again applied to $y_b(t)$. This halving process stops if K reaches its minimum specified value.

The whole sequence is repeated for a new time step to calculate new values of $\underline{x}$ and $\underline{y}$. A simplified flow chart of the above method is shown in Fig. 4-4.

This method is now available as a standard program package under the name SYSTRAN. Program details of SYSTRAN is included in Appendix B.

4.3.2 Implicit Integration Method

The implicit integration method is a relatively new innovation for the computer simulation of non-linear dynamic systems[21,22]. In solving a differential equation of the form shown in Eqn. 4.10 the approach is to approximate the derivative of $x_i(t)$ by a linear combination of the present and N previous points, thus:

$$\dot{x}_i(t_n) = a_0 x_i(t_n) + \sum_{j=1}^{N} a_j \, x_i(t_{n-j}) \qquad 4.18$$

where the coefficients a_0, a_1 .... a_N may be chosen by matching certain number of terms in the Taylor expansion of $x_i(t_{n-j})$ about $x_i(t_n)$; N is a number usually ranging between 1 and 6 depending upon the accuracy desired.

Using the general form of the mixed differential and algebraic equations of Eqns. 4.10 and 4.11, the application of approximation of Eqn. 4.18 results in the formation of (p+q) generally non-linear implicit algebraic equations at each time step, t_n.

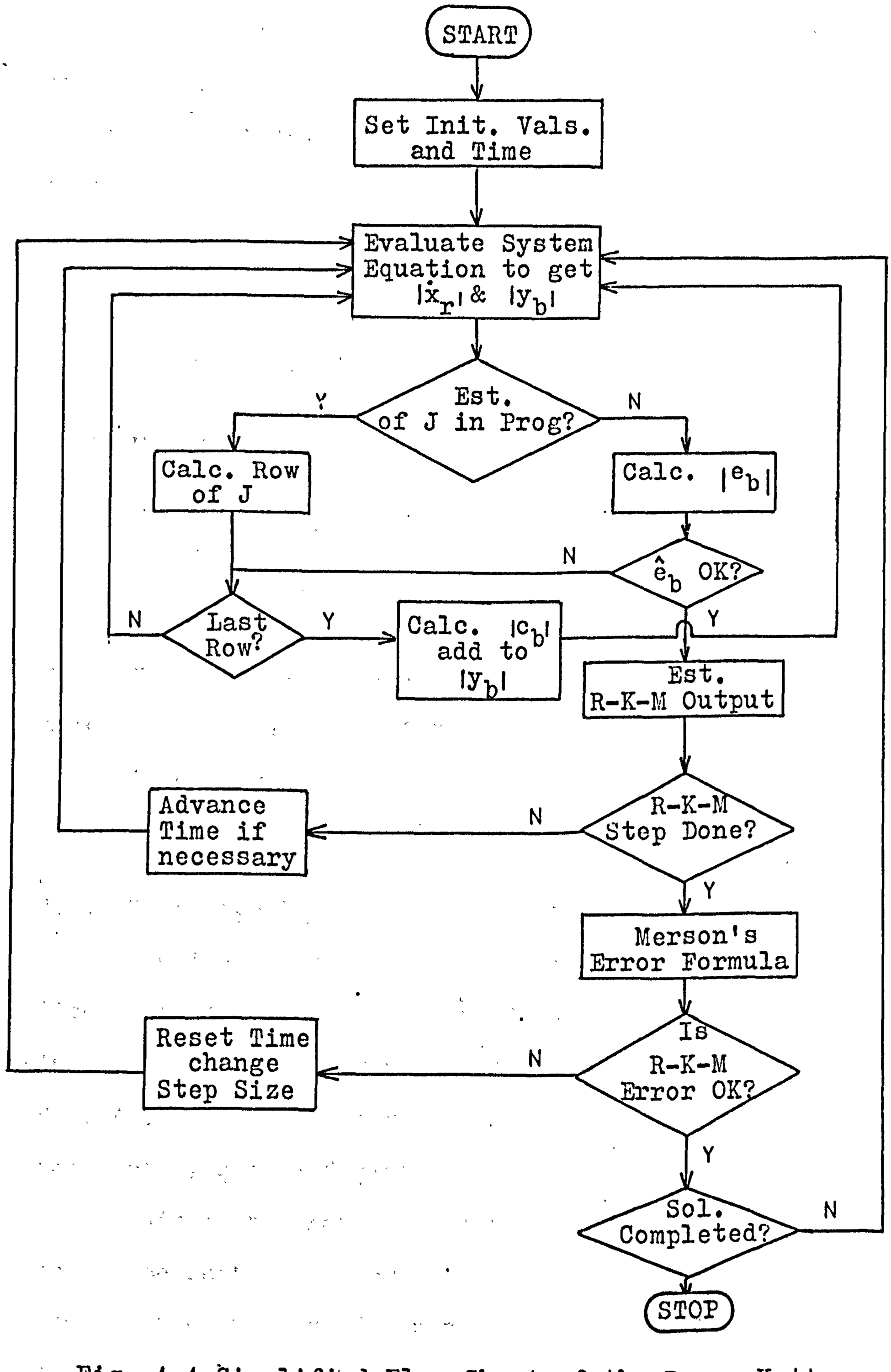

Fig. 4-4 Simplified Flow-Chart of the Runge-Kutta-Merson / Newton-Raphson Method

The equations can then be solved by the Newton iteration process which yields both values of $\underline{x}$ and $\underline{y}$. For a particular time, t_n, Eqns. 4.10, 4.11 and 4.18 can be expressed as:

$$a_o x_r(t_n) + \sum_{j=1}^{N} a_j x_r(t_{n-j}) = F_r\left[t_n, \underline{x}(t_n), \underline{y}(t_n) \right] \qquad 4.19$$

$$0 = G_s\left[t_n, \underline{x}(t_n), \underline{y}(t_n) \right]$$

which may be reduced to:

$$\left.\begin{aligned} F_r'\left[t_n, \underline{x}(t_n), \underline{y}(t_n) \right] &= 0 \\ G_s\left[t_n, \underline{x}(t_n), \underline{y}(t_n) \right] &= 0 \end{aligned}\right\} \qquad 4.20$$

where $\underline{x}(t_n) = x_1, x_2 \ldots x_p$; $\underline{y}(t_n) = y_1, y_2 \ldots y_q$ at time t_n; $r = 1, 2 \ldots p$ and $s = 1, 2 \ldots q$.

A detailed description of the derivation of the approximation in Eqn. 4.18 is given in Appendix C.

4.3.3 Technique for Introducing Non-linear Functions

Non-linear functions are introduced into the equations discussed in section 4.3.1 and 4.3.2 by using linear interpolation and extrapolation routines[20]. As shown in Fig. 4-5, the non-linear function Z_k may be expressed in terms of t, $\underline{x}(t)$ and $\underline{y}(t)$.

This method requires that a relationship between Y_k and Z_k be initially known. In general therefore, to include the effects of m non-linear functions, $\underline{Z} = Z_1, Z_2 \ldots Z_m$, Eqns. 4.10 and 4.11 may be written as:

$$\left.\begin{aligned} \dot{x}_r &= F_r\left[t, \underline{x}(t), \underline{y}(t), \underline{Z} \right] \\ 0 &= G_s\left[t, \underline{x}(t), \underline{y}(t), \underline{Z} \right] \end{aligned}\right\} \qquad 4.21$$

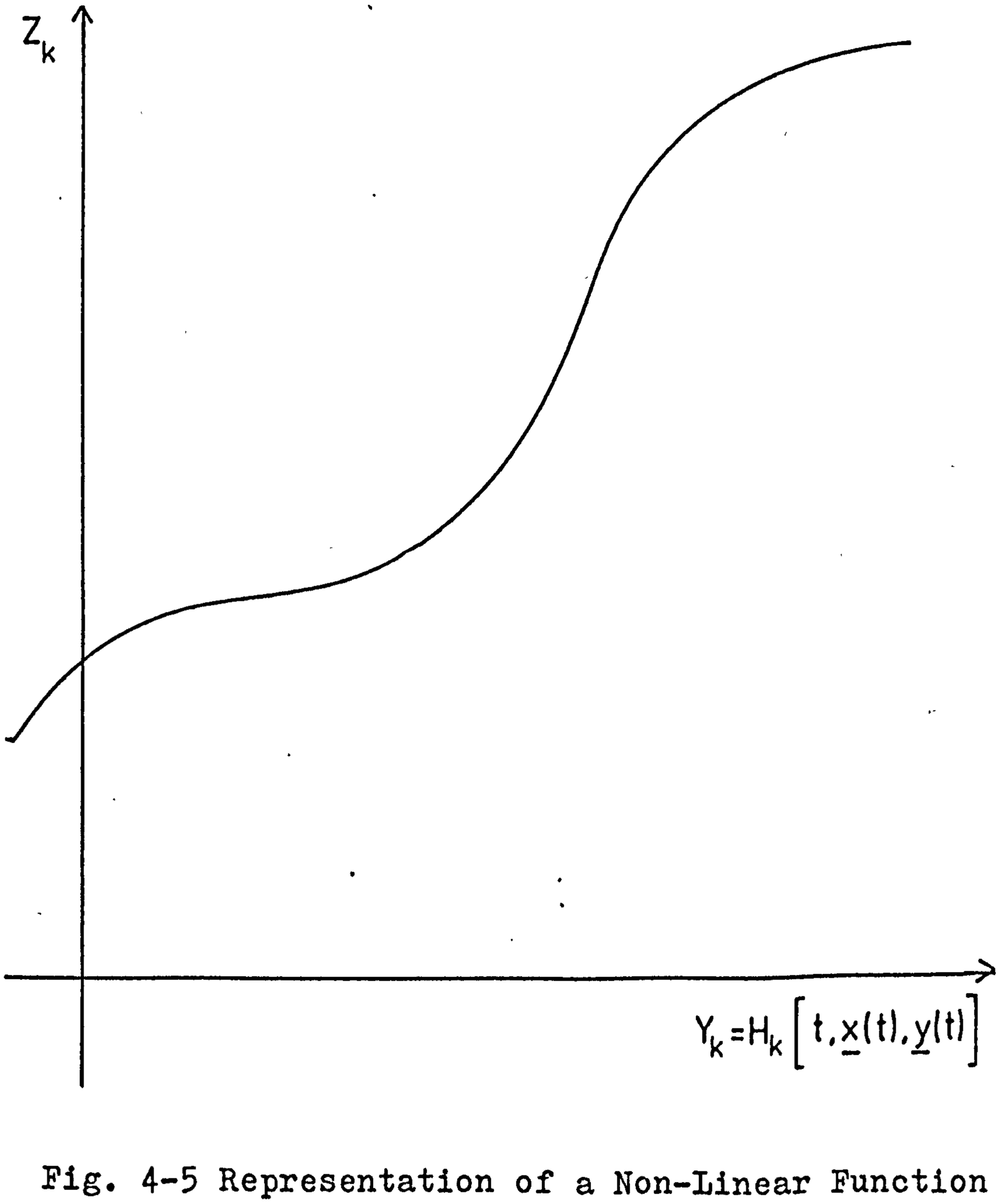

Fig. 4-5 Representation of a Non-Linear Function Z_k

which may be solved by the integration/iteration methods suggested in the preceding sections.

An additional general equation of the form

$$Y_u = H_u\left[t, \underline{x}(t), \underline{y}(t)\right] \qquad 4.22$$

where u = 1, 2 .... m, is necessary to derive the non-linear functions Z. For the kth variable, as shown in Fig. 4-5, a table of the Y_k - Z_k co-ordinate has to be determined and then stored in the appropriate subroutine. At each integration/iteration step Y_k is calculated and the corresponding Z_k is evaluated from Fig. 4-5 using linear interpolation or extrapolation methods.

The basic technique involved the representation of a continuous non-linear function by discrete steps; the accuracy of which depends upon the number of Y_k - Z_k co-ordinates known and the means by which Z_k is updated in the solution process.

4.4 Single-Phase Rotating Machine

In this and the following sections bond graph models of different types of electromechanical energy converters will be developed. A model is used, rather than derivation of the machine equations directly from the inductance matrix, due to the following reasons:

(i) to simplify the mathematical manipulations,

(ii) to accentuate the important features of the machine which may be ignored in pursuit of mathematical expediency, and more importantly,

(iii) to show that the bond graph concept which has been presented in Chapter two for the treatment of multi-

port electromagnetic field system can be used, with minor modifications, for all types of rotating machines.

This method of representing a multiport electromagnetic field system in terms of the basic field proprties, mmf and flux linkages, in the same diagram with the conjugate power variables, voltage and current, enables saturation to be incorporated without difficulty.

In each machine to be simulated the basic assumptions regarding the structure and leakage properties of the windings are made, thus:

(i) the air-gap is of uniform width,

(ii) the coil windings are distributed so as to produce sinusoidal mmf distribution in the air-gap,

(iii) all parts of the magnetic circuit are homogenous, and

(iv) the leakage flux linkage associated with a coil is a linear function of the coil current.

The choice of a single-phase rotating machine as the first model to be developed is due to the fact that it obeys the same physical law as an unbalanced multi-phase machine but without the added complexity to the computation structure of the latter. Since the study of unbalanced behaviours of electromechanical energy converters is an important objective of this chapter, a good understanding of the single-phase rotating machine would be a useful aid in evolving the multi-phase machine model.

4.4.1 Basic Two-Winding Machine

In the two-winding machine shown in Fig. 4-6, Θ is the angular displacement between the coils, sharing a common mutual flux.

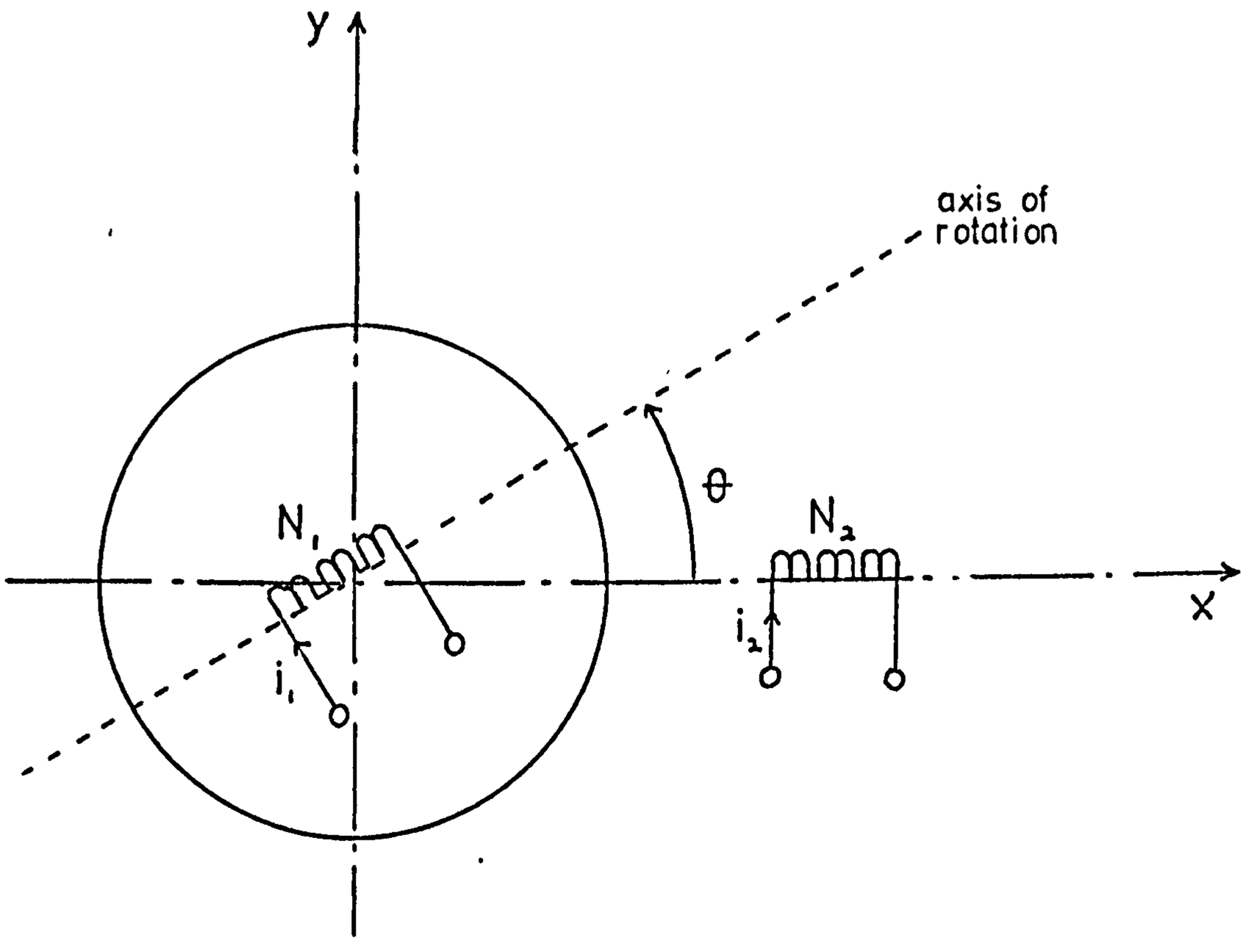

Fig. 4-6 Schematic Diagram of Two-Winding Machine

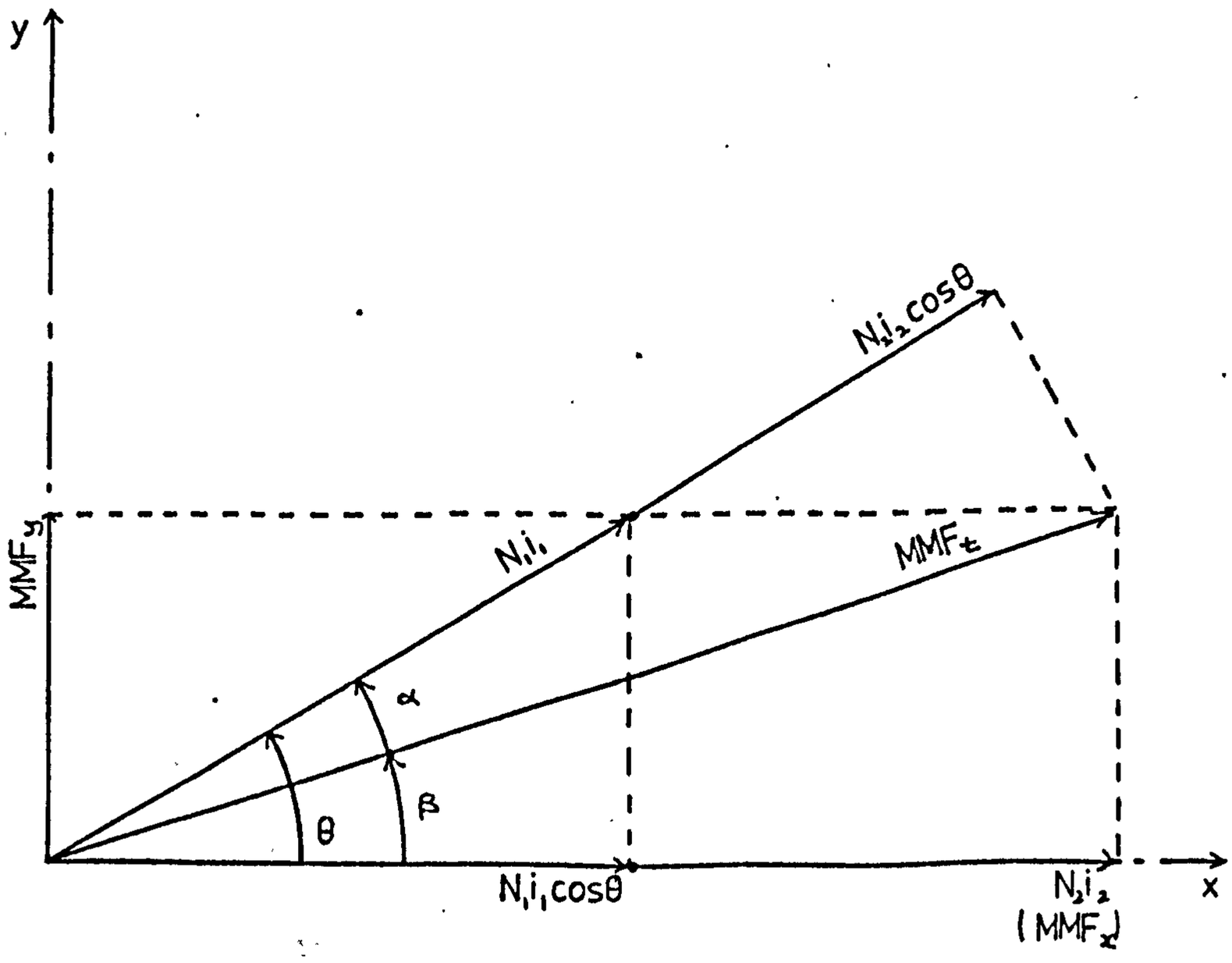

Fig. 4-7 Mmfs' Vector Diagram of Two-Winding Machine

With the assumptions of section 4.4, the mmf may be resolved in the x and y axes in terms of the instantaneous currents i_1 and i_2 shown. Thus the x and y components of the magnetomotive force within the machine are:

$$MMF_x = N_1 i_1 \cos \Theta + N_2 i_2 \qquad 4.23$$

$$MMF_y = N_1 i_1 \sin \Theta \qquad 4.24$$

where N_1 and N_2 are the effective turns ratio of coils 1 and 2 respectively; and these equations may be expressed in magnitudes and direction as:

$$MMF_t = \sqrt{(MMF_x)^2 + (MMF_y)^2} \qquad 4.25$$

and $$\cos \beta = \frac{MMF_x}{MMF_t} \qquad 4.26$$

From Eqns. 4.25 and 4.26 it is possible to determine the magnitude and direction of the total spatial mmf from which the resultant spatial flux distribution can be obtained. This requires that the magnetic properties of the material and the physical structure of the magnetic circuit be accurately known throughout the machine. In fact the method explained in section 4.2.1 may be used for this purpose.

However, in this chapter the no-load magnetisation characteristics are used with the assumptions that all the mmfs are sinusiodally in space, and that three or more windings sharing the same axis have a common mutual flux[4,5].

The relationship between the total mmf and the resultant flux may be written as:

$$\Phi_r = f\ (MMF_t) \qquad 4.27$$

where the function, f (MMF_t), is defined by the no-load magnetisation characteristics; and that a sinusoidal mmf will give rise to a sinusoidal flux[6].

In order to simplify the eventual solution, it is important that the mmfs are all referred to the axis of MMF_t. As such the angle of MMF_t with respect to coil 1 as well as coil 2 must be known. The total mmf component aligned with coil 1 is:

$$MMF_1 = N_1 i_1 + N_2 i_2 \cos \Theta \qquad 4.28$$

From the mmfs vector diagram shown is Fig. 4-7, the angle of the total mmf, MMF_t, with respect to coil 1 is:

$$\cos \alpha = \frac{MMF_1}{MMF_t} \qquad 4.29$$

and β, the angle of the total mmf with respect to coil 2 may be written as:

$$\beta = \Phi - \alpha \qquad 4.30$$

The coil components of the resultant flux, Φ_r, are:

$$\Phi_1 = \Phi_r \cos \alpha \qquad 4.31$$

$$\Phi_2 = \Phi_r \cos \beta$$

$$= \Phi_r \cos (\Theta-\alpha) \qquad 4.32$$

and the corresponding flux linkages are:

$$\lambda_1 = N_1 \Phi_r \cos \alpha \qquad 4.33$$

$$\lambda_2 = N_2 \Phi_r \cos (\Theta-\alpha) \qquad 4.34$$

However, the flux linkages defined by Eqns. 4.33 and 4.34 are only applicable in the ideal case. The actual flux linkages of coils 1 and 2 will have the derived terms as

defined above, as well as leakage terms which account for the associated leakage reactances. Thus, the actual flux linkages are:

$$\lambda_1 = N_1 \Phi_r \cos\alpha + \ell_1 i_1 \qquad 4.35$$

$$\lambda_2 = N_2 \Phi_r \cos(\Theta-\alpha) + \ell_2 i_2 \qquad 4.36$$

where ℓ_1 and ℓ_2 are the leakage inductances of coils 1 and 2 respectively and are assumed to be constant for each particular machine.

The whole existing flux linkage may therefore be sub-divided into:

(i) the main or useful flux linkage which contributes to the energy conversion process, and

(ii) the leakage flux linkage which contributes only to reversible energy storage and endows the coil concerned with the properties of leakage inductance.

In other words, the actual flux linkage may be considered as the superposition of working and leakage flux linkages, each with its own part to play in the electromagnetic action of the rotating machine.

4.4.2 Single-Phase Synchronous Machine

The single-phase synchronous machine is a special case of the basic two-winding machine and as such the equations developed for the latter may, with slight modifications, be effectively applied. Essentially in the single-phase synchronous machine, direct current is fed into the rotating winding which causes a pulsating armature mmf. This difference in the nature of the winding currents, requires that the effective current ratio be

scaled by a $\sqrt{2}$ factor[23]; thus the effective current ratio of the field to the instantaneous armature currents, N_{aF}, is

$$N_{aF} = \frac{N_a}{\sqrt{2}\, N_F} \qquad 4.37$$

where N_a and N_F are the armature winding and the field winding turns ratio respectively.

Similarly, by considering the position of the damper winding with respect to the field winding, as shown in Fig. 4-8, the effective current ratio of the damper to the armature currents is:

$$N_{aD} = \frac{N_a}{\sqrt{2}\, N_D} \qquad 4.38$$

where N_D is the damper winding turns ratio.

Slemon[24] has shown that under transient conditions the field leakage flux, $\Phi_{F\ell}$, can be considered to be excited by the combined effect of armature and damper currents such that:

$$\Phi_{F\ell} = \frac{\ell_F'}{\sqrt{2}\, N_a} \left(i_a - \frac{\sqrt{2}\, N_D i_D}{N_a} \right) \qquad 4.39$$

where ℓ_F' is the field leakage inductance referred to the armature winding; i_a and i_D are the instantaneous armature and damper currents, respectively.

However, the second expression, in the bracket, of Eqn. 4.39 is always small compared to i_a since $N_D << N_a$ and $i_D << i_a$. Thus Eqn. 4.39 may be reduced to:

$$\Phi_{F\ell} = \frac{\ell_F'}{\sqrt{2}\, N_a}\, i_a \qquad 4.40$$

In synchronous machines, the field leakage remains stationary with respect to the field winding and there is no emf of self-inductance developed by the leakage flux under normal working conditions. From Eqn. 4.40 it is evident that an assumption is made such that under transient conditions the field leakage flux is defined by the armature current and that the flux links with the armature and damper windings as shown in Fig. 4-8.

Thus the field leakage inductance referred to the armature winding, under transient conditions, may be defined as:

$$\ell_F' = \frac{\sqrt{2}\, N_a\, \Phi_{F\ell}}{i_a} \qquad 4.41$$

The field leakage inductance referred to the field winding is[24]:

$$\ell_F = \sqrt{2}\, \left(\frac{\sqrt{2}\, N_F}{N_a} \right) \cdot \frac{N_F}{N_a} \cdot \ell_F' \qquad 4.42$$

From Eqns. 4.37, 4.41 and 4.42 the field leakage inductance, ℓ_F, may be expressed as:

$$\ell_F = \frac{2\lambda_{F\ell}}{i_F} \qquad 4.43$$

where $\lambda_{F\ell}$ is the field leakage flux linkage and is equal to $N_F\, \Phi_{F\ell}$.

Similarly, referring to Fig. 4-8, it can be assumed that the damper leakage inductance is defined by the armature current and that $\Phi_{D\ell}$, the damper leakage flux, has the same path as $\Phi_{F\ell}$. Thus the damper leakage inductance referred to the armature winding, under transient conditions is:

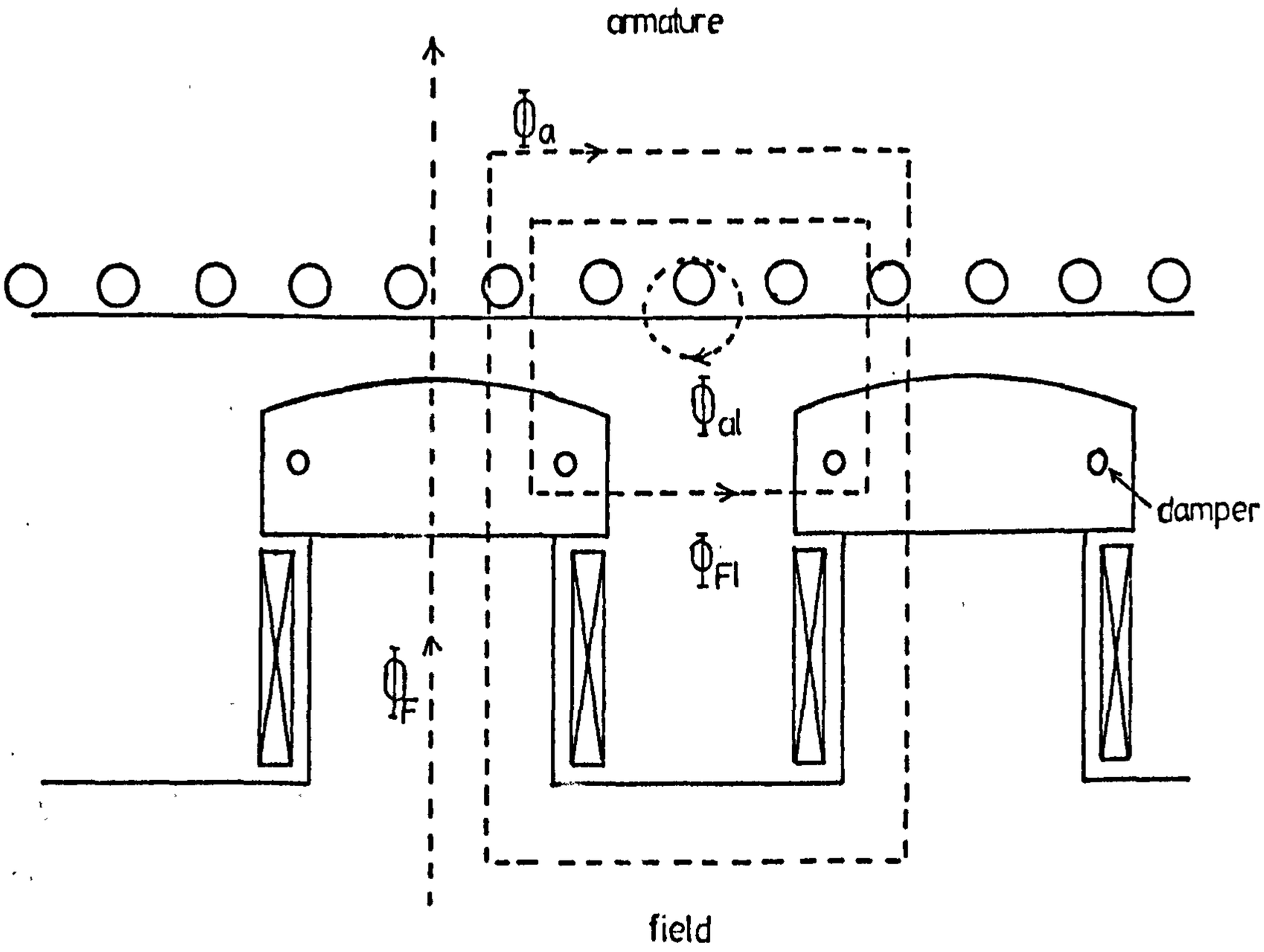

Fig. 4-8 Simplified Developed Diagram of Salient-Pole Synchronous Machine

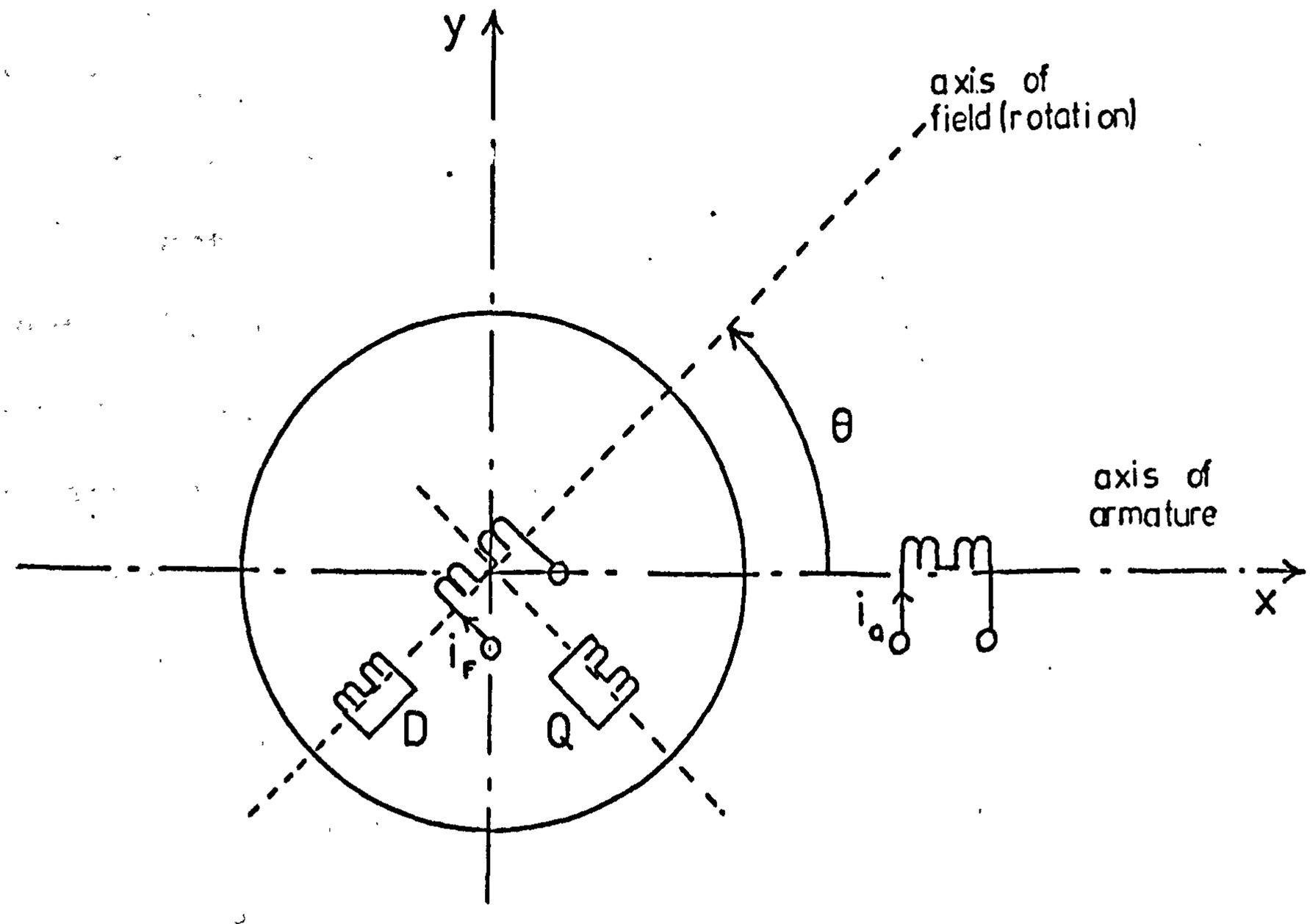

Fig. 4-9 Schematic Diagram of Single-Phase Synchronous Machine with Dampers

$$\ell_D' = \frac{\sqrt{2}\, N_a\, \Phi_{D\ell}}{i_a} \qquad 4.44$$

Following the same procedure as for the field leakage inductance, the damper leakage inductance referred to its own winding may be expressed as:

$$\ell_D = \frac{2\lambda_{D\ell}}{i_D} \qquad 4.45$$

where $\lambda_{D\ell}$ is the damper leakage flux linkage and is equal to $N_D\ \Phi_{D\ell}$.

In the armature winding, the armature leakage flux, $\Phi_{a\ell}$, is defined at rated steady-state values from the rms armature current, turns ratio and permeance[5,25]. Thus the instantaneous armature leakage flux linkage is:

$$\begin{aligned} \lambda_{a\ell} &= N_a\ (\sqrt{2}\,\Phi_{a\ell}) \\ &= \sqrt{2}\,\ell_a\ i_a \end{aligned} \qquad 4.46$$

where $\Phi_{a\ell}$ is the designed steady-state armature leakage flux and ℓ_a is the steady-state armature leakage inductance.

In the single-phase synchronous machine considered in this section the damper windings are assumed to be effectively represented by equivalent damper windings in the direct and quadrature axes. The schematic diagram of the machine and its mmfs' vector diagram are shown in Figs. 4-9 and 4-10 respectively.

From the mmfs' vector diagram, the magnitude and direction of the resultant magnetizing current referred to the field winding may be given by:

$$\left.\begin{aligned} i_{mF}\cos\alpha &= i_F + N_{DF}i_D + N_{aF}i_a\cos\theta \\ i_mF\sin\alpha &= N_{QF}i_Q + N_{aF}\,i_a\sin\theta \end{aligned}\right\} \qquad 4.47$$

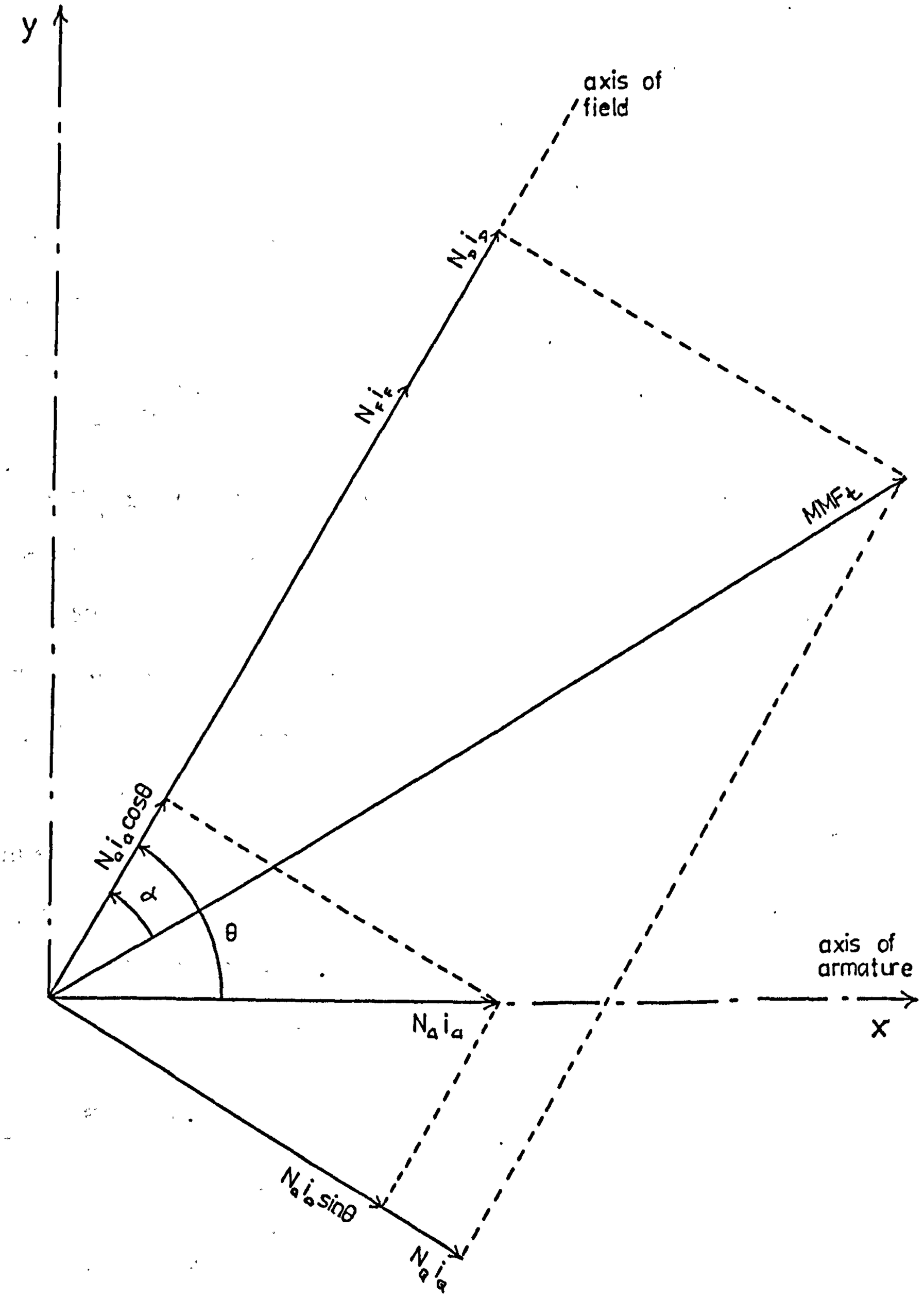

Fig. 4-10 Mmfs' Vector Diagram of Single-Phase Synchronous Machine with Dampers

where i_D and i_Q are the instantaneous damper currents in the direct and quadrature axes respectively, N_{DF} is the direct-axis damper winding to the field winding turns ratio and N_{QF} is the quadrature-axis damper winding to field winding turns ratio.

From the no-load magnetization characteristic of the test generator, shown in Fig. 4-11, the armature flux linkages, λ_{ma}, for various values of i_{mF} may be calculated thus:

$$\lambda_{ma} = \frac{\sqrt{2}\, V_o}{\omega} \qquad 4.48$$

where V_o is the open-circuit armature terminal voltage and ω is the synchronous speed of the generator.

With the resultant magnetizing current, i_{mF}, known from Eqn. 4.47, the value of λ_{ma} can be found from Fig. 4-11 using the technique suggested in Section 4.3.3. Then assuming that a sinusoidal mmf will give rise to a sinusoidal flux, the individual flux linkage may be found by resolving λ_{mA} with the aid of Fig. 4-10 and using Eqns. 4.43, 4.45 and 4.46 for the expressions defining the leakage flux linkages. Thus:

$$\left.\begin{aligned}
\lambda_F &= N_{Fa}\, \lambda_{ma} \cos\alpha + \tfrac{1}{2}\, \ell_F\, i_F \quad)\\
\lambda_D &= N_{Da}\, \lambda_{ma} \cos\alpha + \tfrac{1}{2}\, \ell_D\, i_D \quad)\\
\lambda_Q &= N_{Qa}\, \lambda_{ma} \sin\alpha + \tfrac{1}{2}\, \ell_Q\, i_Q \quad)\\
\lambda_a &= \lambda_{ma} \cos(\theta-\alpha) + \sqrt{2}\, \ell_a\, i_a \quad)
\end{aligned}\right\} \qquad 4.49$$

The equations derived above are very similar to Eqns. 4.35 and 4.36 for the basic two-winding machine. However, in Eqn. 4.49 an attempt is made to take into account the different leakage paths which are unique to

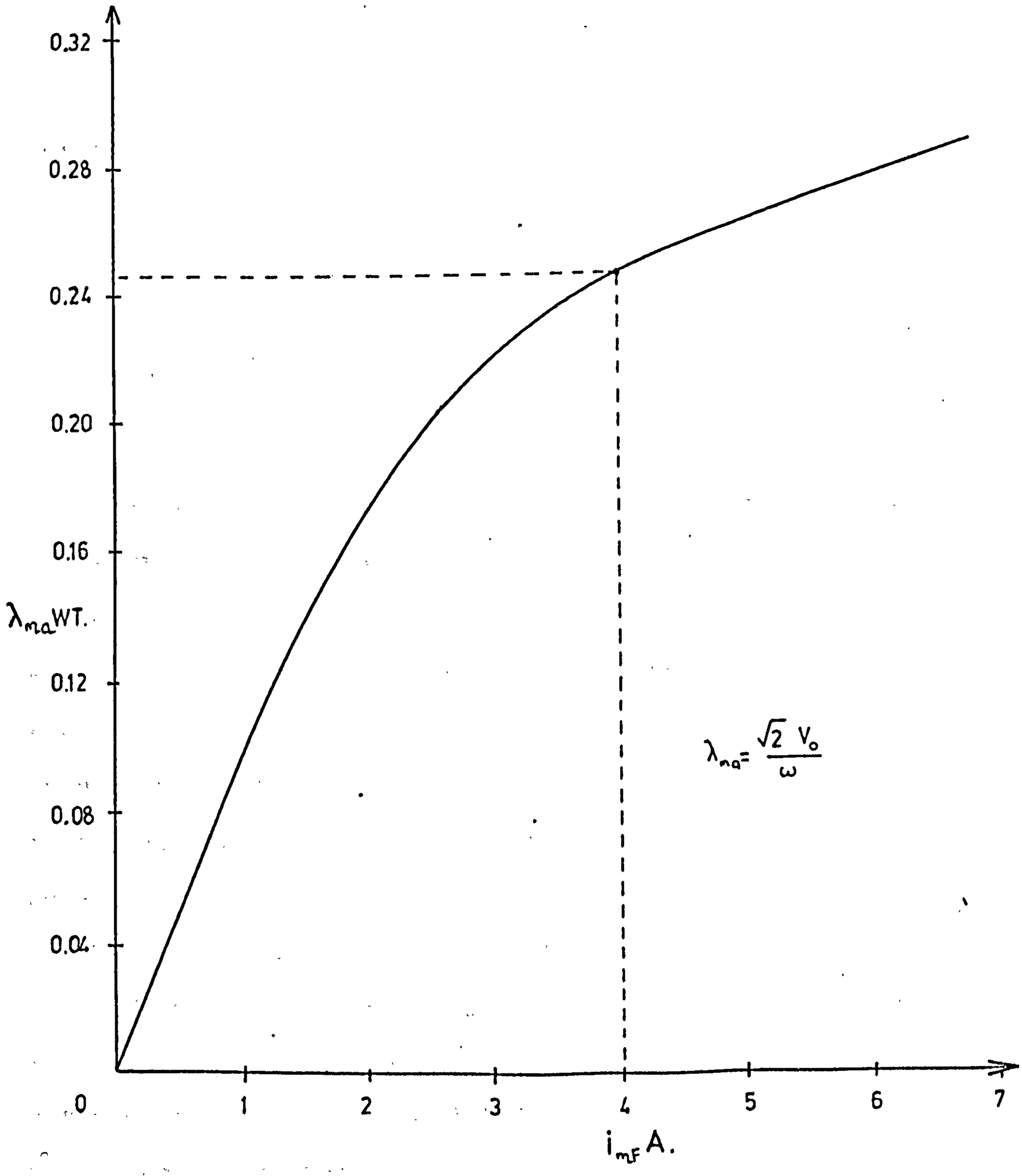

Fig. 4-11 No-Load Magnetization Characteristic of the Test Single-Phase Synchronous Generator

the synchronous machine since direct and alternating currents flow in the rotating and fixed windings respectively. Assumptions are made in this process and in the next sections it is hoped to show that these assumptions are valid to an acceptable degree of accuracy.

The bond graph representation of the single-phase synchronous generator is shown in Fig. 4-12, where the terminal constraint equations for generator action are:

$$\left.\begin{aligned} \dot{\lambda}_F &= \nu_F - i_F R_F \\ \dot{\lambda}_D &= i_D R_D \\ \dot{\lambda}_Q &= i_Q R_Q \\ \dot{\lambda}_a &= \nu_A + i_a R_a \end{aligned}\right\} \qquad 4.50$$

where R are the resistances of the windings and ν are the terminal voltages, with the appropriate subscript indicating the particular winding. In Eqn. 4.50, the constraint equation for the armature winding has a positive term. This is because the convention used is such that all inputs into the system are positive and all outputs are negative. As such for generator action the last three equations of Eqn. 4.49 will have negative leakage terms and Eqn. 4.47 must also undergo the necessary sign changes.

From the bond graph representation, the computation structure may be obtained as shown in Fig. 4-13. It is assumed here that the speed is constant even under unbalanced conditions. To avoid complicating the structure, only the direct-axis damper winding is represented in Fig. 4-13 as the quadrature-axis damper winding is a duplication of the former.

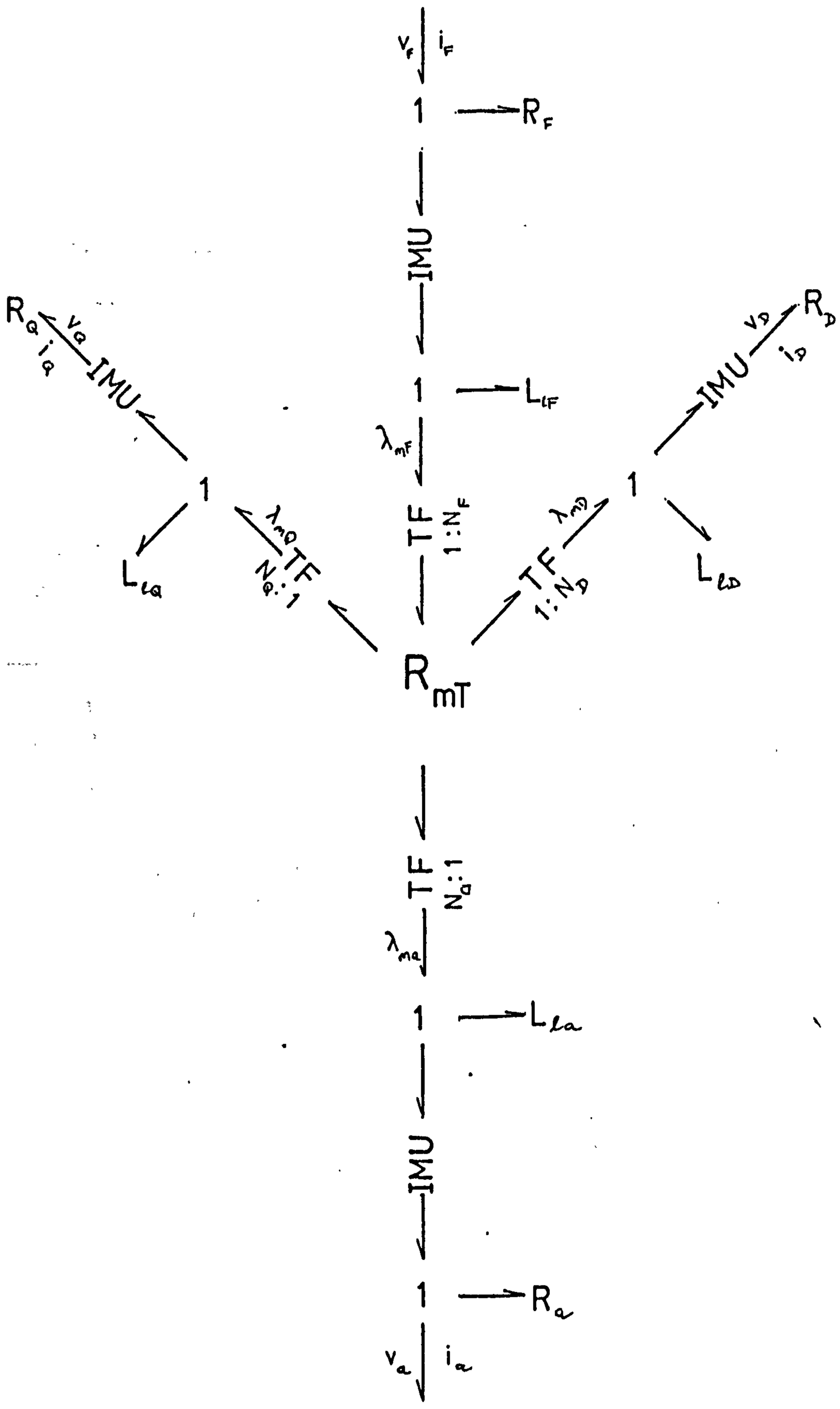

Fig. 4-12 Bond Graph Representation of a Single-Phase Generator with Dampers (constant speed)

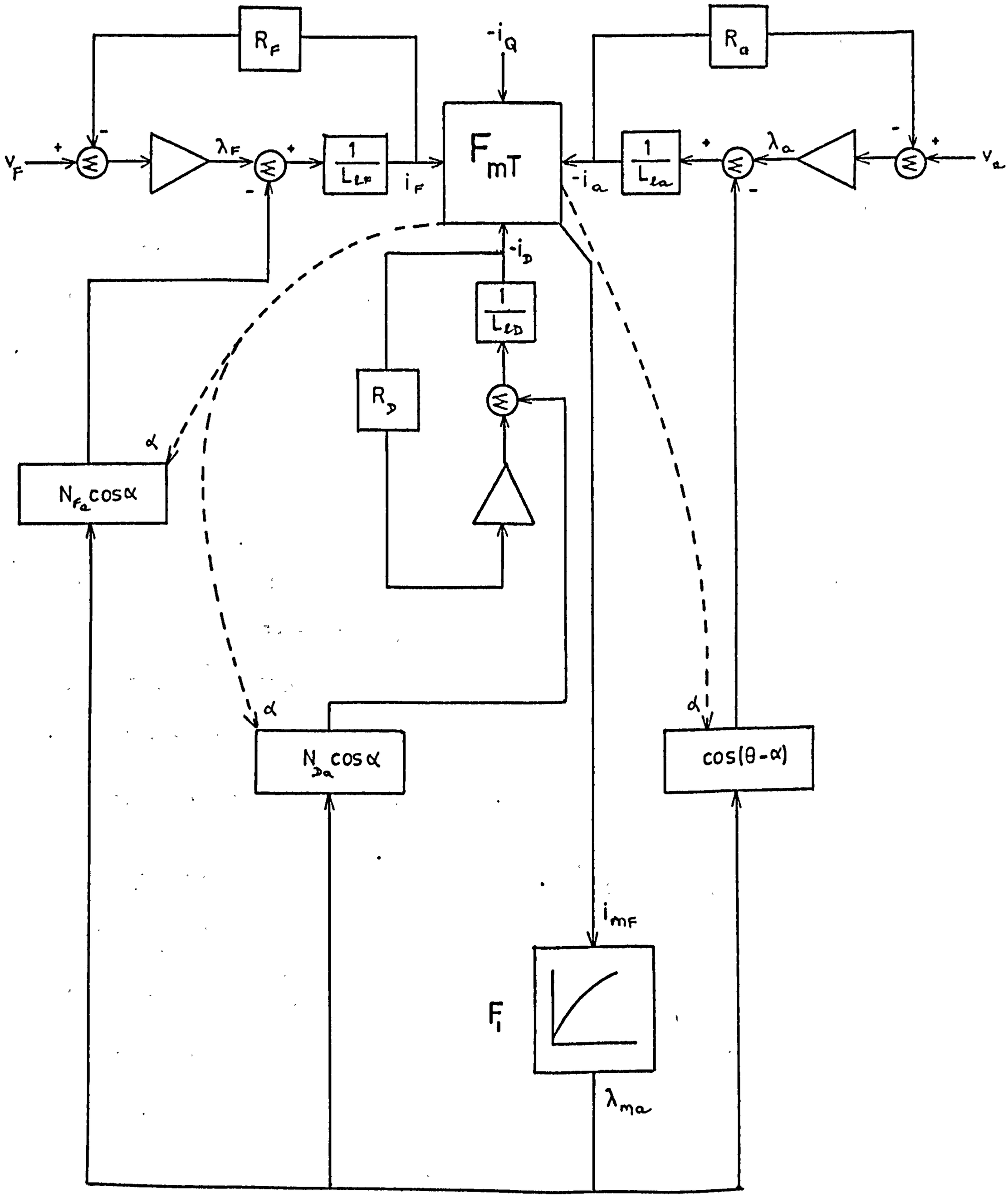

Fig. 4-13 Computation Structure for a Single-Phase Generator with Dampers (constant speed)

4.4.3 Short-Circuit of Single-Phase Synchronous Generator

The computation structure developed in Fig. 4-13 is particularly suitable for solution by the standard computer program, SYSTRAN. Details of this program together with the method of arranging the system equations are given in Appendix B.

In the study of short-circuit of single-phase synchronous generator, the armature constraint equation has to be altered such that $v_a = 0$, thus:

$$\dot{\lambda}_a = i_a R_a \qquad 4.51$$

The mixed differential and algebraic equations obtained in the preceding section are solved by SYSTRAN with a step length of t = 0.0003 second. The simulated results obtained are compared with experimental results as well as with those calculated by the method proposed by Reddy, Ali and Jones[6]. The following tables indicate the differences in the results:

Table 4-1 Comparison of Armature Currents (Amps.)

Method	1st Peak	2nd Peak	3rd Peak	4th Peak
Experimental	348.5	-194.6	149.5	-126.0
Simulated (Bond Graph)	332.5	-197.6	176.1	-147.6
Reedy, Ali & Jones	303.0	-163.5	175.7	-146.5

Table 4-2 Comparison of Field Currents (Amps.)

Methods	1st Peak	2nd Peak	3rd Peak	4th Peak
Experimental	23.8	13.8	11.1	10.0
Simulated (Bond Graph)	23.4	14.3	12.9	11.0
Reedy, Ali & Jones	21.2	12.0	12.8	10.9

A set of oscillogram from the three methods discussed are plotted in Fig. 4-14. It is evident that the method developed in this chapter gives a better estimate of the first subtransient peaks. Perhaps the effort made in trying to approximate the leakage flux paths is valid during this very short initial period. However, eddy current loss which has an important influence on the behaviour of solid rotor synchronous machine immediately after sudden short-circuit is not taken into account. Field theory has shown that this loss is caused by circulating currents in the laminations which make up the machine iron circuit. Indeed the laminations are introduced to keep this loss to an acceptable minimum. The laminations behave as short-circuited windings, and the losses in them are supplied by simple transformer action.

It is probable that these eddy currents provide the extra damping which is observed in the experimental results and is responsible for the discrepancies between the experimental and calculated results particularly after the second and subsequent peaks. Other factors which are not considered in the modelling of the single-phase synchronous generators are:

(i) the in-phase spatial harmonics, although very small have quite a pronounced effect at the first peak,

(ii) hysteresis has been neglected, and

(iii) the leakage flux linkages, although adjusted for the effects of the direct and alternating cirrents in the windings, are assumed linear.

In spite of this, the agreement between the results predicted by the digital model and the experimental results,

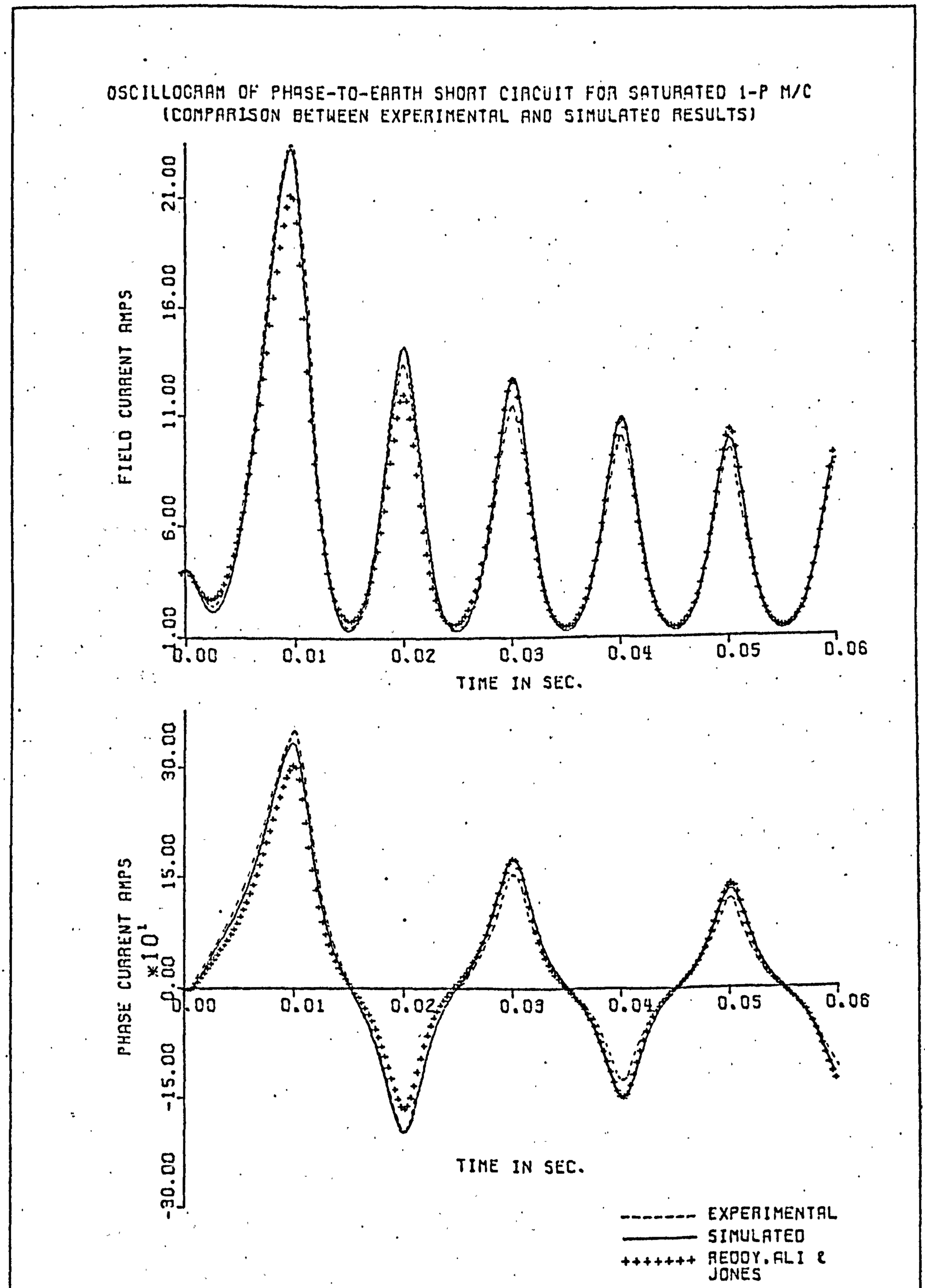

Fig. 4-14 Short-Circuit Currents for the Single-Phase Synchronous Generator

may be regarded as very close, especially since the whole range from sub-transient to steady-state is covered.

The relevant parameters for the single phase synchronous generator tested are given in Appendix D.

4.5 Three-Phase Synchronous Machine

A three-phase synchronous machine differs physically from the single phase machine in as far as the one phase winding is replaced by a balanced three phase windings. In practice the three windings can be achieved by proper inter-connection of a uniform layer of conductors on the cylindrical surface of the stator. In order to get an approximately sinusoidal flux density for the phase windings a large number of conductors is necessary. The mmfs' vector diagram of the three-phase machine is similar to that established for the single-phase machine, shown in Fig. 4-9, however with the single armature mmf being replaced by a balanced three-phase mmf spaced at 120^{o} apart.

For generator action, the magnitude and direction of the resultant magnetizing current referred to the field winding is:

$$i_{mF}\cos\alpha = i_F - N_{DF}i_D - N_{aF}\left[i_a\cos\theta_1 + i_b\cos\theta_2 + i_c\cos\theta_3\right] \quad 4.52$$

$$i_{mF}\sin\alpha = -N_{QF}i_Q - N_{aF}\left[i_a\sin\theta_1 + i_b\cos\theta_2 + i_c\cos\theta_3\right]$$

where θ_1 is the rotor or field axis displacement angle from the axis of phase a, $\theta_2 = \theta_1 - 120^{o}$, $\theta_3 = \theta_1 + 120^{o}$; i_a, i_b and i_c are the instantaneous armature currents in phases a, b and c respectively.

The non-linear relationship between the resultant magnetizing current, i_{mF}, and the armature flux linkage,

λ_{ma}, is given in Appendix D together with the details and relevant parameters of the test three-phase synchronous generator. In general this relationship may be written as:

$$\lambda_{ma} = F\ (i_{mF}) \qquad 4.53$$

where $F\ (i_{mF})$ is a function if i_{mF}.

The currents in the windings of the generator are defined by the algebraic equations identical to Eqn. 2.45, thus:

$$\left.\begin{aligned} i_F &= \frac{1}{\frac{3}{2}\ell_F}\left[\lambda_F - \sqrt{3}\,N_{Fa}\,\lambda_{ma}\cos\alpha\right] \\ i_D &= \frac{1}{\frac{3}{2}\ell_D}\left[\sqrt{3}\,N_{Da}\,\lambda_{ma}\cos\alpha - \lambda_D\right] \\ i_Q &= \frac{1}{\frac{3}{2}\ell_Q}\left[\sqrt{3}\,N_{Qa}\,\lambda_{ma}\sin\alpha - \lambda_Q\right] \end{aligned}\right\} \qquad 4.54$$

$$\left.\begin{aligned} i_a &= \frac{1}{\sqrt{2}\,\ell_a}\left[\lambda_{ma}\cos(\Theta_1 - \alpha) - \lambda_a\right] \\ i_b &= \frac{1}{\sqrt{2}\,\ell_b}\left[\lambda_{ma}\cos(\Theta_2 - \alpha) - \lambda_b\right] \\ i_c &= \frac{1}{\sqrt{2}\,\ell_c}\left[\lambda_{ma}\cos(\Theta_3 - \Theta) - \lambda_c\right] \end{aligned}\right\}$$

where ℓ_a, ℓ_b and ℓ_c are the armature leakage inductances for phases a, b and c. The $\sqrt{3}$ factor included in the first three equations of Eqns. 4.54 is necessary in view of the fact that a three-phase generator is considered[5].

The terminal constraint equations are the derivatives of the flux linkages and are given by:

$$\left.\begin{aligned}
\dot{\lambda}_F &= \nu_F - i_F R_F \\
\dot{\lambda}_D &= i_D R_D \\
\dot{\lambda}_Q &= i_Q R_Q \\
\dot{\lambda}_a &= \nu_a + i_a R_a \\
\dot{\lambda}_b &= \nu_b + i_b R_b \\
\dot{\lambda}_c &= \nu_c + i_c R_c
\end{aligned}\right\} \quad 4.55$$

where R are the resistances of the windings and ν are the terminal voltages, with the appropriate subscript indicating the particular winding.

The bond graph representation of the three-phase synchronous generator is shown in Fig. 4-15. Unlike the case for the single-phase generator, the bond graph for the three-phase generator has a symmetrical configuration. This is expected since the latter is a balanced electromechanical energy conversion device.

The electrical torque expression in terms of three phase quantities is given by[26]:

$$\tau_e = P\,(\tau_a + \tau_b + \tau_c)$$

$$= \frac{P}{\sqrt{3}}\left[\lambda_{mA}(i_b - i_c) + \lambda_{mB}(i_c - i_a) + \lambda_{mC}(i_a - i_b)\right] \quad 4.56$$

where

$$\left.\begin{aligned}
\lambda_{mA} &= \lambda_{ma} \cos(\theta_1 - \alpha) \\
\lambda_{mB} &= \lambda_{ma} \cos(\theta_2 - \alpha) \\
\lambda_{mC} &= \lambda_{ma} \cos(\theta_3 - \alpha)
\end{aligned}\right\} \quad 4.57$$

and P is the number of pole pairs.

Referring to Fig. 4-15, the phase rotational voltages can be obtained at the 1-junction of the hexagonal structure as:

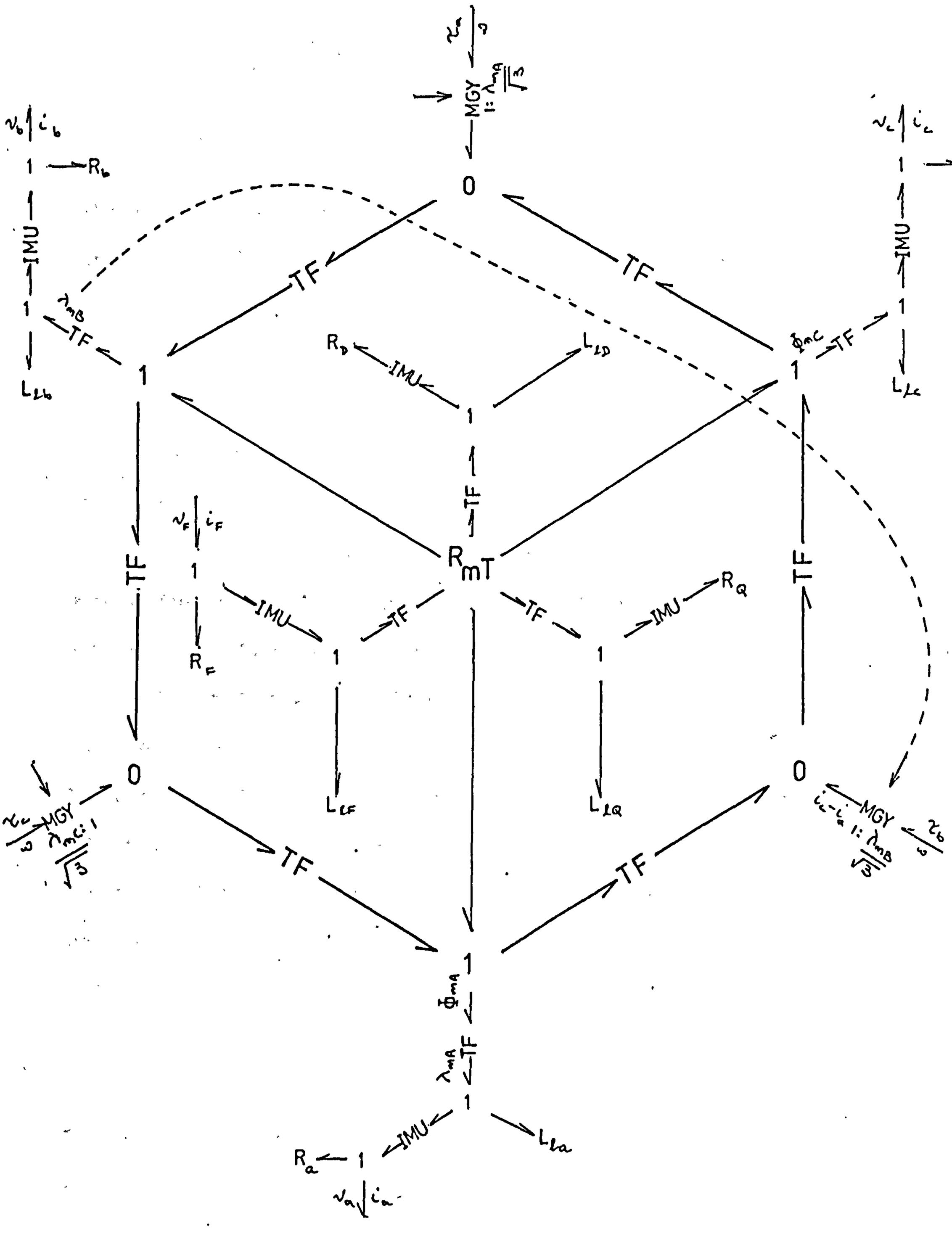

Fig. 4-15 Bond Graph Representation of a Three-Phase Synchronous Generator with Dampers

$$v_{Ra} = \frac{\omega N_a}{\sqrt{3}} (\phi_{mC} - \phi_{mB})$$

$$v_{Rb} = \frac{\omega N_b}{\sqrt{3}} (\phi_{mA} - \phi_{mC}) \qquad 4.58$$

$$v_{Rc} = \frac{\omega N_c}{\sqrt{3}} (\phi_{mB} - \phi_{mA})$$

where $\phi_{mA} = \frac{\lambda_{mA}}{N_a}$ and similarly for ϕ_{mB} and ϕ_{mC}; ω is the angular speed of the rotor and v_R are the rotational voltages with the appropriate subscript indicating the particular winding. In the absence of terminal currents, that is an open circuit, the rotational voltages are the open circuit voltages. There is no component of the rotational voltage in either the field or damper windings. This is expected since their flux linkage expressions are not a function of $\theta = \omega t + \delta$, where δ is the initial rotor angle with phase a at t = 0.

The rotational voltages are contributed exclusively by the power bond comprising the hexagonal structure in Fig. 4-15. From the direction of the power flow, it is observed that energy is exchanged between alternate 'phase' mechanical and electrical junctions, which for this particular balanced operation occurs in the counter-clockwise direction. However, under unbalanced conditions some of the power bonds have to be removed or altered and as such the symmetrical configuration of Fig. 4-15 no longer holds. The bond graph representation of the single-phase synchronous generator shown in Fig. 4-12 is an example of unbalanced operation.

4.5.1 Line-to-Neutral Short-Circuit

The dynamic behaviour of a three-phase synchronous generator under line-to-neutral short-circuit is identical

to that of a short-circuited single-phase generator. With the other two phases on open circuit, the fault currents in the rest of the windings may be calculated using the same equations as developed for the single-phase generator in Sections 4.4.2 and 4.4.3.

The test generator is applied with a line-to-neutral short-circuit at phase c, with phases a and b on open circuit; and oscillograms of this test are recorded. A comparison of this experimental and simulated result obtained from bond graph analysis is tabulated in Tables 4-3 and 4-4.

Table 4-3 Comparison of Phase 'c' Armature Currents (Amps) for Line-to-Neutral Short Circuit

Methods	1st Peak	2nd Peak	3rd Peak	4th Peak
Experimental	482.8	-83.3	421.5	-134.9
Simulated (Bond Graph)	479.1	-78.5	411.6	-132.7

Table 4-4 Comparison of Field Currents (Amps) for Line-to-Neutral Short-Circuit

Methods	1st Peak	2nd Peak	3rd Peak	4th Peak
Experimental	146.9	53.9	131.6	65.5
Simulated (Bond Graph)	146.4	52.3	130.4	64.9

The simulated oscillogram of the short-circuit currents together with that of the magnitude and angle of the resultant magnetizing current is shown in Fig. 4-16. A very interesting feature of these graphs is that at the peak of the armature and field currents, that is when $\frac{di}{dt} = 0$, the magnetizing current undergoes a rapid change equivalent to $\frac{di_{mF}}{dt} \rightarrow \infty$. The rapid change of the magnetizing current or resultant mmf at position 2 occurs when the flux

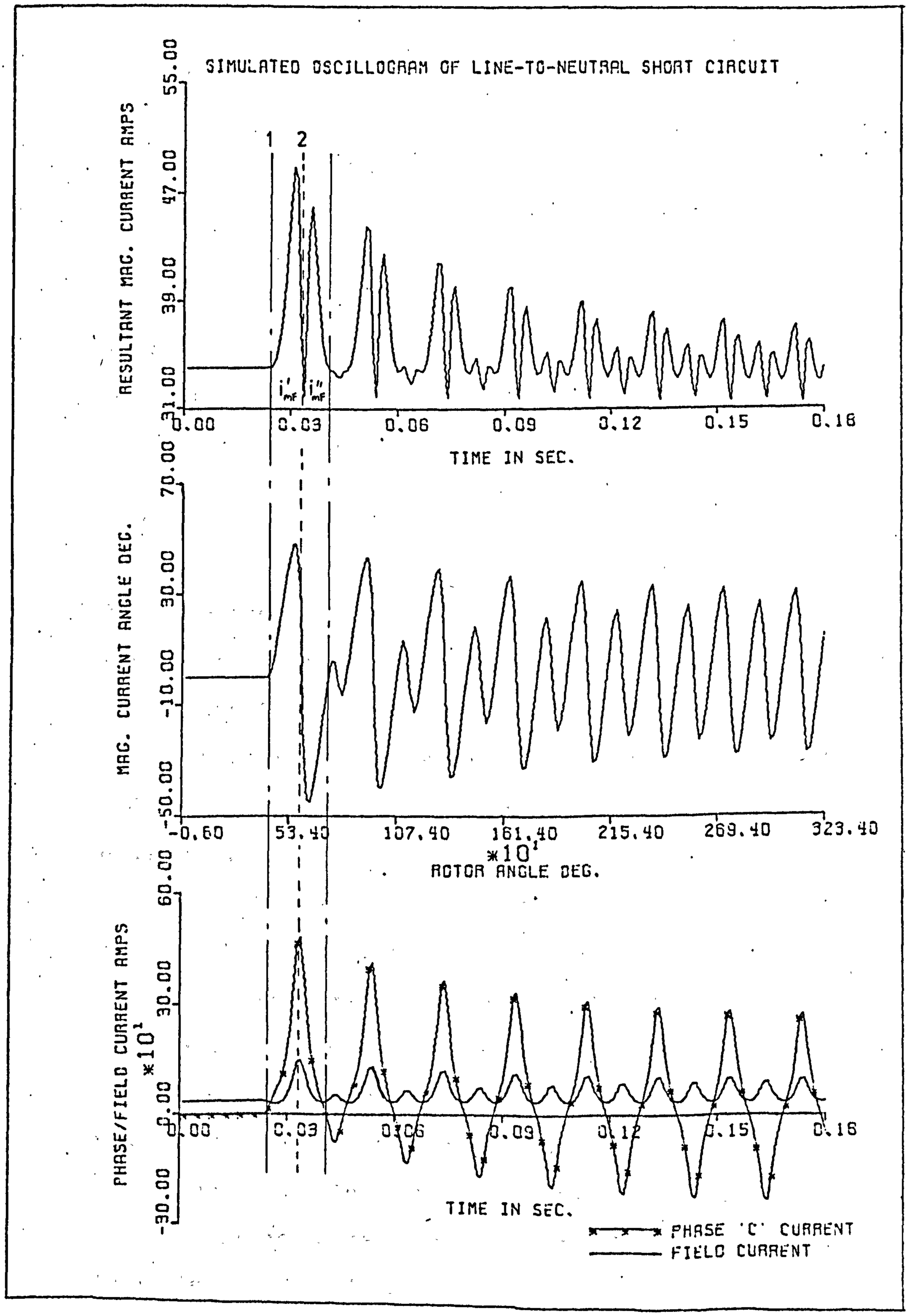

Fig. 4-16 Line-to-Neutral Short-Circuit Currents for the Three-Phase Synchronous Generator

linking the stator and rotor windings is a maximum, as illustrated in Fig. 4-17. With the mmfs' vector diagrams shown, the magnetizing current, i_{mF}, falls to a minimum value and then rises to another maximum value after reaching position 2. During this process the resultant magnetizing current, i_{mF}, oscillates about the field axis at twice the supply frequency.

The simplified mmfs' vector diagrams together with schematic diagrams of a simple single-phase synchronous generator with the damper windings ignored shown in Fig. 4-17, can explain the double frequency phenomenon.

4.5.2 Line-to-Line Short-Circuit

Apart from the line-to neutral short-circuit, the line-to-line short circuit is the more frequently encountered fault for the three-phase synchronous generator. In Section 4.5, the internal characteristics of the synchronous generator is described by Eqns. 4.52, 4.53 and 4.54, while Eqn. 4.55 is the terminal constraint equations.

When the test generator has a line-to-line fault between phases a and c with phase b on open circuit, the generator equations must be modified such that the phase b current and flux linkage equations are omitted since $i_b = 0$ and that a condition is imposed whereby the faulted phase currents have the relationship given by, $i_a = -i_c$.

The peak values of the armature and field currents obtained experimentally and from simulation are compared in Tables 4-5 and 4-6.

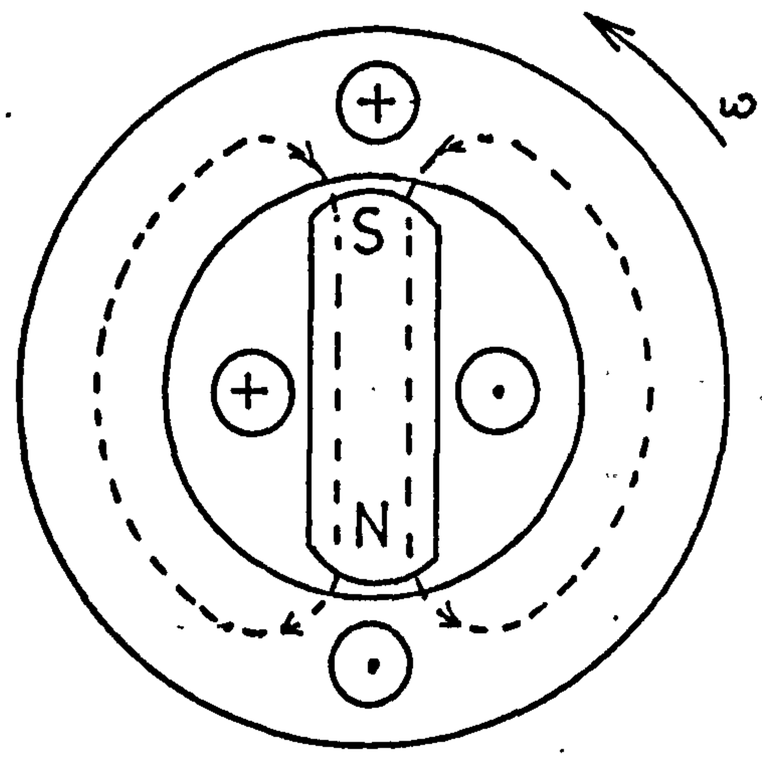

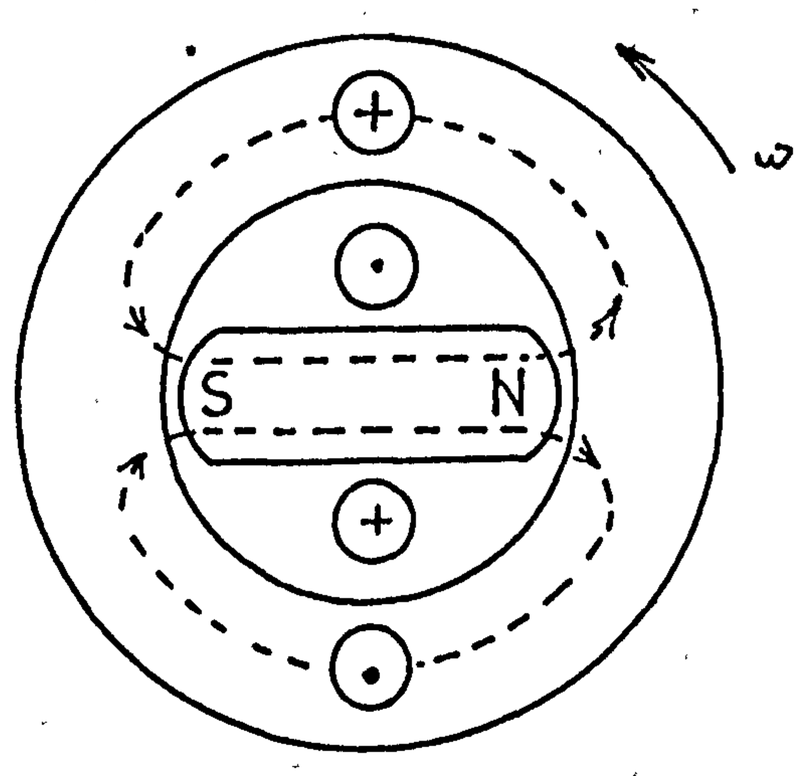

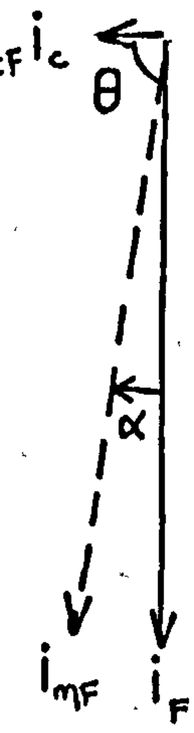

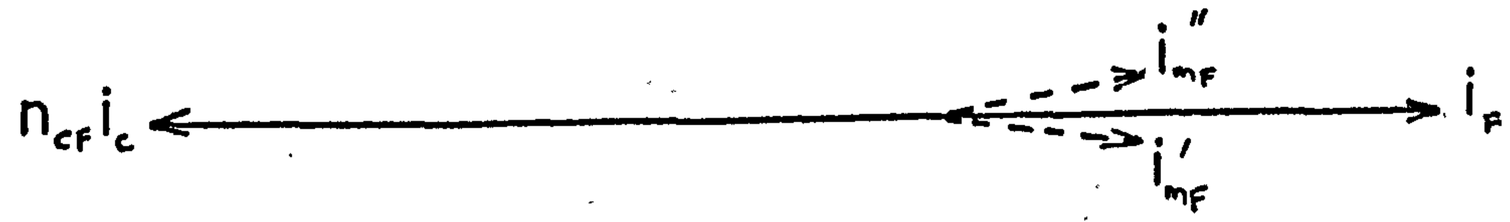

$\theta = 90^{o}$

$i_c \longrightarrow 0$

$\alpha \longrightarrow 0$

For this brief period i_{mF} oscillates rapidly giving rise to the double frequency.

Fig. 4-17 Simplified Mmfs' Vector Diagram for Line-to-Neutral Short-Circuit

Table 4-5 Comparison of Phase 'a' Armature Currents (Amps.) for Line-to-Line Short-Circuit

Methods	1st Peak	2nd Peak	3rd Peak	4th Peak
Experimental	648.6	-112.8	535.8	-141.0
Simulated (Bond Graph)	669.3	-120.1	569.2	-200.5

Table 4-6 Comparison of Field Currents (Amps.) for Line-to-Line Short-Circuit

Methods	1st Peak	2nd Peak	3rd Peak	4th Peak
Experimental	210.2	79.1	185.3	95.6
Simulated (Bond Graph)	212.4	81.1	188.4	100.2

From the tables above, it is observed that the simulated peak currents for line-to-line short-circuit are slightly larger than those obtained experimentally, while for the line-to-neutral short-circuit the simulated and experimental results are in better agreement. Perhaps the assumed leakage path discussed in Section 4.4.2 has to be altered slightly not only for different types of synchronous generators but also for different fault conditions due to varying flux behaviours.

However, apart from the additional damping in the third and subsequent peaks present in the experimental results, the simulation technique used gives a reasonable degree of accuracy particularly for the field current.

The simulated oscillogram of the line-to-line short-circuit is shown in Fig. 4-18.

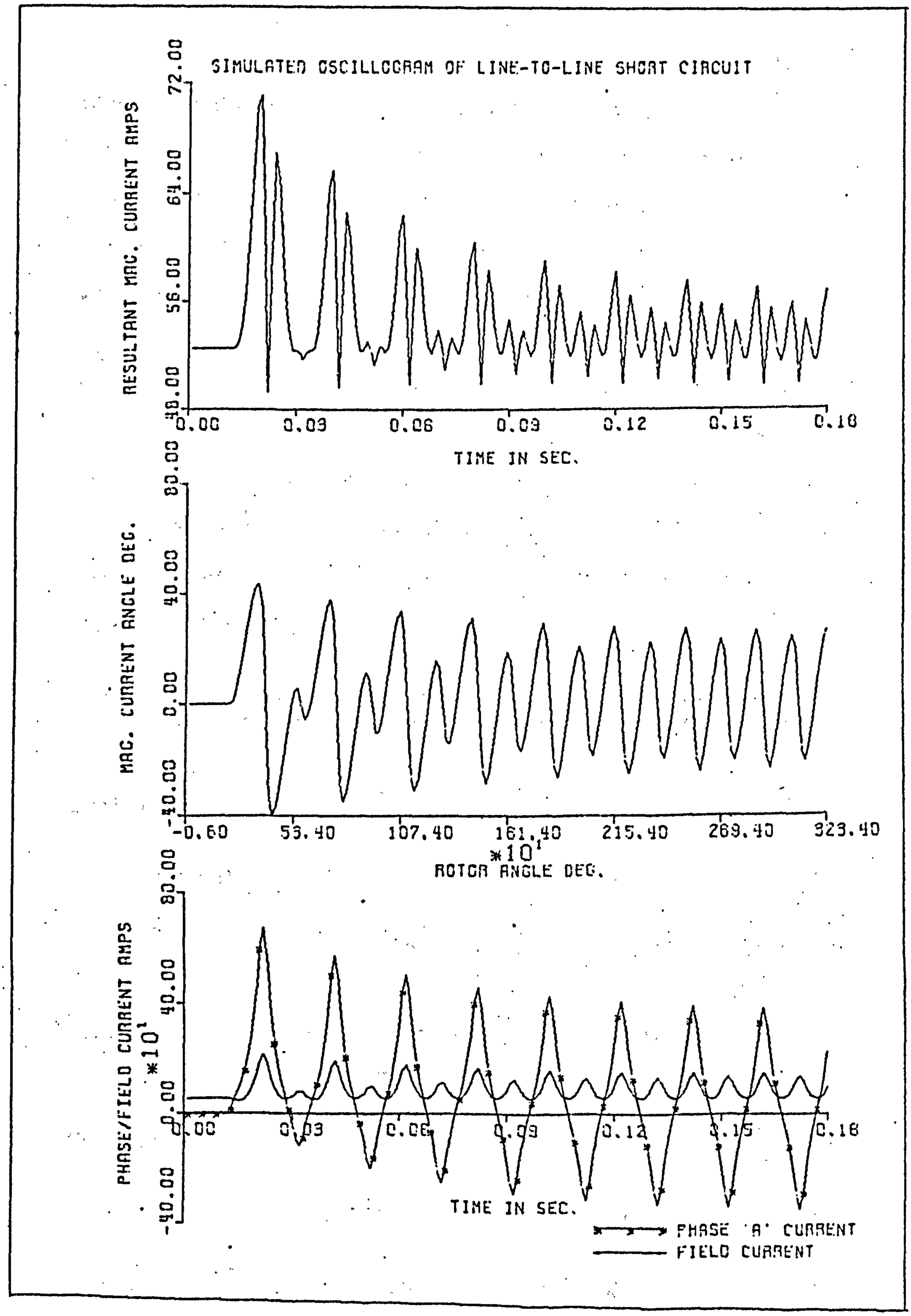

Fig. 4-18 Line-to-Line Short-Circuit Currents for the Three-Phase Synchronous Generator

4.5.3 Symmetrical Three-Phase Short-Circuit

The sudden symmetrical short-circuit of the three-phase synchronous generator, although a comparatively unusual phenomenon, has always been traditionally simpler to analyse[4,5,9]. From Eqns. 4.52, 4.53, 4.54 and 4.55, the symmetrical three-phase short-circuit may be simulated with conditions imposed such that, $v_a = v_b = v_c = 0$ and $i_a + i_b + i_c = 0$, since the generator is operating under balanced short circuit load. As such only two phase currents and two flux linkages need to be calculated as the third can be derived from the two known values.

The differences between the peak currents obtained from experimental and simulated results are shown in Tables 4-7 and 4-8.

Table 4-7 Comparison of Phase 'b' Armature Currents (Amps.) for Symmetrical Three-Phase Short-Circuit

Methods	1st Peak	2nd Peak	3rd Peak	4th Peak
Experimental	701.6	-191.1	600.6	-245.7
Simulated (Bond Graph)	697.2	-224.4	598.3	-286.5

Table 4-8 Comparison of Field Currents (Amps.) for Symmetrical Three-Phase Short-Circuit

Methods	1st Peak	2nd Peak	3rd Peak	4th Peak
Experimental	211.5	81.2	201.0	93.8
Simulated (Bond Graph)	210.6	82.5	185.0	101.8

The simulated oscillogram of the symmetrical short-circuit is shown in Fig. 4-19. The double frequency component caused by the oscillations of the resultant magnetizing current for the unbalanced fault conditions is absent in the field current for symmetrical short-circuit.

4.5.4 Effects of Saturation and Damper Winding Representations

For the sake of analytical expediency, the no-load magnetization characteristic is often linearized by using either the air-gap line or the equivalent unsaturated line which is a straight line through the origin and the rated-voltage point on the magnetization characteristic, as in Fig. 4-20. Based on these representations of the magnetization characteristic, the simulated values of symmetrical short-circuit currents may be obtained and the results are shown in Fig. 4-21.

In the case of this particular machine, the predicted results using the air-gap line are much larger than those obtained from either the exact saturated characteristic or its unsaturated equivalent. Hence methods of fault current prediction based on measured linear inductances normally tend to over-estimate the experimental results[5] since measurements of machine inductances are often performed at reduced voltages and as such are actually parameters on the air-gap line below point Q, in Fig. 4-20.

With respect to the terminal armature and field currents, the results from the saturated and equivalent unsaturated characteristics are in good agreement with each other because in both cases the same initial armature flux linkage, that is, the same operating point on the

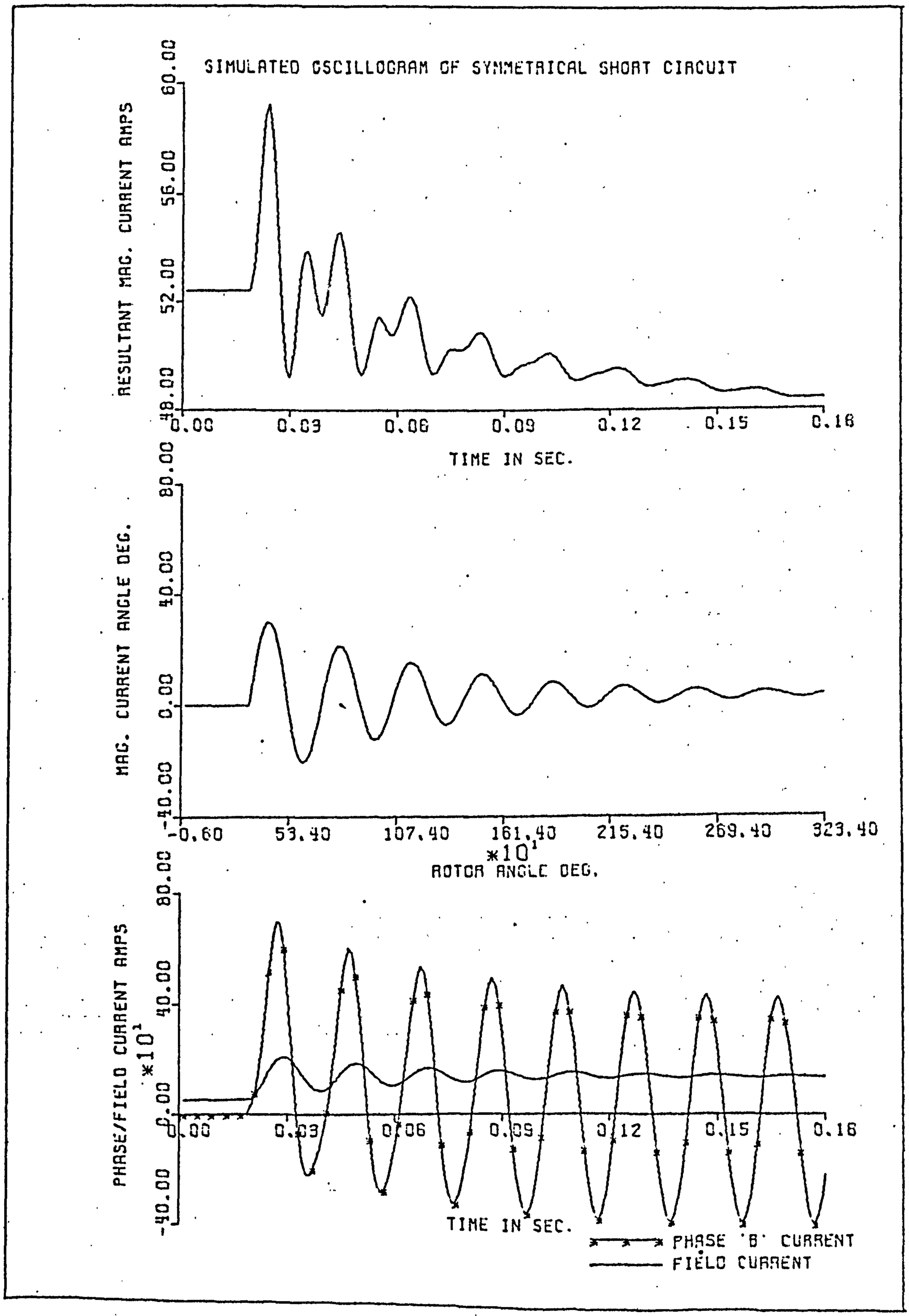

Fig. 4-19 Symmetrical Short-Circuit Currents for the Three-Phase Synchronous Generator

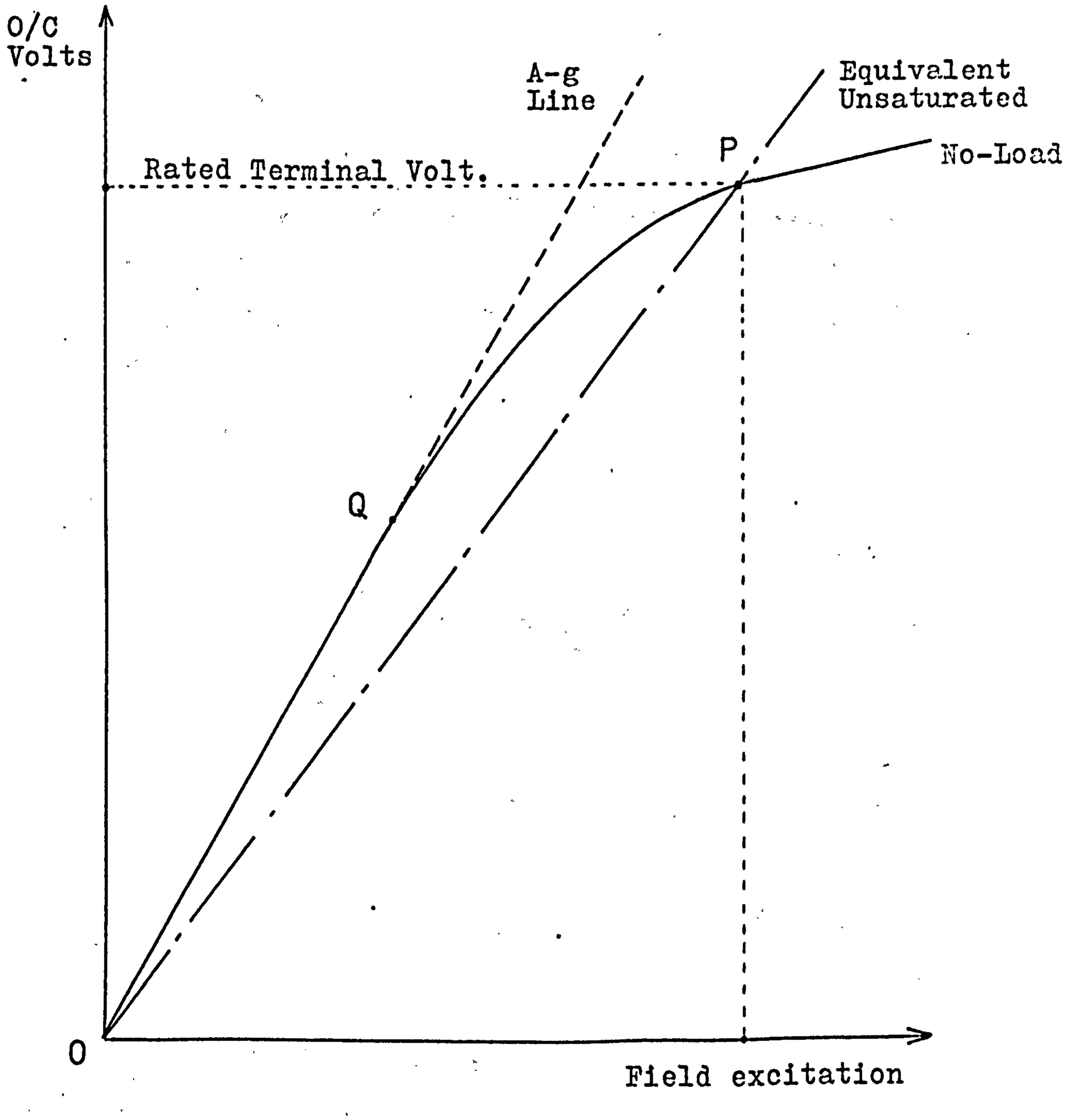

Fig. 4-20 Linearization of the No-Load Magnetization Characteristics

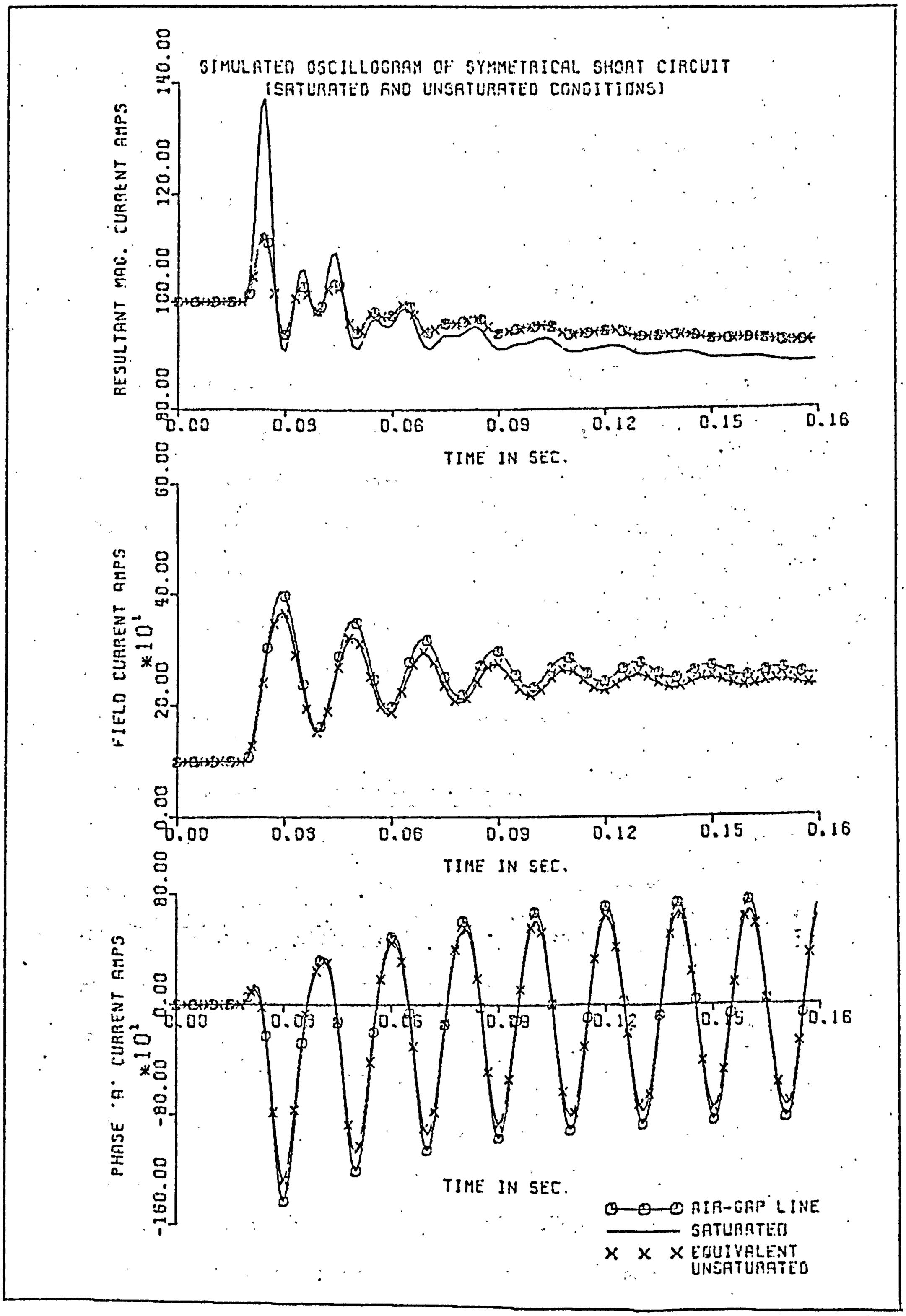

Fig. 4-21 Effects of Linearizing the Magnetization Characteristic on Symmetrical S/C Currents

magnetization characteristic is used. However, there is considerable differences between the values of their magnetizing currents which may perhaps be due to the discrepancies between the slopes of the saturated curve and the equivalent unsaturated line, above and below point P, in Fig. 4-20.

Damping is a complex phenomenon and as such suggests that its representation by only two coils, one in the d-axis and the other in the q-axis may not be sufficient. However, for the machine investigated the representation of damper windings in the two axes is quite valid since the three-phase representation gives identical results to that of the former as shown in Fig. 4.22.

A complete set of the simulated oscillogram for the three-phase generator under both balanced and unbalanced conditions is included in Appendix E.

4.6 Three-Phase Induction Machine

In this section, it is intended to show that the simulation technique developed may be used for all types of electromechanical energy converters. The example chosen is the study of direct-on-line starting of a polyphase induction motor coupled to a mechanically resonant load, details of which appear in Appendix D.

The induction machine, shown schematically in Fig. 4-23, has alternating currents flowing in both the stator and rotor windings, those in the rotor usually being the result of electromagnetic induction from the stator.

Following the steps taken for the basic two winding machine in Section 4.4.1, the total flux linkage in the

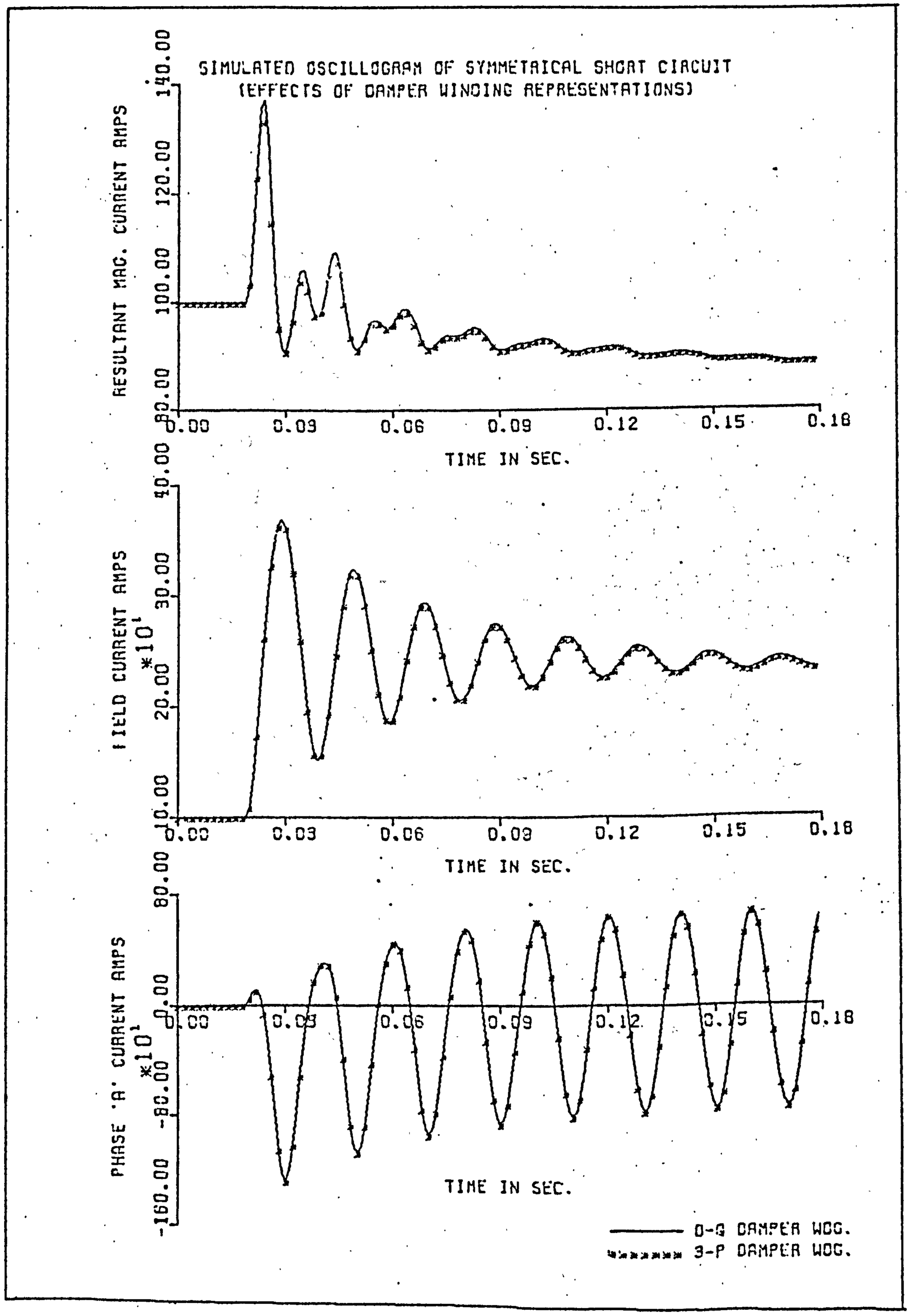

Fig. 4-22 Effects of Three-Phase and d-q Damper Representations

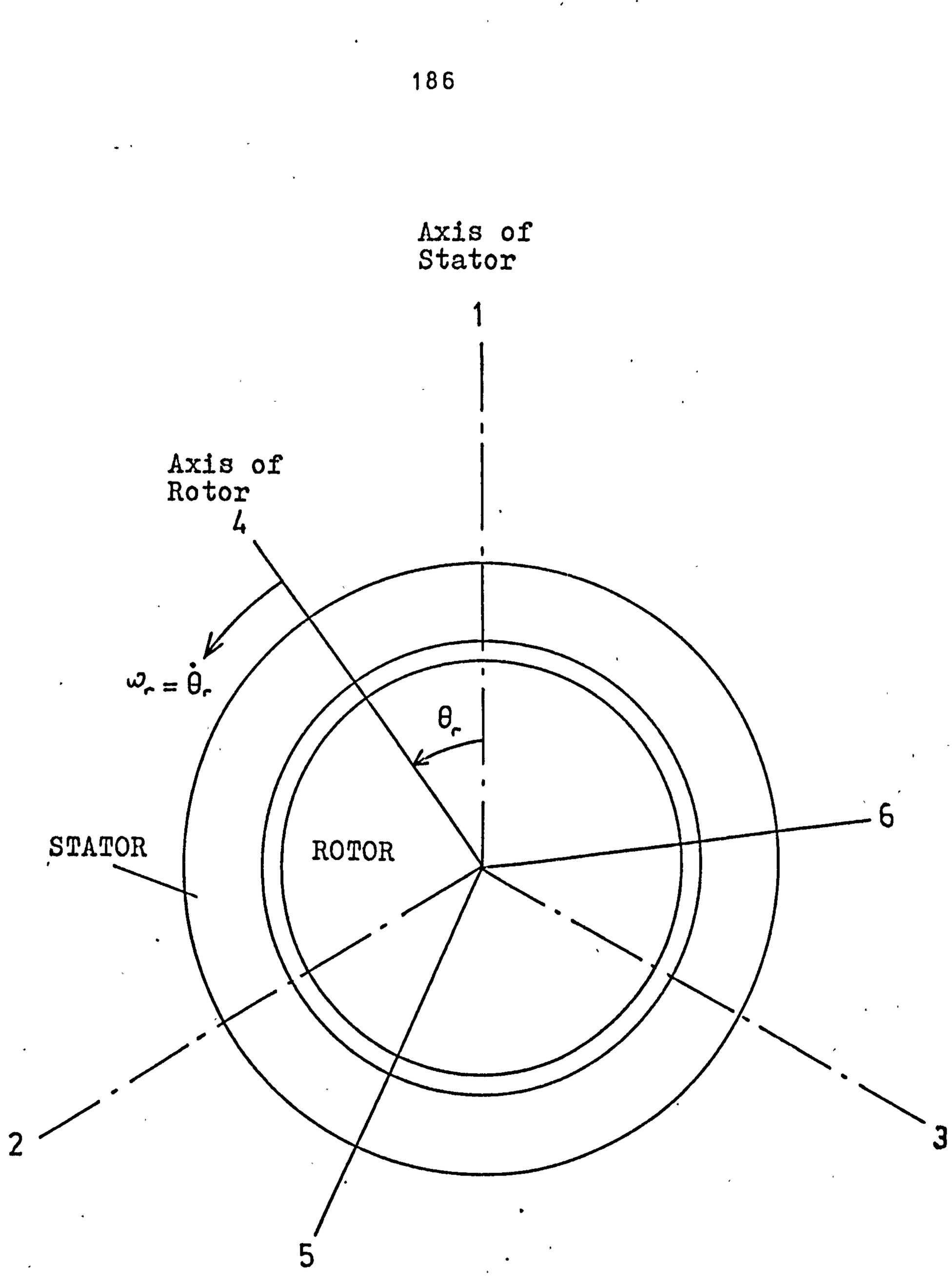

Fig. 4-23 Idealized Three-Phase Induction Machine

stator winding 1 of Fig. 4-23 resolved along its axis may be expressed as[28]:

$$\lambda_1 = L_{ms}\ (i_1 + i_2 \cos 120^o + i_3 \cos 240^o) +$$

$$(\frac{N_r}{N_s}).L_{mr}\left[i_4 \cos \theta_r + i_5 \cos\ (\theta_r + 120^o) + \right.$$

$$\left. i_6 \cos\ (\theta_r - 120)\right] + \ell_1 i_1 \qquad 4.59$$

where L_{ms} and L_{mr} are the stator and rotor magnetizing inductances respectively; θ_r is the rotor displacement angle; N_s and N_r are the stator and rotor turns ratio respectively; ℓ_1 is the leakage inductance for the stator winding 1 and i are the instantaneous winding currents with the appropriate subscripts indicating the particular winding.

Similarly for stator windings 2 and 3, the stator flux linkages may be written in general as:

$$\begin{bmatrix}\lambda_1\\ \lambda_2\\ \lambda_3\end{bmatrix} = L_{ms}\,[A]\begin{bmatrix}i_1\\ i_2\\ i_3\end{bmatrix} + \frac{N_r}{N_s}\cdot L_{mr}\,[B]\begin{bmatrix}i_4\\ i_5\\ i_6\end{bmatrix} + \begin{bmatrix}\ell_1 i_1\\ \ell 2 i_2\\ \ell_3 i_3\end{bmatrix} \qquad 4.60$$

where

$$[A] = \begin{bmatrix} 1 & \cos 120^o & \cos 240^o \\ \cos 240^o & 1 & \cos 120^o \\ \cos 120^o & \cos 240^o & 1 \end{bmatrix}$$

$$[B] = \begin{bmatrix} \cos \theta_r & \cos(\theta_r+120^o) & \cos(\theta_r-120^o) \\ \cos(\theta_r-120^o) & \cos \theta_r & \cos(\theta_r+120^o) \\ \cos(\theta_r+120^o) & \cos(\theta_r-120^o) & \cos \theta_r \end{bmatrix}$$

and the stator windings 1, 2 and 3 correspond to the phases a, b and c respectively.

Also, the rotor flux linkage may be express in matrix form as:

$$\begin{bmatrix}\lambda_4\\ \lambda_5\\ \lambda_6\end{bmatrix} = \left(\frac{N_s}{N_r}\right) L_{ms}\left[B^t\right]\begin{bmatrix}i_1\\ i_2\\ i_3\end{bmatrix} + L_{mr}\left[A\right]\begin{bmatrix}i_4\\ i_5\\ i_6\end{bmatrix} + \begin{bmatrix}\ell_4 i_4\\ \ell_5 i_5\\ \ell_6 i_6\end{bmatrix} \qquad 4.61$$

where $\left[B^t\right]$ is the transpose of $\left[B\right]$.

For both the stator and rotor windings, the terminal constraint equations are:

$$\left.\begin{aligned}
\dot{\lambda}_1 &= \nu_1 - i_1 R_1 \\
\dot{\lambda}_2 &= \nu_2 - i_2 R_2 \\
\dot{\lambda}_3 &= \nu_3 - i_3 R_3 \\
\dot{\lambda}_4 &= -i_4 R_4 \\
\dot{\lambda}_5 &= -i_5 R_5 \\
\dot{\lambda}_6 &= -i_6 R_6
\end{aligned}\right\} \qquad 4.62$$

where ν and R are the voltages and resistances respectively with the appropriate subscript indicating the particular winding.

The torque equation is given by:

$$\tau_m = \frac{P}{\sqrt{3}}\left[\lambda_4(i_5 - i_6) + \lambda_5(i_6 - i_4) + \lambda_6(i_4 - i_5)\right] \qquad 4.63$$

where P is the number of pole pairs. The bond graph representation of the three-phase induction motor is shown in Fig. 4-24.

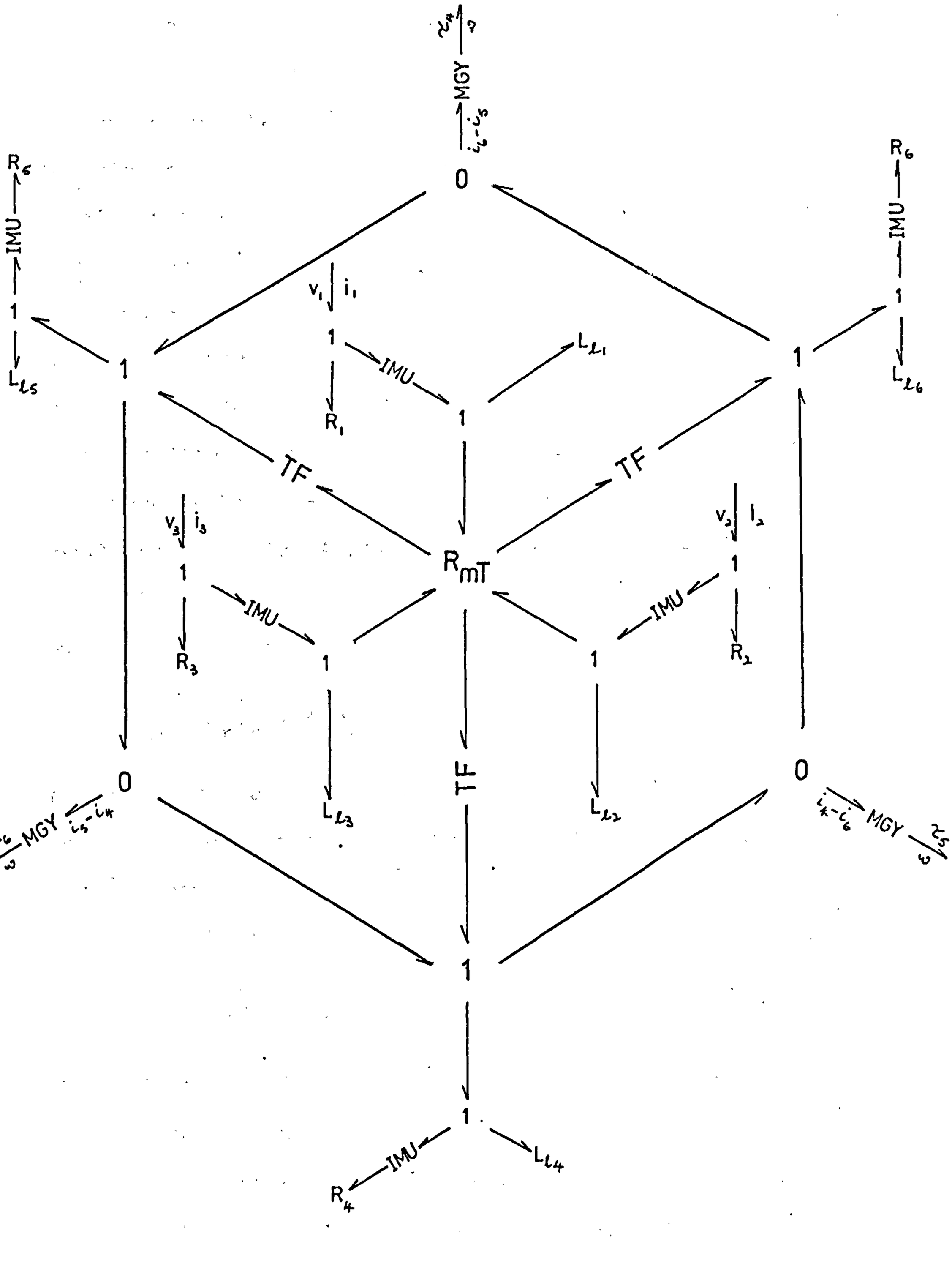

Fig. 4-24 Bond Graph Representation of a Three-Phase Induction Motor

4.6.1 Starting Transients of Induction Motor with Inertia Load

The combine electro-mechanical system consists of a mechanical load of large inertia, which has a natural frequency of the same order as the supply frequency, coupled to the induction motor via a shaft. The motor shaft is somewhat longer than normal and a disc is directly mounted on it so that the induction motor rotor, shaft and disc form a mechanical system which is torsionally stiff. Since the only mechanical losses are bearing friction, air resistance and torsional hysteresis, the system is very lightly damped. The bond graph of the mechanical sub-system is shown in Fig. 4-25 and may be directly connected to the bond graph of Fig. 4-24 to form the complete system.

From Fig. 4-25 the induction motor torque at the rotor end of the shaft is:

$$\tau_m = J_r\dot{\omega}_r + f_r\omega_r + \tau_s \qquad 4.64$$

where J_r is the rotor inertia; f_r is the rotor coefficient of viscous damping; τ_s is the shaft torque and ω_r is the rotor speed.

The shaft torque at the disc is:

$$\tau_s = J_d\dot{\omega}_d + f_d\omega_d \qquad 4.65$$

where J_d is the disc inertia, f_d is the disc coefficient of viscous damping and ω_d is the disc speed.

The shaft torque is related to the shaft twist, $\theta_r - \theta_d$, by its stiffness coefficient σ, that is:

$$\tau_s = \sigma\,(\theta_r - \theta_d) \qquad 4.66$$

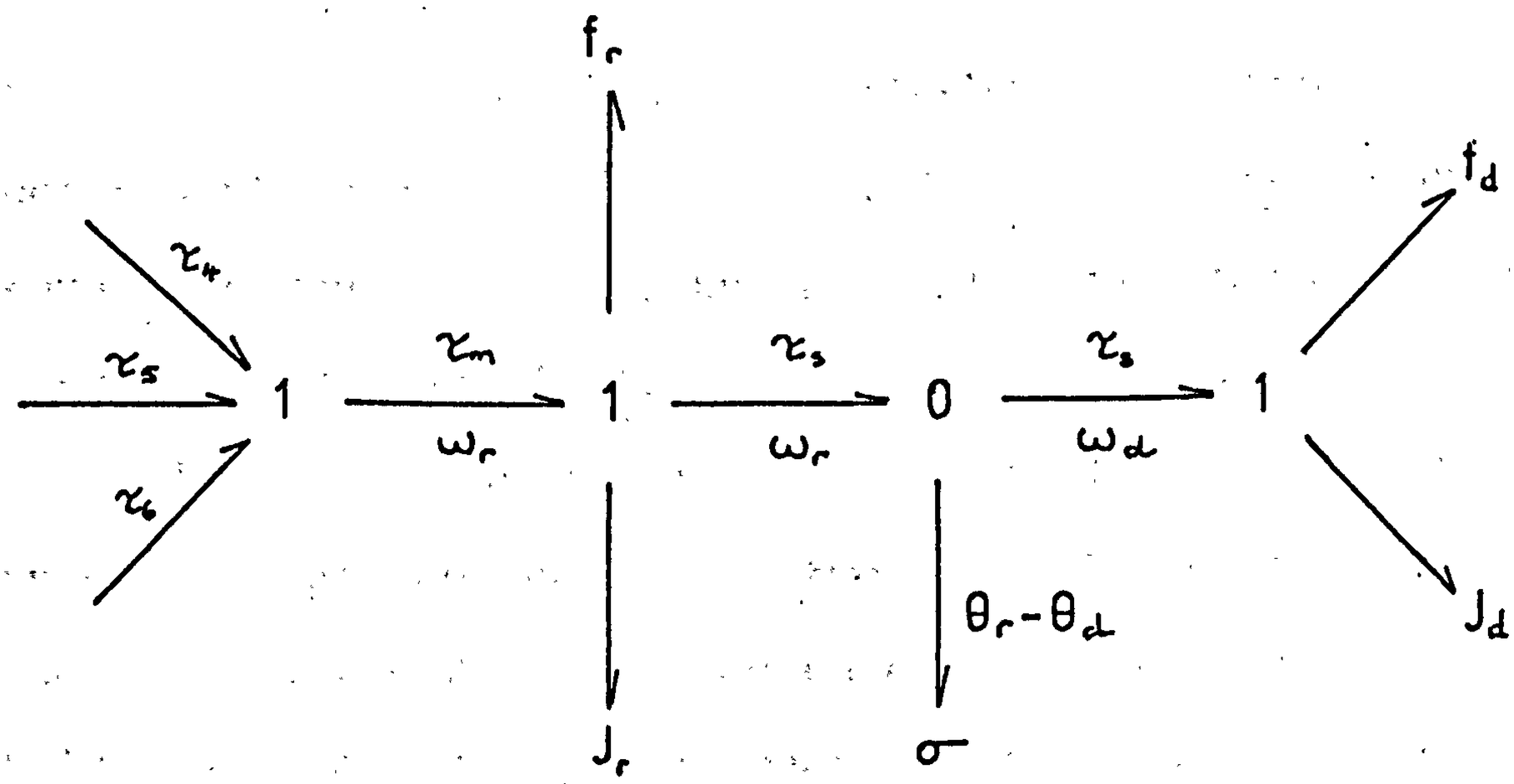

Fig. 4-25 Bond Graph Representation of the Mechanical Sub-System

where Θ_r and Θ_d are the rotor and disc angles respectively measured from a common fixed reference. These angles may be expressed as:

$$\left.\begin{aligned}\dot{\Theta}_r &= \omega_d \\ \ddot{\Theta}_d &= \omega_d\end{aligned}\right\} \qquad 4.67$$

The computation structure needed for solution by SYSTRAN may be obtained directly from the bond graphs in Fig. 4-24 and 4-25. Alternatively, by inspecting Fig. 4-24 the current outputs from the inductive mutators, IMUs, can be easily calculated using Eqns. 4.60 and 4.61 and these are expressed by sets of algebraic equations. The constraints are imposed by Eqns. 4.62; and the torque equations couple the electrical to the mechanical systems, described by Eqns. 4.64, 4.65, 4.66 and 4.67.

The motor torque developed, together with the rotor speed showing the beating of two natural frequencies, is shown in Fig. 4-26. The sequence of events which causes this transient occurs when phases a and b are initially energized while the switch on phase c is closed 0.01 second later.

It is evident that in this high Q system, the natural mode of transient oscillation of the mechanical system, being lightly damped and having a frequency of 74 Hz, is greatly excited. Also the 60 Hz component of the motor torque is amplified resulting in the beating at 14 Hz between the natural and the forced components observed at the rotor. A complete set of the simulated responses of the three-phase induction motor is shown in Appendix E.

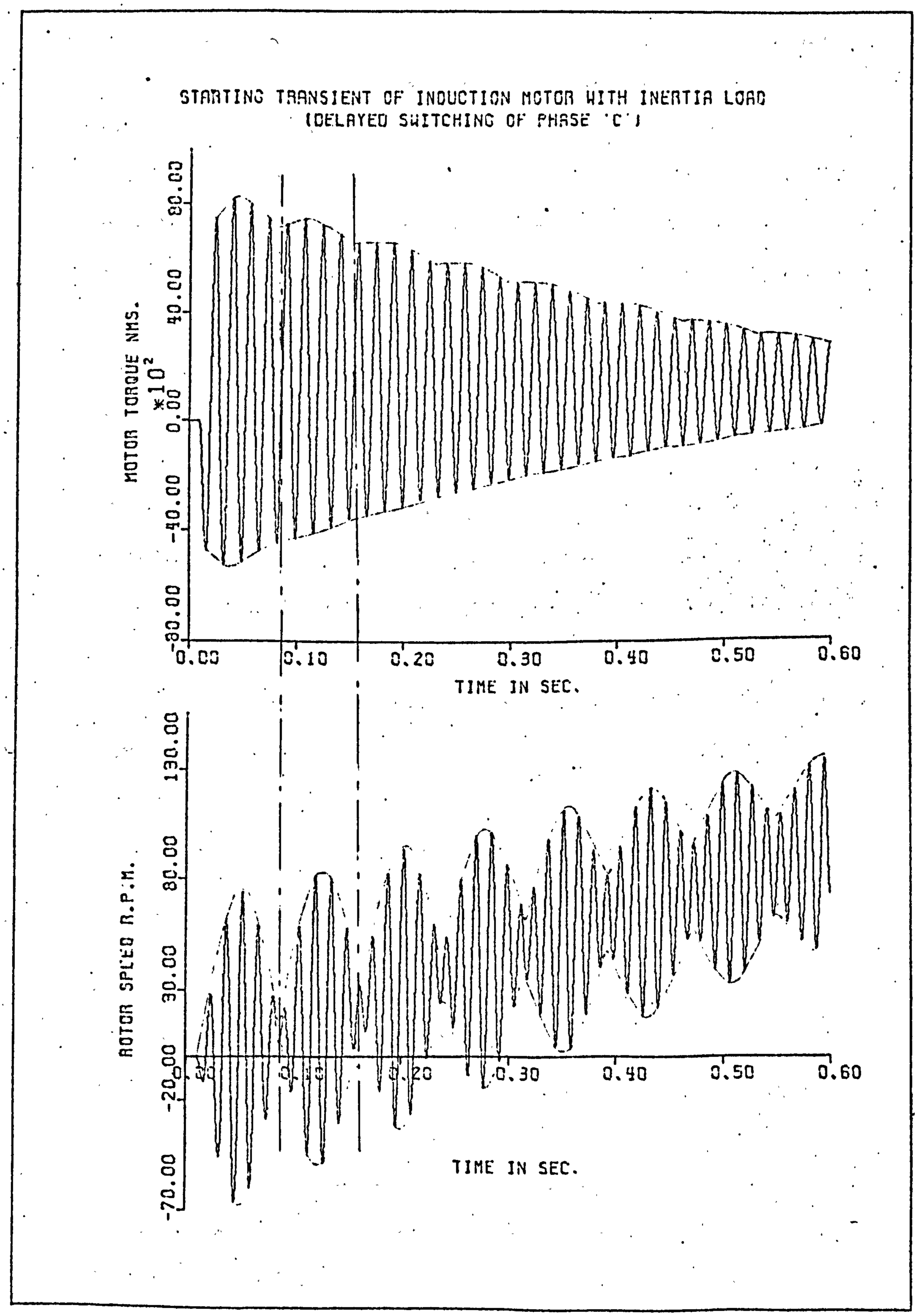

Fig. 4-26 Motor Torque and Rotor Speed of the Induction Motor due to Unsynchronized Switching

4.7 Conclusions

Earlier attempts in the analysis of synchronous machine dynamics have either applied the field theory[7,8,9,10] or used the lumped network parameter approach[4,5,6,26]. The development of the concept of leakage inductance by Hopkinson and others, marked a critical point in machine analysis. On the field theory side, attention began to be paid to the internal features in the construction of the machine which affected the value of the leakage inductance. Analysis based on the lumped parameters, using self and mutual inductances, concentrates on the terminal characteristics of the machine. The bond graph approach enables the magnetic and electric domains to be 'bridged' in a unified diagram from which equations consisting of magnetic and power variables can be derived. Hence, the approach essentially uses both the field theory and lumped parameters techniques to evolve a working model of the system.

In this chapter the unique pattern of the leakage paths for salient pole synchronous generators are considered in arriving at the system equations. Although the leakage path suggested in Section 4.4.2 is idealized, the fault currents obtained for both the single-phase and three-phase generators show a remarkable degree of accuracy when compared with experimental results.

In an attempt to account for the difficulties encountered in representing the rotor circuit accurately, Canay[27] introduced a reactance whose value depends upon the construction of the machine into the equivalent circuit of the synchronous generator. It is in the opinion of the

author that this is an oblique approach to solving the underlying problem of representing the actual leakage path which would be expected to change not only for different types of generator constructions but also for different fault conditions. The leakage path may be determined from flux plotting using the method suggested in Section 4.2.1, and applying the bond graph simulation technique, a reliable and unified approach to the analysis of electromechanical energy converters may be developed.

It has been shown in this chapter that from the general treatment of the basic two-winding machine, the synchronous generator and induction motor bond graphs can be easily derived. The addition and removal of any new windings to the machine present no major obstacle to the technique developed and as such is particularly suitable for the solution of multi-winding machines.

4.7 References

1. Kron, G.: 'The Application of Tensor to the Analysis of Rotating Electrical Machinery', G.E. Review, 1938, 36, pp. 181-211.
2. Gibbs, W.J.: 'The Modern Approach to Electrical Machine Analysis', The Engineers, Oct. 1951.
3. Gibbs, W.J.: 'Tensors in Electrical Machine Theory' (Chapman and Hall, London, 1952).
4. Adkins, B.: 'The General Theory of Electrical Machines', (Chapman and Hall, London, 1957).
5. Jones, C.V.: 'The Unified Theory of Electrical Machine', (Butterworths, London, 1967).

6. Reedy, G., Ali, A.M. and Jones, C.V.: 'Computer-aided Analysis of Saturated Systems', Proc. IEE, 1971, 118, (12), pp. 1791-1799.

7. Binns, K.J.: 'Predetermination of the No-load Magnetization Characteristic of Large Turbo-Generators', Proc. IEE, 1965, 112, pp. 720-732.

8. Chari, M.V.K. and Silvester, P.: 'Analysis of Turboalternator Magnetic Field by Finite Elements', IEEE Trans. on Power Apparatus and System, 1971, PAS-90, pp. 545-564.

9. Fuch, E.F. and Erdelyi, E.A.: 'Non-linear Theory of Turboalternators; I Magnetic Fields at No-load and Balanced Loads', IEEE Trans. on Power Apparatus and System, 1973, PAS-92, (2), pp. 583-591.

10. Fuch, E.F. and Erdelyi, E.A.: 'Non-linear Theory of Turboalternators; II Load Dependent Synchronous Reactances', IEEE Trans. on Power Apparatus and System, 1973, PAS-92, (2), pp. 592-599.

11. Ames, W.F.: 'Numerical Methods for Partial Differential Equations', (Nelson, London, 1969).

12. Binns, K.J. and Lawrenson, P.J.: 'Analysis and Computation of Electric and Magnetic Fields Problems', (Pergamon, New York, 1963).

13. Vitkovitch, D.: 'Field Analysis: Experimental and Computational Methods', (Van Nostrand, New Jersey, 1964).

14. Ahmed, S.V.: 'Accelerated Convergence of Numerical Solution of Linear and Non-linear Vector Field Problems', Computer Journal, 1965, (8), pp. 73-77.

15. Stagg, G.W. and El-Abiad, A.H.: 'Computer Methods in Power System Analysis', (McGraw- Hill, New York, 1968).

16. Clancy, J.J. and Mark, S.F.: 'Digital Simulation Languages: A Critique and a Guide', Proc. of the Joint Computer Conference, 1965, 27, (1), pp. 23-36.

17. Hirst, D.E.: 'Digital Simulation of Non-linear Dynamic System using Standard Fortran', Electronics Letters, 1971, 7, (4), pp. 102-105.

18. Martens, H.R.: 'Simulation of Non-linear Multiport Systems using Bond Graph', ASME Journal of Dynamic Systems, Measurement, and Control, Series G, 1973, 95, (1), pp. 49-54.

19. Fox, L.: 'Numerical Solution of Ordinary and Partial Differential Equations', (Pergamon, London, 1962).

20. Ralston, A.: 'A First Course in Numerical Analysis', (McGraw-Hill, New York, 1965).

21. Brayton, R.K., Gustavson, F.G., and Hachtel, G.D.: 'The Use of Variable-order Variable-step Backward Differentiation Methods for Non-linear Electrical Networks', International IEEE Conference on Systems Networks and Computers, Oaxtepec, Mexico, 1971, pp. 102-106.

22. Branin, F.H., Jr., Hogsett, G.R., Lunde, R.L., and Kugel, L.E.: ECAP II - A New Electronic Circuit Analysis Program', IEEE Journal of Solid-State Circuits, 1971, SC-6, (4), pp. 146-166.

23. Slemon, G.R.: 'Analytical Models for Saturated Synchronous Machines', IEEE Trans. on Power Apparatus and Systems, 1971, PAS-90, (2), pp. 409-417.

24. Slemon, G.R.: 'Magnetoelectric Devices', (Wiley, New York, 1966).

25. Say, M.G.: 'The Performance and Design of Alternating Current Machines', (Pitman, London, 1963).

26. Subramaniam, P. and Malik, O.P.: 'Digital Simulation of a Synchronous Generator in Direct-phase Quantities', Proc. IEE, 1971, 118, (1), pp. 153-160.

27. Canay, I.M.: 'Causes of Discrepancies on Calculation of Rotor Quantities and Exact Equivalent Diagrams of the Synchronous Machine', IEEE Trans. on Power Apparatus and Systems, 1969, PAS-88, (7), pp. 1114-1120

28. Fitzgerald, A.E. and Kingsley, C., Jr.; 'Electric Machinery', (McGraw-Hill, New York, 1961).

CHAPTER FIVE

GENERAL ENERGY APPROACH TO BOND GRAPH ANALYSIS

5.1 Introduction

In Chapter 2 the basic definition of the bond graph language is presented in a compact but general form using a mathematical system of definitions and symbolisms. In the description of storage components there is a choice between power variables and energy variables. Energy variables consist of charge and flux in the electrical domain, displacement and momentum in the mechanical domain, volume and momentum in flow systems, et cetera[1]. However, in the modelling of non-linear storage components energy variables appear to offer greater flexibility. In the previous chapters it has been shown that it is necessary to introduce the inductive and capacitive mutators, in which energy variables are used, to represent non-linearities in a power system component in a concise and mnemonic diagram.

As indicated in the introduction chapter on bond graph concepts, the mutators evolve as a result of the unique characteristic of the gyrator. An interesting topic in the theory of multiports is the quest for a minimal or basic set of irreducible primitives; the strict atoms, of which all dynamic systems are composed. It is no surprise, therefore, that Tellgen's gyrator has hitherto been regarded as an irreducible element. In fact, Paynter and Karnopp[2] have suggested that the variety of distinct elements may be reduced from the necessary proliferation, shown in Tables 2-3 and 2-4, simply to

three elements (C, GY, O), together with passive and active bonds ($\rightharpoonup$, $\rightarrow$) . Preliminary investigations[3,4,5] into the nature of the gyrator have indicated that the gyrator can be used in a wide range of applications to represent new network devices.

Although this line of research may provide future scope for further developments, in this chapter the bond graph derived for lumped energy systems is represented by the usual set (C, I, R, S_e, S_i, TF, GY, O, 1) . In the area of theory and analytic methods, it can be intuitively concluded that the emphasis on power and energy in bond graphs allows interpretations of Lagrangian formulations and the type of tensorial analysis by Kron. It has been shown[6,7,8] that by applying the variational principles to non-conservative lumped systems the dynamic equations of motion may be derived. The bond graph for lumped energy systems developed in this chapter is deduced directly from these equations and forms the basic structure for all energy systems.

From this basic bond graph, a systematic procedure for generating state-space equations has been proposed[9]. The method is based upon a bond graph representation of the system and causal manipulation of the system equations.

As such in this chapter the main aim is to present a formal mathematical approach, involving the formulation and organisation of equations for the general lumped energy system, to solve the resulting mixed differential/ algebraic equations without using either the mutators or the computation structures. While the advantages of this approach are obvious, however, in the pursuit of mathematical

expediency certain salient features of the actual device may be ignored. Thus the general method proposed in this chapter may only be used with extreme care since it lacks the availability of a simple check for correctness of the system relations and of sorting system equations candidly displayed by the computation structures.

5.2 Bond Graph for Lumped Energy Systems in Terms of Transformed Co-ordinates

Since all forces in a system can be deduced from the stored energies to which they are related, excluding, however, externally applied forces and dissipation effects, the equations of motion may be expressed in terms of Lagrange's equations. These equations are a useful tool in the modelling of physical systems, since they are based on expressions for energy and power.

As shown in the preceding chapters, the bond graphs are an equally useful tool in the modelling of physical systems since, by displaying the energy storages and power fluxes, they enhance an understanding of the energy structure and functional behaviour of such systems. Thus from Lagrange's equations for lumped energy systems, a basic bond graph structure may be formulated. This is a standard bond graph constrained and arranged in a special way to permit it to be formed from expressions of energy and power.

A system can be described by the primitive quasi displacements, X_j, $j = i, 2, \ldots, N$, selected in such a way that the recoverable energy stored in the system can be written as:

$$E = \sum_{j=1}^{N} \left[T_j(x_j) + V_j(X_j) \right] \qquad 5.1$$

where $x_j = \frac{dX_j}{dt}$; ΣT_j and ΣV_j are the quasi kinetic and potential energies respectively[10].

In the presence of quasi conservative forces F_j, quasi non-conservative forces F_j', and the quasi forces of internal constraint F_j'', the kinetic energy T_j, may be changed, governed by the conservation of energy such that:

$$\frac{dT_j}{dt} = (F_j + F_j' + F_j'')\, x_j \qquad 5.2$$

The quasi forces of constraint do no net work on the entire system which undergoes arbitrary virtual displacements, δX_1, δX_2 ...., δX_N, satisfying the constraints. Thus:

$$\sum_{j=1}^{N} F_j''\, \delta X_j = 0 \qquad 5.3$$

and using Eqn. 5.2 to eliminate the quasi forces of constraint, Eqn. 5.3 becomes

$$\sum_{j=1}^{N} \left(\frac{1}{x_j} \frac{dT_j}{dt} - F_j - F_j'\right) \delta X_j = 0 \qquad 5.4$$

Introducing a key integral[10] such that this integral vanishes when the variations δT^* and δX_j vanish at the limits $t = t_0$, t_1 and integrating by parts, gives:

$$\int_{t_0}^{t_1} \sum_{j=1}^{N} \left[\frac{d}{dt} \left(\frac{dT_j^*}{dx_j}\right) - F_j - F_j' \right] \delta X_j \, dt = 0 \qquad 5.5$$

where $T^* = \sum_{j=1}^{N} T_j^*(x_j)$ is the quasi kinetic co-energy which is not a real energy, except in dimensions.

Comparing Eqns. 5.4 and 5.5, the relationship between the kinetic energy and co-energy may be defined as:

$$\frac{1}{x_j} \cdot \frac{dT_j}{dt} = \frac{d^2 T_j^*}{dx_j^2} \qquad 5.6$$

or in integral form as:

$$T_j^* = x_j \int_0^{x_j} \frac{T_j(\alpha)}{\alpha^2} \, d\alpha \qquad 5.7$$

where α is a dummy variable of integration.

The term $\sum_{j=1}^{N} F_j \, \delta X_j$ in Eqn. 5.5 is the variation of the work done by the quasi conservative forces, δV.

Defining the Lagrangian as:

$$\mathcal{L} = T^* - V$$

$$= \sum_{j=1}^{N} \left[T_j^* (x_j) - V_j (X_j) \right] \qquad 5.8$$

then Eqn. 5.5 becomes:

$$\int_{t_0}^{t_1} (\delta \mathcal{L} + \sum_{j=1}^{N} F_j' \, \delta X_j) \, dt = 0 \qquad 5.9$$

In order to ensure that the number of primitive displacements or co-ordinates, m, be the minimum possible and be equal to the number of degrees of freedom of the system, the Lagrangian generalised displacements or co-ordinates, $q = q_1, q_2, \ldots, q_m$, and associated Lagrangian generalised velocities or flows, $f = \frac{dq}{dt}$, are introduced.

For physical systems, the generalised geometric internal constraints may be represented by:

$$X_j = X_j (q); \quad j = 1,2,\ldots,N \qquad 5.10$$

Thus q and f together form a sufficient state vector.

From Eqn. 5.10

$$x_j = \frac{dX_j}{dt}$$

$$= \sum_{i=1}^{m} M_{ji}(q) f_i \qquad 5.11$$

where $M_{ji}(q) = \frac{\partial X_j}{\partial q_i}$, which is the transformer modulus.

The term $\sum_{j=1}^{N} F_j' \delta X_j$, from Eqn. 5.9, is the external or non-conservative work variation and can be expressed in terms of generalised forces, $e = e_1, e_2, \ldots, e_m$, and variations, $\delta_q = \delta_{q1}, \delta_{q2}, \ldots, \delta_{qm}$, so that the equation becomes

$$\int_{t_o}^{t_1} (\delta \mathcal{L} + \sum_{i=1}^{m} e_i \delta_{qi})\, dt = 0 \qquad 5.12$$

where $\mathcal{L} = T^*(q,f) - V(q)$, is the Lagrangian in terms of generalised displacements and velocities (or flows). Eqn. 5.12 is the elegant Hamilton's principle, from which can be derived[11] the Lagrange's equations; thus,

$$\frac{d}{dt}\left[\frac{\partial \mathcal{L}(q,f)}{\delta f_i}\right] - \frac{\delta \mathcal{L}(q,f)}{\delta q_i} = e_i \qquad 5.13$$

The bond graph for generalised co-ordinate transformations, as shown in Fig. 5-1(a), may be developed from Eqns. 5-1, 5-11, and 5-13 in which the geometric internal constraints determine the characteristics of the transformers and that the non-conservative forces are absent. The MTF may be further reticulated into

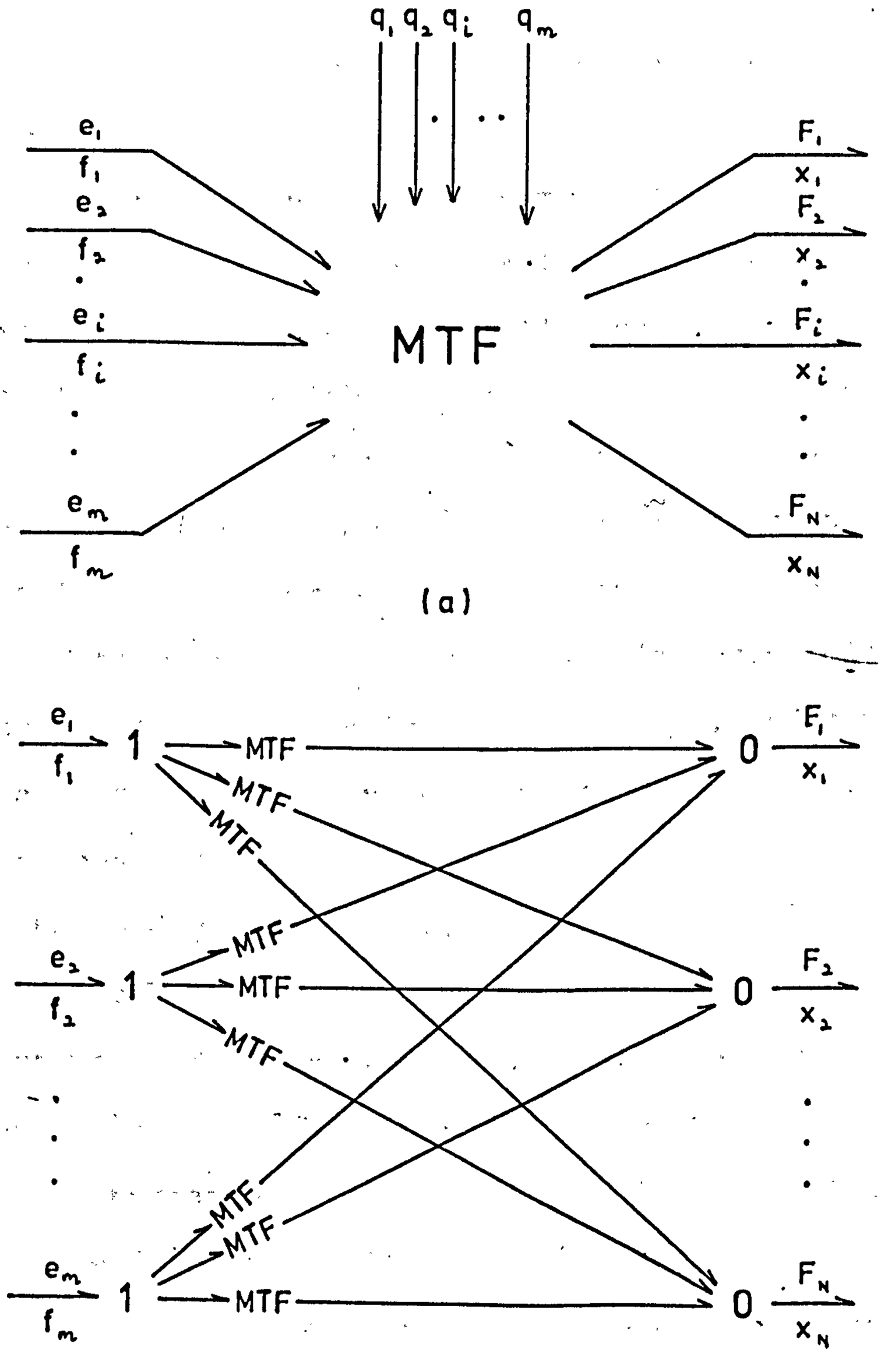

Fig. 5-1 Bond Graph Representations of Generalized Co-ordinate Transformations

O-, 1- junctions and 2-port MTF's as shown in Fig. 5-1(b), if:

$$e_i = \sum_{j=1}^{N} M_{ij}(q)\ F_j \qquad 5.14$$

where $M_{ij}(q) = M_{ji}(q)$, for the transformer to conserve power.

These bond graphs are similar to those obtained by Karnopp[11,12] for power-conserving transformations. Most physical systems are universally associated with these transformations which simultaneiously constrain two sets of variables, the complementary variables. A variety of transformations, for example, symmetrical component transformations for power system studies, d-q transformations in electric machine theory, generalised co-ordinate transformations in analytical mechanics, and constraint equations of ideal devices, can all fit the category of power-conserving transformations and may be represented by the bond graphs of Fig. 5-1.

The basic bond graph for a lumped energy system, as shown in Fig. 5-2 requires a suitable power-conserving transformation such that the storage field can be defined by the inertance L_j, co-inertance L_j^* and compliance C_j with the dissipation field represented by R_j. The expressions for the inertances, co-inertances and compliances in terms of the kinetic energy, kinetic co-energy and potential energy are[10]:

$$T_j = \tfrac{1}{2}\ L_j\ (x_j)\ x^2{}_j \qquad 5.15$$

$$T_j^* = \tfrac{1}{2}\ L_j{}^*(x_j)\ x_j{}^2 \qquad 5.16$$

$$V_j = \frac{1}{2C_j(X_j)}\ X_j{}^2 \qquad 5.17$$

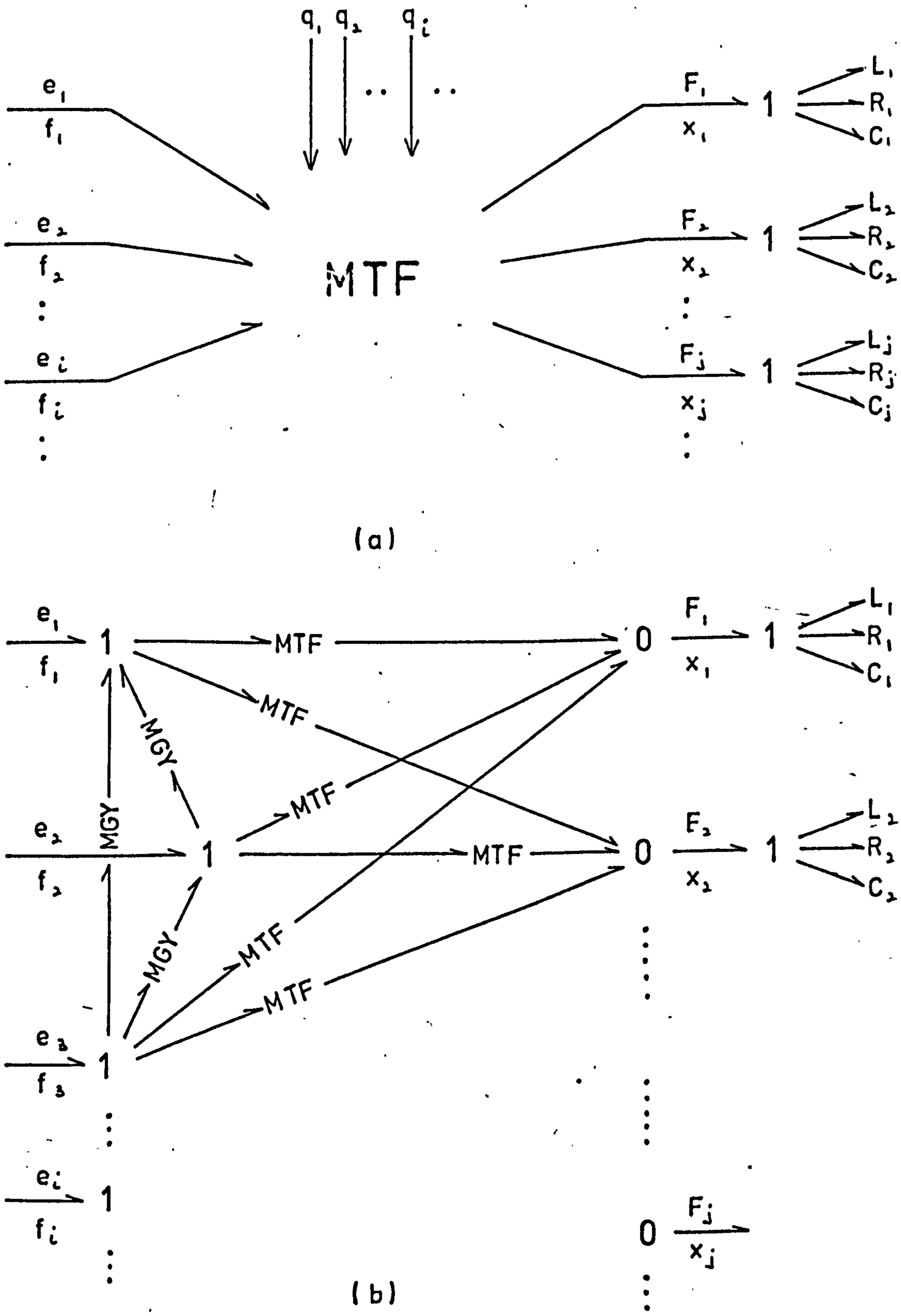

Fig. 5-2 Basic Bond Graph for a Lumped Energy System

The relationship between L_j^* and L_j derived from Eqn. 5.7 is:

$$L_j^* = \frac{1}{x_j} \int_0^{x_j} L_j(\alpha)\, d\alpha \qquad 5.18$$

and energy dissipation can be incorporated into the scheme by the expression:

$$P_d = \sum_{j=1}^{N} P_j(x_j)$$

$$= \sum_{j=1}^{N} R_j(x_j) x_j^2 \qquad 5.19$$

where P_d is the dissipation power.

In the basic bond graph of Fig. 5-2(b), the summations of forces (efforts) about each of the left-hand side 1-junction to give the Lagrange's equations[10], indicate the need to include the gyrators as shown. This reaffirms the suggestion by Karnopp[12,13] that a system consisting of storage fields and multiport power-conserving transformers can under certain circumstances be equivalent to a system consisting of storage elements, gyrators and transformers.

In Fig. 5-2(b), the gyrator modulus joining the ith and kth 1-junctions is[10]:

$$G_{ik} = \sum_{j=1}^{N} \left(L_j^* - \frac{x_j}{2} \frac{dL_j^*}{dx_j}\right) x_j \left(\frac{\partial M_{jk}}{\partial q_i} - \frac{\partial M_{ji}}{\partial q_k}\right) \qquad 5.20$$

As it is necessary for the gyrator to conserve but not to store energy; then:

$$G_{ik}(q,x) = -G_{ki}(q,x) \qquad 5.21$$

From eqn. 5.20, it is evident that the gyrators vanish altogether for the case when the transformer moduli, M_{jk} and M_{ji}, are constant and that in general the C_j and R_j do not influence or contribute to the gyrator moduli.

5.3 Alternative Bond Graph for Lumped Energy Systems in Terms of Actual Co-ordinates

As shown in the previous section, the use of appropriate transformations for an energy system results in the storage and dissipation fields being described by simple functions of inertances $L_j(x_j)$, co-inertances $L_j^*(x_j)$, compliances $C_j(X_j)$ and resistances $R_j(x_j)$. The expressions for the transformer and gyrator moduli are $M_{ij}(q)$ and $G_{ik}(q,x)$ respectively.

However, when constraint transformations cannot be found readily which permit the energy to be put in the form of Eqn. 5.9 or when it is more convenient to work in terms of the actual variables, as for example, in phase co-ordinate methods, the bond graph elements have to be altered for extended flexibility, as shown below:

$$\left.\begin{aligned} R_i &= R_i(f_i,q) \\ C_i &= C_i(q) \\ L_i &= L_i(f_i,q) \\ M_{ij} &= M_{ij}(q,f) \\ G_{ij} &= G_{ij}(q,f) \end{aligned}\right\} \qquad 5.22$$

The transformed variables, F and x, are not used and as such the simulation technique may be more involved.

The first step in the general modelling procedure is the determination of expressions for stored energy and dissipated power, followed by their representation using the appropriate bond graph elements. From the definitions given by Brown[10] for the various elements, the efforts on the assocaited bonds for the alternative bond graph shown in Fig. 5-3 are given by:

Resistance: $$e_i = R_i f_i \tag{5.23}$$

Compliance: $$e_i = \left[\frac{1}{C_i} + \frac{q_i}{2} \frac{\partial (1/C_i)}{\partial q_i} + \sum_{j \neq i} \frac{q_i}{2} \frac{\partial (1/C_i)}{\partial q_j} \frac{f_j}{f_i} \right] q_i \tag{5.24}$$

Inertance: $$e_i = L_i \frac{df_i}{dt} + \frac{f_i}{2} \left(\frac{\partial L_i}{\partial f_i} \frac{df_i}{dt} + \sum_j \frac{\partial L_i}{\partial q_j} f_j \right) \tag{5.25}$$

Transformer: $$e_i = M_{ji} e_j; \quad f_j = M_{ji} f_i \tag{5.26}$$

Gyrator: $$e_i = -G_{ji} f_j; \quad e_j = G_{ji} f_i \tag{5.27}$$

Mutual Resistance: $$e_i = R_{ij} f_j \tag{5.28}$$

Mutual Compliance: $$e_i = \frac{1}{C_{ij}} q_j + \frac{q_i q_j}{2} \sum_k \frac{\partial (1/C_{ij})}{\partial q_k} \frac{f_k}{f_i} \tag{5.29}$$

Mutual Inertance: $$e_i = L_{ij} \frac{df_j}{dt} + \sum_k \frac{\partial L_{ij}}{\partial q_k} \frac{f_i f_k}{2} \tag{5.30}$$

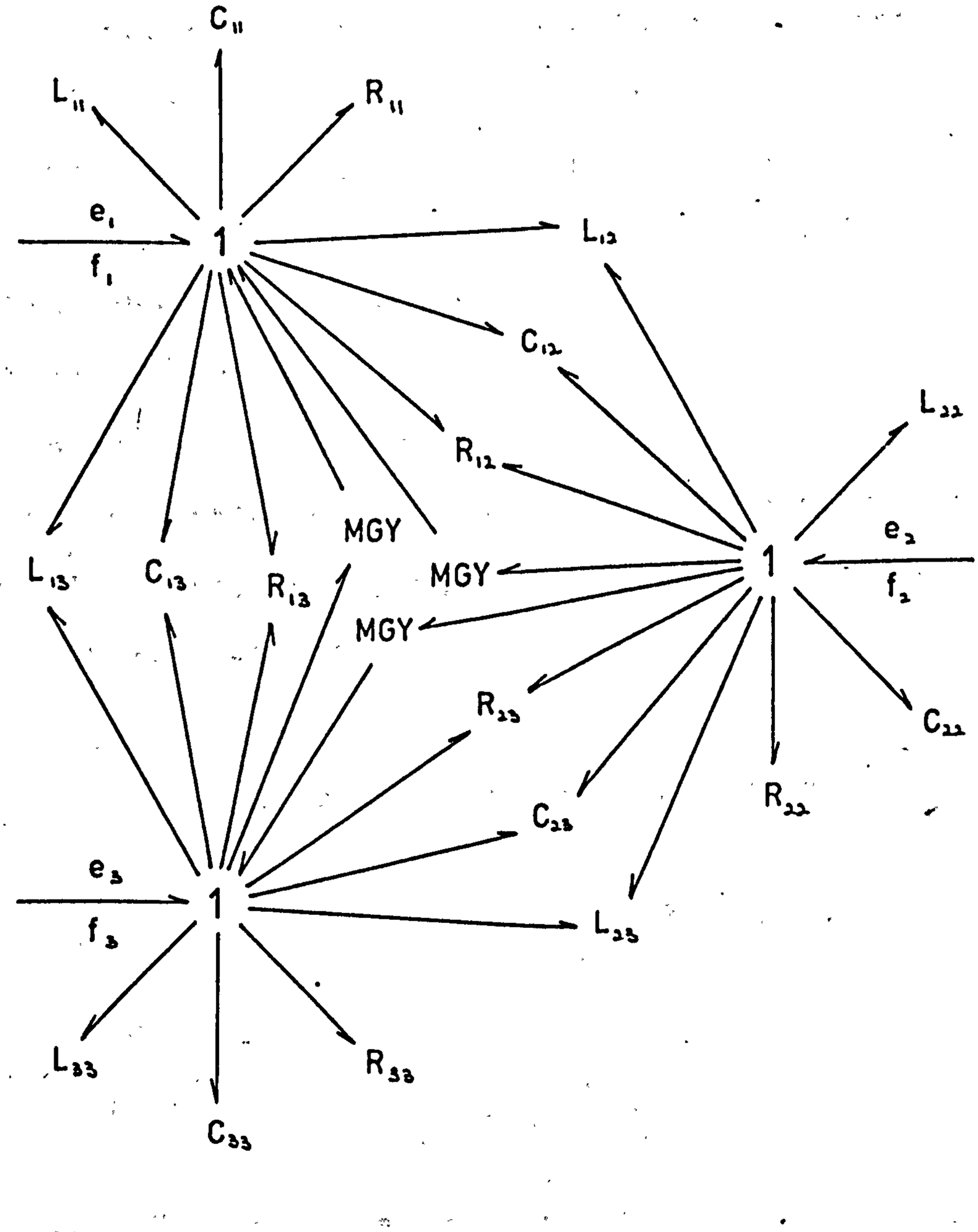

Fig. 5-3 Alternative Bond Graph for a Lumped Energy System with Three-Degree-of-Freedom

The second step in the modelling process is the determination of an expression for the input or terminal power in the form:

$$P_t = \sum_i e_i f_i \qquad 5.31$$

where the vectors e and f may be a function of one or more variables depending upon the terminal constraints.

The final step is the determination of the moduli of the gyrators. Lagrange's equations are used to establish these moduli and the sufficiency of the resulting bond graph.

In order to illustrate the application of Lagrange's equation in setting up the bond graph of dynamic systems, an example involving the two-winding basic rotating machine shown in Figs. 3-1 will be considered.

Example 5-1

The conservative energy function may be written directly as:

$$\mathcal{L} = \tfrac{1}{2}L_{11}i_1^2 + \tfrac{1}{2}L_{12}i_1i_2 + \tfrac{1}{2}L_{22}i_2^2 + \tfrac{1}{2}L_{12}i_1i_2 + \tfrac{1}{2}J\omega^2$$

$$= \tfrac{1}{2}L_{11}\dot{q}_1^2 + \tfrac{1}{2}L_{22}\dot{q}_2^2 + L_{12}\dot{q}_1\dot{q}_2 + \tfrac{1}{2}J\dot{\theta}^2 \qquad El.1$$

where $L_{12} = M_F \cos\theta$, is the mutual inductance[5], L_{11} and L_{22} are the self inductances of coils 1 and 2 respectively; and, J and ω are the moment of inertia and speed of the shaft respectively.

Likewise, the non-conservative energy function is:

$$\mathcal{F} = \tfrac{1}{2}R_{11}i_1^2 + \tfrac{1}{2}R_{22}i_2^2 + \tfrac{1}{2}R_D\omega^2$$

$$= \tfrac{1}{2}R_{11}\dot{q}_1^2 + \tfrac{1}{2}R_{22}\dot{q}_2^2 + \tfrac{1}{2}R_D\dot{\theta}^2 \qquad El.2$$

where R_{11} and R_{22} are the resistances of coils 1 and 2 respectively; and, R_D is the resistance of the mechanical system.

Lagrange's equations given by Eqn. 5.13 may be rewritten to separate the non-conservative function $\mathcal{F}$ as[6]:

$$\frac{d}{dt}\left[\frac{\partial \mathcal{L}(q,f)}{df_i}\right] - \frac{\partial \mathcal{L}(q,f)}{\partial q_i} + \frac{\partial \mathcal{F}}{\partial f_i} = e_i \qquad \text{E1.3}$$

Since the system considered has three degrees of freedom, a Lagrange's equation has to be written for each generalised co-ordinate.

(a) Upon applying the Lagrange's equation to co-ordinate q_1, it follows that

$$\frac{d}{dt}\left[L_{11}\dot{q}_1 + L_{12}\dot{q}_2\right] + R_{11}i_1 = \nu_1 \qquad \text{E1.4}$$

where ν_1 is the terminal voltage for coil 1. For the case in which L_{11} and L_{22} are not dependent upon θ, Eqn. E1.4 becomes:

$$L_{11}\frac{di_1}{dt} + L_{12}\frac{di_2}{dt} - M_F \sin\theta.\omega.i_2 + R_{11}i_1 = \nu_1 \qquad \text{E1.5}$$

(b) When the Lagrange's equation is applied to co-ordinate q_2, then:

$$L_{22}\frac{di_2}{dt} + L_{12}\frac{di_1}{dt} - M_F \sin\theta.\omega.i_1 + R_{22}i_2 = \nu_2 \qquad \text{E1.6}$$

where ν_2 is the terminal voltage for coil 2.

(c) Similarly for the co-ordinate θ, that is, the mechanical energy variable:

$$J\frac{d\omega}{dt} + M_F \sin\theta\, i_1 i_2 + R_D\omega = \tau \qquad \text{E1.7}$$

where τ is the mechanical shaft torque.

The bond graph incorporating Eqns. E1.5, E1.6 and E1.7 is shown in Fig. 5-4, and has the same form as the alternative bond graph for the lumped energy system of Fig. 5-3. For a separately excited D.C. machine, both of the two coils of the basic rotating machine carried direct-current and the bond graph may be derived directly from Fig. 5-4. This is shown in Fig. 5-5.

5.4 Formulation of System Equations from Bond Graphs

A systematic procedure for formulating a set of differential equations for a given bond graph, such as the basic bond graph for lumped energy systems shown in Figs. 5-2 or 5-3, has been proposed by Karnopp and Rosenberg[8,13]. The bond graph is assumed to be composed of elements from the usual set (C, I, R, S_e, S_i, TF, GY, 0, 1) which includes one-port or multiport compliance, inertance, resistance, effort and flow sources, ideal couplers of the transformer or gyrator type, and the common flow and common effort junctions. The variables describing these multiport elements, used in Section 5.2 and 5.3, are for the purpose of this section grouped into the following categories:

Y = the energy vector

Z = the co-energy vector

D_i = the input vector for dissipative elements

D_o = the output vector for dissipative elements

U = the source vector

The field equations for the storage elements are: --

$$Z = S.y \qquad 5.32$$

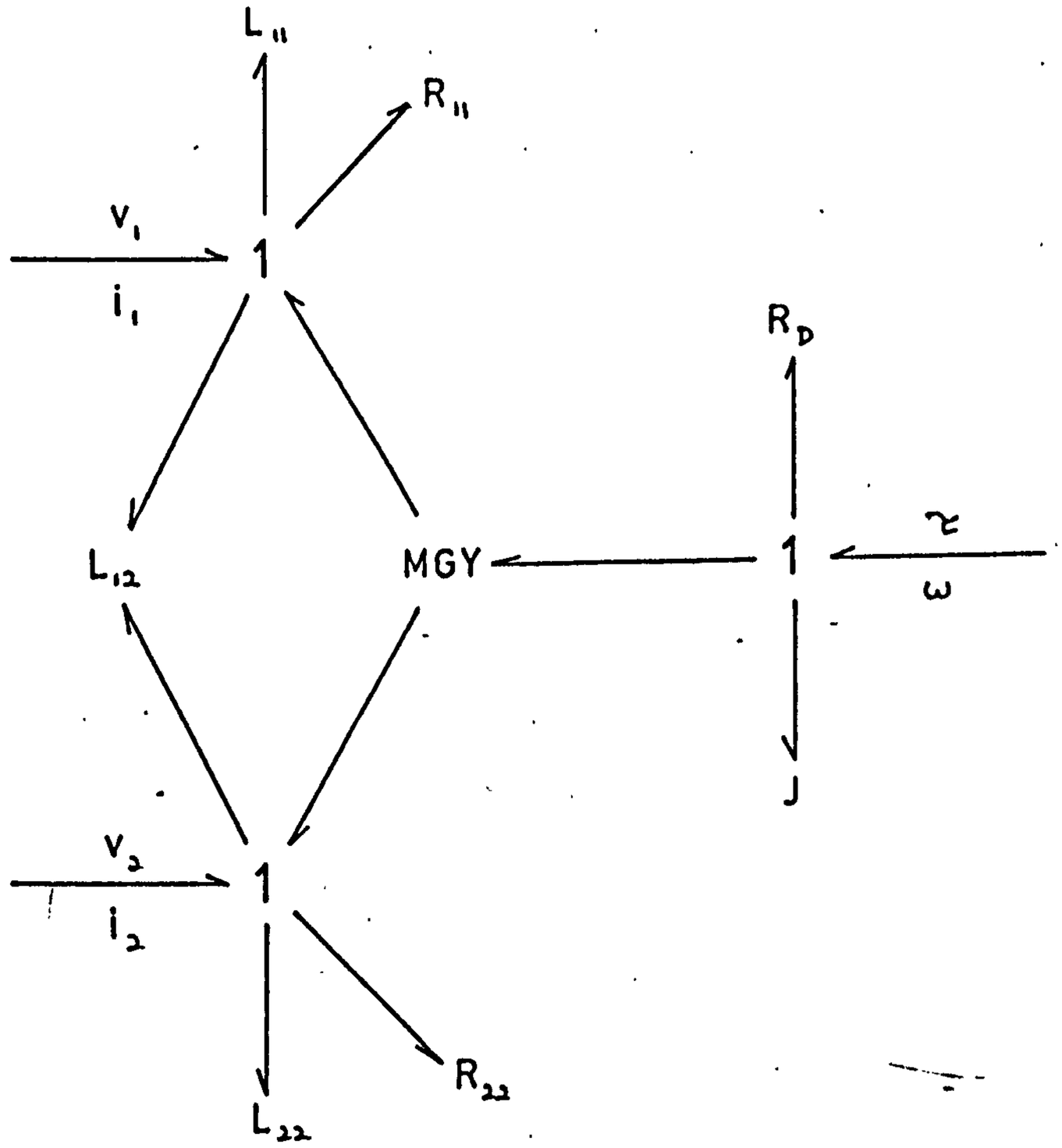

Fig. 5-4 Bond Graph Representation of Basic Rotating Machine

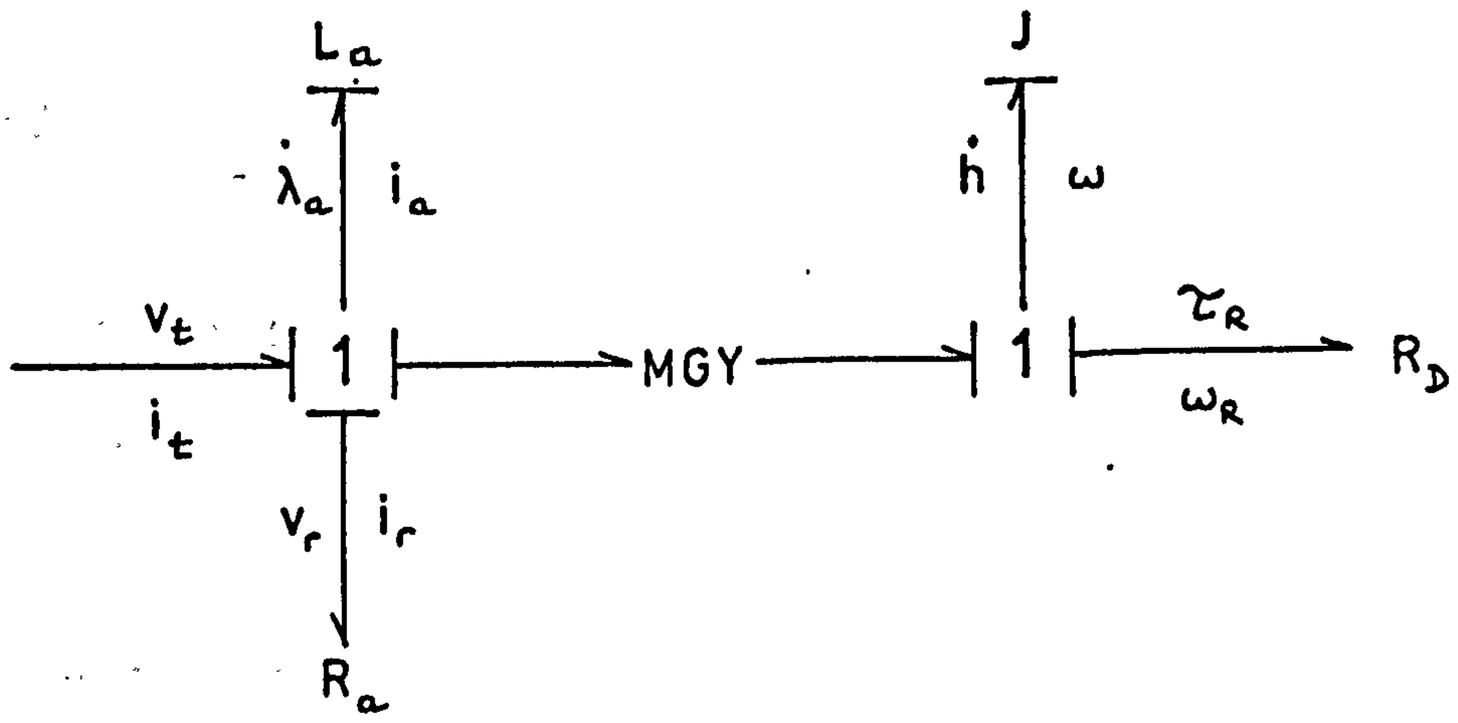

Fig. 5-5 Bond Graph Representation of a Separately Excited D.C. Machine

where S is a square matrix of coefficients.

In general form the dissipative elements may be grouped into two categories:

(i) the dissipation field equation in non-causal form, that is D_{il} on the left-hand side of equation

$$D_{il} = F_D\ (D_{ol}) \qquad 5.33$$

(ii) the dissipation field equation in causal form

$$D_{o2} = G_D\ (D_{i2}) \qquad 5.34$$

where F_D and G_D are non-invertable non-linear functions.

The junction structure yields expressions for the $\dot{Y}$ and D_i vectors in terms of the inputs to the structure namely Z, D_o and U. The structure equations as introduced by Rosenberg[9] are expanded to distinguish between causal and non-causal dissipation fields. If the TF and GY have constant moduli, the junction structure equations are:

$$\begin{bmatrix} \dot{Y} \\ D_{il} \\ D_{i2} \end{bmatrix} = \begin{bmatrix} J_{SS} & J_{SF} & J_{SG} \\ J_{FS} & J_{FF} & J_{FG} \\ J_{GS} & J_{GF} & J_{GG} \end{bmatrix} \cdot \begin{bmatrix} Z \\ D_{ol} \\ D_{o2} \end{bmatrix} + \begin{bmatrix} J_{SU} \\ J_{FU} \\ J_{GU} \end{bmatrix} U \qquad 5.35$$

where $\dot{Y}$ is the derivative of Y and the J sub-matrices are the constraints imposed by the junction structure between sets of ports.

Frequently the J_{GG} sub-matrix is zero as a result of causality being assigned sequentially[9]. This is a frequent occurrence and as such the reduction of Eqns. 5.32, 5.33, 5.34 and 5.35 may take two directions; thus:

(i) when the sub-matrix $J_{GG} = 0$.

From Eqns. 5.32, 5.34 and 5.35, the dissipation field equations are:

$$D_{o2} = G_D\ (J_{GS}\ SY + J_{GF}\ D_{o1} + J_{GU}U)$$

$$= G_D\ (Y,\ D_{o1},\ U) \qquad 5.36$$

Using Eqns. 5.32, 5.33 and 5.36 to eliminate the three vectors, Z, D_{i1} and D_{o2}, yields the computing equations:

$$\begin{bmatrix} \dot{Y} \\ F_D(D_{o1}) \end{bmatrix} = \begin{bmatrix} J_{SS} & J_{SF} & J_{SG} \\ J_{FS} & J_{FF} & J_{FG} \end{bmatrix} \begin{bmatrix} SY \\ D_{o1} \\ G(Y, D_{o1} U) \end{bmatrix} + \begin{bmatrix} J_{SU} \\ J_{FU} \end{bmatrix} U \qquad 5.37$$

The equations for the electromechanical energy converters described in Chapter 4 have the same form as the general equations shown in Eqn. 5.37.

(ii) when the submatrix $J_{GG} \neq 0$

For this particular case it is not possible to eliminate any of the equations. Thus the simplication process is restricted to substitution of Eqns. 5.32, 5.33 and 5.34 into 5.35; thus giving:

$$\begin{bmatrix} \dot{Y} \\ F_D(D_{o1}) \\ D_{i2} \end{bmatrix} = \begin{bmatrix} J_{SS} & J_{SF} & J_{SG} \\ J_{FS} & J_{FF} & J_{FG} \\ J_{GS} & J_{GF} & J_{GG} \end{bmatrix} \begin{bmatrix} SY \\ D_{o1} \\ G_D(D_{i2}) \end{bmatrix} + \begin{bmatrix} J_{SU} \\ J_{FU} \\ J_{GU} \end{bmatrix} U \qquad 5.38$$

It is evident that the form expressed by Eqn. 5.37 is more desirable as it offers a significant reduction in the number of solution variables. As such, should any

linear dissipative elements be present in the system, they could be expressed in Eqn. 5.34 and thus eliminated even if $J_{GG} \neq 0$.

As an example in formulating system equations from bond graphs, the separately excited DC machine whose bond graph is shown in Fig. 5-5 will be considered.

Example 5-2

The detailed bond graph for the DC machine is augmented with causality strokes and the necessary variables are identified. The significant vectors of the graphs are:

the energy vector, $Y = \begin{bmatrix} \lambda_a \\ h \end{bmatrix}$

the derivative vector, $\dot{Y} = \begin{bmatrix} \dot{\lambda}_a \\ \dot{h} \end{bmatrix}$

the co-energy vector, $Z = \begin{bmatrix} i_a \\ \omega \end{bmatrix}$

the input vector for dissipative elements,

$$D_{i2} = \begin{bmatrix} i_r \\ \omega_R \end{bmatrix}$$

the output vector for dissipative elements,

$$D_{o2} = \begin{bmatrix} v_r \\ \tau_R \end{bmatrix}$$

the source vector, $U = \begin{bmatrix} v_t(t) \end{bmatrix}$

where $h = J\omega$ is the angular momentum of the shaft and $\lambda_a = L_a i_a$ is the armature flux linkage.

The causality of the graph indicates that there is no dependent energy variables. Also it may be anticipated that the case $J_{GG} = 0$ applies in the formulation because the causality shows that D_{i2} is explicitly determined by U and Z.

The storage field is characterised by a relation of the form given in Eqn. 5.32; namely:

$$\begin{bmatrix} i_a \\ \omega \end{bmatrix} = \begin{bmatrix} L_a^{-1} & 0 \\ 0 & J^{-1} \end{bmatrix} \cdot \begin{bmatrix} \lambda_a \\ h \end{bmatrix} \qquad \text{E2.1}$$

The loss or dissipation field is assumed to be linear and is described by the causal form of Eqn. 5.34 as:

$$D_{o2} = M.D_{i2} \qquad \text{E2.2}$$

$$\text{or} \quad \begin{bmatrix} \nu_r \\ \tau_R \end{bmatrix} = \begin{bmatrix} r_a & 0 \\ 0 & R_D \end{bmatrix} \cdot \begin{bmatrix} i_r \\ \omega_R \end{bmatrix} \qquad \text{E2.3}$$

The equations of the junction structure are developed from the bond graph according to Eqn. 5.35 with the rows and columns containing the structure for the non-causal dissipation field eliminated; thus;

$$\begin{bmatrix} \dot{Y} \\ D_{i2} \end{bmatrix} = \begin{bmatrix} J_{SS} & J_{SG} \\ J_{GS} & J_{GG} \end{bmatrix} \cdot \begin{bmatrix} Z \\ D_{o2} \end{bmatrix} + \begin{bmatrix} J_{SU} \\ J_{GU} \end{bmatrix} U \qquad \text{E2.4}$$

or

$$\begin{bmatrix} \dot{\lambda}_a \\ \dot{h} \end{bmatrix} = \begin{bmatrix} 0 & -M_F i_F \\ M_F i_F & 0 \end{bmatrix} \cdot \begin{bmatrix} i_a \\ \omega \end{bmatrix} + \begin{bmatrix} -1 & 0 \\ 0 & -1 \end{bmatrix} \cdot \begin{bmatrix} \nu_r \\ \tau_R \end{bmatrix} + \begin{bmatrix} 1 \\ 0 \end{bmatrix} \begin{bmatrix} \nu_t \end{bmatrix} \quad \text{E2.5}$$

and

$$\begin{bmatrix} i_r \\ \omega_R \end{bmatrix} = \begin{bmatrix} 1 & 0 \\ 0 & 1 \end{bmatrix} \cdot \begin{bmatrix} i_a \\ \omega \end{bmatrix} + \begin{bmatrix} 0 & 0 \\ 0 & 0 \end{bmatrix} \cdot \begin{bmatrix} \nu_r \\ \tau_R \end{bmatrix} + \begin{bmatrix} 0 \\ 0 \end{bmatrix} \begin{bmatrix} \nu_t \end{bmatrix} \quad \text{E2.6}$$

Eqns. E2.5 and E2.6 together with Eqns. E2.1 and E2.3 can be simplified to the same form as Eqn. 5.37 and may be directly solved using the computer methods for mixed differential/algebraic equations. However, Eqns. E2.5 and E2.6 can also be expressed in the more familiar form, thus:

$$\dot{Y} = AY + BU \quad \text{E2.7}$$

where the sub-matrices A and B for linear state-space equations are defined as[8],

$$A = \left[J_{SS} + J_{SG} M \left(1 - J_{GG} M\right)^{-1} J_{GS} \right] S$$

$$= \begin{bmatrix} -r_a L_a^{-1} & -M_F i_F J^{-1} \\ M_F i_F L_a^{-1} & -R_D J^{-1} \end{bmatrix} \quad \text{E2.8}$$

in which 1 is a unit matrix and M is defined by Eqn. E2.2 and

$$B = \left[J_{SU} + J_{SG} M \left(1 - J_{GG} M\right)^{-1} J_{GU} \right]$$

$$= \begin{bmatrix} 1 \\ 0 \end{bmatrix} \quad \text{E2.9}$$

Thus the state-space equations are:

$$\begin{bmatrix} \dot{\lambda}_a \\ \dot{h} \end{bmatrix} = \begin{bmatrix} -r_a L_a^{-1} & -M_F i_F J^{-1} \\ M_F i_F L_a^{-1} & -R_D J^{-1} \end{bmatrix} \cdot \begin{bmatrix} \lambda_a \\ h \end{bmatrix} + \begin{bmatrix} 1 \\ 0 \end{bmatrix} \cdot \begin{bmatrix} \nu_t \end{bmatrix} \quad \text{E2.10}$$

5.5 Bond Graphs and Diakoptics

From the bond graph for generalised co-ordinate transformations developed in Section 5.2, it seems that many of the bond graph techniques appear to be intimately related to Kron's work[15,16], although the graphical nature of bond graphs may lead to methods and results which could be difficult to extract from formal matrix and tensor formulations.

In many engineering studies, and particularly in electrical investigations, the analytical work is made much easier firstly by defining the structure components in terms of the simplest possible reference frame and, secondly, by correlating that definition to the actual assembly of components in terms of the particular reference frame demanded by the needs of the problem. The medium by which this correlation is achieved is Kron's transformation matrix - or, in electrical engineering the connection matrix. Paynter[17] interprets Kron's transformation matrix as a physically real ideal mutliport: the junction structure, but makes no attempt to synthesize this structure.

However, in this section an attempt will be made to show that the junction structure can be described adequately by the generalised co-ordinate transformations of Section 5.2. To illustrate this point, an example

involving primitive networks, shown in Fig. 5-6, will be used. The two sub-networks, each of the three branches and two meshes, are to be connected so that $I_a = I_c$, as shown in Fig. 5-8.

Example 5-3

From Fig. 5.6, the four mesh currents may be expressed in terms of the branch current by the equations:

$$\begin{bmatrix} I_1 \\ I_2 \\ I_3 \\ I_4 \\ I_5 \\ I_6 \end{bmatrix} = \begin{bmatrix} 1 & 1 & & \\ 1 & & & \\ & -1 & & \\ & & 1 & 1 \\ & & 1 & \\ & & & -1 \end{bmatrix} \cdot \begin{bmatrix} I_a \\ I_b \\ I_c \\ I_d \end{bmatrix} \qquad \text{E3.1}$$

Using Eqn. E3.1 the bond graph transformations shown in Fig. 5-7, may be derived. The matrices for mesh voltages and impedances can be obtained directly from this diagram without the need for the usual matrix manipulations.

The connected network, shown in Fig. 5-8, has a constraint current such that $I_p = I_a = I_c$ together with mesh currents $I_q = I_b$ and $I_r = I_d$. Based on this constraint, the bond graph of Fig. 5-9 can be constructed. It is interesting to note that both the transformations in Figs. 5-7 and 5-9 have similar structures to that for the generalised co-ordinate transformations shown in Fig. 5-1, however, the transformer moduli of the former are all unity.

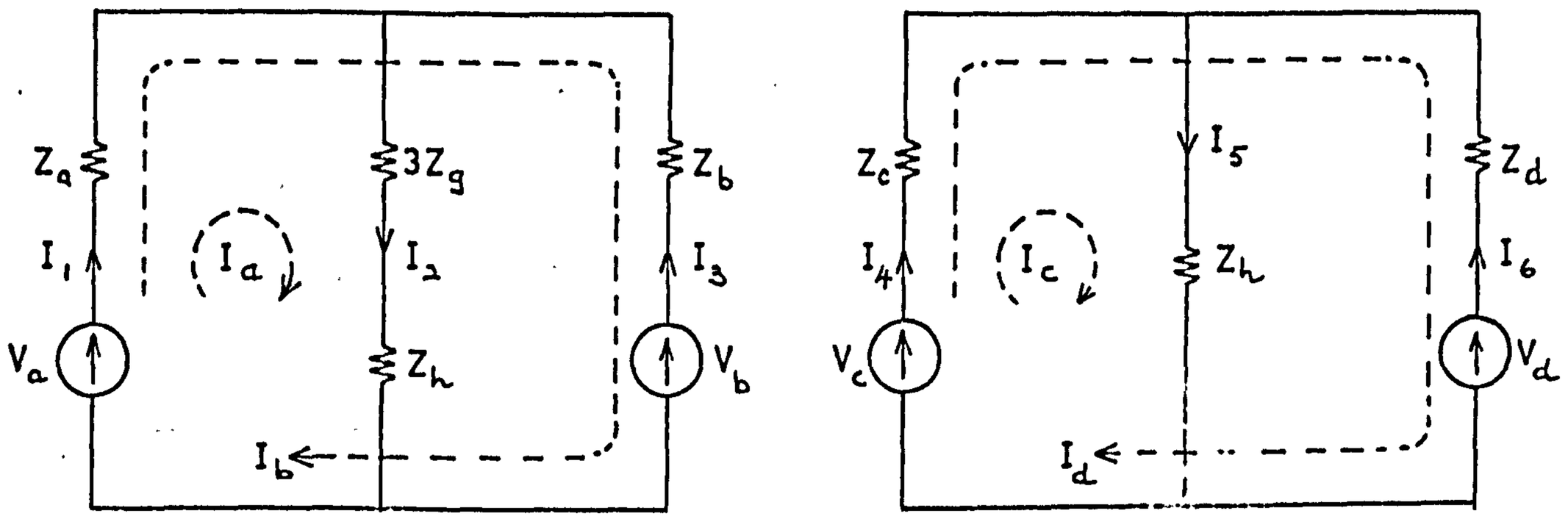

Fig. 5-6 Multimesh Circuits used as Primitive Networks

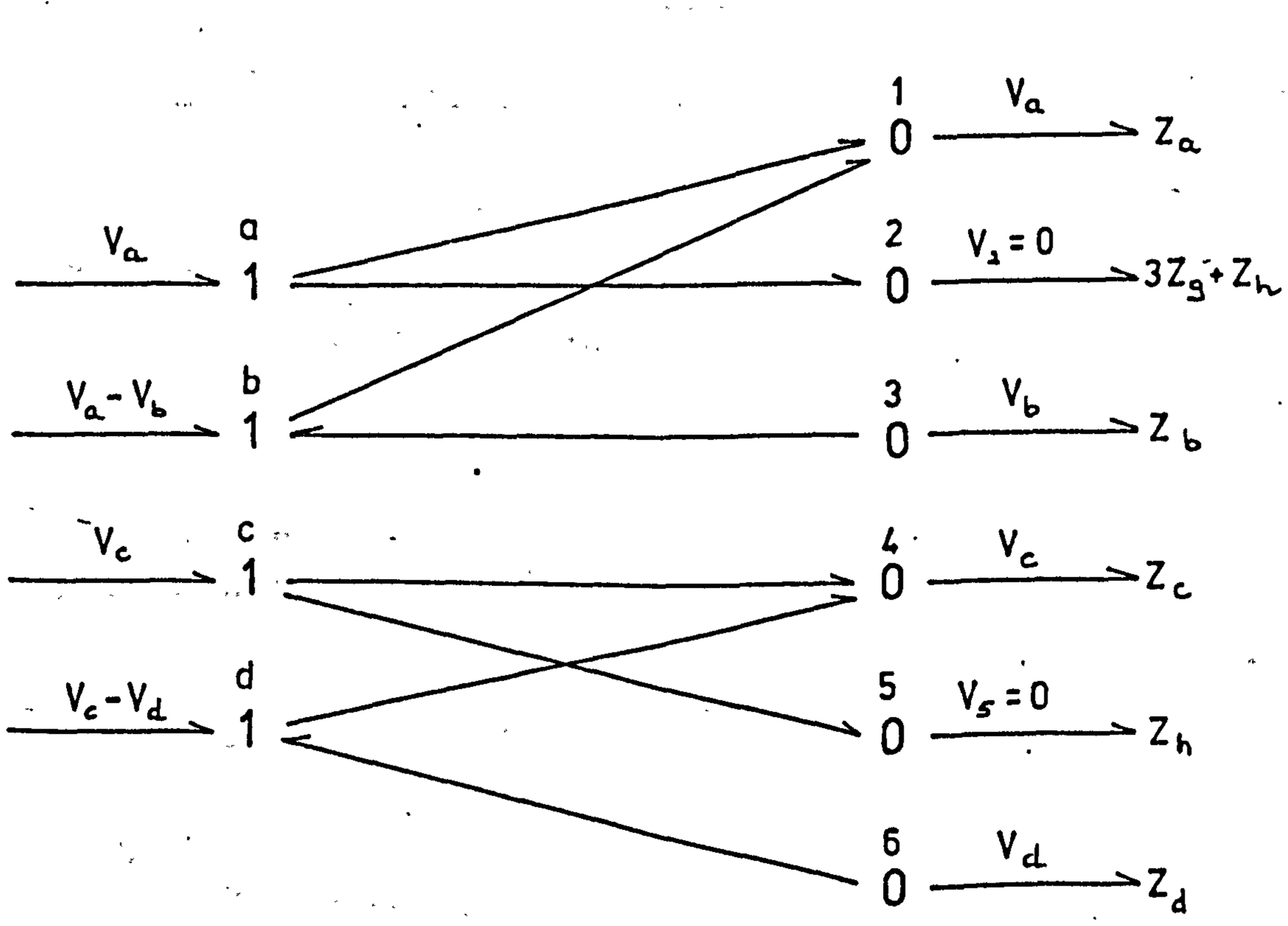

Fig. 5-7 Bond Graph Transformations from Branch to Mesh Equations

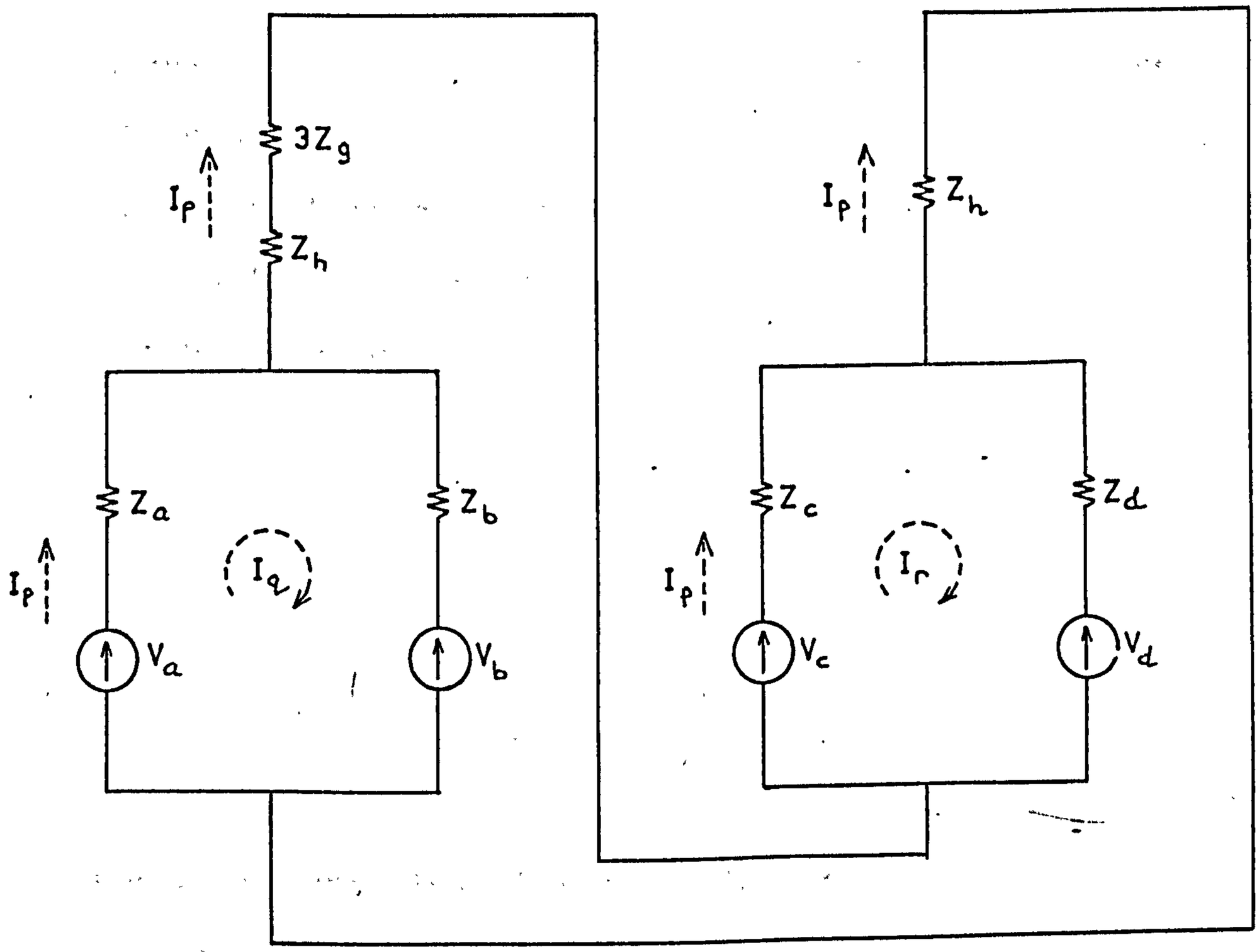

Fig. 5-8 Circuit Formed by Applying the Constraint $I_a = I_c$ to the Networks of Fig. 5-6

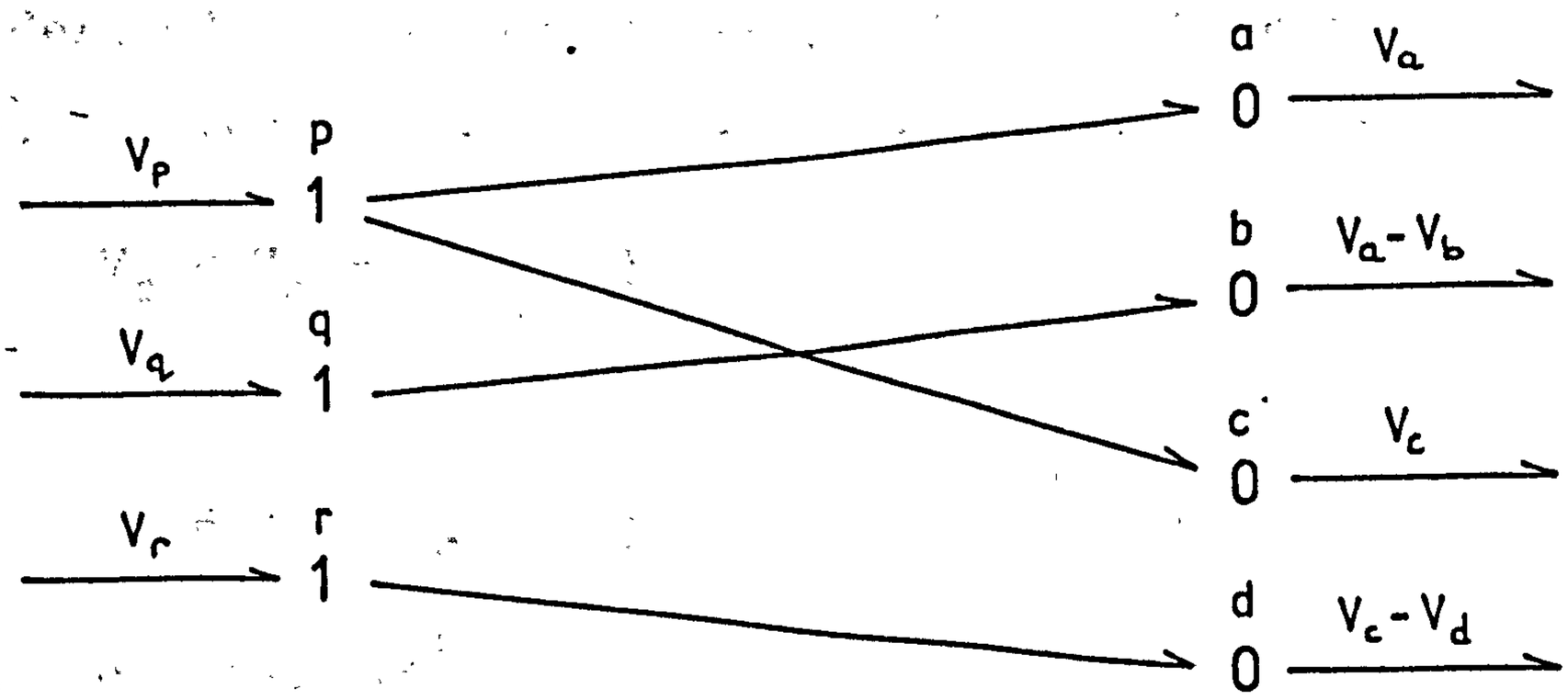

Fig. 5-9 Bond Graph Transformations for the Constraint $I_a = I_c$

The next step is to cascade the bond graph transformations of Figs. 5-7 and 5-9 to represent the transformations from branch equations to that imposed by the constraint $I_a = I_c$ for the connected network. The resulting bond graph may be simplified, as shown in Fig. 5-10, and the impedance matrix of the connected network can be formed; thus,

$$Z = \begin{array}{c} \\ p \\ q \\ r \end{array} \begin{array}{c} \begin{array}{ccc} p & q & r \end{array} \\ \begin{bmatrix} Z_a+3Z_q+2Z_h+Z_c & Z_a & Z_c \\ Z_a & Z_a+Z_b & \\ Z_c & & Z_c+Z_d \end{bmatrix} \end{array} \qquad \text{E3.2}$$

where the principal diagonal element is obtained by summing all the impedances connected to the particular 1-junction and the off-diagonal elements are the impedances between the appropriate 1-junctions.

Similarly the voltages of the connected network can be derived by the summations of all the efforts at the pth, qth and rth 1-junctions respectively; thus:

$$\left.\begin{aligned} V_p &= V_a + V_c \\ V_q &= V_a - V_b \\ V_r &= V_c - V_d \end{aligned}\right) \qquad \text{E3.3}$$

5.5 Conclusions

The application of Lagrange's equations to bond graph analysis results in the diagramatic representation of transformations for the constraint equations of ideal devices. The characteristic of these transformations is

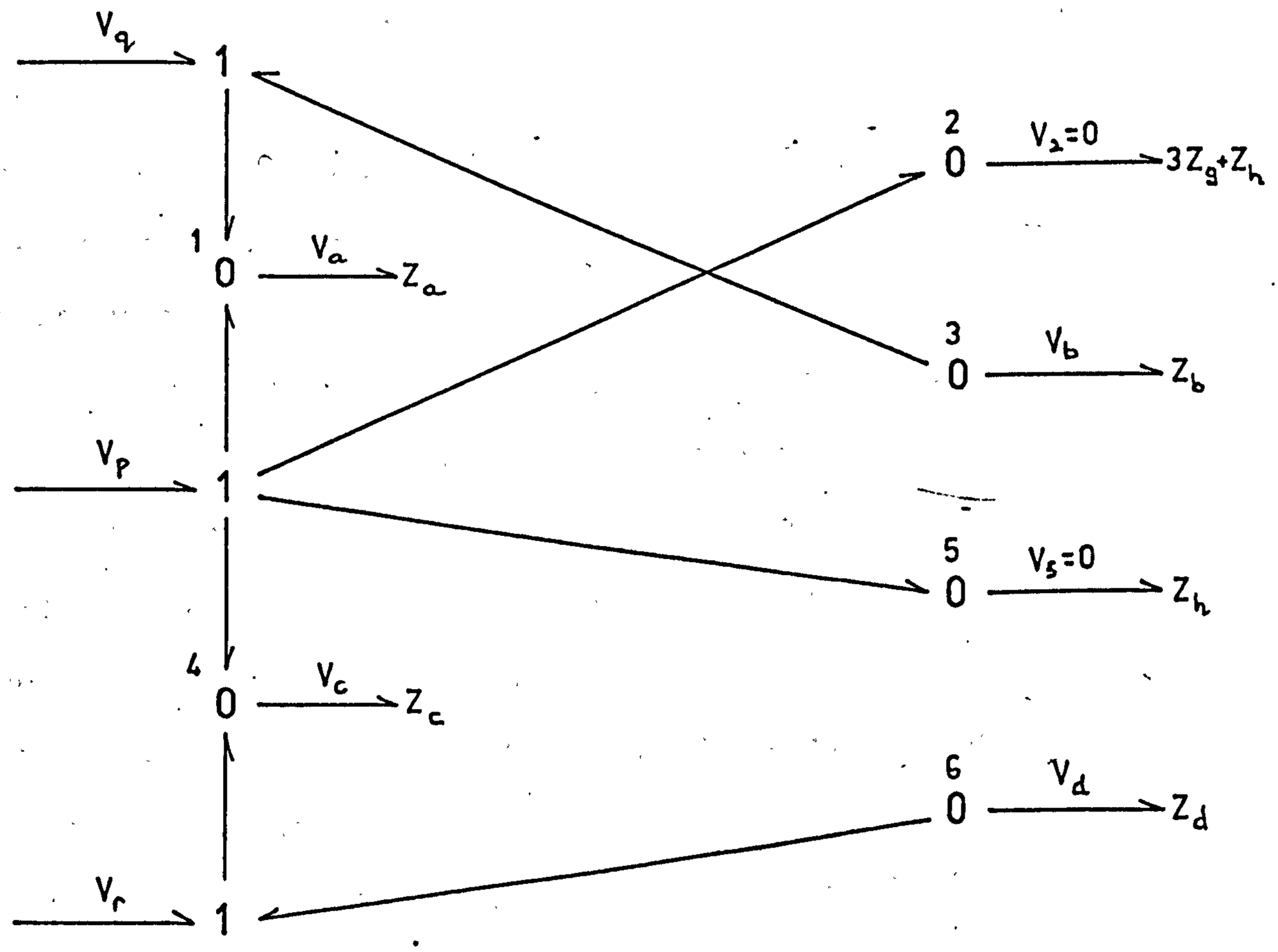

Fig. 5-10 Bond Graph Transformations for the Connected Network

governed by the geometric configurations of the physical structure which constrain and conserve the energy and power. Based on this concept a family of power-conserving transformations may be evolved whose main purpose is to transform variables in dynamic systems so as to obtain simpler representation of the systems or to aid in reducing the complexity of the representation in some rational manner. Many of the useful transformations of variables have been traditionally explained as mathematical transformations which upon close inspection turn out to conserve power and energy.

Bond graphs are mainly used to explain conceptually the nature of component interaction within systems. However, with the introduction of the generalised co-ordinate transformations, it has been possible to trace the relationship between Kron's tensorial method and the corresponding bond graph method. As such a junction structure may be regarded as a physical representation of a connection matrix. Perhaps, the graphical nature of bond graphs, and the wide variety of manipulations which the existence of a graphical notation suggests and permits, may complement and even simplify the highly mathematical style of Kron's presentation of his tensorial method.

In this chapter two methods of representing lumped energy systems using bond graph notations together with Lagrange's equations and variables are presented. The basic form is expressed in simpler transformed equations and more primitive variables. The appropriate state variables for the basic bond graph are the various primitive

quasi displacements X_i, for the compliances and the primitive quasi velocities (or flows) x_i, for the inertance. For the alternative bond graph no transformation of variables is used and as such the generalised displacements q, and the generalised velocities (or flows) f, are the state variables[10]. In this latter case, which is similar to the phase co-ordinate approach, the state equations are the actual Lagrange's equations which are more complicated than the equations in the transformed variables.

Although the use of energy equations provides a general approach to the construction of bond graph structures, the introduction of non-linearities poses certain problems[10] in the representations of the necessary variables in the graphs. In the method for formulating system equations from bond graphs discussed in Section 5.4, the state equations can be expressed in terms of the generalised displacements and the generalised momentums. It appears that by using these variables, the problems of simulating systems with non-linear algebraic characteristics, which often occur in systems containing non-linear dissipative elements, can be effectively solved.

Alternatively as proposed in Chapter 2, actual variables can be used, and the complications in formulating non-linear system equations may be reduced by introducing the mutators. In so far as graphical representations are concerned, the mutators provide greater insight into bond graph structures for non-linear energy systems and ensure that the necessary variables are assigned unambiguously. Also, these devices enable

non-linear electrostatic and electromagnetic field systems to be described by non-linear algebraic equations, which as shown in Section 5.4 is necessary to reduce the system equations into the form of Eqns. 5.37 and 5.38.

5.7 References

1. Martens, H.R.: 'Simulation of Non-Linear Multiport Systems using Bond Graphs', ASME Journal of Dynamic Systems, Measurement and Control, Series G, 1973, 95, (1), pp. 49-54.
2. Paynter, H.M. and Karnopp, D.C.: 'Design and Control of Multiport Engineering Systems', Automatic and Remote Control, Proc. International Federation of Automatic Control, Tokyo, 1965, pp. 443-454.
3. Chua, L.O.: 'The rotator - A New Network Component', Proc. IEEE, 1967, 55, (9), pp. 1566-1577.
4. Chua, L.O.: 'Synthesis of Non-linear Network Elements', Proc. IEEE, 1968, 56, (8), pp. 1325-1340.
5. Chua, L.O.: 'Memristor - The Missing Circuit Elements', IEEE Trans. on Circuit Theory, 1971, CT-18, (5), pp. 507-519.
6. Seely, S.: 'Electromechanical Energy Conversion', (McGraw-Hill, New York, 1962).
7. Messerle, H.K.: 'Dynamic Circuit Theory', (Pergamon, London, 1965).
8. Jones, D.L. and Evans, F.J.: 'A Classification of Physical Variables and its Application in Variational Methods', Journal of the Franklin Institute, 1971, 291, (6), pp. 449-467.

9. Rosenberg, R.C.: 'State-Space Formulation for Bond Graph Models of Multiport Systems', ASME Journal of Dynamic Systems, Measurement and Control, Series G, 1971, 93, (1), pp. 35-40.

10. Brown, F.T.: 'Lagrangian Bond Graph', ASME Journal of Dynamic System, Measurement and Control, Series G, 1972, 94, (3), pp. 213-221.

11. Pars, L.A.: 'A Treatise on Analytical Dynamics', (Heinemann, London, 1965).

12. Karnopp, D.: 'Power-Conserving Transformations: Physical Interpretations and Applications using Bond Graphs', Journal of the Franklin Institute, 1969, 288, (6), pp. 175-201.

13. Karnopp, D.: 'Resolution of a Paradox Involving Mechanical Gyrators and Transformers', Journal of the Franklin Institute, 1971, 291, (3), pp. 211-217.

14. Karnopp, D. and Rosenberg, R.C.: 'Analysis and Simulation of Multiport Systems', (The MIT Press, Cambridge, Mass., 1968).

15. Kron, G.: 'Tensor Analysis of Networks', (John Wiley, New York, 1959).

16. Kron, G.: 'Diakoptics', (MacDonald, London, 1963).

17. Paynter, H.M.: 'Bond Graphs and Diakoptics', The Matrix and Tensor Quarterly, 1969, 19, (3), pp. 104-107.

CHAPTER SIX

CONCLUSIONS

6.1 Introduction

In this thesis it has been emphasized that the main aim is to use the bond graph technique in the modelling and simulation of power system components in terms of their actual variables. Perhaps, the different functions and application of power system components together with the various definitions of the bond graph notations tend to obscure the original aim of this thesis. As such this chapter is intended to unify the seemingly diverse content and to materialize a joint approach in the analysis of energy systems.

Although a concluding section has been included in each chapter, the conclusions derived are based on the results of the investigations pertaining only to the chapter concerned. However, this chapter attempts to present the conclusions and recommendations which relate to the whole bond graph approach used for the modelling of power system components. The role of the mutators and other associated network devices[1,2,3] will be discussed.

6.2 Application of Bond Graph Methods to Power System Studies

It is felt that the major contribution presented is this thesis is in the application and extension of bond graph methods for power system analysis. The definitions of bond graph notations in Chapter 2 are geared and directed to achieve this goal. Consequently, the inductive

and capacitive mutators are proposed to represent graphically the non-linear n-port electromagnetic and electrostatic field systems.

As an initial attempt in the modelling of power system components only steady-state operating conditions are considered in Chapter 3. Models under these conditions are relatively simpler. In addition efforts are made to reduce these models into their elemental parts before restructuring the complete component models. The bond graph of the n-port electromagnetic field system, although developed as a dynamic model, can be readily adapted for steady-state operating conditions and when appropriately used becomes the main constituent in the modelling of power system components. By assembling the component models derived, the behaviours of a power system complex under fault conditions are analysed and compared with known results; thus confirming the validity of the bond graph models.

In order to study the individual characteristics of a power system component, a detailed model is required. The bond graphs of synchronous generators derived in Chapter Four are used to accurately predict the dynamic behaviours of these machines. The n-port electromagnetic field system, which forms the basis for the generator models, enables the effects of saturation to be included with no added complication to the system equations. The computation structure derived directly from the bond graph of the synchronous generator organises the system equations and consequently enables rapid convergence of ——

the solution process. This technique is also used in the study of an induction motor system and may effectively provide a unified approach to the analysis of all types of electromechanical energy converters.

In the preceding chapters, the fundamental modelling technique involves the initial construction of the bond graphs of sub-systems, each describing the relationships of a pertinent collection of variables. These bond graphs are then assembled appropriately to form the model of the actual device. However, in Chapter 5 an alternative approach is proposed by using Lagrange's equations. The bond graphs of lumped energy systems in terms of both the transformed and actual variables as well as the bond graph for generalised co-ordinate transformations are derived. The method of organising system equations from bond graphs of energy systems attempts to incorporate non-linear effects and provides a general mathematical approach for formulating equations of non-linear systems which in the previous chapters are graphically represented by the mutators.

The models of power components developed in this thesis require associated developments in computer technique for their analysis. In the steady-state analysis of the power system complex in Chapter 3, the supplemented nodal phase admittance matrix is formed from the bond graph models. The available computer methods for the solution of linear algebraic equations are adapted to enable the phase admittance matrix to be used for the analysis of balanced and unbalanced fault problems in terms of their phase co-ordinates.

Another important development in computer technique involves the solution of equations for non-linear systems described by mixed differential/algebraic equations. It frequently occurs that in representing power system components non-linear effects may be characterised by algebraic equations. The computer simulation of the saturated synchronous generators in Chapter 4 provides a good starting point for using and extending this technique to other non-linear systems.

6.3 Possible Developments of Bond Graph Models for Power System Components

One of the consequences of introducing the mutators in the analysis of non-linear systems is that energy and power bonds connecting the various elements and junction structures are represented by the same conventional notations. The only distinction between these bonds is expressed by the types of variables describing them; the energy variables for the energy bonds and the conjugate power variables for the power bonds. It is felt that this is a desirable feature for the purpose of the present study since it not only emphasises the energy and power interactions but also enables energy and power variables to be represented in the same diagram.

Also the inductive mutator is able to exploit the common phenomenon occurring in most power system devices which consists basically of a single magnetic circuit interlinked with several separate electric circuits. The n-port electromagnetic field system is formed by using the inductive mutator. Under both steady-state and

dynamic conditions, this system is shown to be a necessary ingredient in the bond graph representation of power system components.

The origin of the inductive and capacitive mutators can be traced to the three classes of mutators suggested by Chua[1] as early as 1968. Since then their use as network elements has been quite extensive. Other elements such as the reflector[1], the scalor[1], the rotator[2] and the memristor[3] have also been introduced. Of these elements, perhaps the memristor seems to offer a new scope for use beyond the traditional electrical domain.

In one of the earlier books[4] on bond graphs, Paynter draw a 'tetrahedron of state', as shown in Fig. 6-1, which summarises the relationship between the state variables (e, i, λ, q), that is, the effort, flow, momentum and displacement respectively. There are six binary relationships possible between these four state variables. Two of these can be defined as the displacement (or electric charge), $q(t) = \int^t i(t)\, dt$, and the momentum (or flux linkage), $\lambda(t) = \int^t e(t)\, dt$.

Of the remaining four possible relations, three are the elementary constitutive relations for the energy storage and dissipative elements:

$$q = F_C\ (e) \qquad 6.1$$

$$\lambda = F_L\ (i) \qquad 6.2$$

$$e = F_R\ (i) \qquad 6.3$$

From a purely logical view point, the remaining constitutive relation, shown as a dotted line in Fig. 6-1,

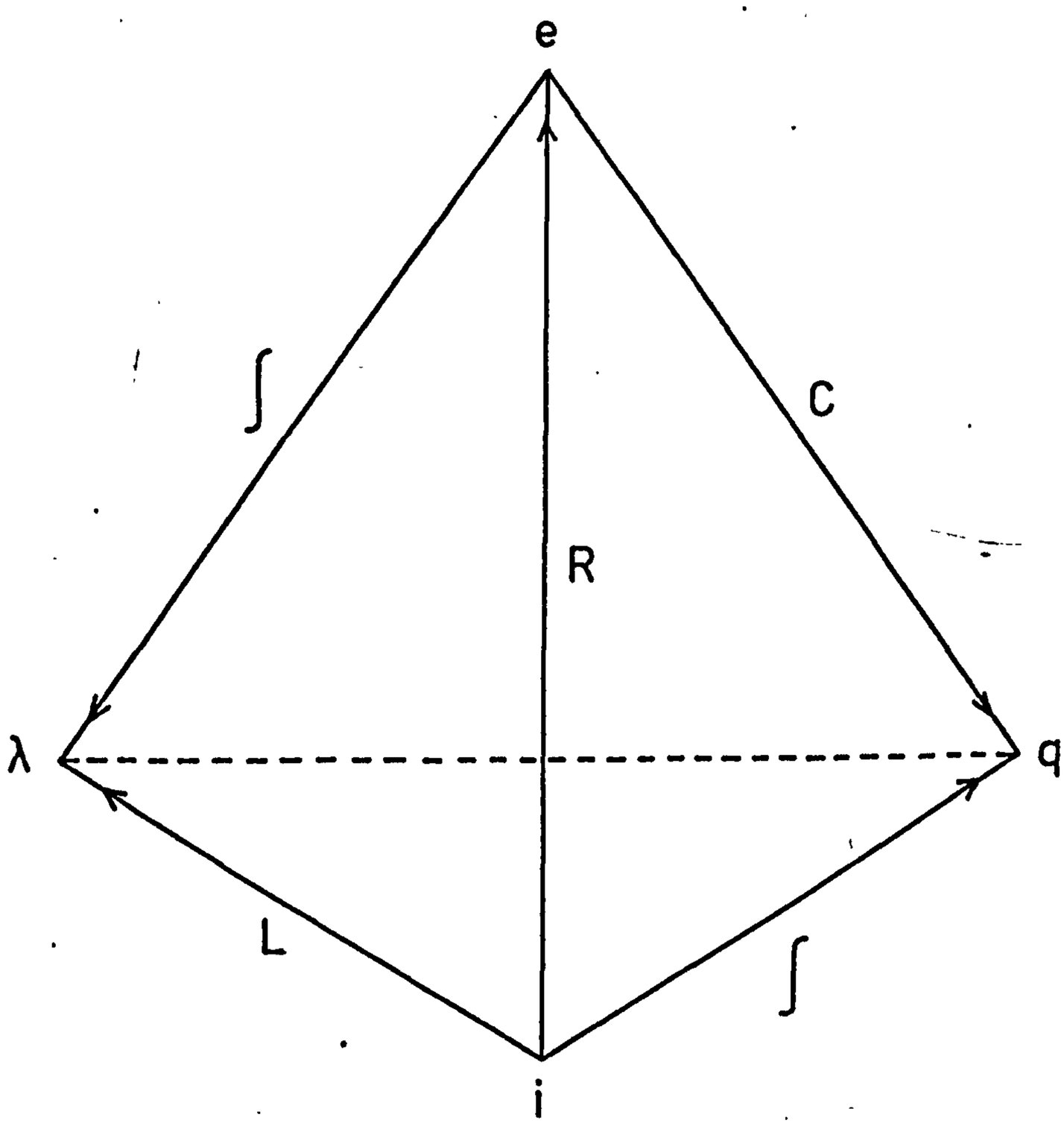

Fig. 6-1 State Variables and Constitutive Relations

may be regarded as fundamental as the other three elements expressed by Eqns. 6.1, 6.2 and 6.3. Chua[3] proposed that the missing constitutive relation,

$$\left.\begin{aligned} \lambda &= F_M(q) \\ \text{or} \quad q &= G_M(\lambda) \end{aligned}\right\} \qquad 6.4$$

be called a memristor.

It is felt that an important use of the memristor lies in the mechanical-electrical domain. In the study on the electromechanical energy converters a major problem involves the representation of the complex mechanical-electrical energy interactions within the machine. In this thesis an attempt is made to represent these energy interactions in simple terms by introducing the concept of the 'phase' torque. However, in the opinion of the author, a detailed understanding and representation of these energy interactions is needed.

Expressed in terms of the mechanical angular displacement Θ, and the electrical flux linkage λ, then Eqn. 6.4 may be written as:

$$\left.\begin{aligned} \lambda &= F_M(\Theta) \\ \text{or} \quad \Theta &= G_M(\lambda) \end{aligned}\right\} \qquad 6.5$$

If the relationships given by Eqn. 6.5 are physically realisable, then the memristor may be effectively used in the bond graph modelling of energy converters to display the complete electromechanical energy conversion process. Perhaps this may result in a new and radical approach to the analysis and synthesis of all types of electrical machines.

6.4 Bond Graph Analysis of Multiport Energy Systems

In the initial stages of the research, one of the major preoccupations is in identifying the fundamental structure for energy systems. Basically, the n-port electromagnetic and electrostatic field systems can be regarded as a necessary structure for representing power system components in the study of power system behaviours.

However, the bond graph of a large power system complex consisting of assembled components is far too complicated to be of real practical value. This limitation in using bond graphs to represent a large system graphically may perhaps be remedied by introducing rules for the reduction of bond graph structures into their equivalent simpler forms.

Alternatively, another approach may be considered in which a form of structural formula for each component model is classified and catalogued in a special computer program. Thus, the assembly of a representation of any particular portion of the large power system merely requires ordering the parts from a catalogue by an appropriate alphameric computer language together with other specifications, and constructing an assembly diagram.

An important intention of this thesis is to explore the possible use of bond graphs in power system studies. It is hoped that in some way this has been achieved. As a teaching tool, the use of bond graphs to represent power system components in terms of their phase co-ordinates may provide a direct approach to illustrate system interactions which hitherto can be obscured by the need to comprehend transformation theory.

In this thesis only the application of bond graphs to power system problems has been presented in detail, and of the many manipulations the emphasis is in the setting up of component models with the appropriate developments of the associated computer techniques. The work presented here includes some original contributions towards an attempt to understand power system behaviours, but the author would concede that more rigorous methods are required in the extension and further usage of bond graph techniques.

6.5 References

1. Chua, L.O.: 'Synthesis of New Non-linear Network Elements', Proc. IEEE, 1968, 56, (8), pp. 1325-1340.
2. Chua, L.O.: 'The rotator - A New Network Component', Proc. IEEE, 1967, 55, (9), pp. 1566-1577.
3. Chua, L.O.: 'Memristor - The Missing Circuit Elements', IEEE Trans. on Circuit Theory, 1971, CT-18, (5), pp. 507-519.
4. Paynter, H.M.: 'Analysis and Design of Engineering Systems', (The MIT Press, Cambridge, Mass., 1961).

APPENDICES

APPENDIX A

DETAILS OF PHASECO - PROGRAM FOR THE SOLUTION OF FAULT PROBLEMS USING PHASE CO-ORDINATE METHOD

PHASECO is a program specially written to solve fault problems in power systems using the method of phase co-ordinates. The input data, in the form of node numbers, transformer tap values and system admittances, are used to assemble the component matrices from the bond graph models described in Chapter 3. The supplemented nodal phase admittance matrix may then be constructed by a subroutine incorporated in the program.

The original program is developed to handle all types of fault conditions, such as, direct earth faults, direct phase-to-phase short-circuits, earth faults via impedances, phase-to-phase short-circuits via impedances as well as for open conductor conditions. Fault occuring at different geographical locations can be included in the program without added difficulties to the data organisations.

For the purpose of the study in this thesis, the original phase co-ordinate program is modified to solve only direct earth faults so as to reduce the core storage needed. Initially this modified program, called PHASECO Mk. I, is used to test the validity of the bond graph models of power system components; however, its use can be extended to include the investigations into the effects of removing power bonds from these models.

The summaries of program details and performance guide of PHASECO Mk I are given below:

PROGRAM DETAILS

(a) Language: Subset of ICL 1900 FORTRAN which is similar to FORTRAN IV.

(b) Number of routines:

Main Program 1

Subroutines 15

In Fig. A-1, the interaction between the principal subroutines of program PHASECO is shown. The functions of the various subroutines are given below:

1. PHASECO - Main program for reading data and calling the appropriate subroutines.
2. YLOAD - Forms the load admittance matrix.
3. YIMLOD - Forms the induction motor admittance matrix.
4. YTLINE - Forms the transmission line admittance matrix.
5. YSPSTM - Forms the generator admittance matrix.
6. YEARTH - Forms the earth admittance matrix
7. YTRYD - Forms the delta-star transformer admittance matrix.
8. YTRYY - Forms the star-star transformer admittance matrix.
9. YTRDD - Forms the delta-delta transformer admittance matrix.
10. YTRYYD - Forms the star-star-delta transformer admittance matrix.
11. ASSAM - Assembles the supplemented nodal phase admittance matrix from matrices formed by subroutines 2 to 10.
12. FLTLVL - Calculates the fault levels and single-phase earth fault currents.

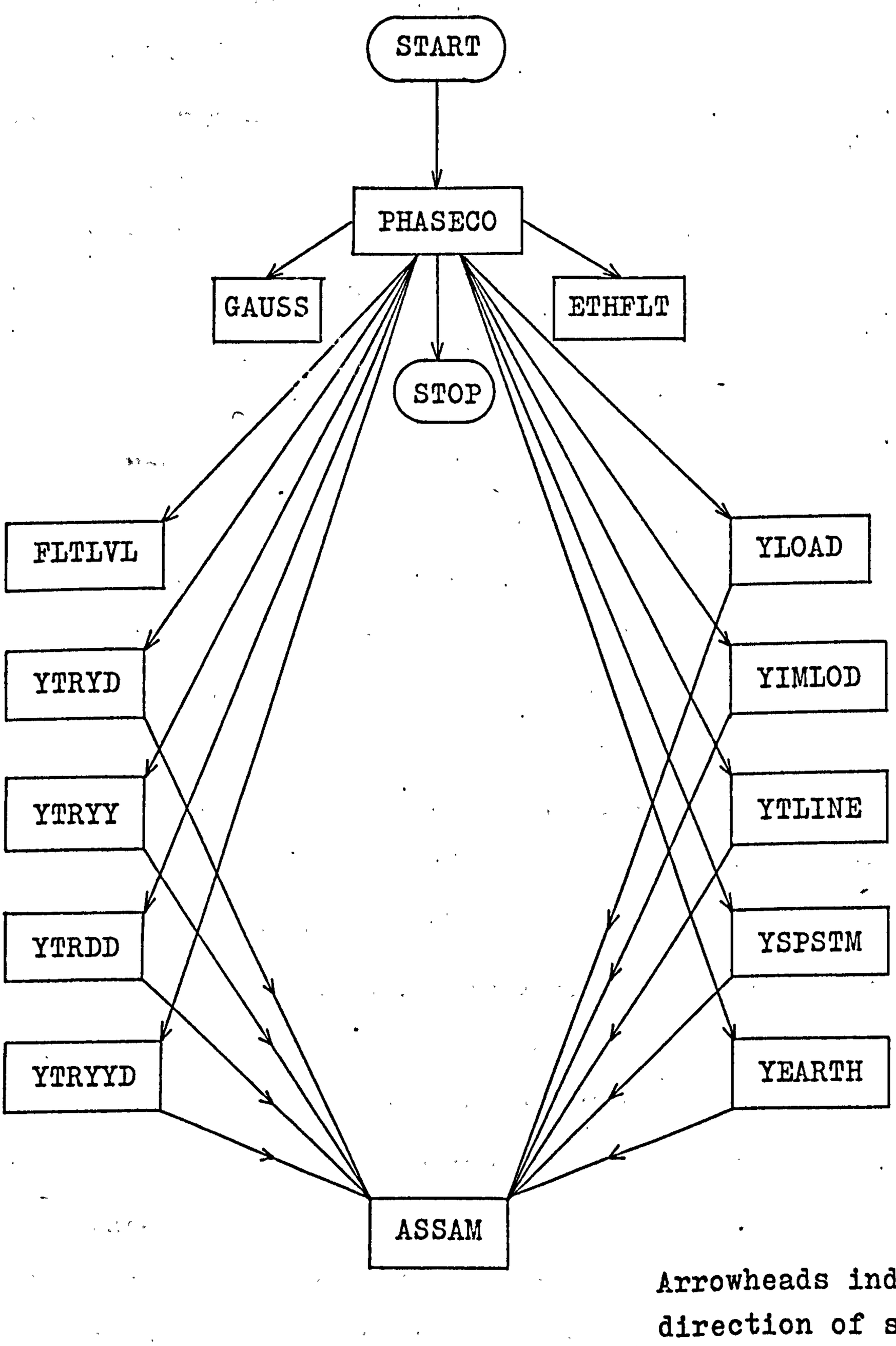

Fig. A-1 Interaction between Principal Subroutines

13. GAUSS - Performs the iterative calculations for fault currents at different locations using the distributed source method.

14. ETHFLT - Calculates simultaneous earth fault currents by the source transformation method.

(c) Number of variables:

Labelled COMMON:	complex	10,010
	real	140
	integer	322
Non-COMMON:	real	36
	integer	25

(d) Size of source program:

Source statement lines	1234
Comment	47
Total	1281 cards

(e) Organisation: The program is specially written to ensure that overlaying techniques may be effectively applied. The core size requirement is greatly reduced by using this technique. However, it is essential that a temporary file be created to accommodate the binary output from the overlay program. The depth of the overlay is equal to the number of overlay units which in this case it two.

(f) Method of use: Each power system component considered must be labelled with the appropriate node numbers and these together with its admittances form the input data. The sequence, by which the card containing individual data of each component is to be read, is given in the operating manual.

PERFORMANCE GUIDE

(a) Computer used: PHASECO Mk I runs without modification on ICL 1900 series machines with GEORGE operating system. The program may, with minor alternations, be adapted for use with any other machine.

(b) Core size required: Using COMPRESS INTEGER AND LOGICAL mode:

Non-overlaid : approximately 60K words

Overlaid : approximately 48K words

(c) Input media: Any valid 1900 series media can be used.

Preferred media:

PHASECO program : input from disc file

Data : punched cards

Control card deck: punched cards

(d) Output medium: One line printer with a minimum line length of 120 characters.

(e) Work file for compilation/consolidation: When run in overlaid mode, a program file is required.

(f) Limiations:

(i) The maximum number of nodes, that is, the number of busbars, multiplied by 3, plus the number of floating neutrals must not exceed 70.

(ii) The maximum number of each type of power system components, for example, loads, transformers, induction machines, transmission lines, and synchronous generators must not exceed 20.

(iii) The maximum number of simultaneous earth faults occurring for any one study must not be more than 7.

APPENDIX B

DETAILS OF SYSTRAN - PROGRAM FOR THE SIMULATION OF NON-LINEAR DYNAMIC SYSTEMS

Using SYSTRAN, the setting up and running of a system simulation may be approached in the following way. The set of equations representing the system is first written out by the user in the form of a Fortran SUBROUTINE Subprogram called EQNS. This subroutine specifies all of those aspects of the system which on an analogue computer are dependent on the patchboard wiring and is combined with the basic Systran routines under the control of a standard Fortran compiler, to produce a complete Object Program ready to solve the user's particular set of system equations.

The problem solving capacity of Systran Mk 3D may best be defined in terms of an equivalent analogue computer configuration. This would include 40 Integrators, 20 Function Generators, 10 Electronically-controlled Multiway Switches, 5 Variable Delay Units, and a more or less unlimited number of Multipliers, Summers, Inverters, Potentiometers, Comparators, Logic Elements, etc. Also as with analogue, the preferred formulation is the familiar Block Diagram in which the dynamic elements should be represented in terms of simple integrators.

The summaries of program details and performance are given below:

PROGRAM DETAILS

(a) Language: Subset of ICL 1900 FORTRAN which is as close as possible to USASI FORTRAN

(b) Number of routines:

Main Program	1
BLOCK DATA Subprogram	1
Subroutine Subprograms	9
Function Subprograms	7
User-written Subprogram	1

(c) Number of variables:

Blank COMMON:	real	2347
	integer	356
	logical	5
Labelled COMMON:	real	663
	integer	25
Non-COMMON	real	303
	integer	117
	logical	1

(d) Word-length requirements: Integer variables: capacity to store 4 or more characters; Real variables; preferably 8 or more significant digits. On ICL 1900 machines, integer and logical variables may be stored in compressed mode.

(e) Size of source program:

Source statement lines (excluding user's subroutine)	885
Comment lines	188
Total	1073 cards
Source lines in typical user's subroutine	20-100

(f) Organisation: Division of program into subprograms is arranged so that maximum benefit is obtained from overlaying subprograms, using one overlay area with two

overlay units. The program may be run in overlaid or non-overlaid mode without modification. The organisation also permits very simple adaptation of chaining instead of overlaying, where the computer to be used provides this facility. Three core loads are recommended.

(g) Method of use: Form of system to be simulated is specified by writing a FORTRAN subroutine. Particular solutions required, and values of adjustable constants etc., are specified for each computer run via a 'control card deck'.

PERFORMANCE GUIDE

(a) Computer used: SYSTRAN/S as supplied runs without modification on ICL 1900 series machines, with or without the GEORGE operating system. The program is specifically designed for easy adaptation to any other machine. Performance details below refer to 1905E computer using the ICL disc compiler XFAE.

(b) Core size required: Using COMPRESS INTEGER AND LOGICAL mode:

Non-overlaid: approximately 21K words

Overlaid: approximately 18.5K words

Exact core requirement varies somewhat with size of user's subroutine. Note that the minimum machine store size required is determined by the above figures plus any space needed for executive and operating system.

(c) Input media: Any valid 1900 series media can be used.

Preferred media:

SYSTRAN program : input from disc file

User's subroutine: cards or paper tape

Control card deck: punched cards

(d) Output medium: One line printer with a minimum line length of 120 characters.

(e) Work files for execution: One scratch file, preferably disc, to hold formatted data. Maximum size determined by largest line printer graph-plot to be output (typically 50-100 records of 121 information characters each).

(f) Work files for compilation/consolidation: If run in overlaid form, a program file is required.

(g) Processing time: Job run time varies widely with size and nature of problem. Built-in limits set maximum time per solution of the order 1-5 minutes, unless explicitly over-ridden by the user.

(h) Limitations:

(i) Maximum problem size is similar to that following equivalent analogue computer complement

Integrators	: 40
Variable-function generators	: 20
Delay units	: 5

Multipliers, summers, potentiomenters etc: virtually unlimited.

(ii) Algorithm for solving implicit algebraic equations (multidimensional Newton-Raphson iteration) may not always converge e.g. when solution passes over discontinuity.

(iii). Integration and iteration processes are error controlled to user-specified limits, with practical maximum accuracy of about 6-7 significant figures.

As a practical example in the use of Systran, the computation structure of Fig. 4-13 for the test single-phase generator will be used to derive the mixed differential and algebraic equations. The process of calculating system derivatives in the presence of algebraic loops proceeds in the following way. The Systran user first 'break' all such loops in the system by inserting a special unity-gain 'Buffer Block' somewhere in each loop. A notation, y'_b and y_b is introduced for input and output respectively of a Buffer Block and each y'_b term is rewritten on the LHS of one equation as already done with derivative terms, $\dot{x}_i$.

Considering the algebraic loop for the field winding in Fig. 4-13, the input to the Buffer Block placed between the block diagrams containing $L_{\ell F}$ and F_{mT} terms is:

$$i'_F = \frac{1}{L_{\ell F}} \left[\lambda_F - N_{Fa} \lambda_{ma} \cos \alpha \right] \qquad \text{B.1}$$

where $L_{\ell F} = \frac{1}{2} \ell_F$ and ℓ_F is the field leakage inductance.

The set of equations suitable for Subroutine EQNS are obtained by tracing the appropriate loops in Fig. 4-13, thus:

$$
\left.
\begin{aligned}
i_{mF} &= F_{mT}\ (i_a,\ i_F,\ i_D,\ i_Q,\ \Theta,\ \alpha) \\
\lambda_{ma} &= F_l\ (i_{mF}) \\
i_F' &= \frac{1}{L_{\ell F}} \left[\lambda_F - N_{Fa}\ \lambda_{ma} \cos \alpha \right] \\
\dot{\lambda}_F &= \nu_F - i_F R_F \\
i_a' &= \frac{1}{L_{\ell a}} \left[\lambda_{ma} \cos\ (\Theta-\alpha) - \lambda_a \right] \\
\dot{\lambda}_a &= \nu_a + i_a R_a \\
i_D' &= \frac{1}{L_{\ell D}} \left[N_{Da}\ \lambda_{ma} \cos \alpha - \lambda_D \right] \\
\dot{\lambda}_D &= i_D R_D \\
i_Q' &= \frac{1}{L_{\ell Q}} \left[N_{Qa}\ \lambda_{ma} \sin \alpha - \lambda_Q \right] \\
\dot{\lambda}_Q &= i_Q R_Q
\end{aligned}
\right\} \quad \text{B.2}
$$

where $L_{\ell a} = \sqrt{2}\ \ell_a$; $L_{\ell D} = \frac{1}{2}\ \ell_D$; $L_{\ell Q} = \frac{1}{2}\ \ell_Q$; F_l is defined by the no-load magnetization characteristic and F_{mT} may be derived from Eqn. 4.47.

APPENDIX C

DERIVATION OF THE DERIVATIVE APPROXIMATION FOR IMPLICIT INTEGRATION

The approach taken in solving a differential equation of the form $\dot{x} = f(x,t)$ is to approximate this equation by a difference equation of the general form

$$x_n = a_1 x_{n-1} + a_2 x_{n-2} + \cdots + h\left[b_o \dot{x}_n + b_1 \dot{x}_{n-1} + b_2 \dot{x}_{n-2} + \cdots\right] \quad C.1$$

where h is the integration step size and where $x_n = x(t_n) = x\,(nh)$. The coefficients a_i and b_i are determined usually by matching a certain number of terms in the Taylor expansion of x(t) about a point.

If the coefficient $b_o = 0$, the formula represents an explicit method of integration since all the data on the right-hand side are already known from previous integration steps. However, if $b_o \neq 0$, the term $\dot{x}_n$, which has not yet been computed, is required to calculate the new value of x_n. In this case, the formula represents an implicit method of integration and it requires that a system of equations relating $\dot{x}_n$ and x_n be solved at every integration step. If these equations are non-linear, then an iterative process of solution must be used.

From Fig. C-1, let x_n, x_{n-1}, x_{n-2} ..., x_{n-k} be the ordinates and let t_n, t_{n-1}, t_{n-2} ..., t_{n-k} be the abscissas of k+1 points on the curve x(t). Further, let $h_i = t_n - t_{n-i}$ with $h_1 = h$ and let $\lambda_i = h_i/h$. Then the derivative $\dot{x}_n$ may be defined as a linear combination of the x_{n-i}; thus:

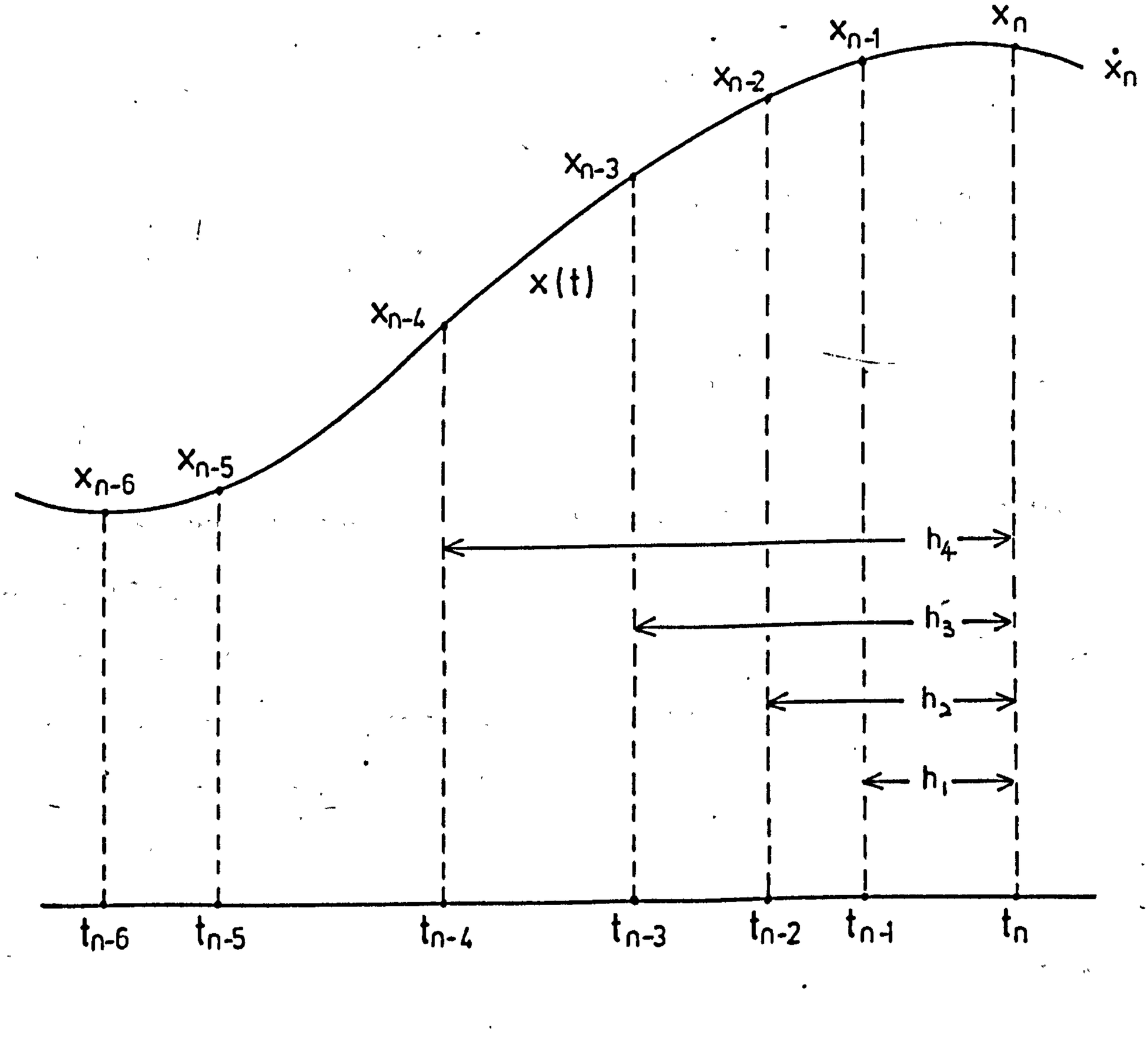

Fig. C-1 Polynomial Approximation to x(t) using $\dot{x}_n$ and x_{n-i}

$$h\dot{x}_n = \sum_{i=0}^{k} p_i \, x_{n-i} + E_k \qquad C.2$$

where the coefficients p_i are to be determined by requiring Eqn. C.2 to be exact for any x(t), which is a polynomial of degree k or less.

By substituting into Eqn. C.2 the Taylor expansion of x_{n-i} about the point x_n and then collecting terms, it turns out that:

$$h\dot{x}_n = p_o \, x_n + \sum_{i=1}^{k} \left[p_i x_n - h_i p_i \, \dot{x}_n + \frac{h^2_i}{2!} p_i \ddot{x}_n + \ldots + \frac{(-h_i)^k}{k!} p_i x_n^{(k)} \right] + \sum_{i=1}^{k} \frac{(-h_i)^{k+1}}{(k+1)!} p_i x_n^{(k+1)} + \ldots \qquad C.3$$

where the leading term of the truncation error E_k is shown explicitly.

If Eqn. C.2 and hence Eqn. C.3 are to be exact for polynomials up to degree k, then E_k must be zero and the coefficients of all derivatives up to the kth must also vanish. This leads to the conditions:

$$\sum_{i=1}^{k} p_i = 0 \qquad C.4$$

$$-\sum_{i=1}^{k} h_i p_i = h$$

or

$$\sum_{i=1}^{k} \lambda_i p_i = -1 \qquad C.5$$

and

$$h^m \sum_{i=1}^{k} \lambda_i^m \, p_i = 0, \quad m = 2,3,\ldots,k \qquad C.6$$

These relationships show that the p_i are determined solely by the λ_i, which in turn depend on the relative sizes of the time intervals $t_n - t_{n-i}$. Eqns. C.4, C.5 and C.6 must be solved afresh at each time step, but this is a minor task. By letting:

$$\left.\begin{aligned} x_n &= x_{n-1} + \Delta x_n \\ x_{n-1} &= x_{n-1} \\ x_{n-2} &= x_{n-1} - \Delta x_{n-1} \\ x_{n-3} &= x_{n-1} - \Delta x_{n-1} - \Delta x_{n-2} \\ &\text{etc.} \end{aligned}\right\} \quad \text{C.7}$$

it can be shown that Eqn. C.2 is equivalent to

$$\dot{x}_n = \frac{b_o}{h} \Delta x_n + \sum_{i=1}^{k-1} \frac{b_i}{h} \Delta x_{n-1} + \frac{E_k}{h} \qquad \text{C.8}$$

where

$$b_i = \sum_{j=0}^{i} p_j \qquad \text{C.9}$$

Eqn. C.8 requires Δx_n to be known before $\dot{x}_n$ can be computed. In other words, the implicit nature of C.8 requires an iterative process to obtain self-consistent values of both $\dot{x}_n$ and Δx_n. Fortunately, the modified Newton iteration scheme can readily be extended to achieve this result simultaneously with reduction of the error vector u(x) to acceptably small value.

Actually, a predicted value of Δx_n, obtained as outline below, is used in Eqn. C.8 at the beginning of each integration step to calculate a first approximation to $\dot{x}_n$. This approximation, designated x', is updated during the Newton iteration process according to the relation:

$$\dot{x} = \frac{Rb_o}{h} \Delta x + x' \qquad C.10$$

Here, Δx is the correction vector obtained by solving the Jacobian equation and R is the step-size factor.

The truncation error E_k is computed using the leading terms only, as displayed in Eqn. C.3, written in the form:

$$E_k = \frac{h^{k+1}}{k+1} x_n^{(k+1)} \sum_{i=1}^{k} \frac{\lambda_i^{k+1} p_i}{k!} \qquad C.11$$

using the relationship

$$\varrho_k = \sum_{i=1}^{k} \frac{\lambda_i^{k+1} p_i}{k!} = \prod_{i=1}^{k} \lambda_i / i \qquad C.12$$

Eqn. C.11 becomes:

$$E_k = \varrho_k \left[\frac{h^{k+1} x_n^{(k+1)}}{k+1} \right] \qquad C.13$$

The bracketed quantity in Eqn. C.13 can be computed from a linear combination of x_{n-i} or Δx_{n-i} in a manner quite similar to that already described for $\dot{x}_n$. In fact the same coefficient matrix as that derived for Eqns. C.4, C.5 and C.6 can be used - extended by one additional row and column - but with a different right hand side. The resulting $\underline{p_i}$ are used in a formula identical in form to Eqn. C.9 for computing the coefficients b_i in the expression:

$$E_k = \varrho_k \sum_{i=0}^{k} \underline{b}_i \Delta x_{n-i} \qquad C.14$$

Finally, a third set of coefficients $\underline{p_i}$ and $\underline{b_i}$ are computed - again using the same coefficient matrix but a still different right-hand side - for predicting Δx_n

according to the relationship:

$$\Delta x_n = \sum_{i=1}^{k+1} \underline{b_i}\ \Delta x_{n-i} \qquad \text{C.15}$$

APPENDIX D

DATA OF ANALYSED SYSTEMS

D.1 One-Line Diagram and Power System Component Parameters

The impedances and admittances of the power system components labelled as in Fig. D-1 are given below:

Generator No.	Node No.	Reactances	
		Generator Transformer	Generator Sub-transient
1	1	0.133	0.160
2	4	0.100	0.080
3	13	0.267	0.320
4	56	0.100	0.080
5	50	0.067	0.080
6	61	0.0696	0.145

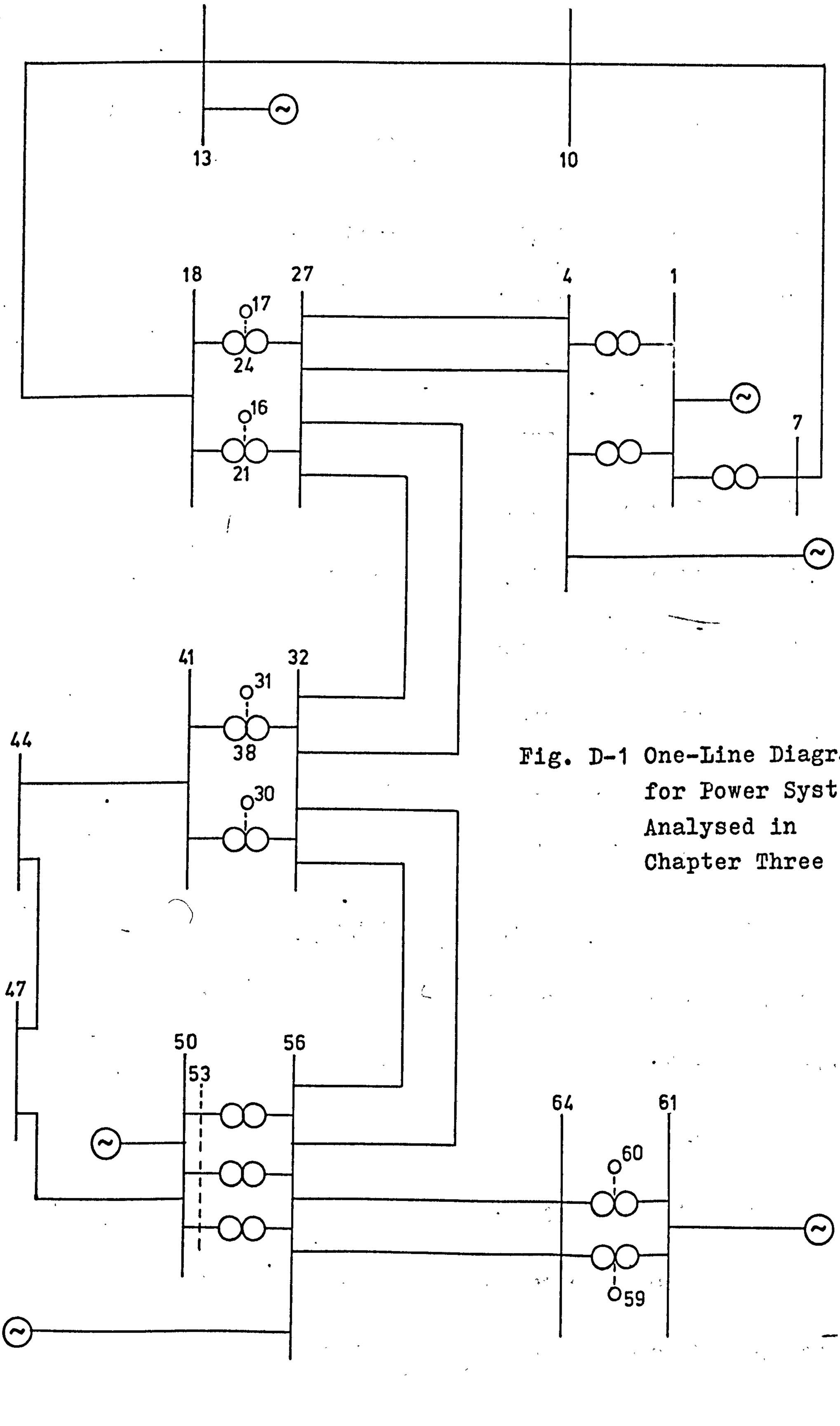

Fig. D-1 One-Line Diagram for Power System Analysed in Chapter Three

T/Line No.	Between Node Nos.	R	X	B
1	7/10	0.1982	0.4657	0.0046
2	10/13	0.0330	0.0760	0.0030
3	13/18	0.057	0.1303	0.0052
4	4/24	0.0226	0.0717	0.1010
5	4/24	0.0226	0.0717	0.1010
6	27/32	0.0311	0.0985	0.1385
7	27/32	0.0311	0.0985	0.1385
8	41/44	0.475	1.087	0.00065
9	44/47	0.646	1.497	0.00089
10	47/50	0.570	1.305	0.00079
11	50/53	0.0103	0.0706	0.00011
12	50/53	0.0103	0.0706	0.00011
13	50/53	0.0103	0.0706	0.00011
14	32/56	0.0269	0.0851	0.1197
15	32/56	0.0269	0.0851	0.1197
16	56/64	0.00566	0.01788	0.0252
17	56/64	0.00566	0.01788	0.0252

Y-D Transformer

Transformer No.	Between Node Nos.	Tap %	Reactances
1	1/4	-	0.20
2	1/4	-	0.20
3	1/7	-	0.60
4	53/56	7.5	0.20
5	53/56	7.5	0.20
6	53/56	7.5	0.20
7	61/64	-10.0	0.30
8	61/64	-10.0	0.30

Y-Y-D Transformer

Transformer No.	Between Node Nos.	Tap %	Reactances
1	18/27	-7.5	0.60
2	18/27	-7.5	0.60
3	32/41	-5.0	0.60
4	32/41	-5.0	0.60

D.2 Parameters for the Single-Phase Synchronous Generator

The magnetization characteristic for this machine has already been given in Fig. 4-11. The following relevant parameters are taken from the paper by Reedy, Ali and Jones given in Reference 6 of Chapter 4.

$\ell_a = 0.000239H$

$\ell_F = 0.1141H$

$\ell_D = \ell_Q = 0.0191H$

$R_a = 0.150\Omega$

$R_F = 15.38\Omega$

$R_D = R_Q = 1.40\ \Omega$

$N_{Fa} = 11.85$

$N_{Da} = 2.30$

$N_{FD} = 5.15$

D.3 Parameters for the Three-Phase Synchronous Generator

The magnetization characteristic for the three-phase synchronous generator is given in Fig. D-2. The following designed details of the 1290 KVA, 6 KV, 50 Hz, 20 poles machine were supplied by the manufacturer, GEC Machine Limited, Mill Road, Rugby, England.

$\ell_a = 0.01331H$

$\ell_F = 0.04270H$

$\ell_D = \ell_Q = 0.0866H$

$R_a = 0.587\Omega$ at 75^oC

$R_F = 0.20\Omega$ at 75^oC

$R_D = R_Q = 1.28\Omega$ at 75^oC

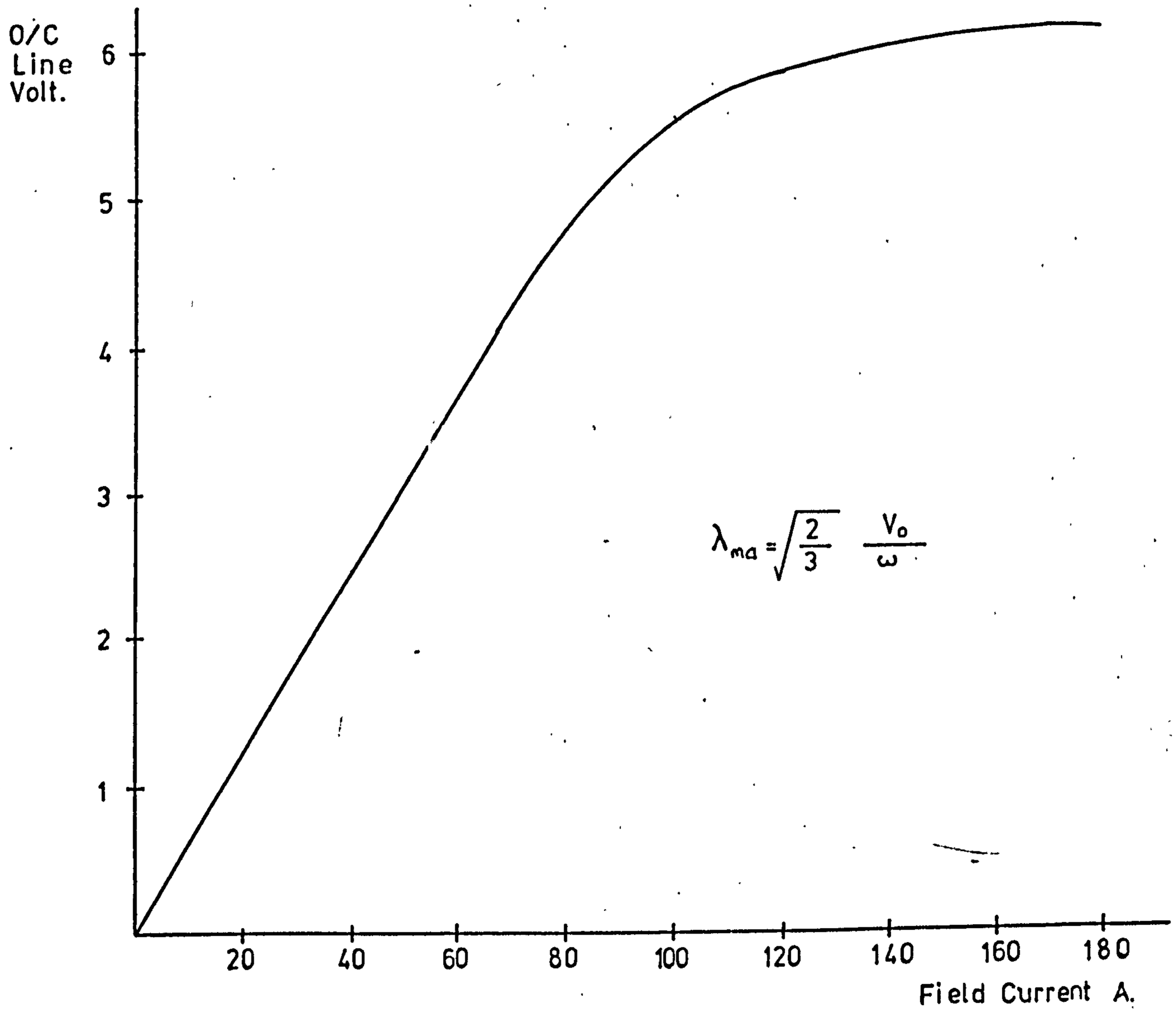

Fig. D-2 Magnetization Characteristic of the Three-Phase Synchronous Generator

From the above curve the armature flux linkage table may be obtained:

i_{mF}(Amp.)	λ_{ma}(Wb.T.)
0.0	0.0
40.0	6.40
60.0	9.45
80.0	12.50
100.0	14.34
110.0	14.81
120.0	15.17
140.0	15.70

Effective number of turns of armature winding/phase = 364

Effective number of turns of field winding/pole = 52½

Effective number of turns of damper winding/pole = 8

D.4 Parameters for the Three-Phase Induction Motor and Inertia Load

The electrical and mechanical system parameters are given below:

Rated Power	200	HP
Rated Line Voltage	550	Volt
Frequency	60	Hz
Stator Connection	Y	
Stator Resistance	0.0285	Ω
Stator Leakage Inductance	0.291	mH
Rotor Resistance	0.0549	Ω
Rotor Leakage Inductance	0.291	mH
Magnetizing Inductance	7.103	mH
Stator/Rotor Turns Ratio	1.0	
Number of Poles	6	
Rotor Inertia	7.73	Kg. m^2
Rotor Damping Coefficient	20.0	Nm/rad/sec
Disc Inertia	68.75	Kg. m^2
Disc Damping Coefficient	20.0	Nm/rad/sec
Shaft Stiffness	1.5×10^6	Nm/rad

APPENDIX E

SETS OF SIMULATED OSCILLOGRAM FOR THE THREE-PHASE SYNCHRONOUS GENERATOR AND INDUCTION MOTOR

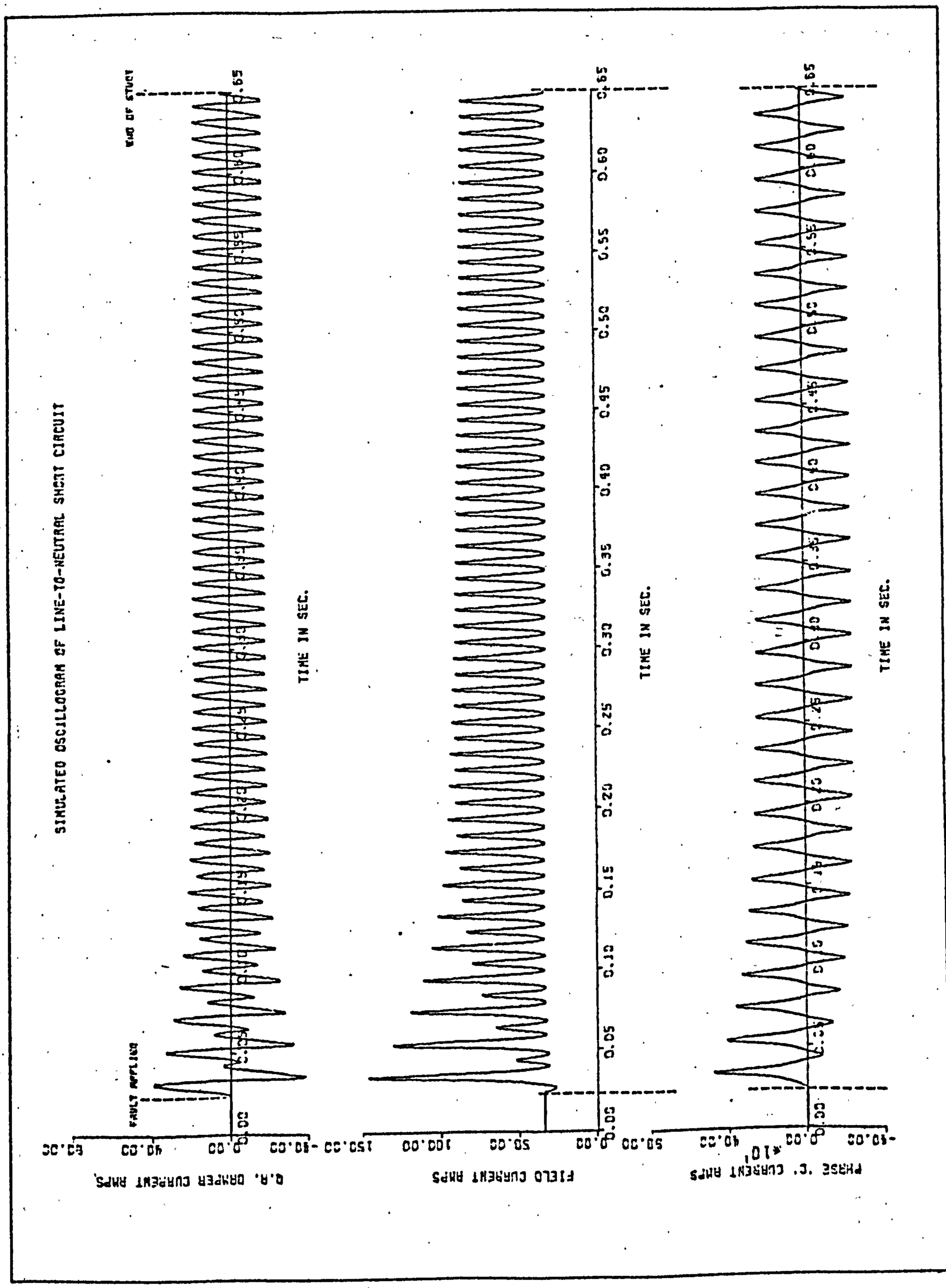
SIMULATED OSCILLOGRAM OF LINE-TO-NEUTRAL SHORT CIRCUIT
END OF STUDY
FAULT APPLIED
TIME IN SEC.
TIME IN SEC.
TIME IN SEC.
A.R. ARMATURE CURRENT AMPS.
FIELD CURRENT AMPS
PHASE 'C' CURRENT AMPS
«10'

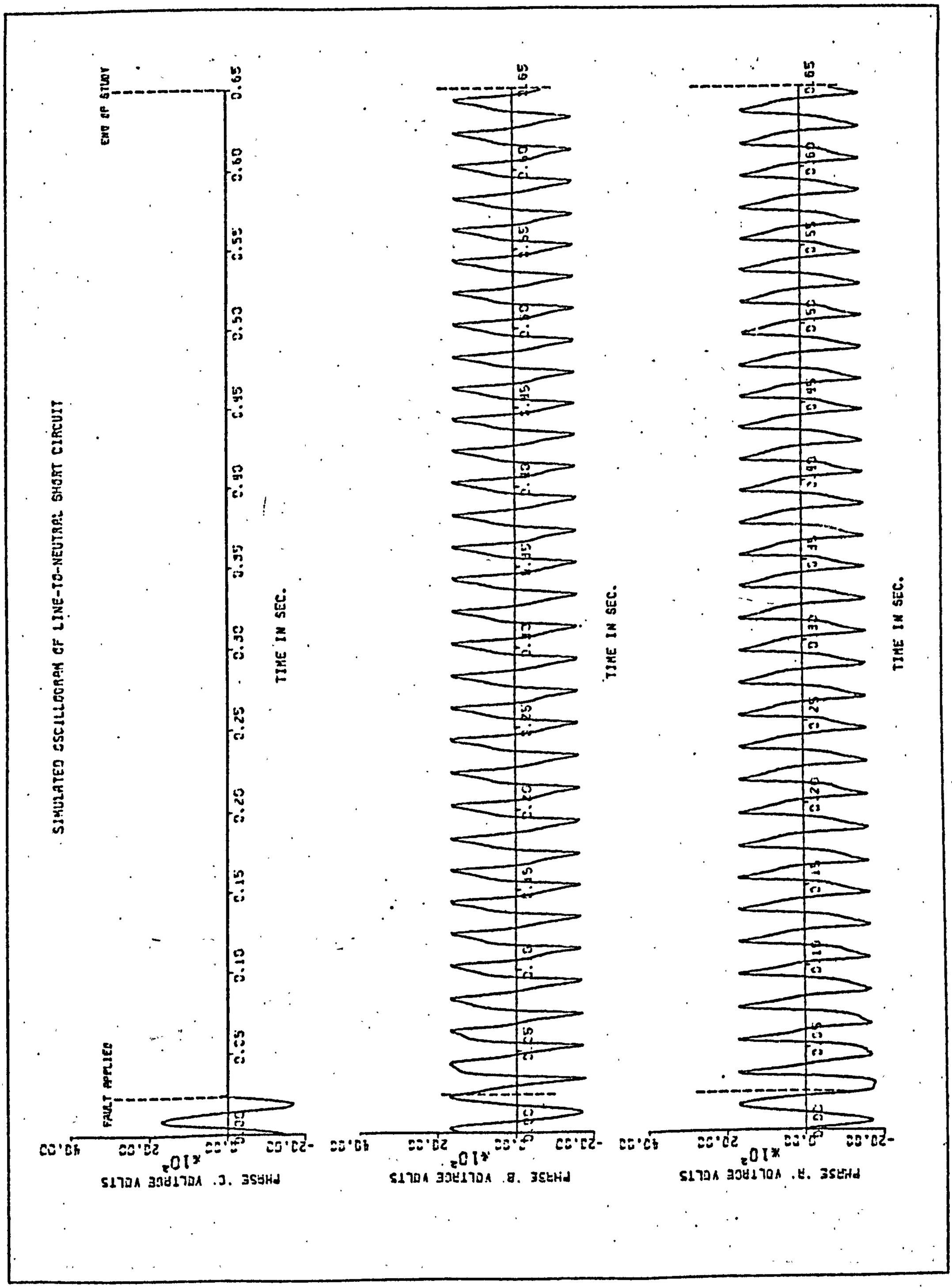
SIMULATED OSCILLOGRAM OF LINE-TO-NEUTRAL SHORT CIRCUIT
FAULT APPLIED
END OF STUDY
TIME IN SEC.
PHASE A. VOLTAGE VOLTS
PHASE B. VOLTAGE VOLTS
PHASE C. VOLTAGE VOLTS
*10²

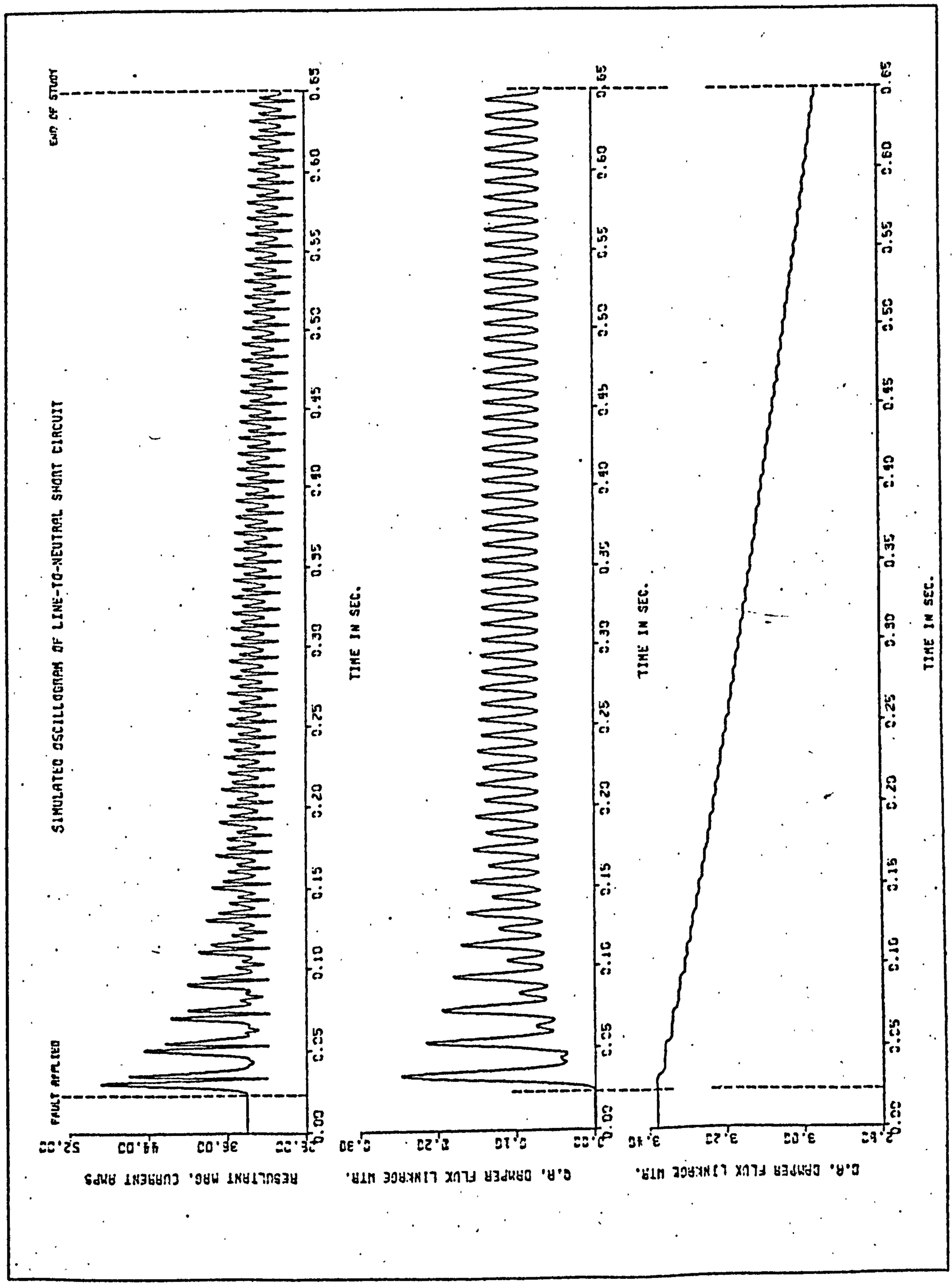
SIMULATED OSCILLOGRAM OF LINE-TO-NEUTRAL SHORT CIRCUIT
FAULT APPLIED
END OF STUDY
TIME IN SEC.
0.00
0.05
0.10
0.15
0.20
0.25
0.30
0.35
0.40
0.45
0.50
0.55
0.60
0.65
52.00
44.00
36.00
28.00
3.40
3.20
3.00
2.80
C.R. DAMPER FLUX LINKAGE WTR.
G.R. DAMPER FLUX LINKAGE WTR.
RESULTANT MAG. CURRENT AMPS

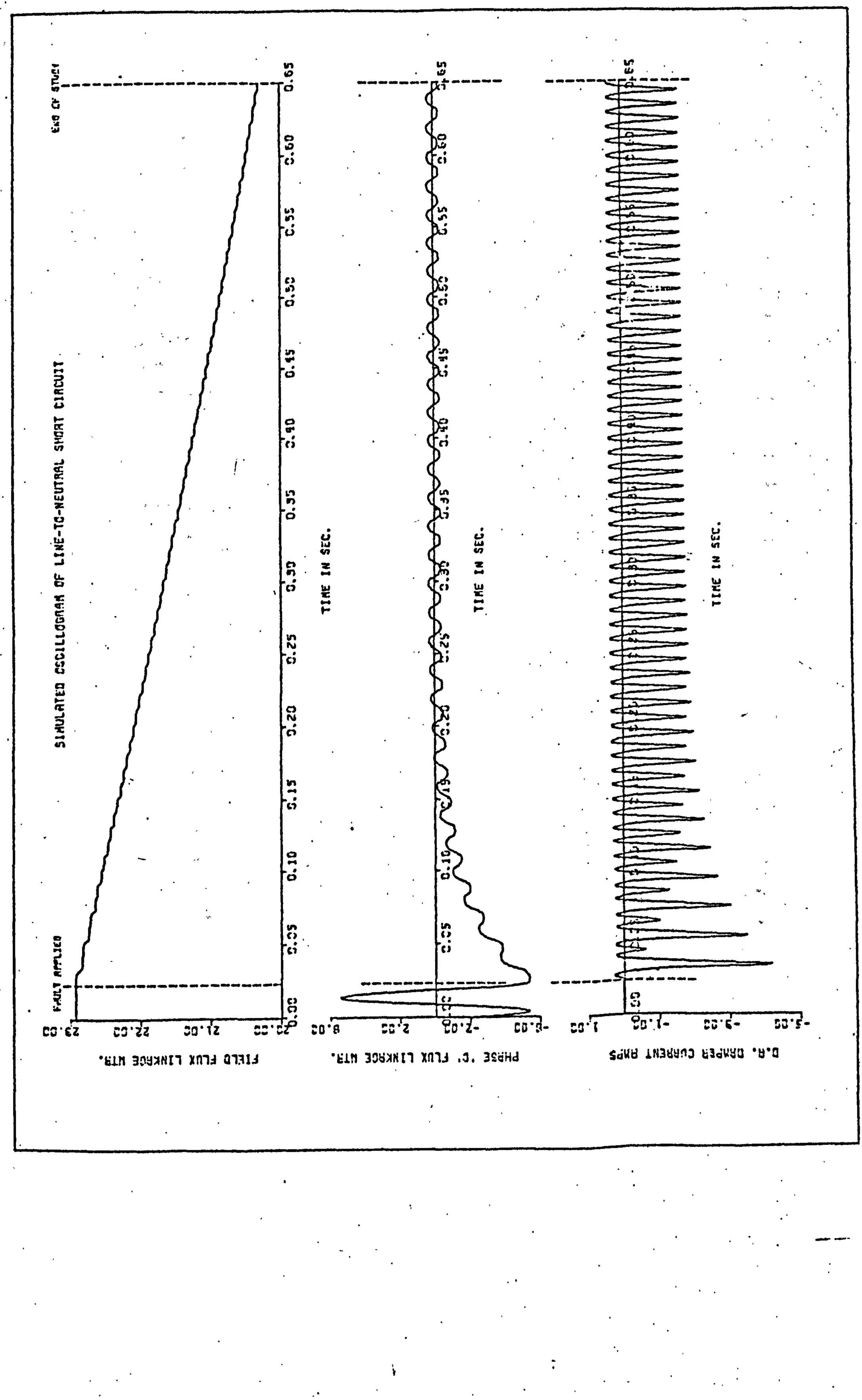
SIMULATED OSCILLOGRAM OF LINE-TO-NEUTRAL SHORT CIRCUIT
FAULT APPLIED
END OF STUDY
TIME IN SEC.
PHASE 'C' FLUX LINKAGE WTR.
FIELD FLUX LINKAGE WTR.
D.R. DAMPER CURRENT AMPS

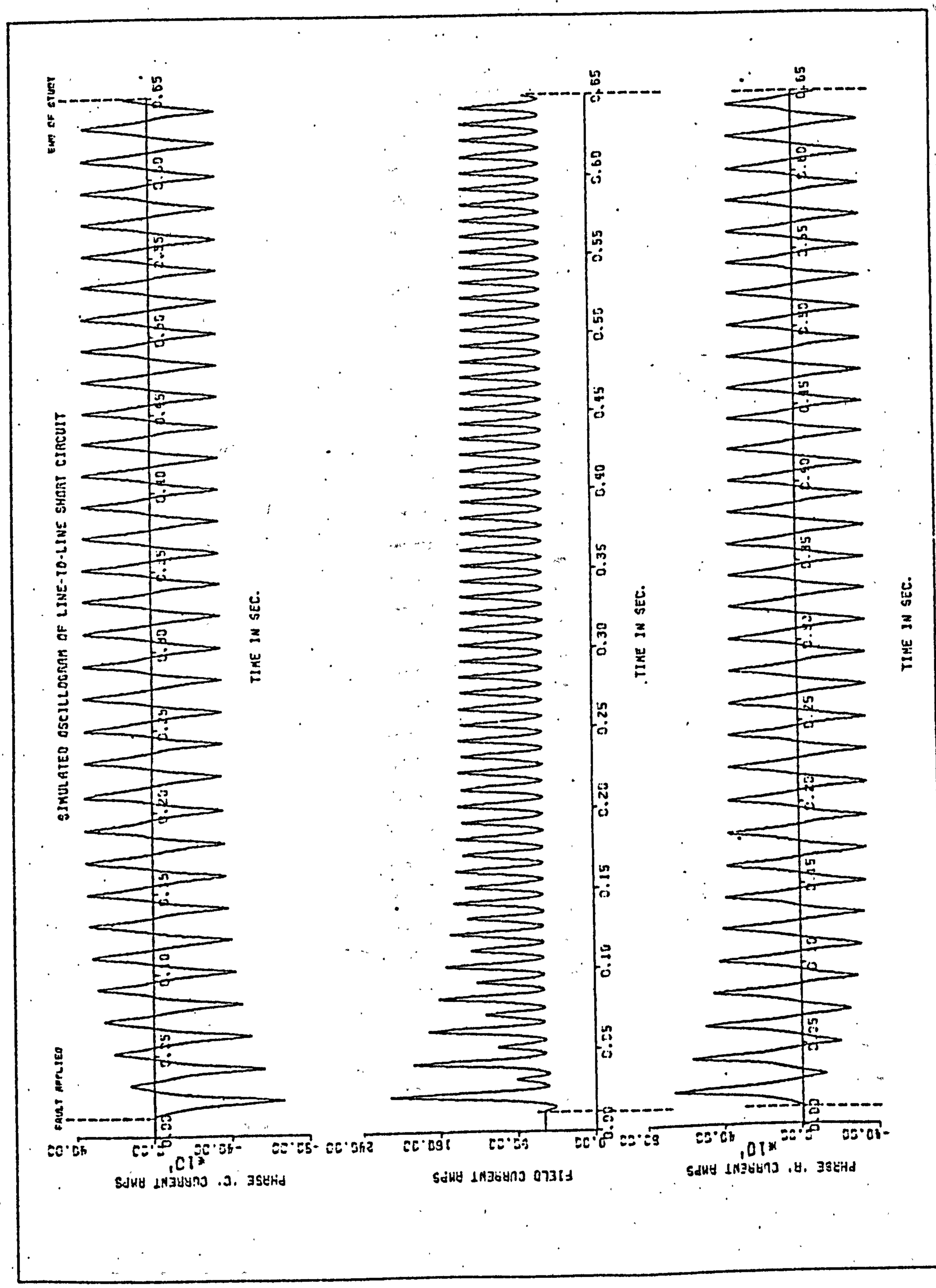
SIMULATED OSCILLOGRAM OF LINE-TO-LINE SHORT CIRCUIT
FAULT APPLIED
END OF STUDY
TIME IN SEC.
PHASE 'C' CURRENT AMPS
FIELD CURRENT AMPS
PHASE 'R' CURRENT AMPS

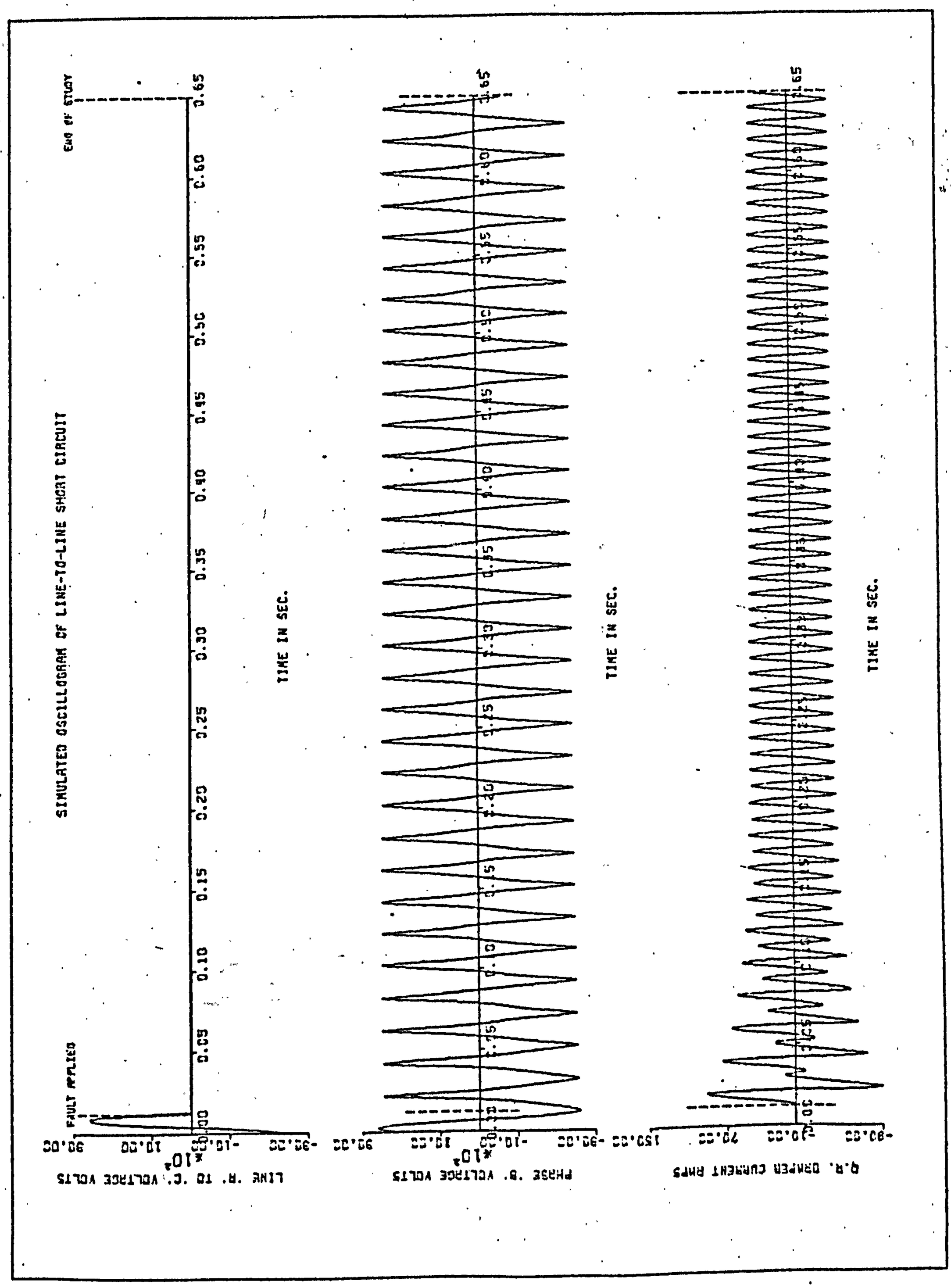
SIMULATED OSCILLOGRAM OF LINE-TO-LINE SHORT CIRCUIT
FAULT APPLIED
END OF STUDY
0.00
0.05
0.10
0.15
0.20
0.25
0.30
0.35
0.40
0.45
0.50
0.55
0.60
0.65
TIME IN SEC.
LINE 'B' TO 'C' VOLTAGE VOLTS
PHASE 'B' VOLTAGE VOLTS
Q.R. DAMPER CURRENT AMPS

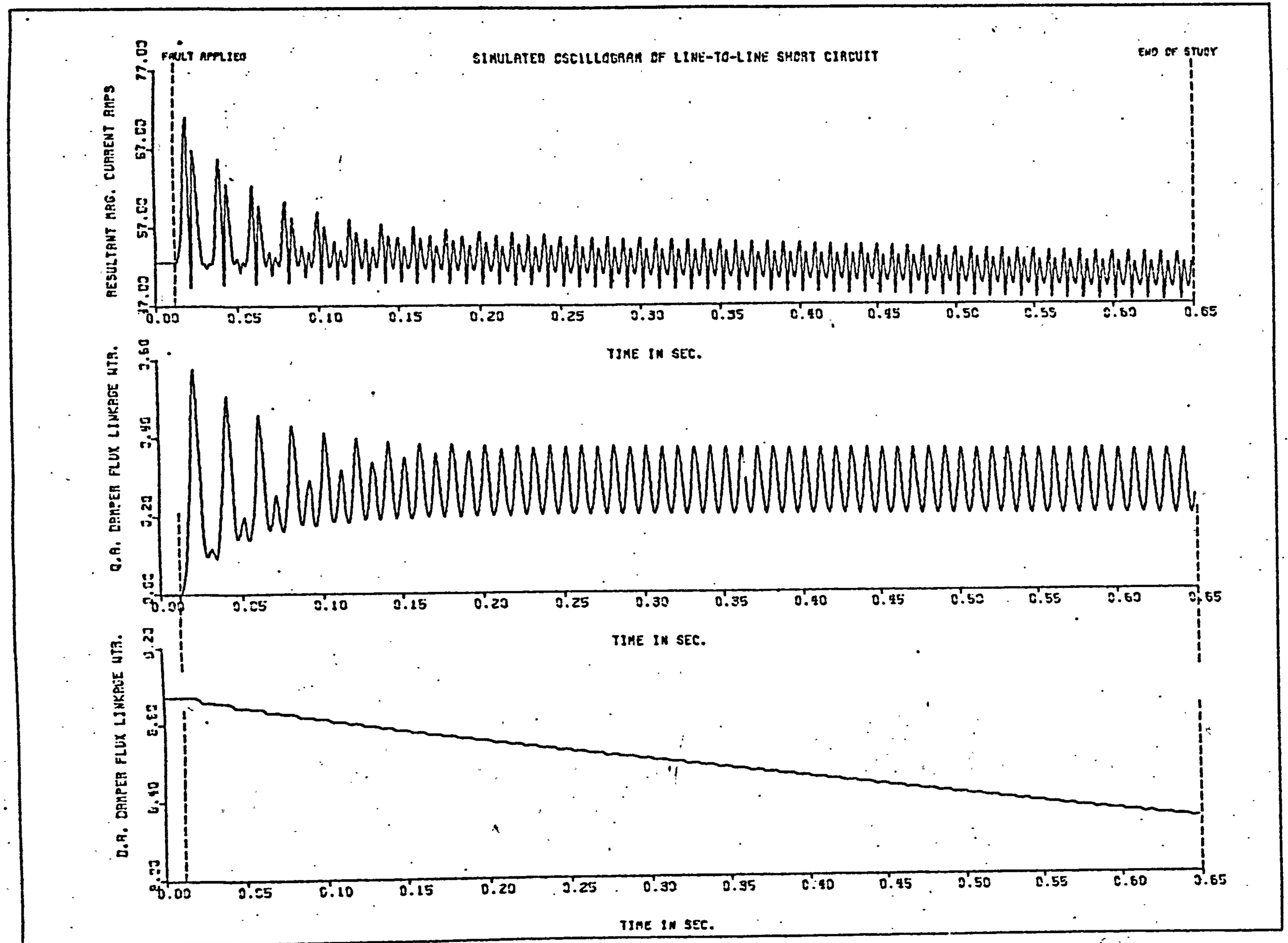
SIMULATED OSCILLOGRAM OF LINE-TO-LINE SHORT CIRCUIT
FAULT APPLIED
END OF STUDY
RESULTANT ARG. CURRENT AMPS
37.00
57.00
67.00
77.00
0.00
0.05
0.10
0.15
0.20
0.25
0.30
0.35
0.40
0.45
0.50
0.55
0.60
0.65
TIME IN SEC.
Q.A. DAMPER FLUX LINKAGE WTR.
TIME IN SEC.
D.A. DAMPER FLUX LINKAGE WTR.
TIME IN SEC.

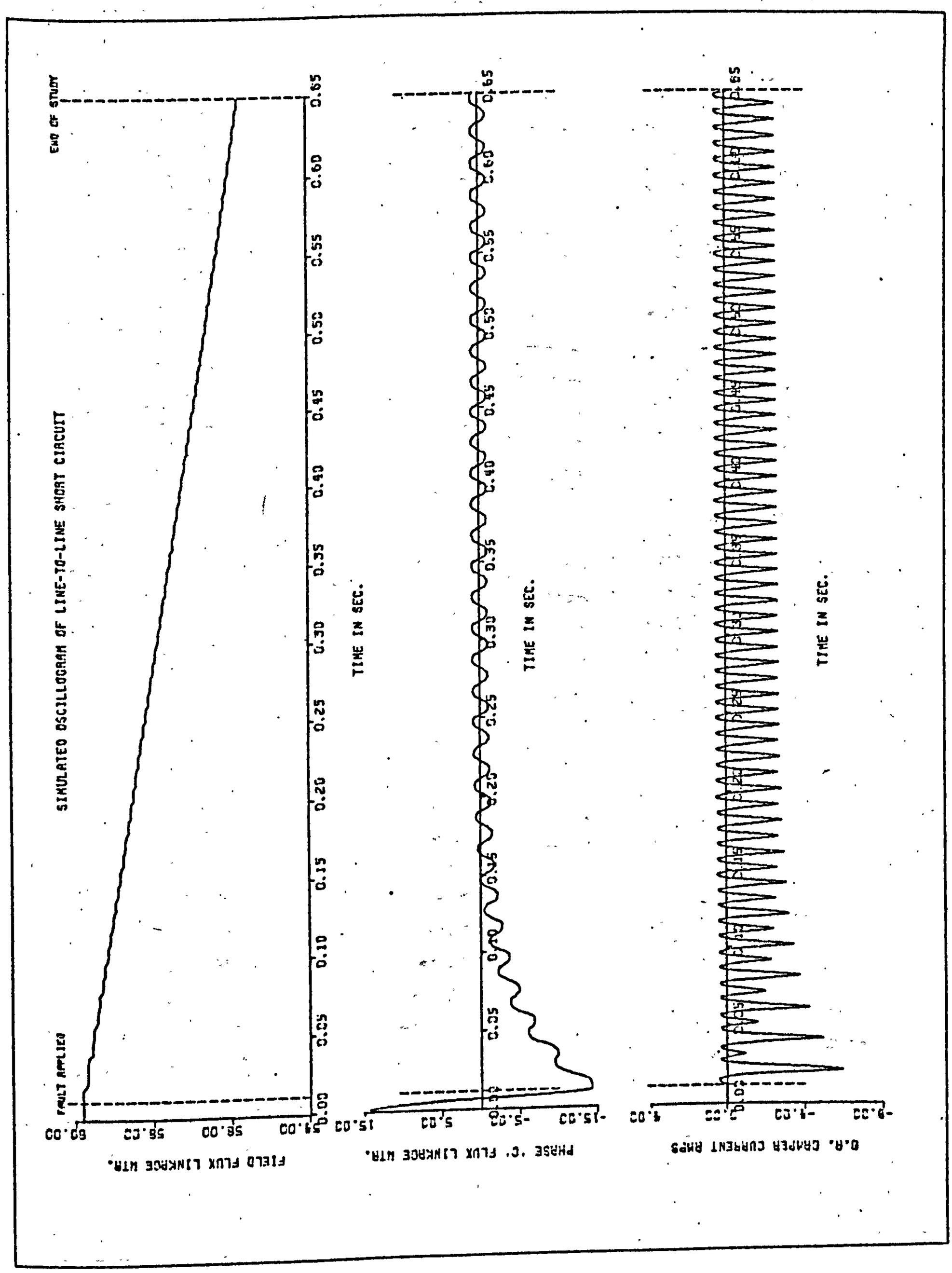
SIMULATED OSCILLOGRAM OF LINE-TO-LINE SHORT CIRCUIT
FAULT APPLIED
END OF STUDY
FIELD FLUX LINKAGE WTR.
PHASE 'C' FLUX LINKAGE WTR.
D.R. CRAPER CURRENT AMPS
TIME IN SEC.
TIME IN SEC.
TIME IN SEC.

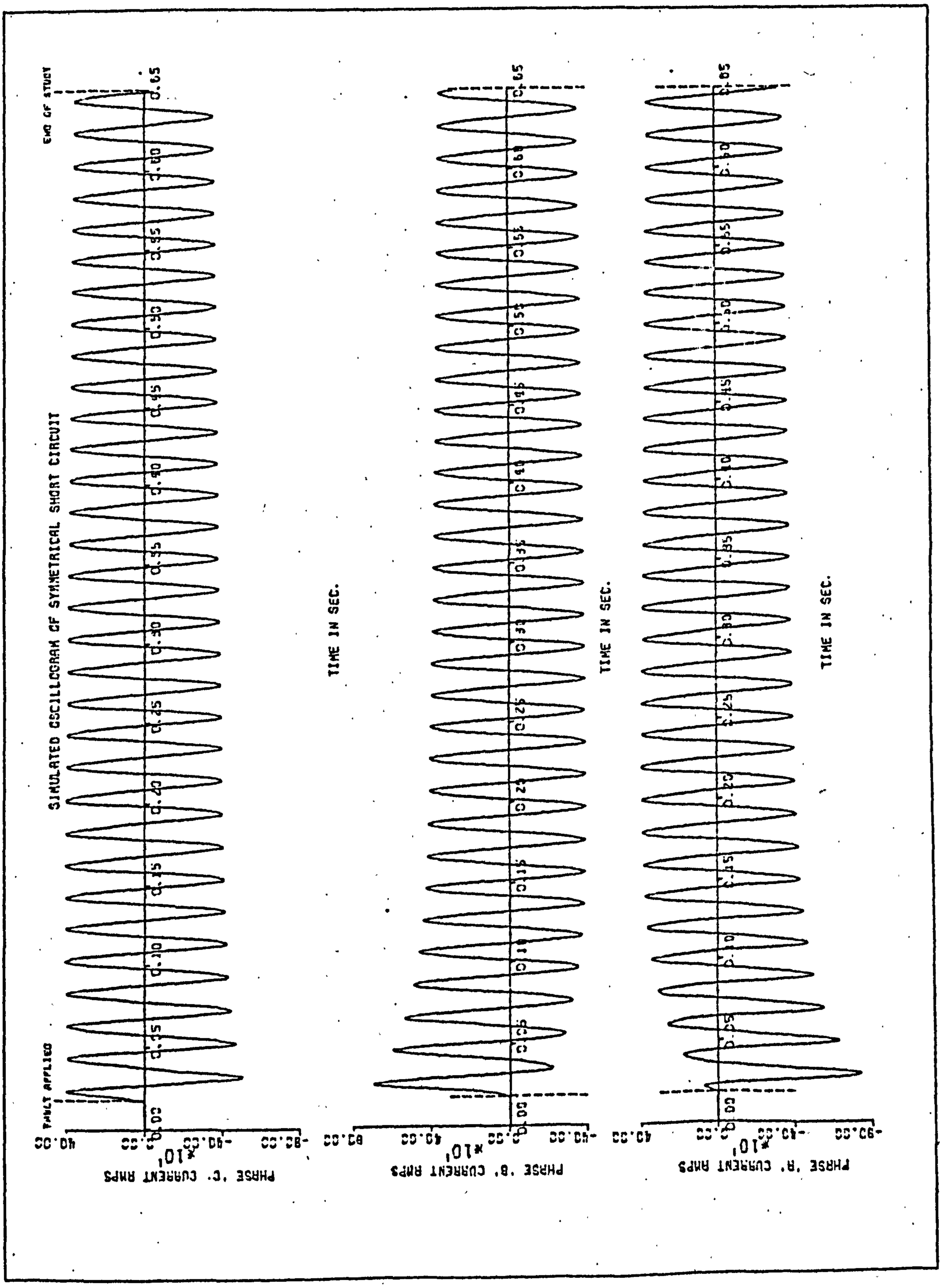
SIMULATED OSCILLOGRAM OF SYMMETRICAL SHORT CIRCUIT
FAULT APPLIED
END OF STUDY
PHASE 'R' CURRENT AMPS
PHASE 'B' CURRENT AMPS
PHASE 'C' CURRENT AMPS
TIME IN SEC.
TIME IN SEC.
TIME IN SEC.

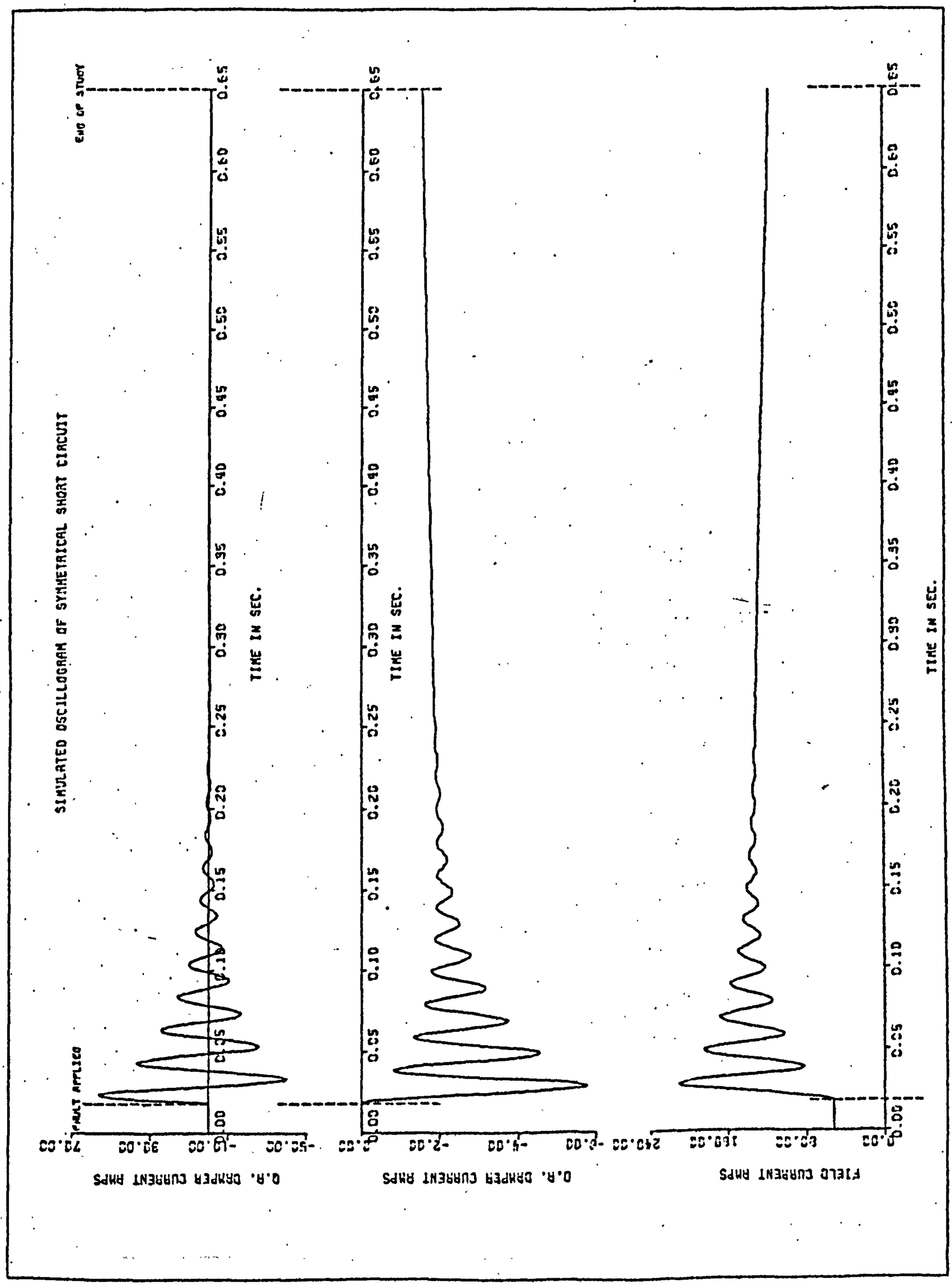
SIMULATED OSCILLOGRAM OF SYMMETRICAL SHORT CIRCUIT
FAULT APPLIED
END OF STUDY
TIME IN SEC.
TIME IN SEC.
TIME IN SEC.
0.R. DAMPED CURRENT AMPS
0.R. DAMPED CURRENT AMPS
FIELD CURRENT AMPS

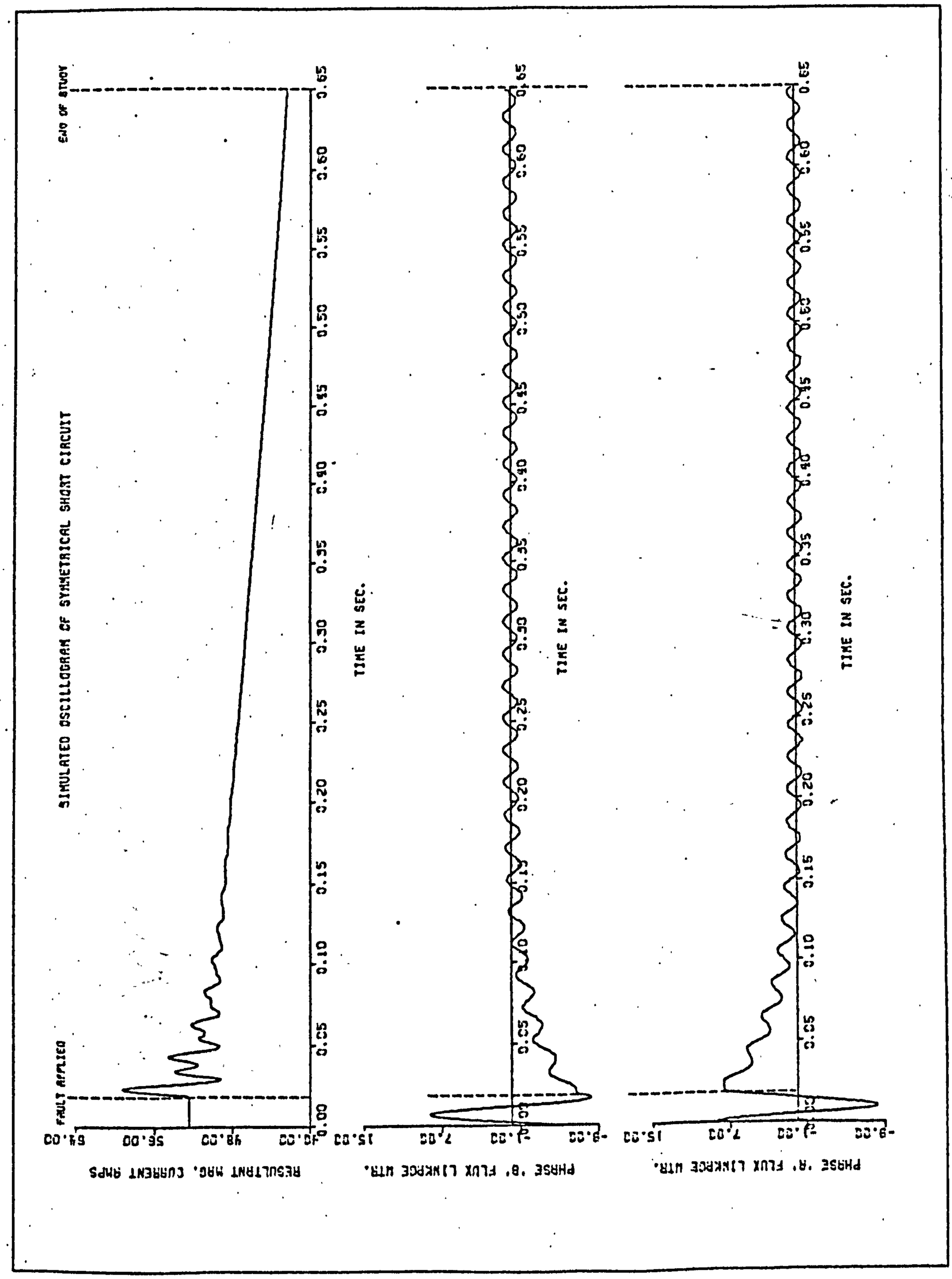
SIMULATED OSCILLOGRAM OF SYMMETRICAL SHORT CIRCUIT
FAULT APPLIED
END OF STUDY
TIME IN SEC.
PHASE 'R' FLUX LINKAGE WTR.
PHASE 'B' FLUX LINKAGE WTR.
RESULTANT MAG. CURRENT AMPS

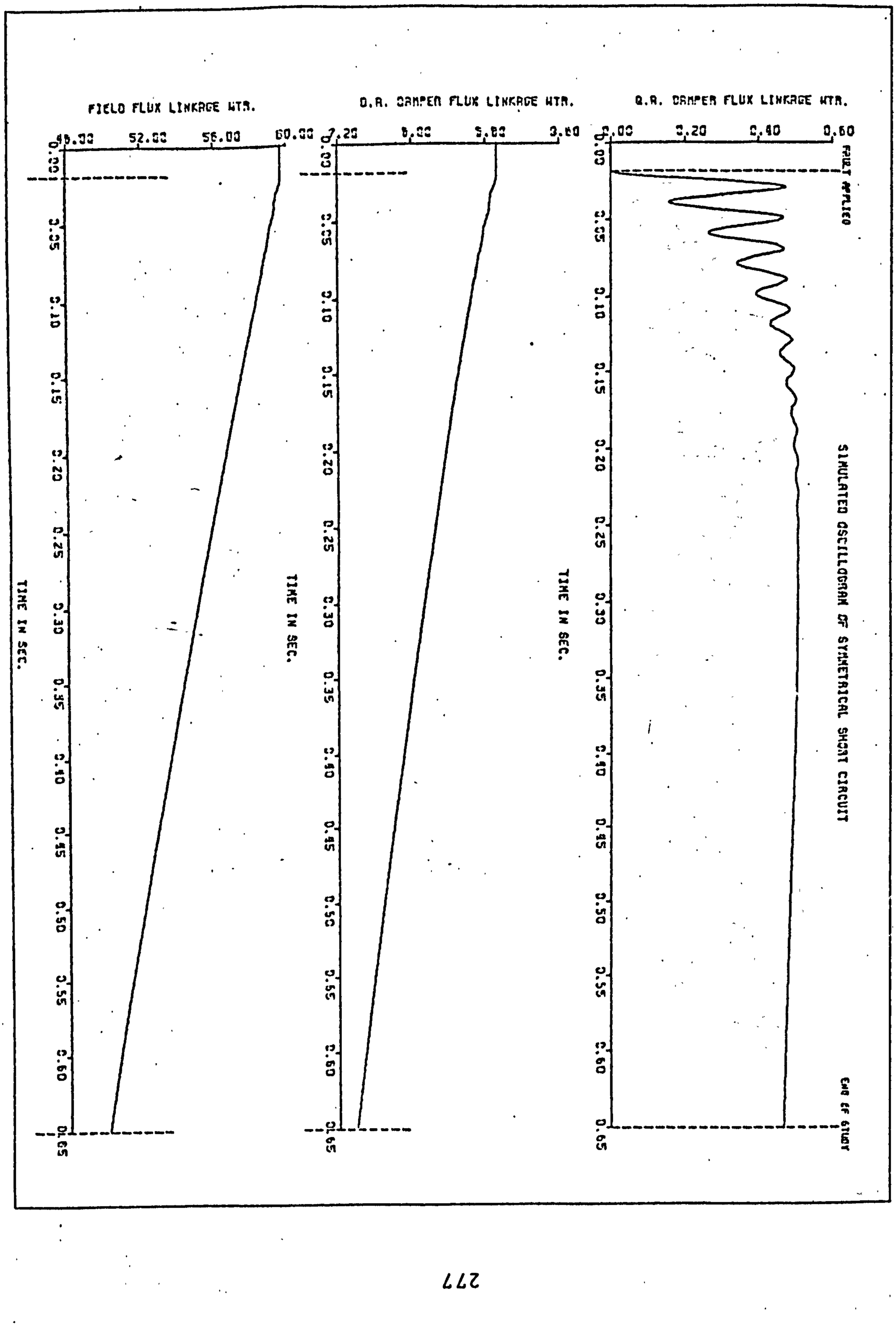
FIELD FLUX LINKAGE WTR.
48.00
52.00
56.00
60.00
TIME IN SEC.
D.R. DAMPER FLUX LINKAGE WTR.
2.20
3.00
3.80
TIME IN SEC.
Q.R. DAMPER FLUX LINKAGE WTR.
3.00
3.20
3.40
3.60
FAULT APPLIED
SIMULATED OSCILLOGRAM OF SYMMETRICAL SHORT CIRCUIT
TIME IN SEC.
0.00
0.05
0.10
0.15
0.20
0.25
0.30
0.35
0.40
0.45
0.50
0.55
0.60
0.65
END OF STUDY

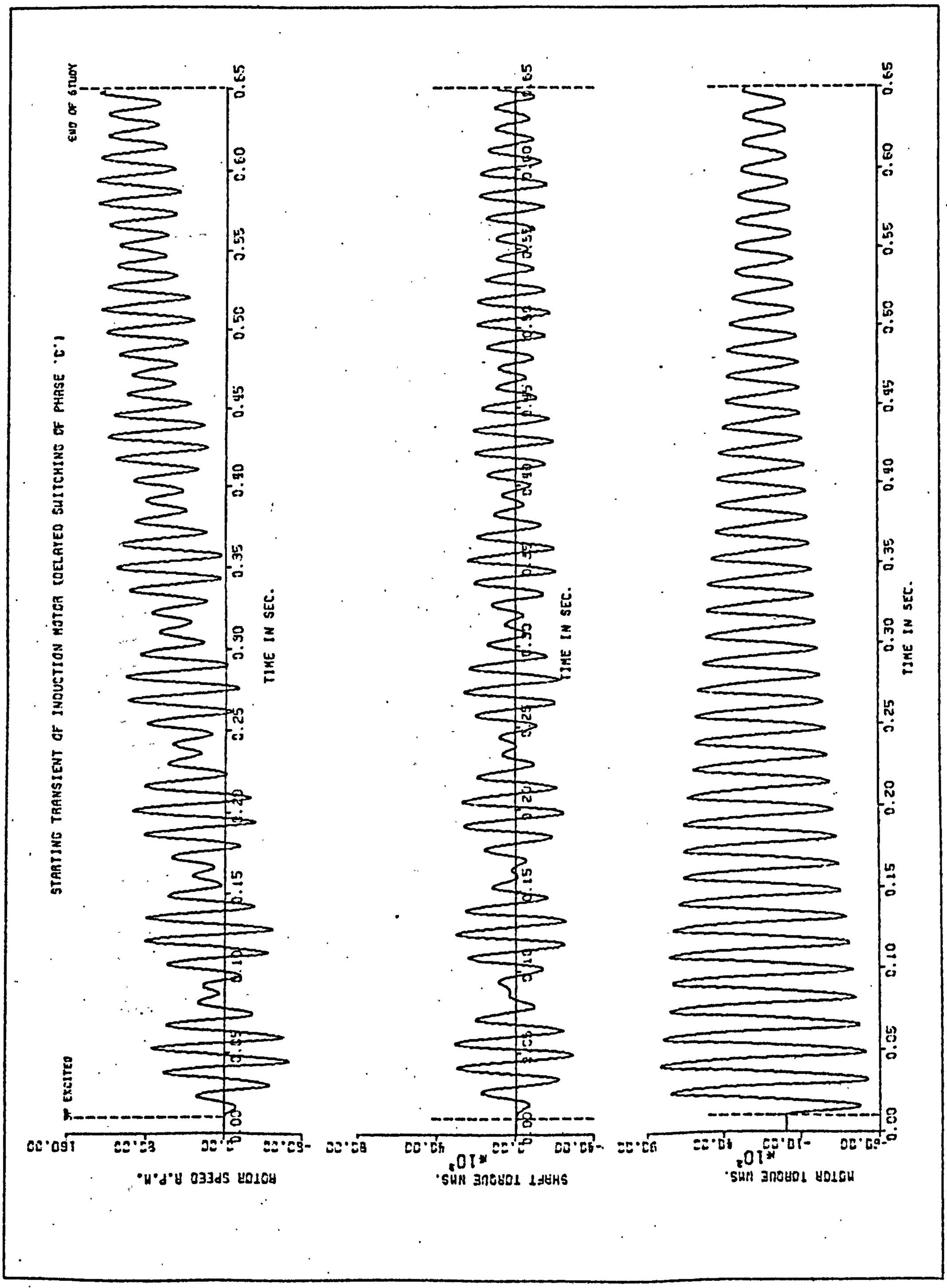
STARTING TRANSIENT OF INDUCTION MOTOR (DELAYED SWITCHING OF PHASE 'C')
MOTOR TORQUE NMS.
*10³
SHAFT TORQUE NMS.
*10³
ROTOR SPEED R.P.M.
TIME IN SEC.
TIME IN SEC.
TIME IN SEC.
END OF STUDY
'A' EXCITED

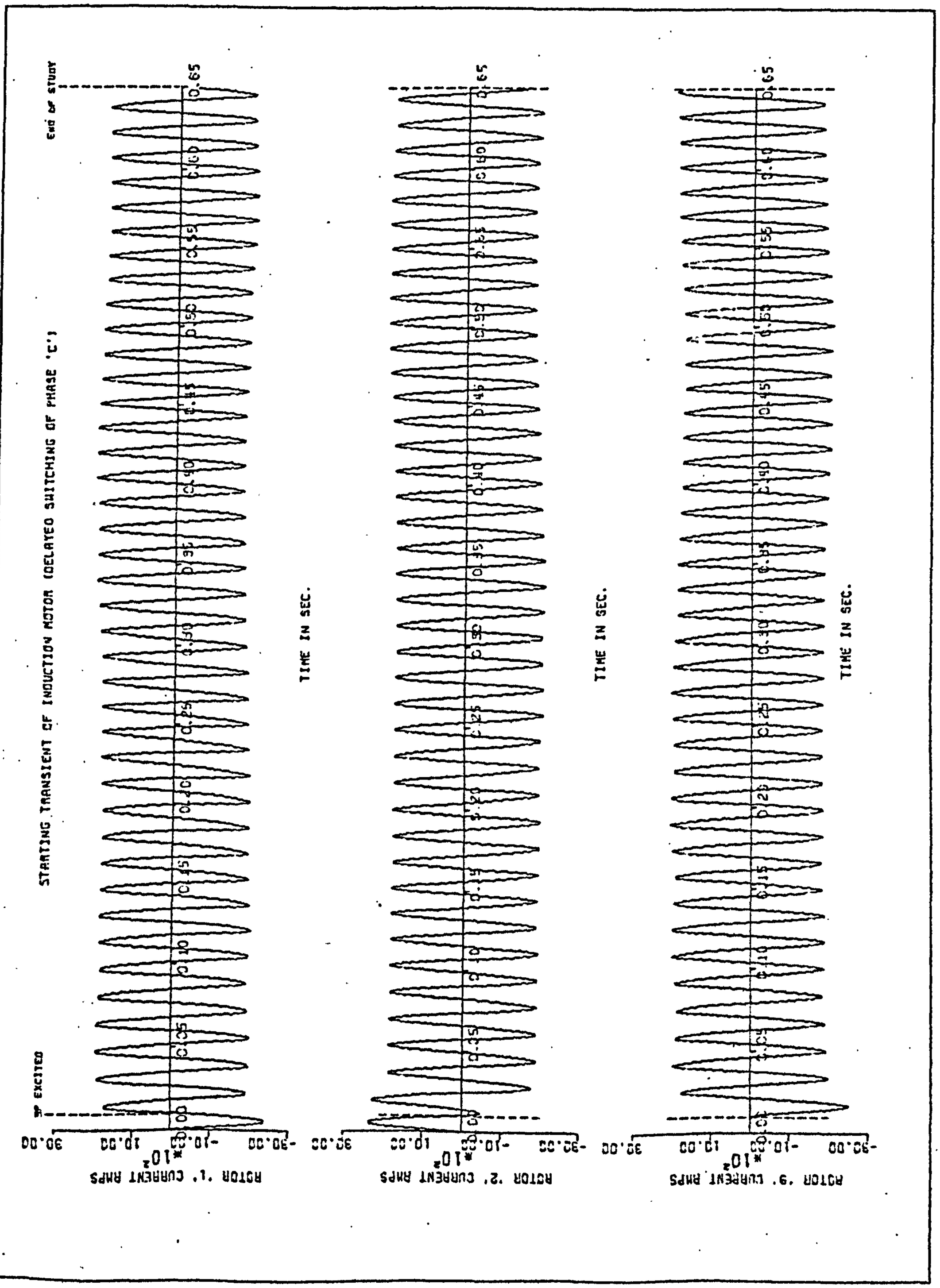
STARTING TRANSIENT OF INDUCTION MOTOR (DELAYED SWITCHING OF PHASE 'C')
EXCITED
END OF STUDY
TIME IN SEC.
ROTOR '1' CURRENT AMPS
ROTOR '2' CURRENT AMPS
ROTOR '9' CURRENT AMPS
*10²